HEAD TRACKING TWO-IMAGE 3D TELEVISION DISPLAYS

by

Phil Surman

Imaging and Displays Research Group

Faculty of Computing Science and Engineering

De Montfort University, The Gateway, Leicester

June 2002

PAGINATED
BLANK PAGES
ARE SCANNED AS
FOUND IN
ORIGINAL
THESIS

NO
INFORMATION
MISSING

Head Tracking Two-image 3D Television Displays

by

Phil Surman

The research covered in this thesis encompasses the design of novel 3D displays, a consideration of 3D television requirements and a survey of autostereoscopic methods is also presented. The principle of operation of simple 3D display prototypes is described, and design of the components of optical systems is considered. A description of an appropriate non-contact infrared head tracking method suitable for use with 3D television displays is also included.

The thesis describes how the operating principle of the displays is based upon a two-image system comprising a pair of images presented to the appropriate viewers' eyes. This is achieved by means of novel steering optics positioned behind a direct view liquid crystal display (LCD) that is controlled by a head position tracker. Within the work, two separate prototypes are described, both of which provide 3D to a single viewer who has limited movement. The thesis goes on to describe how these prototypes can be developed into a multiple-viewer display that is suitable for television use.

A consideration of 3D television requirements is documented showing that glasses-free viewing (autostereoscopic), freedom of viewer movement and practical designs are important factors for 3D television displays.

The displays are novel in design in several important aspects that comply with the requirements for 3D television. Firstly they do not require viewers to wear special glasses, secondly the displays allow viewers to move freely when viewing and finally the design of the displays is practical with a housing size similar to modern television sets and a cost that is not excessive. Surveys of other autostereoscopic methods included within the work suggest that no contemporary 3D display offers all of these important factors.

CONTENTS

SECTION 4 - PROTOTYPES

SECTION 5 – HEAD TRACKING

LIST OF ILLUSTRATIONS

LIST OF TABLES

ABBREVIATIONS

Abbreviation	Meaning
A/R	Antireflection
AOM	Acousto-optic modulator
AMLCD	Active-matrix liquid crystal display
CFF	Critical flicker frequency
CGH	Computer generated hologram
CRT	Cathode ray tube
DFT	Discrete Fourier transform
DLP	Digital light processor
DMD	Digital micromirror device
EASLM	Electrically addressed spatial light modulator
EL	Electroluminescent
FFT	Fast Fourier transform
FLA	Focused light array
FLC	Ferroelectric crystal
FWHM	Full-width half-maximum
HDTV	High definition television
HOE	Holographic optical element
LCD	Liquid crystal display
LED	Light emitting diode
LICOS	Liquid crystal on silicon
LSD	Light shaping diffuser
MDF	Medium density fibreboard
MTF	Modulation transfer function
OASLM	Optically addressed spatial light modulator
PCB	Printed circuit board
PDP	Plasma display panel
PSF	Point spread function
RGB	Red green blue
SLM	Spatial light modulator
SMM	Stretchable membrane mirror
SMV	Super multi-view
STN	Supertwist nematic
SVGA	Super VGA
TFT	Thin film transistor
VGA	Video graphics array

ACKNOWLEDGEMENTS

My sincere thanks to Dr Ian Sexton and Dr Tim Bardsley for their judicious supervision throughout this research programme.

A special note of appreciation to David Surman for his support in building demonstrator models and in proof reading the thesis.

PAGE
MISSING
IN
ORIGINAL

CHAPTER 1
INTRODUCTION

1.1) Preface

The ultimate aim of the research is the design, production and evaluation of a stereoscopic display that is suitable for television applications. This display will meet the particular requirements for television that are set out in this chapter. It is envisaged that the proposed display will fulfil the demands of the third generation of television that is likely to be around for about twenty-five years. The time is overdue for the commencement of 3D television - our eyes have colour receptors and we have two of them. The first generation of television, monochrome, was prominent from the nineteen thirties until the nineteen sixties and seventies, when colour took over. Once colour had been established, monochrome was considered unacceptable. The same pattern will probably happen with 3D. It is interesting to note that children, the customers of the future, are fascinated by 3D and also generally have little difficulty fusing stereo pairs.

Although the delivery of picture information is currently undergoing dramatic changes, the interface with the viewer is still the same monoscopic picture. The need for 3D television is not unanimous, even amongst workers in the field of stereoscopy. However, it is the author's opinion that the enhanced picture quality provided by the addition of 3D will fuel a market that is enormous. At a conservative estimate, the total number of units could be in excess one hundred million. A 3D television will undoubtedly be more expensive, say €1,500, which gives a total of one hundred and fifty billion euros.

Display requirements fall into three broad categories. These are: single-viewer, for displaying on computer monitors and arcade games: two to around six viewers where television (and some arcade games) is viewed: and tens to hundreds of viewers for theatre presentation. The consensus of opinion is that a 3D television display should be autostereoscopic, i.e. it does not require the wearing of special glasses. There are several single-viewer autostereoscopic systems under development, and the presentation of autostereo to a theatre-sized audience has been achieved [VALY62a], albeit with viewers having restricted movement. The object of the current research is

to produce a display that provides 3D without glasses to several viewers over a room-sized area. This will necessarily be more difficult to achieve than for a single-viewer 3D display, and will therefore be somewhat more complex.

Due to increased personal computer use, viewing patterns are changing so that there are more individual viewers within a household. However, the author considers that television will remain a shared experience to a sufficient degree for multiple-viewer television to be a widely used display mode for the foreseeable future.

1.2) Aims and Objectives of Research

Investigation into the most suitable method of providing 3D to viewers under typical television viewing conditions has suggested that the optimum solution is to provide the same stereo image-pair to every viewer. As the bottleneck in any 3D system is the amount of information the screen can display, the use of two images only keeps this to a minimum.

Until now, the research has concentrated on investigation into the properties of the various components of the display, the construction of low-cost single-viewer prototypes and head tracker. These are still under construction at the time of writing, but much valuable work has been carried out to date. The research has attracted funding from the European Commission under the Information Society Technology (IST) programme. The project is called ATTEST (Advanced Three-dimensional Television System Technologies) and is an ambitious two-year programme whose aim is to develop a complete 3D television chain from the production and synthesis of 3D material, through to the display itself. De Montfort University will be providing the multiple-viewer prototype displays.

These prototypes will present the same left image to the left eyes of every viewer, and the same right image to their right eyes. This is achieved by using a direct-view liquid crystal display (LCD) where the conventional backlight is replaced by novel steering optics that steer the light to the appropriate viewers' eyes. The regions in which the eyes are located are referred to in this work as the exit pupils, and are regions where a left image only, or a right image only, is seen across the complete width of the screen. The steering optics are controlled by the output of a head position tracker that

determines the positions of the viewers' eyes. Both left and right images are presented simultaneously on the screen on alternate rows of pixels.

A simple infrared head tracker is also under development. This has the advantage of being non-intrusive to the viewer – it does not need any attachments worn on the head. This has been developed for single-viewer use, but it is capable of being adapted to serve multiple-viewers.

1.3) 3D Television Requirements

Cost must be an important consideration; there is little doubt that 3D television displays will be more expensive than current monoscopic sets. However, when colour television was introduced, the cost of a colour set was around five times that of black and white, yet this did not deter consumers from buying them.

There have been several papers published relating to the requirements for 3D television, amongst these are [FORS78a] [SMIT88a] [PAST91a]. These mention such things as compatibility, cost, desirability, motion parallax (the ability to look around objects in the image), viewing distance and screen size. However, the aspects mentioned in the following sections are likely to be the most important.

1.3.1) Display Availability

This might appear to be a rather obvious requirement but there would be no point, for example, in pursuing a method using a direct-view LCD if a device of sufficient size and with a low enough cost was not likely to be available in the near future. This point seems to be rarely acknowledged in published work on stereo displays. It must be borne in mind that *any* stereo display will have to provide a minimum of twice the number of images necessary for monoscopic presentation. The current research has been carried out for a number of years and during that period LCDs have gradually increased in size so that 20" displays are readily available at a cost that is not exorbitant, and 28" LCDs, and even tiled 40" versions, are now available. This is encouraging as it was not certain when the research started that a sufficiently large LCD would ever become available.

1.3.2) Multiple Viewers

Unlike computer monitors, which in general need to provide an image to only one viewer, television has to serve a maximum of around six viewers. The proposed method only addresses the requirements of the television market, and no attempt will be made to present stereo to a theatre-sized audience. In an article in the Scientific American, the interesting point relating to viewing audiences was made that there is a trend for consumers with access to CD-ROMs and the Web to become somewhat disenchanted with television [BROW96]. Although there appears to be a need for some viewers to have *anything* on a screen, the viewing pattern of television, which has existed for the past forty to fifty years, seems likely continue substantially unchanged into the foreseeable future.

1.3.3) Autostereoscopic

It is generally recognised that 3D television would not be as acceptable if special glasses had to be worn. As television is watched intermittently, usually with many interruptions - unlike the cinema, it is unlikely that viewers will want to keep putting on and taking off special glasses [SMIT88b].

1.3.4) Viewing Volume

Television viewers must be able to move freely over a large viewing volume - possibly between 1 to 6 metres from the screen, and up to 40° from the centre-line. Within this volume, stereo must be able to be seen for any head position. Methods such as simple lenticular displays which have alternate stereoscopic and pseudoscopic zones, or integral imaging which have around three or four unusable regions across the width of the viewing field, would place unacceptable restrictions on the viewers' freedom of movement. In many autostereoscopic displays, the viewers are restricted to being close to an optimum-viewing plane.

1.3.5) Housing Size

The light in a stereo display will require some degree of manipulation that would not be necessary in a monoscopic display, therefore it is possible that the overall housing size may be larger. When a direct-view LCD is used in its normal mode of operation, the housing could be of 'hang-on-the-wall' size. However, with an LCD used in the

proposed stereo display, the housing will be of a size comparable to that of currently available rear projection televisions. This may not be a particular disadvantage as there is no real necessity for the depth of a television set to be very small. The folded optical system, to be used in the prototype, will enable the housing to have considerably less depth than a CRT set.

1.4) The Case for Two-image Head Tracking

It is the author's opinion that a two-image head tracked display is the most appropriate for the next generation of television. The advantages of head tracking will now be considered. The limitation of any stereo system will most likely be determined by the display itself owing to the increased amount of information that has to be displayed. Bearing in mind that the increased resolution and size requirement for HDTV alone will be quite difficult to achieve, any stereo method that requires the display to either run many times faster, or have many times the resolution, is unlikely to be implemented in the near future. A system supplying the minimum of only two images will provide the only realistic solution for the next generation of television.

If these two images occupy fixed positions in the viewing field, as in the case of the simple lenticular or parallax barrier displays, then the restriction on head position will be unacceptable, as already mentioned. The wearing of special glasses in order for the images to be directed to the appropriate eyes irrespective of head position is also unacceptable.

If the display is able to direct the left and right views to the correct eyes, but without the need for glasses, then the minimum display requirement is the presentation of two images.. It is clear that the only way this can be achieved is by directing the images to the positions that the eyes are known to occupy. This will necessitate the use of head tracking do determine the eyes' positions.

The earliest reference to head tracking known to the author is that of Alfred Schwartz in 1985 [SCHW85]. This described a method that uses two projection CRTs and a large Fresnel lens, and could serve only one viewer. Since that time there have been

an increasing number of papers published describing various head tracking displays, and these are surveyed in Chapter 3). None of these are particularly suited for 3D television, but the growing interest indicates that some form of head tracking would possibly be the preferred method for this application.

There are three important points regarding the presentation of two-image head tracking stereo that should be made. Firstly, *if* head motion parallax were considered to be absolutely necessary, then in principle, head tracking could be used to provide this. If there are N viewers in the viewing field, then 2N views must be presented. This would enable motion parallax to be obtained with the minimum amount of information being displayed. If eventually a display technology does become available that is sufficiently fast, or has a sufficiently high resolution, to show this amount of information, the optics of the multiple-viewer prototypes will be sufficiently flexible to cope with this.

The second point is for the sound, but rarely acknowledged reason, that motion parallax might actually be undesirable owing to the fact that the camera used for the image capture would have to be very wide. Consider the case of an object, for example a head, located at the plane of the screen. If the viewing field is ± 40° either side of the centre line, and the camera is 2 metres away from the head, it would have to capture images over a width of around 3 metres.

Thirdly, if true motion parallax is presented, the edge of the screen can be considered as being a 'window' through which the scene is observed. It is evident that a completely different image will be seen at either side of the viewing field if the scene being shown was at infinity. In practice, this will not be the case as the amount of disparity is limited in order to reduce the effect of the difference between accommodation and convergence of the eyes. The compression of apparent depth necessary to avoid this would mean that the images seen would never be completely different. The effect will also be less pronounced for a 16:9, as opposed to a 4:3, aspect ratio screen. Nevertheless, this is another factor that never appears to be taken into account. There are also other reasons for the desirability of having all viewers see

the same pair of images [KLEI90]. These last two points are considered in more detail in Section **8.3)**.

1.5) Principle of Operation of Prototypes

As there is no simple method of forming exit pupils with an *emissive* display, i.e. one that produces its own illumination such as a cathode ray tube, a *transmission* display must be used. In this type of display, illumination is provided by a backlight. This provides the capability of the light being manipulated in order to steer the pupils. Although some LCDs operate in the reflective mode, the majority of them require a backlight. Also the display will have to be direct-view, as opposed to projection. The use of a projection display has been investigated in some detail by the author as, at first sight, projection appears to be an attractive means of producing 3D. This led to the conclusion that unfortunately it would not be suitable for producing exit pupils over the large areas required for television. The investigation is not included in this thesis.

One benefit offered by some projection displays is that of speed. Digital micromirror devices (DMDs) [YOUN93] and liquid crystal on silicon dislays (LICOS) can operate sufficiently fast for two images to be presented alternately in what is termed the field-sequential mode. Unfortunately, these devices are small and can only be used in a projection system, not for direct-view applications.

The majority of direct-view LCDs are either supertwist nematic (STN), or use thin film transistors (TFT). The devices can only run at a frame rate of around 60 Hz and are too slow for field-sequential operation without the appearance of flicker. The frame rate at which flicker disappears, the critical flicker frequency, is dependent on various factors such as brightness and contrast in the image [KING83] [KNAP90] [MAXW92]. However, the frame rate would have to be in excess of around 120 Hz for flicker to be imperceptible. Ferroelectric liquid crystal displays have the ability to switch quickly, but as these are essentially bistable devices, they cannot be made to run at a sufficiently fast frame rate when grey-scale is required in the image.

Some 3D methods use a separate display for each image [SMIT88c] [EZRA95], but this gives a housing size that is impracticably large for television use. The alternative method of presenting two images on one screen is to display the left-image information on the odd rows of pixels, and right-image information on the even rows – this is termed spatial multiplexing. In our research, the latest prototypes use high resolution LCDs to compensate for this. It is most likely, at least in the near future, that greater image content will be obtained from an LCD by increased resolution rather than speed.

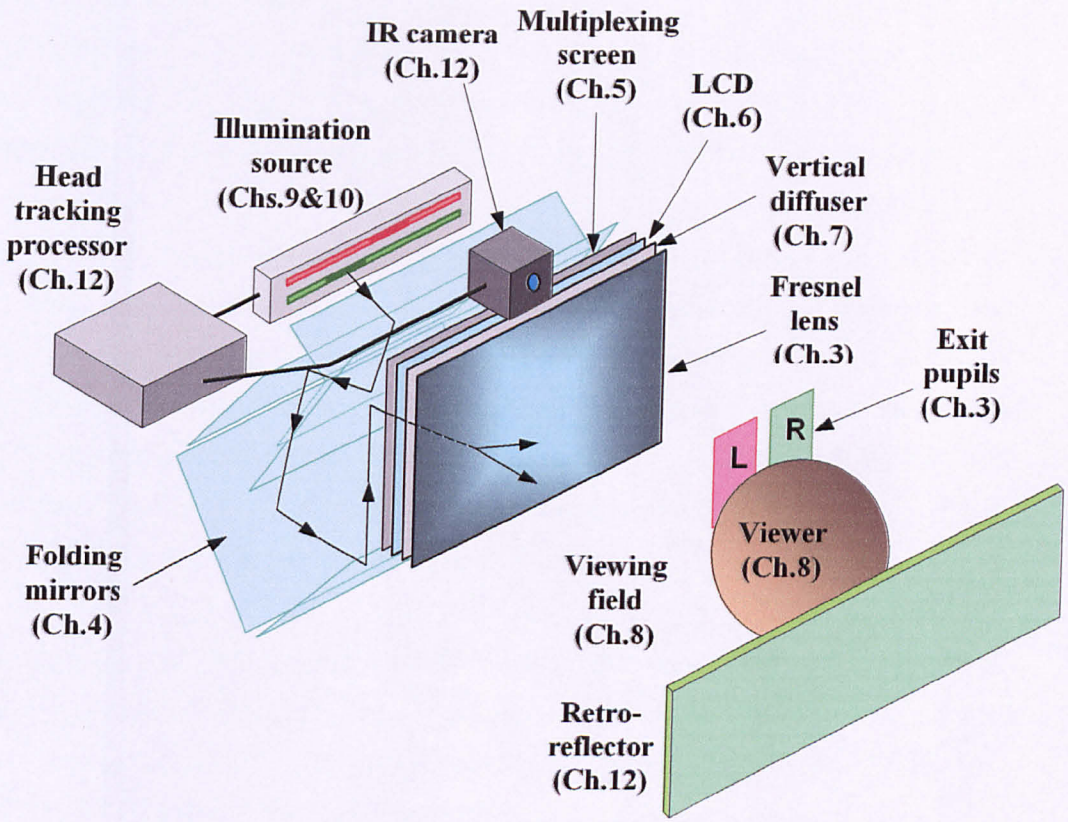

FIG.1.1 SCHEMATIC DIAGRAM OF PROTOTYPE 3D DISPLAY

The light forming the left and right exit pupils must be directed to the appropriate pixel rows by an image-multiplexing screen located between the steering optics and the LCD. In the simple single-viewer prototypes under construction, the exit pupils are formed by Fresnel lenses and lenticular screen. The lens forms real images of the

illumination sources, and a lenticular screen scatters the light vertically to create the exit pupils. The pupils can be steered by either physically moving a pair of light sources, or by shifting the illuminated regions on a pair of white LED arrays. This gives only a narrow range of distance from the screen. Also, the lateral movement is restricted due to spherical aberration in the lens.

Fig.1.1 is a schematic diagram of the prototype single-viewer displays. This shows its components, and the numbers of the chapters in the thesis that cover these.

1.6) Thesis Overview

The thesis covers four broad areas: these are, a survey of autostereoscopic displays, the theory of the optics of the proposed prototypes and other related subjects, a description of the practical work carried out on the prototypes and head tracking.

In Chapter 2, various methods of autostereoscopic displays that do not utilise head tracking are described. These include holographic, volumetric, holoform and binocular. These terms are defined, and the relative merits of each type with regard to suitability for 3D television are examined. Although research into human factors has not been undertaken, the last section in Chapter 2 covers some of the relevant published work. It is not intended to be an exhaustive study of the subject as this is beyond the scope of the present research.

The principles of head tracking operation and image multiplexing are considered in the first sections of Chapter 3. Head tracking is becoming increasingly popular for use in 3D displays, and the various implementations of this are described next. In the final section, the operation of the single-viewer prototypes is outlined.

Chapters 4 to 7 cover general optical considerations that apply to both the single-viewer prototypes under construction and to the forthcoming multiple-viewer prototypes. The nature of the optics in the single and the multiple viewer versions requires mirrors in order to reduce the overall housing size to a reasonable level. This is achieved by the use of folding mirrors that are located between the steering optics and the LCD. In the single-viewer prototypes the light only needs to be folded in the vertical plane, and a simple method of optimising this is described. The wide angle of

view of the multiple-viewer displays requires the light to be folded in both the vertical and horizontal planes. The way in which this works can be quite difficult to comprehend and demonstration models that help the understanding of this folding are described.

An image-multiplexing screen that separates the left and right image must be located immediately behind the LCD. One simple method of achieving this is to use a parallax barrier that consists of a series of horizontal apertures that direct light to the appropriate rows of pixels. The dimensions of this barrier are crucial and Chapter 5 gives a rigorous analysis of the design procedure.

One potentially serious problem encountered, when passing light from steering optics through an LCD to form exit pupils in the viewing field, is that of diffraction at the LCD. Virtually every suitable LCD consists of red, green and blue (RGB) pixels in the vertical stripe configuration. This has the effect of making the LCD act as a diffraction grating. This causes horizontal scattering and can be a large contributory factor to the crosstalk. Crosstalk is where the left image is seen faintly by the right eye, and vice versa. Diffraction grating theory in relation to an LCD is analysed in Chapter 6.

Another contribution to crosstalk will be the lenticular screen vertical diffuser. When light falls on its surface orthogonally, it is scattered in the vertical direction only, with no horizontal deviation. However, when the light is not at right angles to the surface, deviation can occur. In Chapter 7 the results of measurements of this deviation are given. A polynomial equation has been derived from this empirical data. This is particularly useful as it applies to *any* lenticular screen. The results of experiments that simulate the lenticular screen in a typical 3D viewing situation are described. An alternative to a lenticular diffuser is a holographic optical element (HOE), and its use is considered.

One unavoidable artefact of two-image 3D displays is that of stereoscopic distortions in the perceived image. Spotiswoode and Spotiswoode originally pointed this out as long ago as 1953 [SPOT53a], but they did not treat the subject rigorously. In Chapter 8 equations are derived for the effect of viewer position on these distortions. Although

the distortions have no bearing on the *design* of the display, it is useful to know their effect. This could be particularly important where the viewing field is large, as it will be in a multiple-viewer television set.

It is envisaged that the optics necessary to steer the exit pupils in the multiple-viewer display could consist of some form of discontinuous illumination source. This possibly could give the appearance of bright or dark vertical bands on the observed image on the LCD. In order to carry out some preparatory work for future multiple-viewer prototypes, measurements were carried out into the subjective effects of intensity variation. Again, these results are not relevant to the design of the prototypes under construction, but may be extremely useful in future design work.

Around three years ago, when LCDs were considerably more expensive than they are at present, the construction of a prototype using a 5.6" LCD was commenced. Using the Fresnel lens that forms the exit pupils as a magnifier compensates for this rather small size. This is achieved by locating the Fresnel lens some distance in front of the LCD. The prototype is not yet complete, but the useful results obtained from it are described in Chapter 9.

Chapter 10 describes another prototype under construction. This is a 12" version where the lens is adjacent to the LCD. Originally, the illumination source for this was a pair of 150-watt linear halogen lamps. These performed satisfactorily, but the continued reduction in cost of white LEDs made these a more viable alternative. The LCD required modification in order for the backlight to be replaced with steering optics. Work on this prototype came to a halt when the LCD was damaged by the modification. The optics have been adapted to accommodate a 10" display that did not require modification. Due to the small screen size, magnification is also utilised in this version.

Chapter 11 covers the subject of head tracking. First, methods carried out by other groups are surveyed. The non-intrusive methods considered fall into the categories of infrared reflection off the head, infrared reflection from the retinas and machine vision. The required accuracy of the head tracker is considered in the second half of

this chapter. This is an important consideration as tracking errors are one of the many factors that contribute to crosstalk.

Although the display optics is the main concern of this research, some form of head tracking is necessary for the optics to operate and be evaluated. A Polhemus electromagnetic head tracker is available in the laboratory but this requires the wearing of an attachment to the head, and is also susceptible to interference from ferrous objects in the vicinity of the wearer. A simple and robust infrared head tracker that does not require the wearing any attachment is described in Chapter 12.

At an early stage of the research, the use of an acoustic head tracker was considered. One reason for adopting this approach is that it is extremely simple to obtain range information acoustically. Inexpensive acoustic 'tape measures', with sufficient accuracy for a display application, are readily available off-the-shelf. The wavelength of a suitable sound frequency is rather too long for the horizontal accuracy required for tracking and possible increase in resolution using deconvolution is considered in Chapter 13. Possible methods of simplifying the hardware are also considered.

Although the work carried out to date has not resulted in a completed prototype, it forms the basis for continuing research into the production of a television display. Two prototypes are being built within the ATTEST project. One of these is a single-viewer 3D display that is a 21" version that operates on the same principles as the prototypes described in this thesis. Multiple-viewer versions will also be built. These utilise 21" LCDs, and provide 3D to four viewers who have a high degree of freedom of movement over a large viewing area. The optics is considerably more advanced, however, many of the same principles apply to both the single and the multiple-viewer versions.

CHAPTER 2

AUTOSTEREOSCOPIC DISPLAY TYPES AND HUMAN FACTORS

2.1) Preface

In the first part of this chapter, the implementation and the various advantages and disadvantages of non-head tracking autostereoscopic displays, are considered. The particular classification system used is, in the author's opinion, the most appropriate for determining the suitability for television applications. Although experiments on human factors are not within the scope of the present research, a survey of some of the relevant work in this area is covered in the latter part of the chapter.

2.2) Autostereoscopic Display Types.

The three basic autostereoscopic display types are **holographic** where the image is formed by wave-front reconstruction, **volumetric** where the image is formed within a volume of space without the use of light interference and **multiple image** where different two-dimensional images are seen across the viewing field. These basic types, along with sub-divisions, are shown in Fig.2.1.

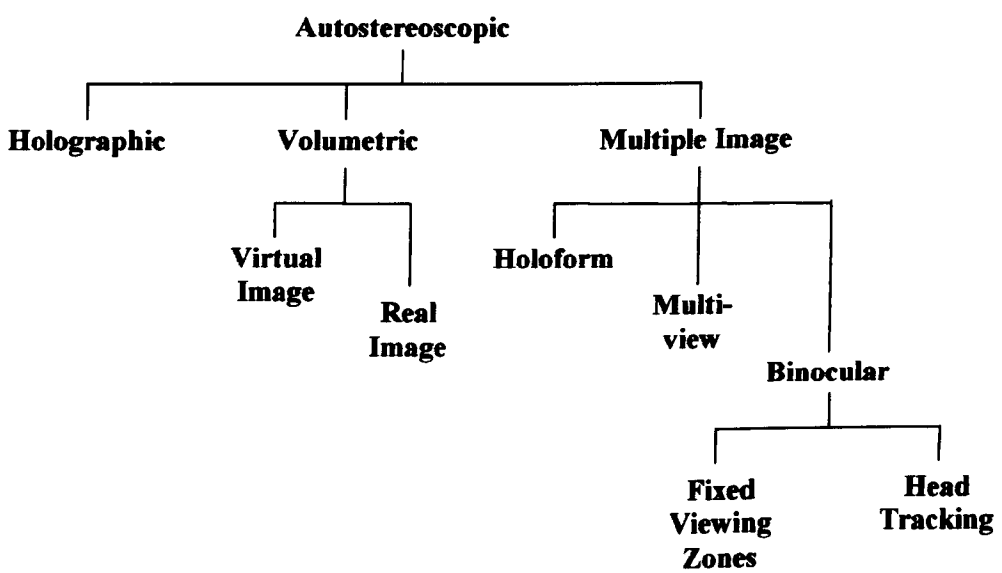

FIG.2.1 CLASSIFICATION OF AUTOSTEREOSCOPIC TYPES

Other workers in this field have used various other classification systems. Siegmund Pastoor of the Heinrich Hertz Institut [PAST97] gives the basic categories as 'aided viewing' (stereoscopic), 'free viewing' and 'autostereoscopic'. Displays within the category of 'free viewing' are called 'multi-view' in the author's terminology, and these do not require the wearing of special glasses. There are several other classification systems [VALY66b] [FARI94] [BARD95a], but none of these include head tracking and are therefore not particularly useful.

2.3) Holographic

The 'Holy Grail' of all stereoscopic displays would be the production in real time of images that exhibit *all* the characteristics of the original scene. This would require the reconstructed wavefront to be identical and could only be achieved using holographic techniques. The difficulties of this approach are the huge amounts of computation necessary to calculate the fringe pattern, and the high resolution of the display, which has to be of the order of a wavelength of light (around 0.5 micron). Approximately ten million discretized samples per square millimetre are required to match the resolution of an optically produced hologram. This means that large amounts of redundant information have to be displayed.

2.3.1) MIT Electroholography

A display was first demonstrated by the Spatial Imaging Group at MIT in 1989. They created an image the size of a golf ball by using an acousto-optic modulator (AOM) and moving mirrors [LUCE95]. Computation of the fringe pattern took several minutes using traditional methods. The speed of this was limited by the large number of samples in the discretized fringe pattern, and by the complexity of the physical simulation of the light propagation used to calculate each sample value.

In 1990 faster computational algorithms were developed that enabled the first interactive Holovideo display system to be implemented. A new method known as diffraction-specific computation was used [LUCE94]. This is particularly appropriate to the diffraction that occurs during the reconstruction of a holographic image.

Another strategy employed to reduce the information content in the fringe pattern is to dispense with vertical parallax. This reduces the spatial resolution required in the

vertical direction from around 1000 lines per millimetre to approximately 10 lines per millimetre, therefore giving a reduction factor of roughly 100 in the information content. A horizontal parallax only hologram can be considered as being an array of one-dimensional holograms known as hololines. Each of these hololines diffracts light into a single horizontal slice of the image.

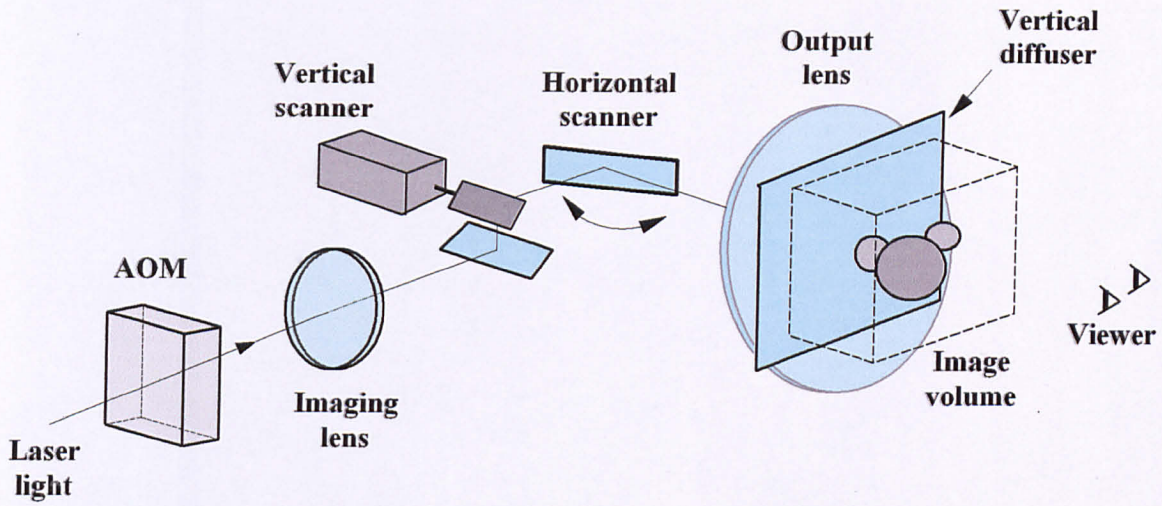

FIG.2.2 SIMPLIFIED SCHEMATIC DIAGRAM OF MIT DISPLAY

The use of an AOM time-multiplexed spatial light modulator makes the display configuration similar to the Scophony television system of the thirties. The AOMs are crossfired (run alternately in each direction) to provide a bidirectional Scophony geometry that utilises the mirror scan in both directions.

The hardware of the display is very large in relation to the size of the image (150 x 75 x 150 millimetres). The most recently published work by MIT describes a large he-ne laser, an 18 channel AOM, a vertical scanning mirror, a beamsplitter, six tiled horizontal scanning mirrors, a screen-sized output lens and a vertical diffuser [LUCE97]. This is shown in the simplified schematic diagram in Fig.2.2.

2.3.2) Japanese and Korean Holographic Displays

Moving parts can be eliminated by replacing the AOM with an LCD. One of the projects within a five-year initiative by the Telecommunications Advancement Organization of Japan (TAO) utilised a fifteen million pixel LCD that consists of five separate LCD panels [HOND95] [MAEN96]. The configuration of this display is illustrated in Fig.2.3. This produces an image that is 50 millimetres wide, 150 millimetres high and 50 millimetres deep. The viewing zone is 65 millimetres wide at around one metre distance. As in the MIT display, vertical parallax is dispensed with.

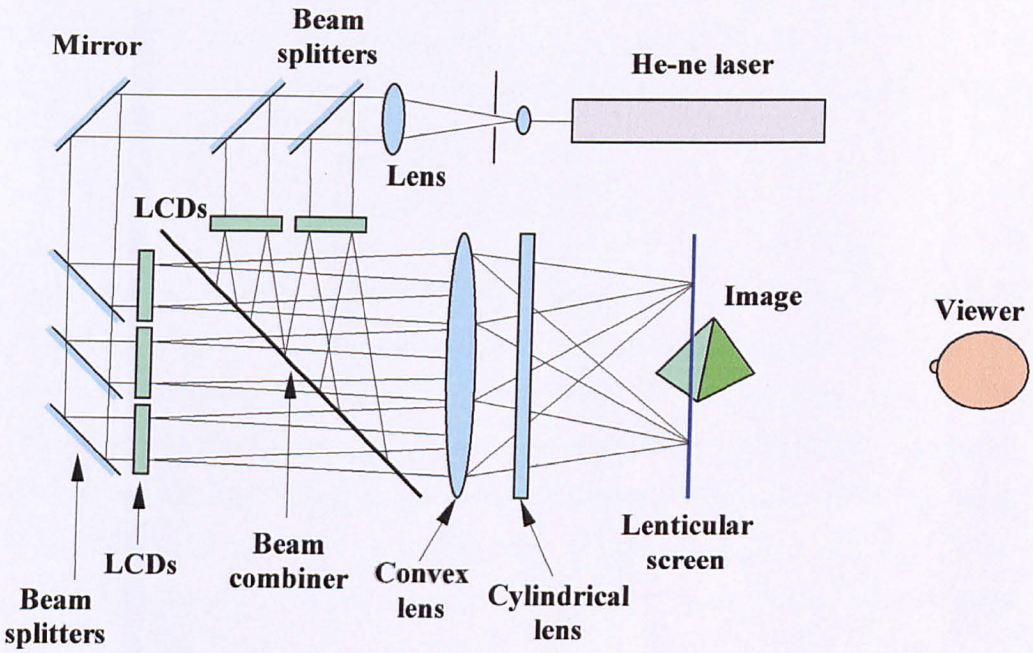

FIG.2.3 TAO 15-MILLION PIXEL DISPLAY

A pulsed laser light source can be used to eliminate the rotating polygon mirrors that are generally used to 'freeze' the motion of the acoustic waves on the AOM. A combined Korean/Russian team is working on a system that gives a 74 x 50 x 50 millimetres image with a 60 Hz frame rate [SON96].

A holographic display using a CCD camera to record fringe patterns, and an active-matrix LCD has been described [HASH91]. A he-ne laser is used to generate the hologram. A semi-silvered mirror splits the beam into the object beam and the reference beam. The light diffracted by the object interferes with the reference beam at the CCD where the image is recorded. This hologram is transmitted to the LCD that is illuminated by a second he-ne laser in order to produce the image.

The MIT display has been improved in a project undertaken by the Telecommunications Advancement Organization of Japan (TAO) [KAJI96]. In this display the AOM is replaced with a focused light array (FLA) consisting of laser diodes, or LEDs, and microlenses. The final monochrome image is produced by 32 discrete images that change semi-continuously across the viewing field. Apart from the replacement of the AOM, the optics of the display are virtually identical to those of the MIT display.

2.3.3) QinetiQ Holographic Display

The problem of obtaining a giga-pixel computer-generated hologram (CGH) has been addressed by QinetiQ (formerly DERA Malvern). This utilises the high speed of some electrically addressed spatial light modulators (EASLMs), and the high spatial resolution afforded by optically-addressed spatial modulators (OASLMs) [STAN00]. EASLMs include digital micromirror devices (DMDs) [YOUN93] [GOVE94], liquid crystal on silicon (LCOS) and a ferroelectric liquid crystal (FLC) on silicon, developed at QinetiQ. EASLMs can have more than 10^6 pixels and operate at speeds in excess of 1KHz.

The OASLM consists of an essentially continuous layer that does not require expensive lithography. It is addressed by applying a voltage to a transparent layer that is in contact with a photoconductor layer, and then allowing the addressing light to fall on the surface. When the control voltage is removed, the photoconductive layer causes an adjacent liquid crystal layer to pass light in the regions where addressing light has fallen. The OASLM is addressed with incoherent light in order to minimise speckle, but is illuminated with coherent light to form the hologram. The output of the OASLM *could* be resolved into a hologram by a simple Fourier transform lens, but the paper suggests that a more efficient replay mechanism is used.

The trade-off between the speed of the EASLM and the resolution of the OASLM can be achieved by transferring the information to the OASLM via replication optics, as shown in simplified form in Fig.2.4. This consists of a 5 x 5 array of lenses that de-magnify the EASLM image. The appropriate regions of the OASLM can be selected by either allowing individual regions of the shutter array to successively pass light, or by enabling separate regions of the OASLM to be written by applying a control voltage to them.

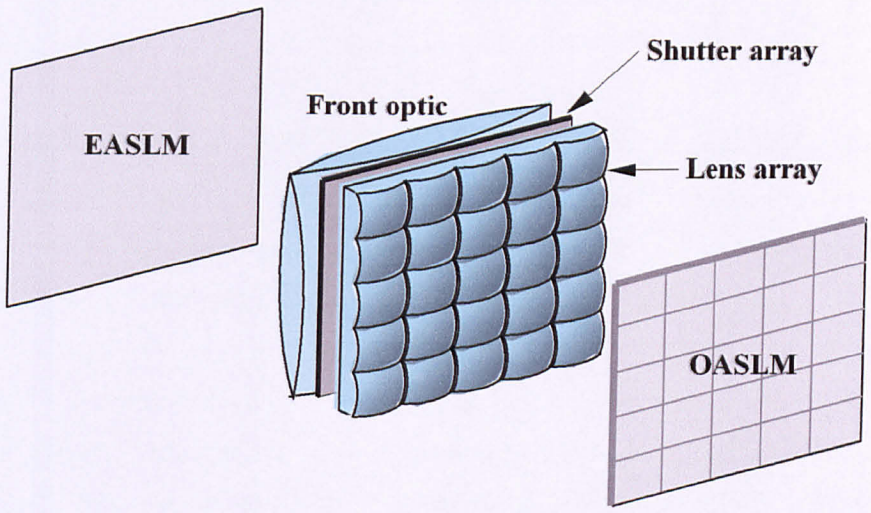

FIG.2,4 FUNCTIONAL DIAGRAM OF QINETIQ ACTIVE TILING

The QinetiQ approach is interesting as it has the potential to provide an SLM with a sufficiently large number of pixels for replicating holographic images in real time. Their estimation is that 10^9 pixels will be needed to produce a hologram in a 0.5 metre^2 volume with a field of view of ± 30°. Consider, for example, a 2,000 x 2,000 EASLM being magnified by 5 x 5. This gives a figure of 10^8 pixels, which is not that far away from the 10^9 that is needed. If the EASLM runs at 1 KHz, the magnification of 25 times will presumably make the refresh rate of the OASLM around 40 Hz.

The usefulness of the OASLM / EASLM approach for providing high pixel density in 3D display types other than holographic is being investigated. A joint Cambridge University / KIST group is developing a device of this type for multi-view display applications [JEON00].

2.3.4) The Future of Holographic Displays

Even given the fact that there is a possibility that holography might be used eventually for television, it seems unlikely that the hardware will be sufficiently simple for it to be used in the next generation of television, which will hopefully be available within the next ten years. Image capture and transmission are also going to be very challenging.

Another problem with holography that might prove very difficult, if not impossible, to easily overcome, is that of the reproduction of naturally lit scenes. The principal author of the QinetiQ paper has stated that *simulation* of external lighting is possible with CGH: however, this might not be of great use for natural scenes.

The future of electro-holography depends on more computing power, higher bandwidth optical modulation, and improvements in holographic information processing. Computing power is likely to increase sufficiently quickly to support electro-holography within the next few years.

2.4) Volumetric

The second class of display is volumetric, where the surface of the image is actually produced within a volume of space. The elements of the surface are referred to as 'voxels', as opposed to 'pixels', on a two-dimensional surface. Volumetric displays can be of two basic types: these are **virtual image** where the voxels are formed by a moving or deformable lens or mirror, and **real image** where the voxels are on a moving screen or are produced on static regions.

A problem with volumetric displays is that they usually suffer from image transparency. This is where parts of an image that are normally occluded are seen through the foreground object. Whilst this might not be a disadvantage with some

computer-generated images, it is unacceptable for video. Another difficulty that is possibly less important than transparency, but could give an unrealistic appearance to natural images, is that of the inability to display surfaces with a non-Lambertian intensity distribution

2.4.1) Virtual Image

One of the earliest virtual image methods described is that of Traub [TRAU66] [TRAU67] where a mirror of varying focal length (varifocal) is used to produce a series of images at differing apparent distances. The variable surface curvature of the mirror entails smaller movement than would be required from a moving flat surface GIVING the same effect. The mirror consists of a thin silvered Mylar film that is attached to the front of a loudspeaker. The loudspeaker can be driven between twenty and several hundred Hz. and sound levels are reported to be tolerable. Three-dimensional Lissajous figures, simulations of air traffic control display and the presentation of a series of slides to give ten depth planes are described.

The University of Strathclyde is developing a version of this using a stretchable membrane mirror (SMM) [MCKA99] [MCKA00]. The mirror is 1.2 metres diameter and can vary over a large range of F-numbers. The image can be produced both in front of, and behind the plane of the mirror.

Lenses can also be used to produce the same effect. In the xyzscope [FAJA92] a rotating lens is used to effectively vary the distance between the object and the lens centre. The method is not described in great detail, but this will presumably be a very cumbersome means of achieving the same effect as the varifocal mirror. A lens the size of the screen rotating at 1200 rpm or more is likely to create considerable windage problems.

A combination of variable focus lenses and integral photography has been proposed [YANA97]. The paper describes a lens array that would be difficult to make, due to a lenslets that have a varying radius of curvature.

2.4.2) Moving Screen

A solid image can be produced in a volume of space by displaying 'slices' of the image on a moving screen. If, for example, a sphere has to be displayed, this can be achieved by displaying a series of circles of varying size on to a moving surface.

The US Navy has developed a system where the image is produced on a 36" diameter, 18" high double helix. An acousto-optic system is used to scan the light from a he-ne laser in order to produce an image of 40,000 voxels. The image is viewable from 360° so that viewers can walk around the display and look down from above [LYTL95]. A display with a volume of 120 x 120 x 100 millimetres has been produced by the Korea Institute of Science and Technology (KIST) [SON99a]. The images are displayed at a frame rate of 15 to 25 Hz. and consist of 250,000 voxels.

A system that has a voxel resolution sufficient for video display has been described [FAVA01]. The 90-million voxel resolution is obtained by presenting 200 radially disposed slices consisting of 768 x 768 pixel images. These are provided from a modified Texas Instruments projector that can supply eight-colour images at around 4kHz. Images are projected on to a disc that rotates at 600 r.p.m. and frames are updated at 20Hz.

2.4.3) Static Images

In this type of display voxels are produced on stationary regions in the image space. An interesting point with these displays is that some of them have the potential to overcome the problem of image transparency.

In the voxel-based display of the University of Texas [MACF94] ultraviolet light is piped to the individual voxels via fibre optics. This causes the dye to fluoresce. Although the fluorescing region is not entirely opaque, it is not be completely transparent as in virtual image or moving screen methods. The device described consists of a stack of transparent spacers, with layers of fluorescent dye in between them. The device was small at 11 x 11 x 5 voxels, but it was envisaged this would be capable of being scaled up to 10^3 x 10^3 x 10^3 voxels. However, it is unclear whether this research was continued as no further references have been found since.

A simple two-plane method by Floating Images Inc. [DOLG97] uses a partially reflecting mirror to combine the real foreground image behind it with the reflected background image. The foreground image is brighter in order for it to appear opaque. This type of display is not suitable for video, but it does provide a simple a simple and inexpensive display that can be very effective in applications such as advertising.

An attempt to overcome the transparency problem has been made by a group at KIST [SON97]. This proposes the use of an SLM in front of a translucent volumetric image in order to block light in directions that would normally be occluded. The paper is not very clear, but appears to conclude that the speed and spatial resolution of the SLM will be insufficient for this method to be effective.

2.5. Multiple Image Displays

Multiple image displays, where two or more images are seen across the width of the viewing field, can take three basic forms. In the first category, a large number of views are produced in order to give the appearance of smooth motion parallax. As these give a hologram-like appearance, they are referred to here as **holoform**. Displays where a smaller number of discrete views are presented across the viewing field are termed **multi-view**. The simplest multiple image displays are **binocular** where only a single stereo pair is displayed. Head tracked displays come under the category of multiple-image, and will be considered in Chapter 3.

2.5.1) Holoform

The object of holoform displays is to provide smooth motion parallax as the viewer traverses the viewing field laterally. This is achieved by producing a large number of closely spaced discrete views that give an image with a hologram-like appearance.

In the 1980's, a method called the Stereoptiplexer was developed by Robert Collender [COLL86]. This used picture information from rapidly moving cine film to produce a moving 'aerial exit pupil' from scanning mirrors. The exit pupil is effectively a vertical narrow aperture that traverses the region between the viewer and the virtual 3D scene. The paper describes the apparatus and shows a photograph of it, so presumably this system actually worked. In a later paper a system with no moving

parts is described [COLL87], but it is unlikely this was ever built as it required devices that did not exist. Even today, it is very difficult to find hardware that can display sufficient information to exploit this type of solution.

Another variation on this approach is to replace the 'aerial exit pupil' with a physical slit. The earliest work on this appears to be the Parallactiscope of Homer Tilton [TILT85]. In this display a slit is moved rapidly in front of a CRT screen. At any instant, the view of the 3D image that would be seen through the slit is displayed on the CRT. This is updated as the slit traverses the viewed region. In this way a complete 3D image can be built up. This method suffers from the disadvantage of not being suitable for the display of video information, due to the extremely fast frame rate that would be required – a new frame would have to be displayed on the CRT every time the slit had traversed only a small lateral distance. Also, the luminous efficiency will be very low due to the slit capturing light from a small angle from the CRT. Another problem that could possibly occur, but only at quite large viewing distances, is that of diffraction at the slit. However, if the slit is sufficiently narrow for diffraction to be appreciable, the light throughput is likely to be extremely poor.

A version of this display with no moving parts has been developed in the Imaging and Displays Group at De Montfort University [SEXT92]. In this display the moving slit is replaced by a 150-millimetre square 400-element ferroelectric array.

Research is also being carried out by another group at De Montfort University into the use of integral imaging to produce an autostereoscopic display with full motion parallax [MCCO92]. Integral imaging is a technique using an array of small lenses that are either spherical or cylindrical. Integral photography is used to produce the familiar stereoscopic photographs, where a lenticular sheet of vertically aligned cylindrical lenses provide pictures with horizontal parallax-only 3D image. If a photographic emulsion is located in the focal plane of an array of small lenses, parallax information is recorded. If this information is used to reconstruct an image after being developed, the image produced will be pseudoscopic - that is it will be stereoscopically inverted. As long ago as 1908 it was proposed by Lipmann [LIPM08] that a two-stage process should be carried out to restore the image to its original orthoscopic form.

The implementation of the De Montfort display using integral imaging is shown in the schematic diagram in Fig.2.5. The optical transfer required to produce orthoscopic images *could* be achieved by using a semi-silvered mirror and a retro-reflecting screen. The disadvantages of this arrangement are the light loss at the semi-silvered mirror, and the relatively low modulation transfer function of the retro-reflecting screen. For these reasons, a two-tier transmission screen has been adopted for the first stage of the capture system.

This screen consists of three stages. The first stage is an input macro lens array that produces a series of pseudoscopic real images. Within the volume of these images lie two back-to-back microlens arrays that have a common focal plane. Light leaving these arrays is focused by an output *macrolens* array into a single pseudoscopic image. The recording microlens array is situated within the volume of this pseudoscopic image. It is the image on the focal plane of this array that is transmitted to the display.

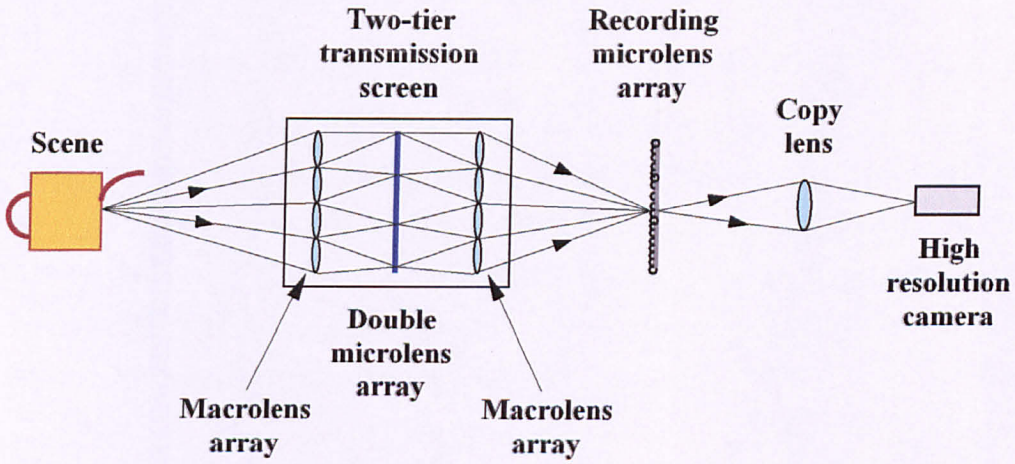

Fig.2.5 INTEGRAL IMAGE CAPTURE

The construction of the display is simple as it consists of a high resolution TFT LCD and a microlens array only.

The resolution required is higher than is required for two-dimensional imaging, but the team working on the project anticipate that an increase in the information content by a small factor will enable the transmission of full parallax images. Work is also being carried out into compression algorithms that are appropriate to the nature of the image formed by the recording microlens array.

A research group in the 3D project at TAO have identified the need for a large number of views in order to overcome problems caused by the difference between accommodation and convergence [KAJI97]. Their approach is to provide what they term 'super multi-view' (SMV). Under these conditions, the pupil receives two or more parallax images. The authors claim this will cause the eye to focus at the same distance as the convergence. This is a very significant finding regarding the minimum amount of information that has to be displayed in order for the accommodation and convergence of the eyes to be the same. The paper does not state where this finding originates – a rigorous examination would allow for variations in pupil diameter with light levels, and also the fact that the pupil is circular. This consideration is similar to the way in which the pupil function is allowed for in determining crosstalk in Section **12.2.2)**.

The display itself is implemented by using a focused light array (FLA) in order to obtain the necessary horizontal spatial resolution required for the production of 45 views. Effective resolution is obtained by modulating the output of an array of LEDs or laser diodes, and mechanically scanning the light in a similar manner to the TAO 32-image holographically-derived display, which is in turn inspired by the MIT electroholographic system.

Although not mentioned in the references in this paper, holographic stereograms, i.e. where multiple views across the viewing field are produced holographically, are analysed in a paper by Pierre St Hilaire [HILA95]. In this paper, the effect of the image appearing to 'jump' between adjacent views is considered. This phenomenon is similar to aliasing when a waveform is undersampled, i.e. when the sampling rate is less than half the maximum frequency in the original signal. This optimum is in the same order as the figure obtained from research at the Heinrich Hertz Institut where it

has been determined that typically, 20 views per interocular distance are required for the appearance of smooth motion parallax [PAST92].

2.5.2) Multi-view Displays

In multi-view displays, a series of discrete views are presented across the viewing field. One eye will lie in a region where one perspective is seen, and the other eye in a position where the adjacent perspective is seen. The number of views is too small for continuous motion parallax, but strategies, such as merging one image into the adjacent image, and limiting the disparity in order to keep the apparent image content close to the plane of the screen, can minimise the apparent 'jumping' between views. This section is not an exhaustive selection of work carried out in this area but it is a fair representation of the various methods being researched in the past few years.

The methods fall within four broad categories. These are: lenses, either in the form of Fresnel lenses or sheets of cylindrical lenses, parallax with 'point' light sources: holographic viewing zone formation and 'Cambridge' type displays with fast light shutters giving spatio-temporal formation of zones.

A method that is simple in principle, but rather cumbersome to implement, is described in a paper by Stephen Hines [HINE97]. This uses an arrangement of projection lenses, a Fresnel field lens and vertical diffuser (horizontally aligned lenticular sheet) to produce a series of viewing zones across the viewing field. Various configurations of the optics are used to provide 4,7,13 or 21 zones. This gives an inevitable trade-off between the number of views and resolution. The drawings of the apparatus indicate that the housing size is extremely large in relation to the restricted viewing field. This rather limits this approach to being suitable only for arcade games.

Lenticular screens, with the lenses running vertically, can be used to direct the light from columns of pixels on an LCD into viewing zones across the viewing field. The principle of operation is shown in Fig.2.6. The liquid crystal layer lies in the focal plane of the lenses, and the lens pitch is slightly less than the horizontal pitch of the pixels in order to give viewing zones at the chosen optimum distance from the screen. In this case, three columns of pixels contribute to three viewing zones. Early multi-

view displays with four zones were produced at NHK [ISON90]. There were two versions, one using a 12" plasma display panel (PDP) and one with 9" electroluminescent (EL) panel.

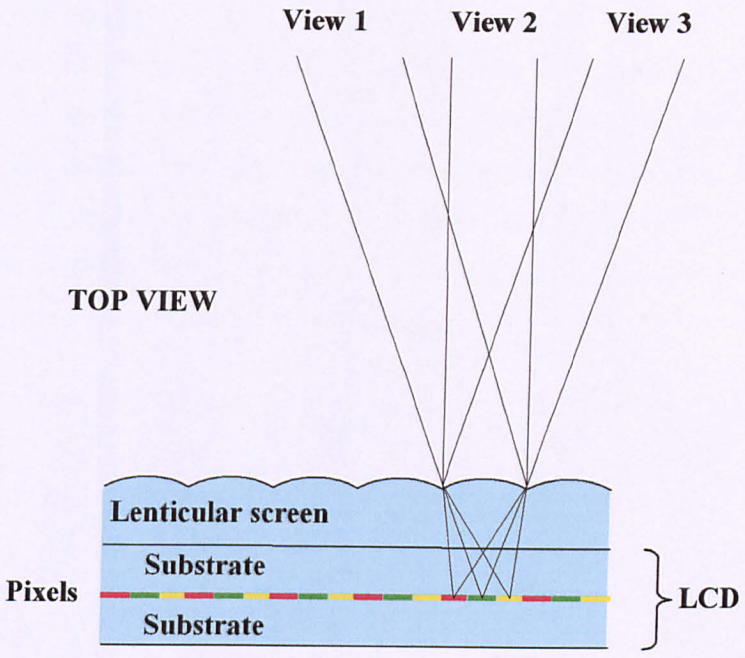

FIG.2.6 PRINCIPLE OF LCD MULTIVIEW OPERATION

A simple multiview display with the above construction suffers from two quite serious drawbacks. Firstly, the mask between the columns of pixels in the LCD gives rise to the appearance of vertical banding on the image known as the 'picket fence' effect. Secondly, when a viewer's eye traverses the region between two viewing zones, the image appears to 'flip' between views.

These problems have been addressed by the Philips Research Laboratories in the UK by the simple expedient of slanting the lenticular sheet in relation to the LCD [BERK96], [BERK97] [BERK99]. An observer moving sideways in front of the display always sees a constant amount of black mask, therefore rendering it invisible and eliminating the appearance of the 'picket fence' effect. The transition between adjacent views is also softened so that the appearance to the viewer is closer to the

continuous motion parallax of natural images rather than a succession of flipping views.

Fig.2.7 shows the relationship between the pixels and the slanted lenticular sheet for a seven-view display. As the LCD is located in the focal plane of the lenticular sheet, the horizontal position on the LCD corresponds to the viewing angle. Therefore all points on the line XX direct view 3 in a given direction, and all points on line YY direct view 4 in another direction. The way in which the effect of flipping is reduced is evident by examining line XX where view 3 predominates, but with some contribution from view 2. Similarly, for the angle corresponding to line YY, view 4, with some contribution from view 3 is seen.

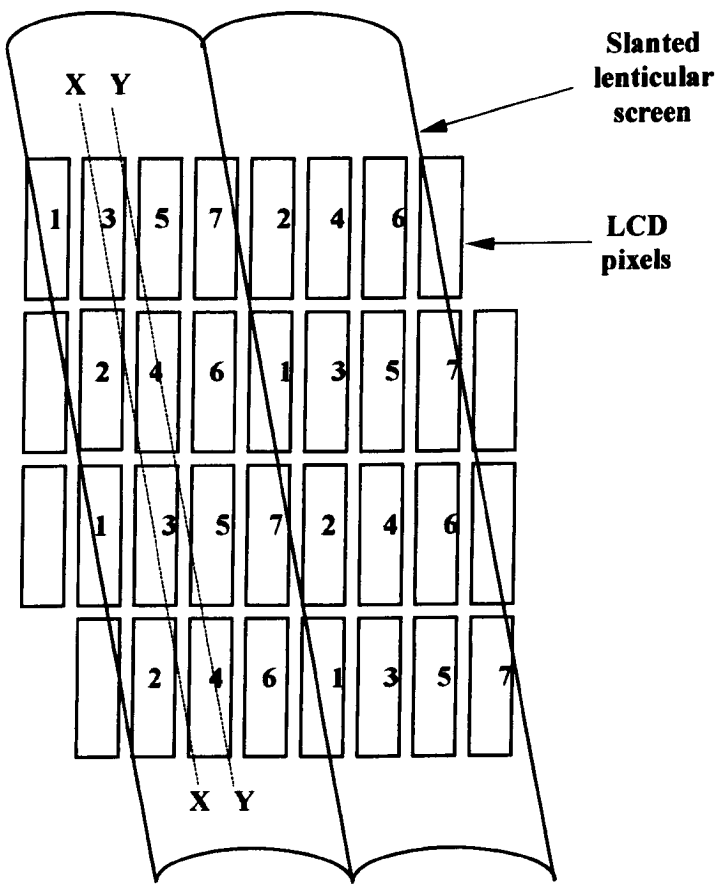

FIG.2.7 ARRANGEMENT OF PIXELS IN PHILIPS DISPLAY

Although by their very nature, multi-view displays are limited in the quality of the stereo effect, the size of the usable viewing region and the restricted depth of image field, the actual appearance of the Philips display is remarkably good, especially bearing in mind its simplicity.

'Point' light sources behind an LCD are used by a Korean group to direct images to the viewing zones [KIM01]. A simple 32 x 32 pixel display is described, where the light sources are obtained from a collimated blue laser beam passing through a microlens array. Each light source lies behind a 6 x 6 array of pixels, therefore providing both horizontal and vertical parallax. The paper acknowledges that the display suffers from the loss of resolution – this is particularly severe where both parallaxes are available.

A holographic optical element (HOE) is used by Osaka City University to form viewing zones [SAKA95] [TAKA96]. In this display an HOE mounted behind an LCD forms four viewing zones in the viewing field as illustrated in Fig.2.8.

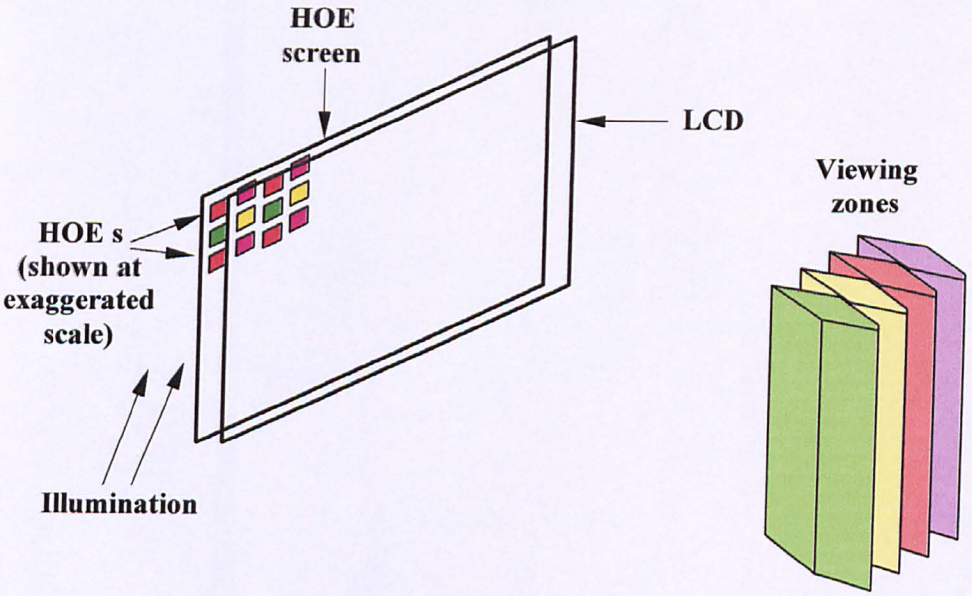

FIG.2.8 OSAKA HOE DISPLAY

A team at Cambridge University has opted for temporal multiplexing where the series of images is presented in sequence [TRAV91] [MOOR 92] [MOOR 96]. Although a sufficiently fast device is not available to perform this function, the operation of the display can be best understood by imagining a transmission LCD as shown in Fig.2.9 (a). If a large Fresnel lens is located adjacent to the LCD, a vertical illumination source behind the lens will form a real image in the viewing field. This image is the exit pupil for the view being displayed on the LCD at that particular time. The illumination will be even over the complete area of the LCD, and the view will only be visible over the area of the exit pupil.

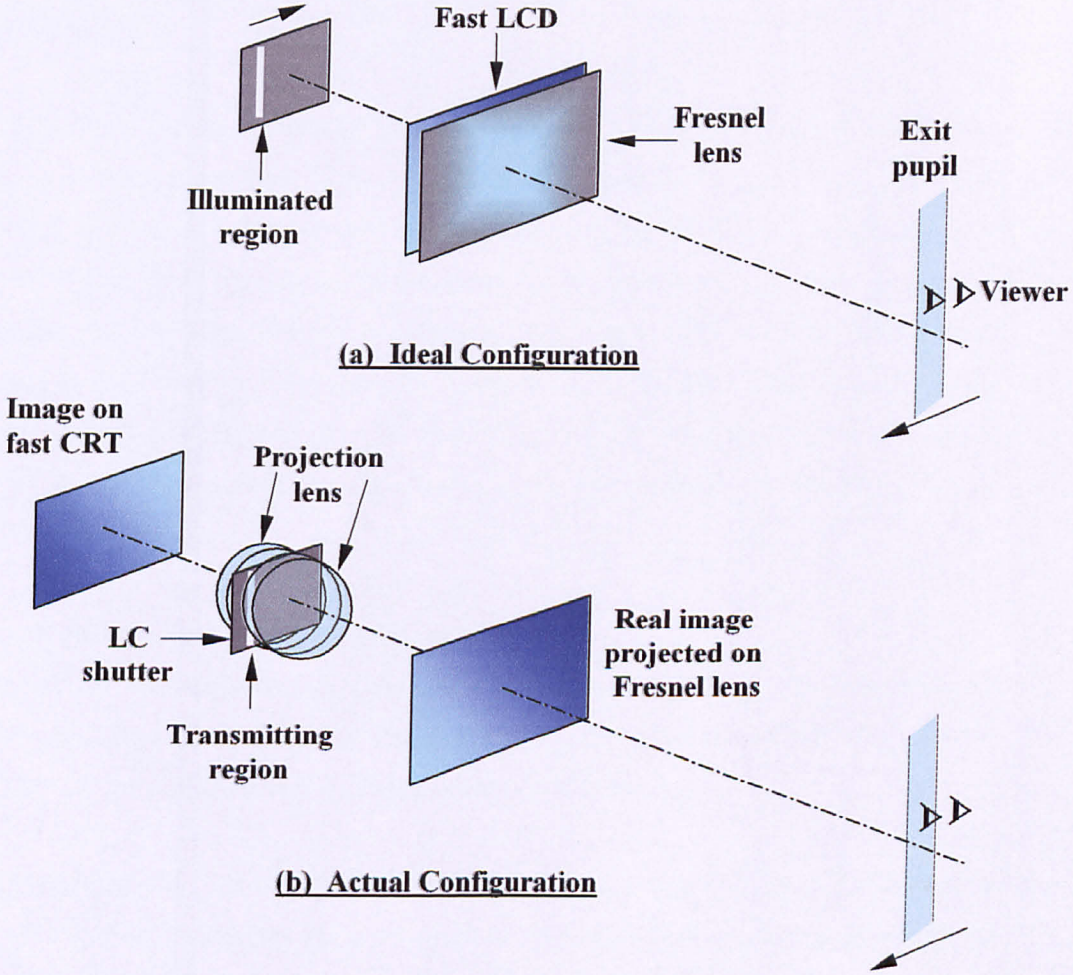

FIG.2.9 CAMBRIDGE MULTI-VIEW DISPLAY

If the adjacent view is next displayed on the LCD, the illumination source moves laterally to form an exit pupil in a position next to the previous one. This process is repeated until the complete series of views is presented across the viewing field. Operation in this mode would require the LCD to be running at N times the normal video rate, where N is the number of views.

The display is implemented using a CRT that is able to operate at a sufficiently fast frame rate. Instead of a view being displayed on an LCD, it is projected on to the Fresnel lens by a projection lens located where the illumination sources were, as shown in Fig 2.9 (b). A ferroelectric liquid crystal shutter replaces the illumination sources. This shutter is in the Fourier transform plane of the projection lens, and its real image forms the exit pupil. However, this is not seen on the image perceived by the viewer.

Various versions of the display have been built with up to 16 views, and with colour and monochrome images. Colour is obtained by using a Tektronix sequential liquid crystal shutter. A recent version of this display uses a 50" concave spherical mirror [DODG00]. This overcomes the problem of scattering ambient light from which Fresnel lenses suffer. Images are derived from three primary-colour CRTs whose outputs are combined by dichroic mirrors for maximum efficiency. A further development provides two sets of viewing zones that are derived from two sets of CRT subsystems. This makes the display particularly suitable for two-player arcade games.

2.5.3) Multi-view Display Limitations

There are two fundamental reasons why multi-view displays are unsuitable for television. In order to perceive stereo correctly, the right eye of a viewer must be located in one exit pupil and the other in the adjacent pupil.

Reference to Fig.2.10 shows that the regions where the eyes may be located is restricted. This is possibly not a very severe problem with a small display, where the pupils are quite deep. However, as the screen becomes wider the pupils become foreshortened as shown in Fig.2.10 (b). The exit pupil depth is approximately inversely proportional to the screen width.

A 28″ diagonal screen with an exit pupil pitch of 6.5 cm. would give exit pupil depths of approximately 400 millimetres when the pupils are formed 2 metres (approximately 5 times picture height) from the screen. This requires viewers to be located close to an optimum-viewing plane, hence restricting their movement.

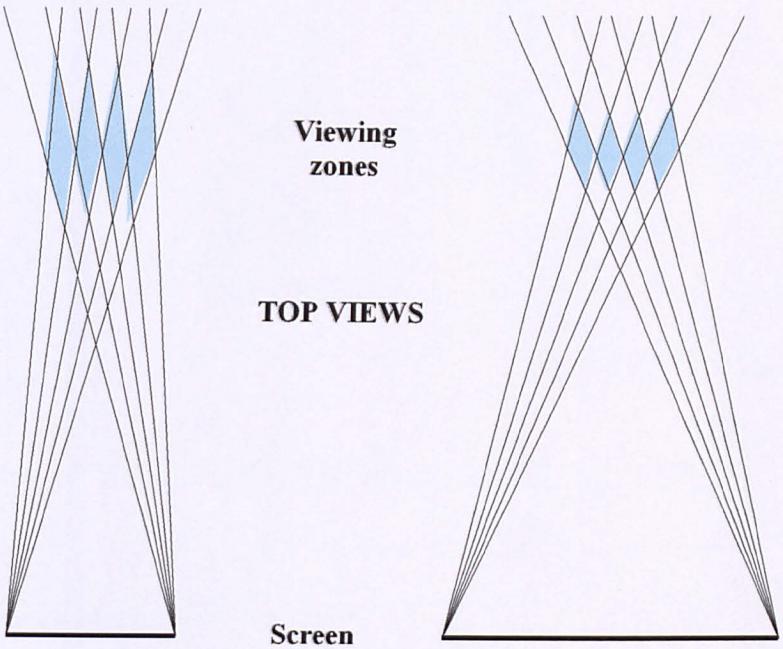

FIG.2.10 MULTI-VIEW: EFFECT OF SCREEN WIDTH

Next, it is necessary to consider the image seen by an eye that is not situated within an exit pupil. An eye located at the position indicated in Fig.2.11 will see parts of images 2, 3 and 4 across the width of the screen. If a region of the image appears to be in the plane of the screen, a continuous image will be observed with no breaks at the boundaries between the different images. However, discontinuities will be seen at the boundaries for areas that do not appear to be in the plane of the screen. Even though the effect will be made less objectionable due to the overlapping of images at the boundaries, unacceptable discontinuities will occur, especially where the *subject* of the scene is away from the plane of the screen

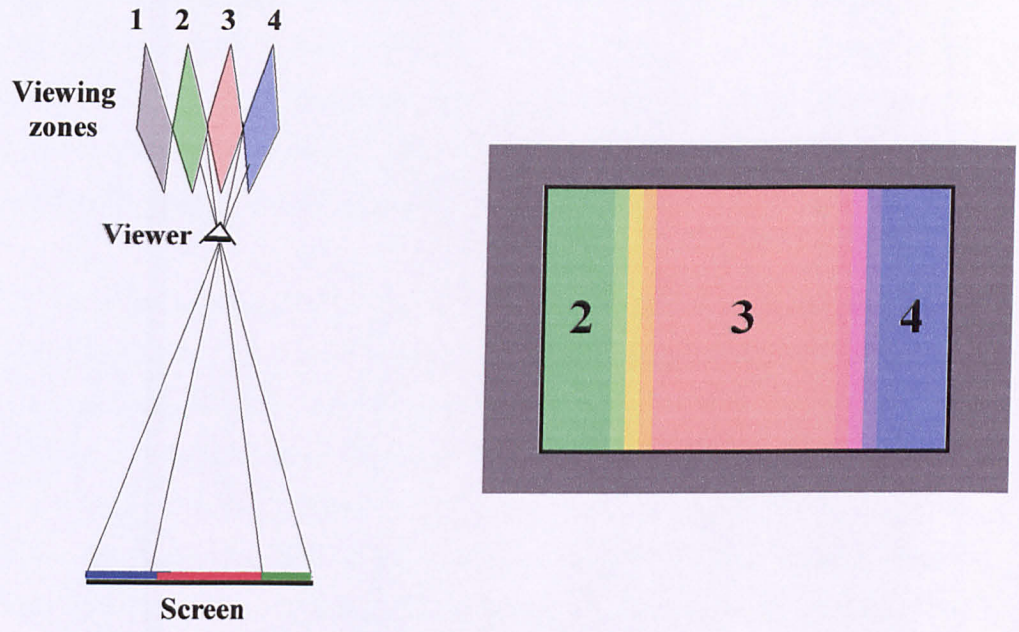

(a) Top View (b) Appearance of Screen

FIG.2.11 MULTI-VIEW DEPTH LIMITATION

2.5.4) Binocular Display Types

The simplest type of display is binocular or two-image, where a single pair of viewing zones is produced. These can be of four basic types; the viewing zones can be formed by lenticular screens, with twin projectors, by parallax methods or by HOEs. In its simplest form, the lenticular screen display operates in the same way as described in section **2.5.2)**. Twin projector methods produce exit pupils that are real images of the projector lenses, with the image formed on a double lenticular screen or a special reflecting screen. Parallax displays use an opaque mask, an array of orthogonally polarised image multiplexing elements or a series of line illumination sources behind an LCD.

The simple lenticular screen display consists of an LCD with a lenticular screen in front of it. The screen consists of a series of vertically aligned cylindrical lenses with a pitch slightly less than double the horizontal LCD pitch. This allows for the fact that the viewer is at a finite distance from the screen and parallax has to be allowed for. As

the majority of LCDs have the RGB sub-pixels in the vertical stripe configuration, the LCD has to be operated in the portrait mode in order to avoid coloration and distortion of the colours in the image. Left and right images are displayed on alternate columns (parallel to the lenticular lenses). A display of this type has been built and evaluated in the Imaging and Displays Group at De Montfort University [BARD95b].

An LCD can be operated in the normal landscape mode in a display utilising a chequered mask and orthogonally aligned lenticular screens [MORI98]. The left and right images are multiplexed on alternate pixel rows. The display consists of five layers, these are, in order from the back; the backlight panel, the chequered pattern mask, a vertically aligned lenticular sheet, a horizontally aligned lenticular sheet and the LCD. The horizontal pitch of the mask and the pitch of the vertically aligned lenticular sheet are around double the LCD horizontal pitch. These perform the same *function*, but in a different manner, to the lenticular screen in the previous method. Rows of the chequered pattern are directed to the appropriate rows of pixels by the horizontally aligned lenticular sheet.

Twin projectors are used in conjunction with double lenticular screens to make large screen displays for single viewers [ISON95]. Real images of the projector lenses are formed into vertical exit pupils by the double lenticular screen. With the correct pitches and focal lengths, this screen acts as a two-dimensional version of a Gabor superlens [HEMB97]. This is a type of lens that is normally made from two-dimensional arrays of microlenses, and has unusual imaging properties. The double lenticular screen performs focusing in the horizontal direction, and scattering in the vertical direction, to form vertical viewing zones that allow a degree of vertical viewer movement.

A special reflecting screen, where retroreflection occurs in the horizontal direction, and scattering in the vertical direction, also performs the same purpose [OHSH97]. This is referred to as a 'curved directional reflecting '(CDR) screen. Retroreflection is achieved with micro corner reflectors with vertical alignment, and vertical scattering with a lenticular sheet.

The first of the parallax methods uses thin vertical illumination lines behind the LCD in order to direct the light to the appropriate viewing regions [EICH94] [EICH95] [EICH96] [EICH97]. The lines are produced on a diffusing screen by a lenticular sheet that is mounted behind it. The primary light sources are a series of vertical lamps that are located behind slit apertures and are focused by the lenticular sheet.

The Sanyo display uses masks to produce a simple and effective means of supplying 3D to a single viewer [HAMA95]. In the most advanced version of their optics, parallax barriers, both behind and in front of an LCD, are used to present images with virtually no Moire fringing. These barriers consist of masks that have vertical apertures in them. The operation of the optics was clarified in a communication from Sanyo's laboratories [MASH97]. At first sight, it appeared that the LCD would require RGB sub-pixels to be in the horizontal orientation in order to avoid coloration problems.

The information supplied regarding the configuration of the pixels is as follows –

Table 1.1 Sanyo RGB Sub-pixel Configuration

Colour filter configuration	**Red**	**Green**	**Blue**	**Red**	**Green**	**Blue**
Parallax image configuration	**Right eye**	**Left eye**	**Right eye**	**Left eye**	**Right eye**	**Left eye**

This is very interesting as it implies that individual triads of RGB sub-pixels are used for both left and right images. Modification of the LCD drivers will be necessary but presumably this would not be difficult for Sanyo as an LCD manufacturer. This has a useful implication for lenticular displays, as a lenticular screen with a pitch of 2 / 3 the horizontal LCD pitch would enable the LCD to be used in the landscape mode, provided the drivers were modified.

Polarization can be used to provide what is effectively a vertical slit mask A display that uses a dichroic type polarisation plate is described in a paper by KIST [SON99b]. The image-multiplexing screen consists of an array of vertical strips of dichroic

polarizing material of alternating orientation. A Fresnel lens produces exit pupils from a pair of illumination sources that have polarizers in front of them to select the odd and even columns of pixels. The conclusions of the paper state that difficulties were encountered with the manufacture of the multiplexing screen. The optics are very basic as the pupils are produced with a Fresnel lens. Also, the multiplexing barrier would probably have been more simply obtained by using an off-the-shelf micropolarizer array from Reveo Inc. [FARI01].

HOEs can be used to provide the viewing zones, and RealityVision [TRAY97] has developed a display of this type. As this will be a head tracked display in its final form, it is considered in greater detail in Chapter 3.

2.5.5) Limitations of Binocular Displays

Binocular displays without head tracking impose a greater restriction on viewer movement than any other autostereoscopic display method. When lenticular screens or parallax barriers are used, the viewing field will be as shown in Fig.2.12 (b). In the diamond shaped regions marked **R**, a right image is seen across the complete width of the screen, and a left image in the regions marked **L**. In order to see 3D, the viewers right eye must lie in an **R** zone, and the left eye in an **L** zone. This means that the eye-centre must occupy the shaded region shown in Fig.2.12 (b). The geometry of the displays is designed to give zone regions with a width of around the average inter-ocular distance of 65 millimetres. It can be seen that at the optimum viewing distance from the screen, 3D can only be seen for a maximum of half the width of the viewing field. In practice this will be less due to the edges of the zones not being sharp.

When the eye-centre is located between the shaded regions, pseudoscopic images are seen. This is where the stereo pair is reversed, and unusual stereo effects are observed, As the viewer moves away from the optimum viewing distance, the proportion of the field over which 3D can be seen becomes less. As with multi-view displays, the zones become foreshortened with increasing screen width. If there are sufficient viewing zones across the field, more than one viewer could be accommodated [VALY62b].

In projection displays, only a single pair of viewing regions is formed, thereby restricting the viewing region even more. A larger viewing region is provided by the

RealityVision HOE display[TRAY96]. Instead of producing diamond-shaped regions, the right image is directed to the right side of the viewing field, and the left image to the left side. The distance from the screen over which 3D can be seen is considerably increased. Also, when both eyes are in the right side of the field, a right image is seen by both of them, and a left image by both eyes when they are in the left side of the field.

.

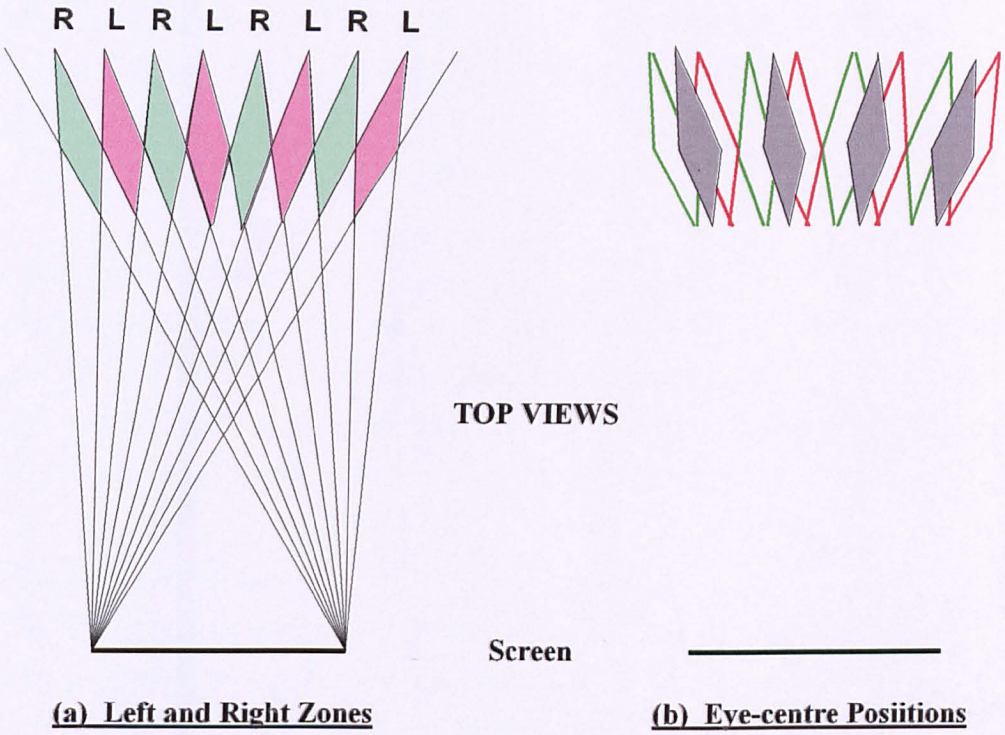

FIG.2.12 BINOCULAR VIEWING ZONES

CHAPTER 3
HEAD TRACKING PRINCIPLES AND SURVEY OF METHODS

3.1) Preface

This chapter covers the principle of operation of the prototype displays under construction, and a survey of head tracking display methods. The principle of operation is described in the first part of the chapter as this will facilitate the understanding of other methods where similar techniques are frequently used. The survey is not exhaustive, but it does cover a representative selection of the various methods.

3.2 Exit Pupil Formation

The principle of operation is most easily understood by initially giving the optical analogies of the displays. Section **3.2.1)** describes the principle of exit pupil formation that is used in the single-user prototype. The way in which this principle can be used provide stereo to more that one viewer is given in Section **3.2.2)**.

3.2.1) Single-user Display

In order to present stereo to a viewer who does not have to wear special glasses, regions must be formed in the viewing field where a left image only is seen on the screen, and another region where a right image is seen on the screen. These are referred to as the exit pupils. As an exit pupil has to be produced for each of the viewer's eyes, the optics effectively consist of a separate system for each eye.

Methods that employ a separate display for each eye make the overall housing size impracticably large, therefore one display only is used in the prototype to present both left and right images. The use of transmission displays, where the illuminating light passes through it, is pursued in this research as these appear to provide the easiest means of enabling the necessary manipulation of the light. Emissive displays that produce their own light, or projection methods, *can* be used, but the resulting implementations are generally not particularly practicable.

LCDs provide the necessary transmission display. Unfortunately, these cannot run at a frame rate that is sufficiently fast to provide left and right images alternately without the appearance of flicker. The two images therefore have to be presented simultaneously on either alternate rows or columns of pixels: this is referred to as spatial image multiplexing. Multiplexing on alternate pixel rows is chosen for the current research and is discussed in Section **3.3)** and in Chapter 4.

The formation of an exit pupil can be explained by referring to Fig. 3.1 which shows the real image formed by a vertical illumination source and a convex lens. If an eye is located in the exit pupil region, it will see illumination over the complete area of the lens. If it is located in the region within the lines from the corners of the lens to the top and bottom of the exit pupil, illumination will be seen across part of the lens. Outside this region no illumination is seen. This pupil is located at the appropriate eye of the viewer, and its position determined by the output of a head position tracker.

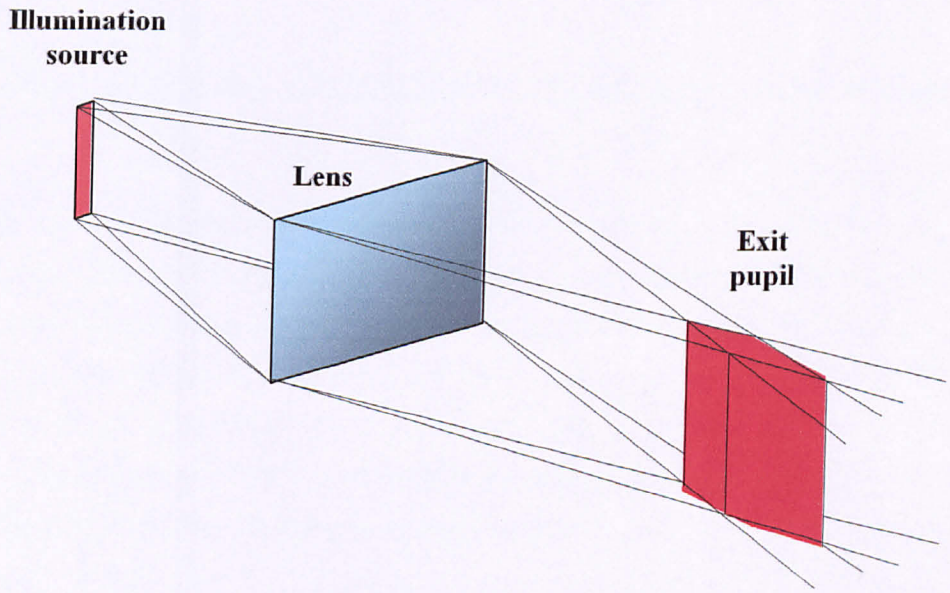

EIG.3.1 EXIT PUPIL FORMATION WITH LENS

The use of a vertical source makes the overall display size inconveniently large and this can be avoided with the use of a spherical lens and a diffuser that scatters light in the vertical direction only. This enables the illumination source to be reduced from a vertical strip to a narrow region as in Fig.3.2. Lateral movement of this strip, which is

controlled by the output of a head position tracker, enables the exit pupil to follow the movement of the viewer's eye. Although the light source *could* move fore-and-aft in order to allow for more viewer movement in the z-direction, it is rather more difficult to achieve, and is not done in the prototypes described in Chapters 9 and 10.

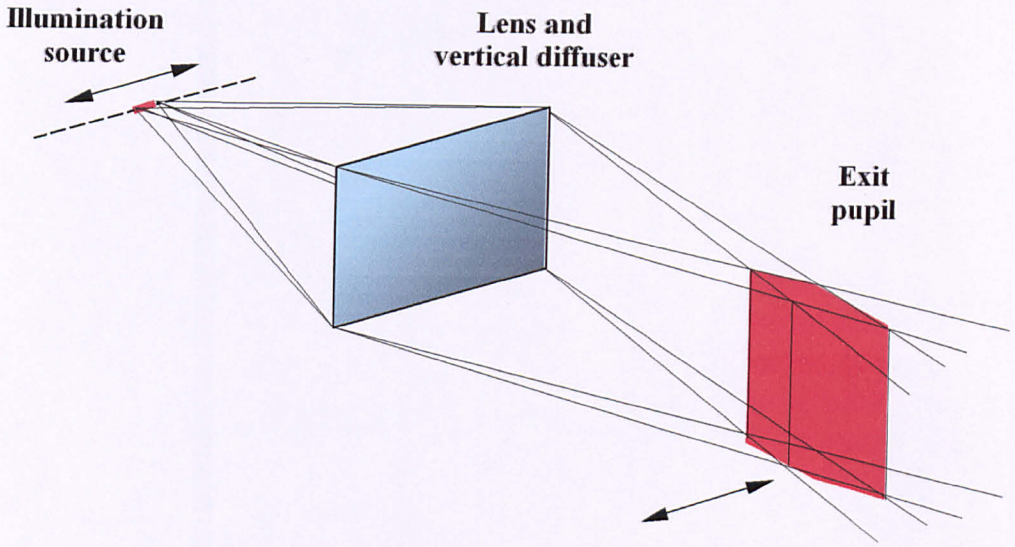

FIG.3.2 EXIT PUPIL FORMATION WITH LENS AND VERTICAL DIFFUSER

The prototype optics produces a pair of adjacent pupils as in Fig.3.3 where the same lens and diffuser are used for each pupil. The vertical diffuser is a lenticular screen with its lenses running horizontally, or a holographic diffuser. The lenticular screen is a sheet that consists of an array of cylindrical lenses whose pitch is sufficiently small for it not to be resolved by the eye at the typical viewing distance. In practice, although the exit pupils will have the diamond-shaped sections as shown, the top and bottom of them will not actually be sharply defined. They are merely depicted this way for clarity.

As there is no movement of the illumination sources in the z-direction, the pupils can only move laterally between the extreme positions shown by the broken lines. This restricts the viewer to being located close to an optimum viewing plane, however a far greater degree of freedom of viewer movement is allowed over that of a display with fixed pupils.

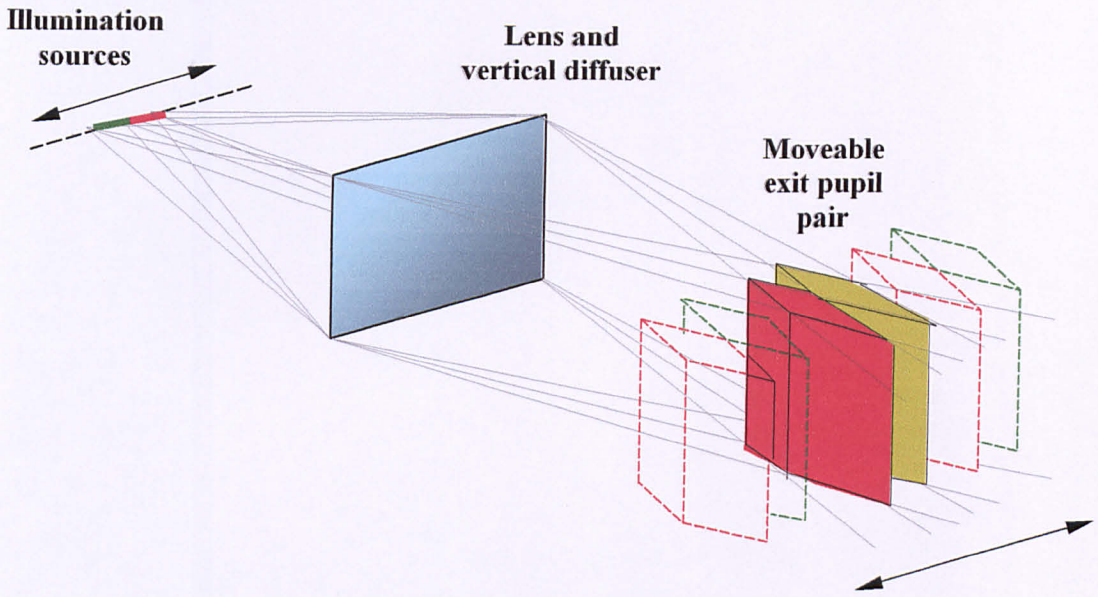

FIG.3.3 EXIT PUPILS IN SINGLE-VIEWER PROTOTYPE

The effective positions of the illumination sources can be moved in various ways, amongst these being the use of fixed sources whose output is controlled with a spatial light modulator (SLM), polarization rotation, physically moving sources or switched arrays of lights, for example white LEDs. The prototypes use the latter two methods. The illumination sources are shown as lying on the same line in Fig.3.3, but in practice, these will be separated in the vertical direction as is described in Section **3.3.2**).

3.2.2) Multiple-user Display

A multiple-user stereo display is not within the area of this research; however, the way in which the principle is extended to serving several viewers is considered. Fig.3.4 illustrates the formation of three exit pupils with three illumination sources, a spherical lens and a vertical diffuser. If the sources move in the x and the z-direction in a single plane, three steered exit pupils will be formed. A Fresnel lens *could* be used in this application, but in practice, aberrations would limit the viewing field to a size that is rather too small for even two viewers to comfortably see stereo.

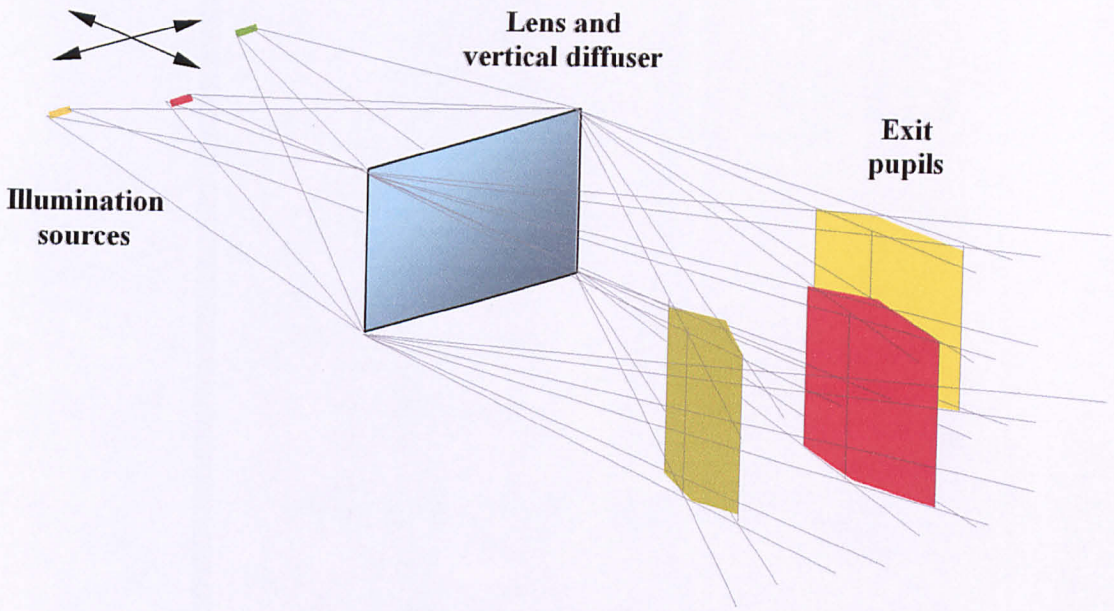

EIG.3.4 MULTIPLE EXIT PUPIL FORMATION

Fig.3.5 (a) is a top view of the arrangement in Fig.3.4. Although confined to a single plane, the illumination sources would still have to move over a large area. The overall housing size can be reduced by replacing the lens and the multiple illumination sources with a compact steering optics unit as in Fig 3.5 (b).

The design of the multiple exit pupil optics is beyond the scope of the current work, but it is envisaged that it will most likely take the form of a compact assembly that is possibly in the order of a few centimetres high. The emergent light from this would need to be contained within an angle of around 25°. If this angle is too large, unacceptable horizontal deviation occurs at the vertical diffuser. This deviation causes crosstalk and is considered in some detail in Chapter 7.

The relatively small emergent vertical angle also means that the steering optics has to be some distance behind the LCD, and therefore considerably wider than the LCD in order to produce pupils away from the axis. Ideally, the steering optics would cover around the same area as the LCD, and be shallow. However, preliminary investigation into the design indicates that such a configuration might be difficult to realise.

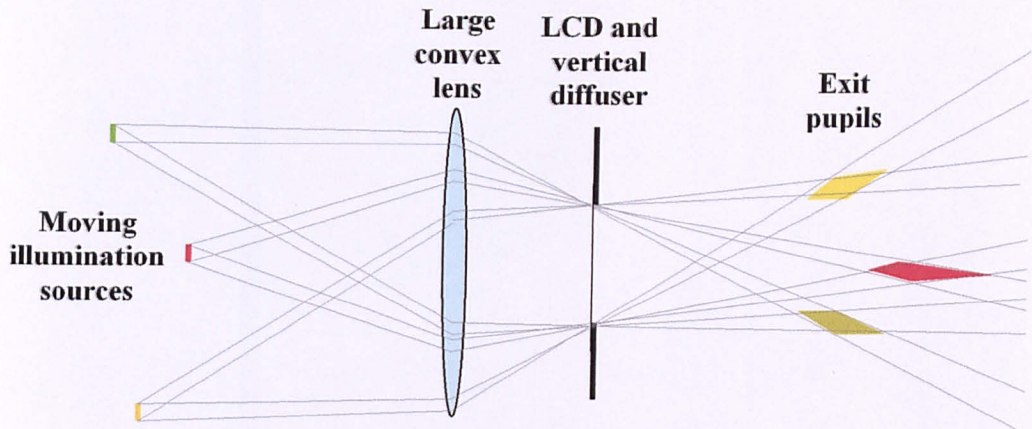

(a) Lens and Multiple Moving Sources

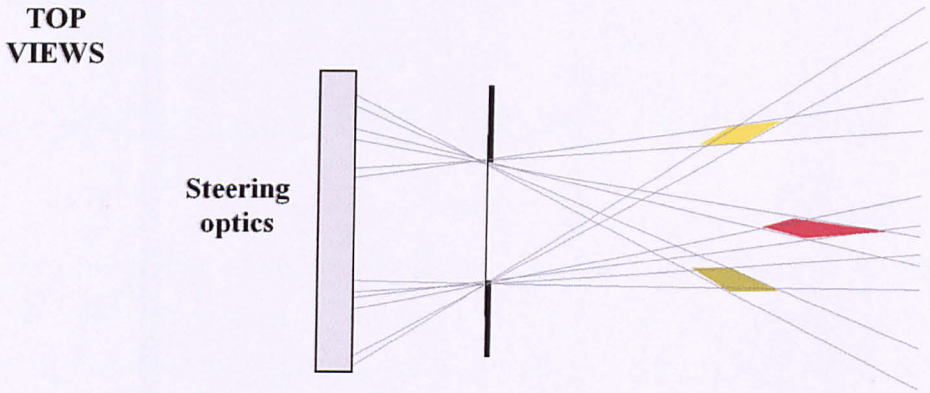

(b) Steering Optics

FIG.3.5 STEERING OPTICS REPLACEMENT OF LENS

A perspective view of the multiple-viewer display is shown in Fig.3.6. It can be seen that the housing would need to be extremely large in relation to the screen size. However, if the optics could be designed so that they can place exit pupils anywhere over a large region, side mirrors can be employed in order to produce virtual images of the array that effectively increase its length. Also, using a series of mirrors that are orthogonal to the side mirrors can reduce the housing depth. These techniques are described in Chapter 4.

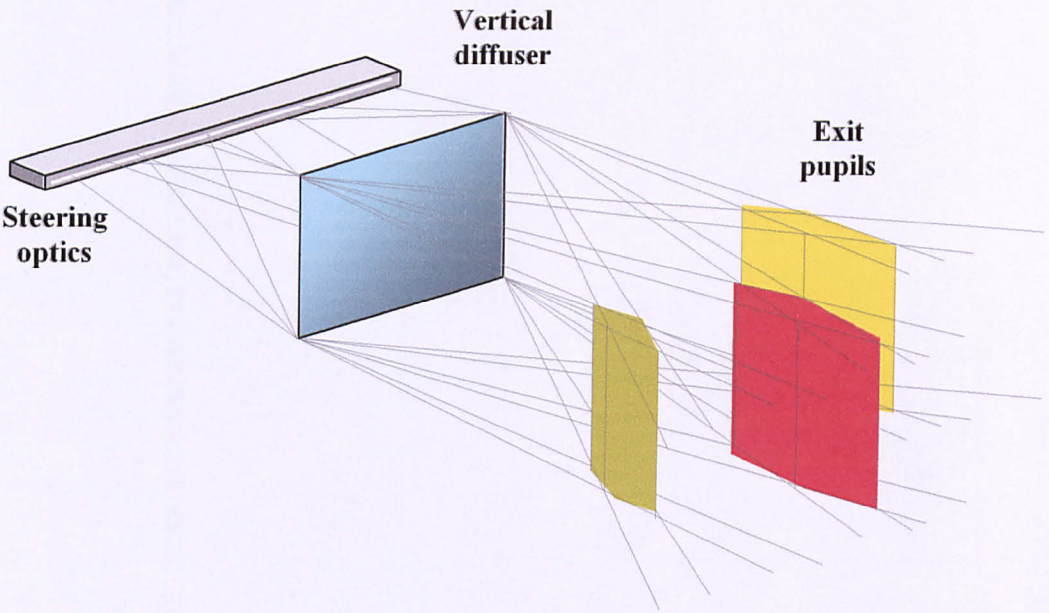

FIG.3.6 MULTIPLE EXIT PUPIL FORMATION WITH STEERING OPTICS

There are two ways in which the same stereo pair can be presented to several viewers simultaneously. Either a basic right (or left) image field is presented across the complete viewing field, with left (or right) image pupils formed within it, as illustrated in Fig.3.7, or an exit pupil-pair created for each viewer, as in Fig.3.8.

In Fig.3.7 a left image is seen across the complete width of the screen in the exit pupil region. In the regions outside the lines from the screen sides to the exit pupils, a right image is seen across the complete width of the screen. In the hatched regions that lie in front of, and behind the exit pupil, parts of both images are seen across the screen width as illustrated in the 'Appearance of screen a seen by viewer' figures. With this presentation, the right eye will lie in the region to the right of the exit pupil detected by a head tracker. In the event of a head not being detected, the exit pupil is not formed and both eyes will be in the right image region so that a monoscopic image is seen.

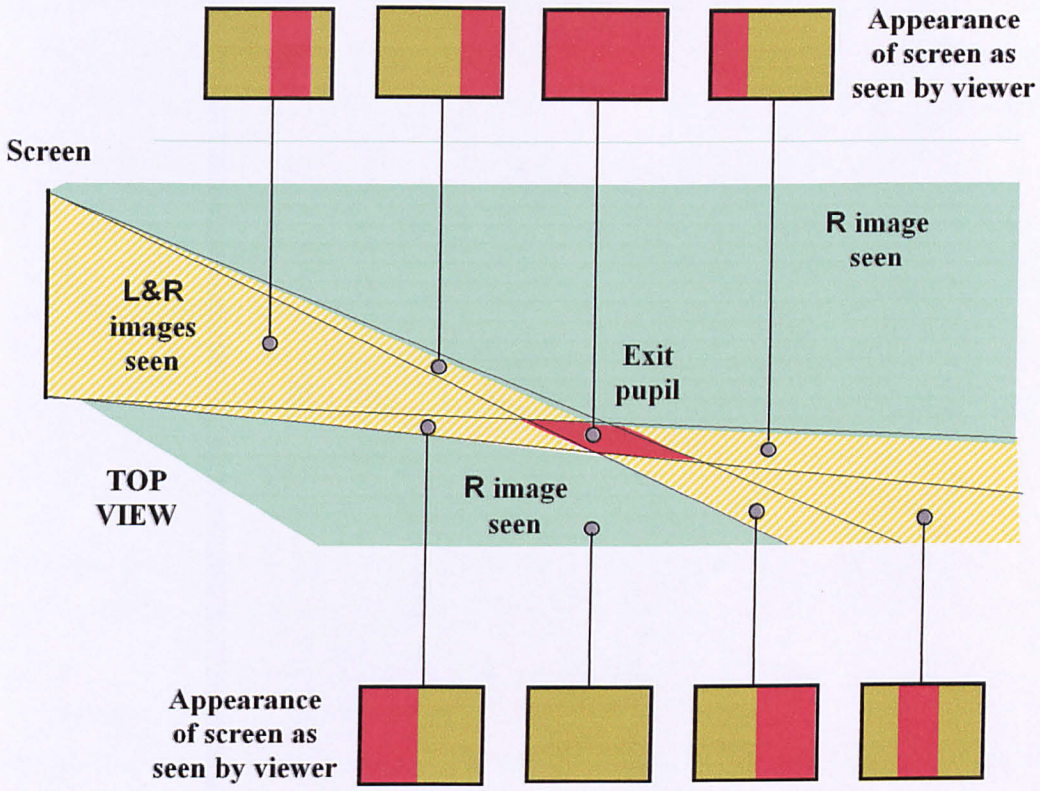

FIG.3.7 APPEARANCE OF SCREEN ACROSS VIEWING FIELD

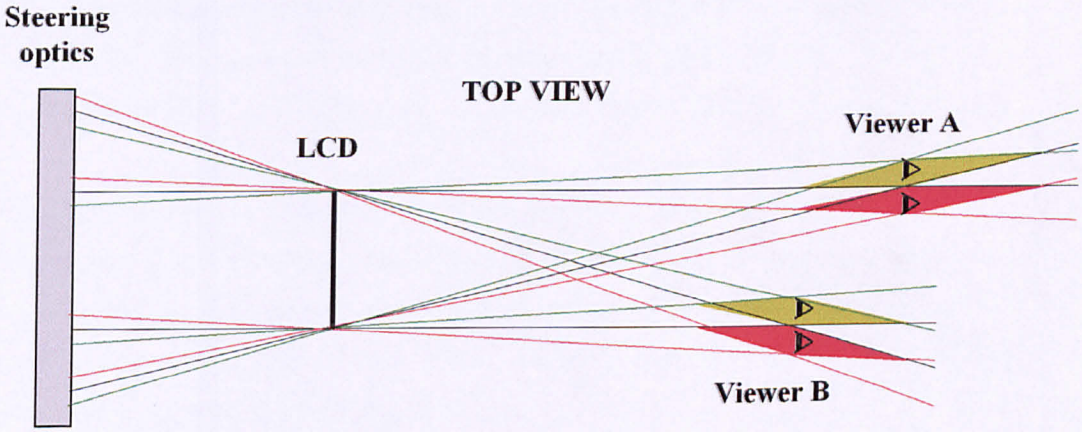

FIG.3.8 EXIT PUPIL PAIRS

The production of a separate exit pupil-pair for each viewer does not have the advantage of supplying a monoscopic image when a head is not detected. However, this requires less total illumination as exit pupils are placed only where there is a viewer. This could well be an important consideration, as illumination levels will have to be high due light loss within the steering optics being greater than in a conventional LCD backlight.

3.3) Image Multiplexing

There are several forms image multiplexing can take, these include holographic optical elements (HOEs), micropolarizer arrays, lenticular sheets and parallax barriers. The parallax barrier approach is used in the prototypes under construction as it provides an inexpensive, if rather optically inefficient, solution. An HOE is used by RealityVision [TRAY97], both to perform the multiplexing and produce the exit pupils. This elegant solution is described in Section **3.4.5)**.

3.3.1) Micropolarizer Multiplexing

At an earlier stage of the research, the use of a micropolarizer array was considered. This is an array of polarizers where the polarization is orthogonal on alternate rows. These are aligned with alternate pixel rows so that light with one polarization alignment passes through the odd rows, and the other orientation through the even rows. The light entering the array can be manipulated to produce the separate left and right pupils. Some methods using this are described in Section **3.4.1)**. The arrays are manufactured by VRex [FARI01] and are used for various stereoscopic applications.

Although the use of a micropolarizer is not envisaged for the prototype, the principle is used to in a spatial multiplexing demonstrator that has been constructed. Exit pupils are produced by focusing the real images of various polarizer configurations into the viewing field with a convex lens. These images form regions where either the left image only, or the right image only, are seen.

The demonstrator screen consists of a pair of simple 12-line images. This is illustrated in Fig.3.9 where the right image regions are indicated by the green rows, and the left image by the red rows. The screen is only 33 millimetres high by 72 millimetres wide,

and the vertical resolution is 1.4 millimetres. However, the demonstrator does illustrate effectively the principle of exit pupil production. This screen consists of strips of orthogonally aligned Polaroid on alternate rows, on which a mask containing the simple images is attached. The mask is arranged to give the appearance of four squares of differing size and apparent distance. These range from the small square in the top right hand corner, that appears to be in the plane of the screen, to the large square in the middle that appears to be the furthest behind the screen.

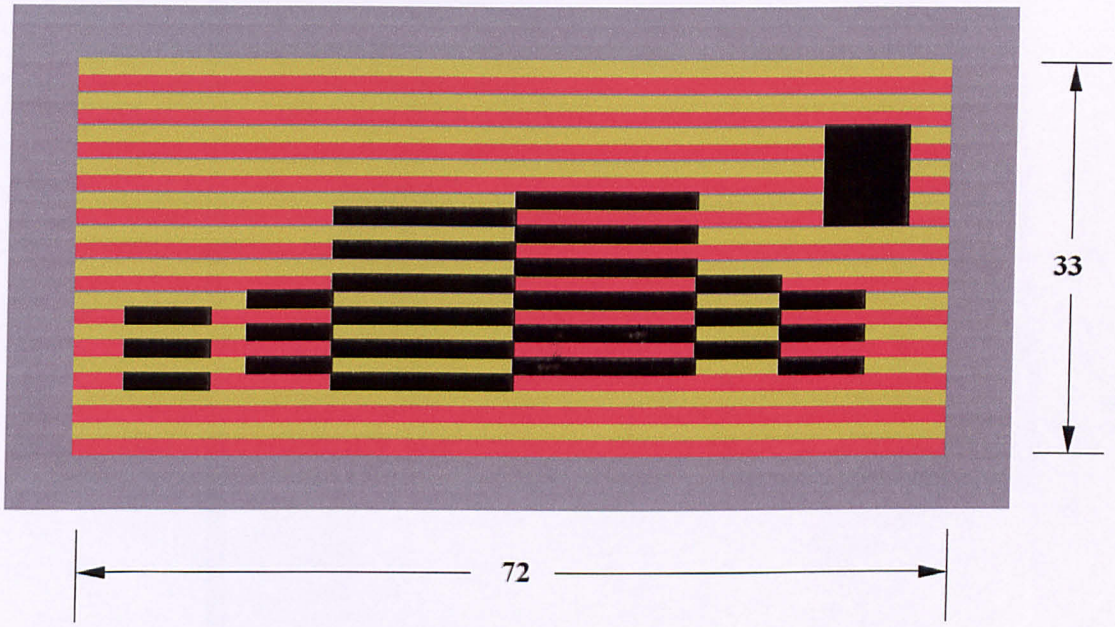

'Left' image on lines indicated red
'Right' image on lines indicated green
Dimensions in millimetres

FIG.3.9 IMAGE MULTIPLEXING DEMONSTRATOR SCREEN

This screen is mounted in the assembly shown in Fig 3.10. This consists of a box that also houses a lamp unit, the polarizer and the lens. The polarizer can be configured in various ways in order to demonstrate various modes of operation of the display. The illumination source has a diffuser 150 millimetres high that forms exit pupils around a metre high. A diffuser can be mounted to the bezel around the screen to eliminate the appearance of the coarse line structure in the images. Figs.3.10 and 3.11 show the

demonstrator with movable retardation film. This shows that two exit pupils can be steered independently.

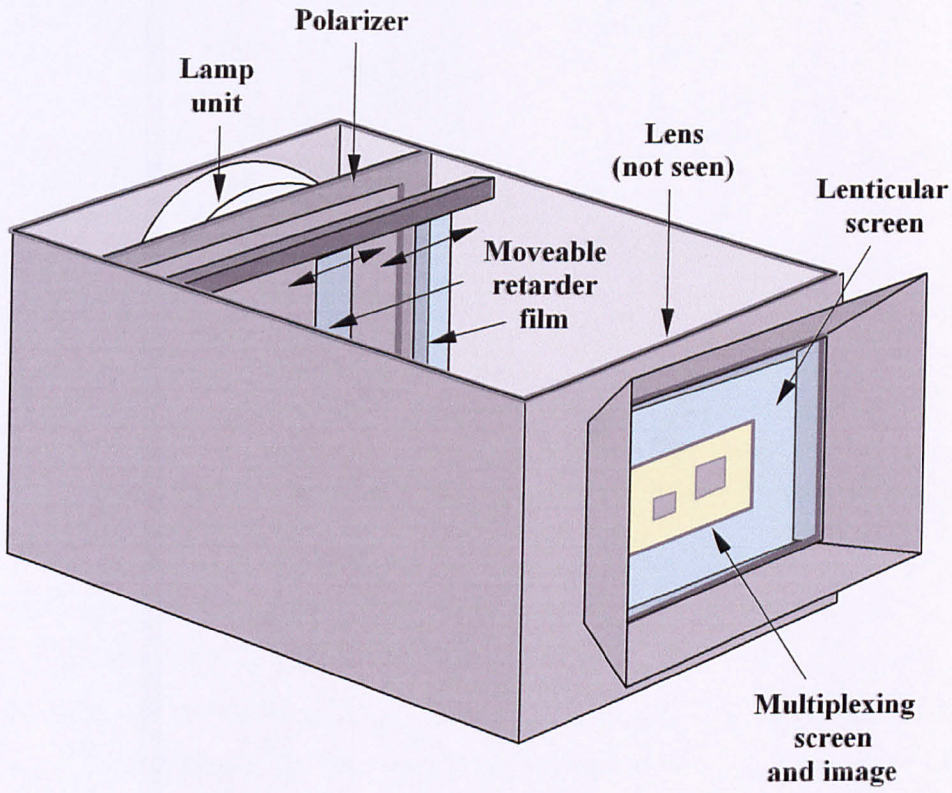

FIG.3.10 POLARIZED LIGHT MULTIPLEXING DEMONSTRATOR

Fig.3.11 shows the formation of two left exit pupils within a basic right image field. Light from a polarizer passes through the retarder film and emerges with its polarization rotated through 90°. This goes through the left image lines only and forms the exit pupils where the left image is seen. Light that passes directly from the polarizer to the screen goes through the right image lines and enables this image to be seen in the regions between the pupils. As the screen is very small, the pupils are narrow, and are extensive in the z-direction.

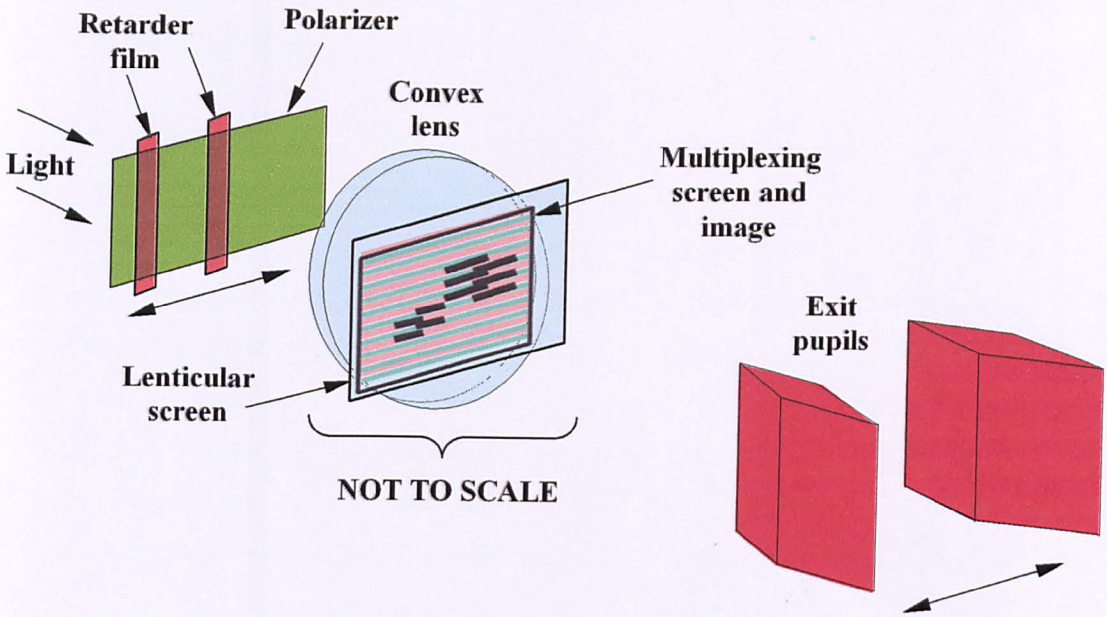

EIG.3.11 MULTIPLEXING DEMONSTRATOR OPTICS

The demonstrator can be used in four modes that are selected by the choice of the polarizer located in front of the lamp unit. These are as follows –

a) Non-autostereoscopic: In this mode there is no polarizer in front of the lamp unit and the screen is viewed through a pair of polarized glasses.

b) Three Fixed Autostereoscopic Regions: A polarizer screen with six vertical bands of alternating polarization is inserted in front of the lamp. This produces six exit pupils across the viewing field. Normal stereo can be seen in three regions, with two pseudoscopic regions in between these. The polarizer glasses are not required in order to observe stereo. In this mode, the display is operating in a similar manner to lenticular displays where the lenses run vertically. It should be noted that the demonstrator was built with the intention to merely illustrate the way in which polarization can be used to form exit pupils by observation of the screen with one eye covered. It was not anticipated that the low-definition 12-line images would provide a

stereo picture. However, it has been found that in excess of 75% of viewers are actually able to fuse the images.

c) Two Exit Pupils in Right Image Field: In this case the polarizer consists of a sheet which has the majority of its area polarized in order to allow light to pass through the right image lines on the screen. Within this there are two ten-millimetre wide vertical regions where the polarizer is orthogonal to the rest of the area. This demonstrates the formation of left exit pupils within a basic right-image field. A viewer, with one eye covered, traversing the field at around two metres from the screen will observe the image change. At the extreme left, a right image is seen. As the viewer moves to the right there are two regions around 100 millimetres wide where the left image is seen. In these regions the squares appear to 'jump' to the right.

d) Two Moveable Exit Pupils: The ability of the exit pupils to be steered is demonstrated by inserting a plain right-image selecting polarizer in front of the lamp. Movable left-image pupils are produced by placing two ten-millimetre strips of retarder in front of the polarizer. These rotate the polarization by 90° to produce left exit pupils. These strips can be moved laterally as shown in Figs.3.10 and 3.11.

3.3.2) Parallax Barrier Multiplexing

Left and right exit pupils can be produced from two separate sets of optics whose outputs are directed to left and right rows of pixels using a barrier that has horizontal apertures as shown in Fig.3.12. The pitch of these apertures is slightly less than double the LCD vertical pitch in order to allow for the effect of parallax due to the optics being at a finite distance from the barrier. The geometry of the barrier is analysed rigorously in Chapter 5.

The barrier has the advantage of being inexpensive, but has the disadvantage of having a low light throughput. This problem can be overcome by replacing the barrier with a lenticular screen that has its lenses running horizontally. The pitch of these lenses will be the same as for the parallax barrier. Although a custom-built lenticular screen can be very expensive, it has the advantage of capturing almost 100% of the

light as this is directed to the appropriate pixel rows by focusing the light, as opposed to blocking it.

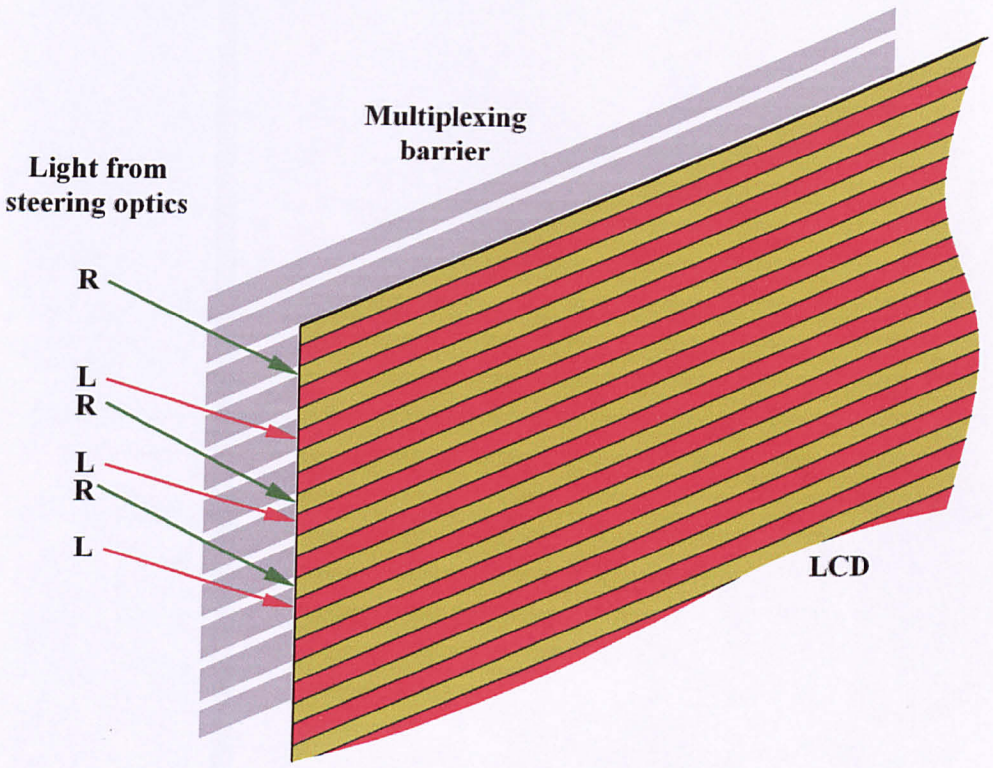

FIG.3.12 PARALLAX IMAGE MULTIPLEXING

3.4) Survey of Head Tracking Display Types

Head tracking is becoming increasingly used as a 3D display method. The most likely reason for this being that it enables freedom of viewer movement, with the display showing the minimum amount of information. The various 3D display types can be categorised in different ways, for example by their means of multiplexing: spatial, temporal or twin displays. However, the classification system chosen for this survey is based on the optical configuration as this has an important bearing on the size and performance of the particular display.

The categories are - Fresnel lens; lenticular; projection; parallax and other methods, e.g. holographic optical elements (HOEs). Some displays do not fall completely within one category and the author has used his discretion as to the most appropriate. The descriptions of the displays in this chapter cover only their optical configurations as the head tracking aspects are covered separately in Chapter 11.

3.4.1) Fresnel Lens Displays

Fresnel lenses are widely used in this application as they provide an inexpensive means of producing the exit pupils. The earliest reference to a head tracking display known to the author is that of Alfred Schwartz [SCHW85]. Fig.3.13 is a simplified schematic diagram – the actual display incorporates a folding mirror and the head tracker. The CRT projection modules project the left and right images on to the Fresnel lens that acts as a field lens with respect to the image information.

Exit pupils are formed by this lens focusing real images of the projector lenses in the viewing field, and then extending these images vertically in a similar way to the method described in Section **3.2.1)**. The pupils are steered by moving the Fresnel lens laterally with a servo-motor controlled by the head tracker output.

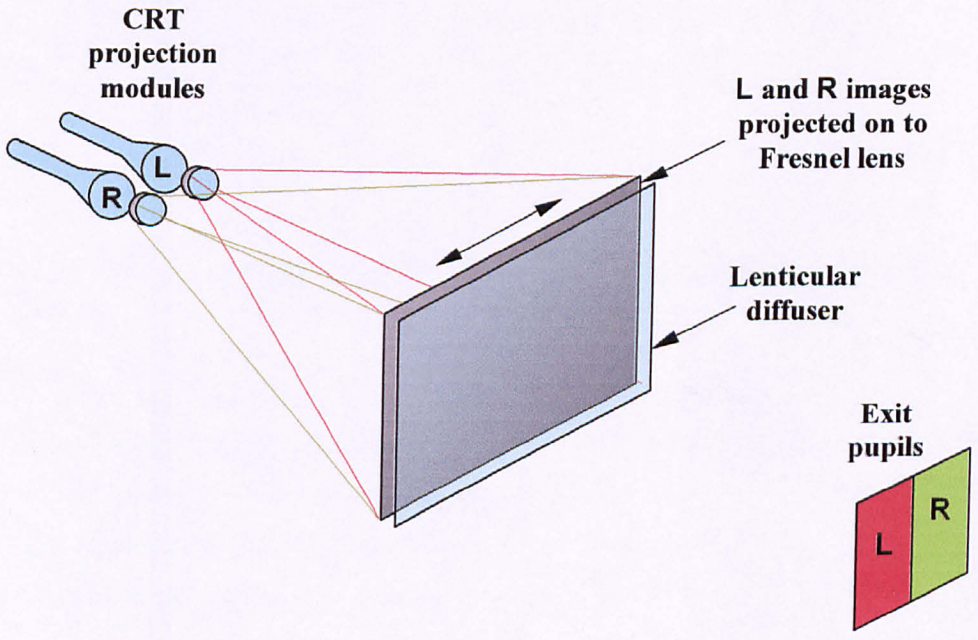

FIG.3.13 1985 SCHWARTZ DISPLAY

In order to retain full resolution, Sharp use two LCDs whose images are combined with a semi-silvered mirror [EZRA95] [WOOD97]. Lenses are used to produce the exit pupils (referred to by Sharp as 'windows'). The light source consists of an array of cold cathode fluorescent tubes whose outputs are guided by Perspex wedges. Incidentally, although the optical components are shown as being vertical in Fig.3.14, which is based on Sharp's report, the display seen by the author at their laboratory obviously had the light path folded in the vertical direction, not horizontally as shown. This display is termed 'macro-optic' by Sharp, as the focusing element is of a size comparable to the LCD.

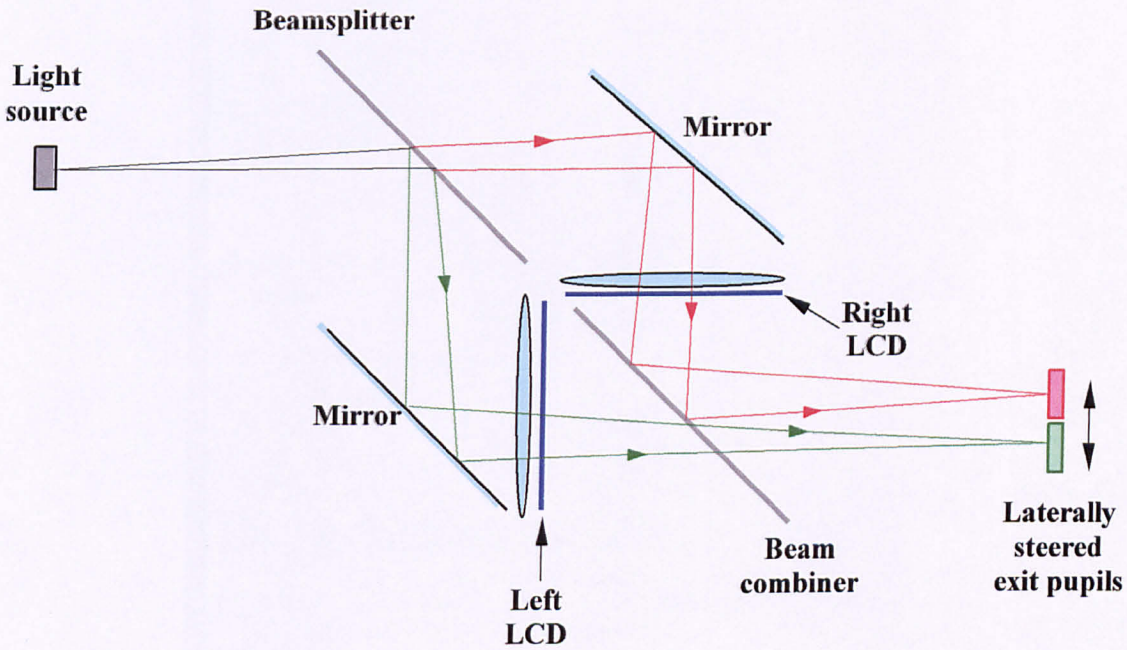

FIG.3.14 SHARP TWIN SCREEN DISPLAY

The Massachusetts Institute of Technology (MIT) Media Lab have built a display that works on the same principle as the demonstrator described in Section **3.3.1)** that was built two years before the MIT patent application was filed in 1998 [BENT02]. The Patent describes the use of a two-dimensional SLM that rotates the polarization by 90° in the region that produces an exit pupil in the right-eye area of the viewing zone. This corresponds to the retarder region in the demonstrator decribed in Section **3.3.1).**

Head tracking is achieved simply by imaging the right side of the viewer's head with reflection from an infrared source. This is similar to the tracking method used in various Japanese systems that are mentioned in Section **11.1.2).**

The schematic diagram of Fig.3.15 shows the configuration as described in an SPIE report [BENT99]. In this case, head tracking is carried out with a machine vision system, and the region of rotated polarization on the SLM forms a vertical band.

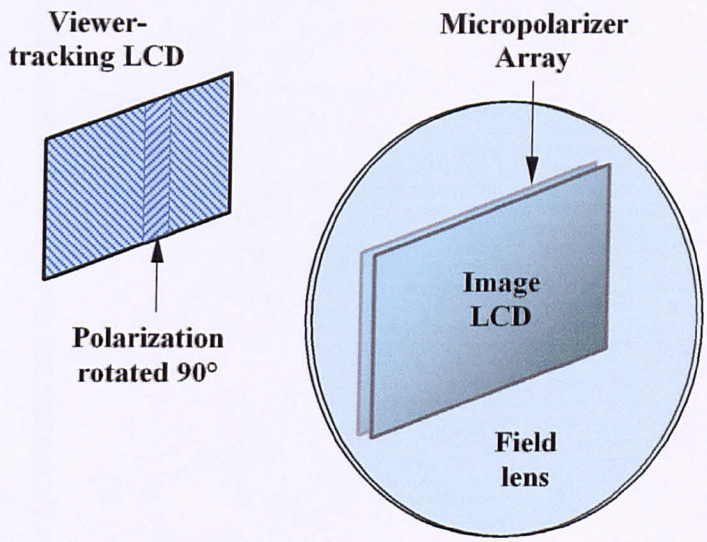

FIG.3.15 MIT MICROPOLARIZER DISPLAY

A twin-screen display that uses Fresnel lenses is described in information from Sea Phone, a Japanese company [HATT00a]. This uses a semi-silvered mirror to combine the images from two LCDs as shown in Fig.3.16. The principle of operation is very similar to that of Sharp, with the exception that the illumination is provided from two two-dimensional monochrome displays, as opposed to the single linear array and beamsplitter.

The monochrome displays show images of each side of the head, as the figure illustrates. This enables exit pupils to be formed around the regions of the respective viewer's eyes. These are captured with an infrared camera that uses the same optics as the display in order to eliminate parallax error. An infrared reflecting mirror is

mounted at 45° to the vertical in the light path between the left-image LCD and its monochrome display – this in not shown in the figure. Earlier embodiments of this display have been described in previous papers [NISH94] [HATT94(a)]. The only difference with these is the means of head tracking image capture.

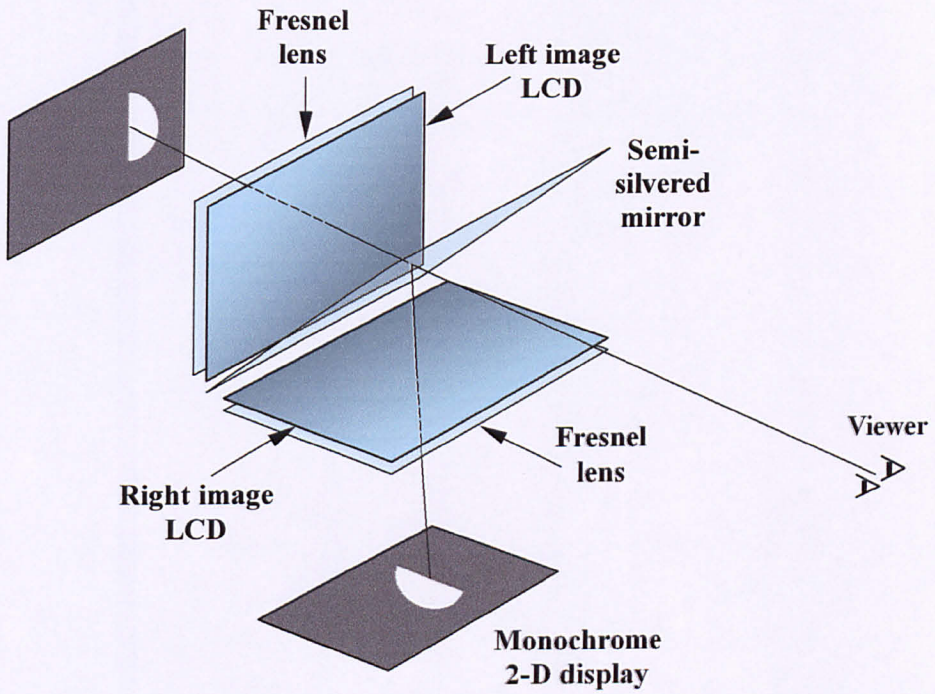

FIG.3.16 SEA PHONE TWIN SCREEN DISPLAY

Another method of 3D display, illustrated in Fig.3.17, is also described in the Sea Phone report [HATT00b]. Like the MIT display, it uses a micropolarizer array to separate the illumination to the left and right pixel rows, and a Fresnel lens to form the exit pupils. In this case, however, the light is provided from linear arrays of white LEDs that have polarizers in front of them. The arrangement is similar to that described in Section **3.2.1)** and requires a vertical diffuser to produce vertical exit pupil regions. The only difference between the Sea Phone display and the prototype under construction by the author is in the method of image multiplexing – micropolarizer, as opposed to parallax barrier.

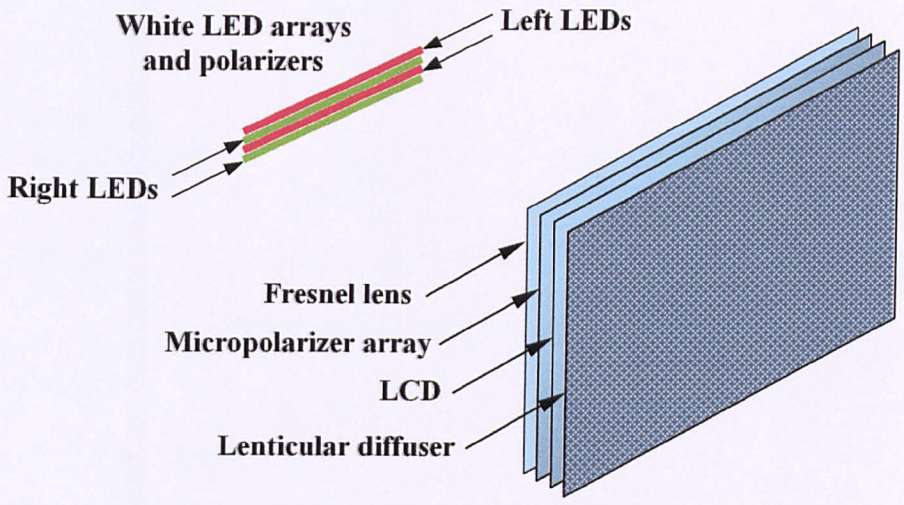

FIG.3.17 SEA PHONE MICROPOLARIZER DISPLAY

The Korea Institute of Science and Technology (KIST) have developed a system that projects the images of two 6.5" LCD panels on to a 20" diagonal Fresnel lens [SON01]. Exit pupil steering is achieved with the use of an SLM that selectively blocks the light in two separate paths, one path for the right exit pupil and one for the left.

The principle of operation is most easily understood by simplifying the optics into the optical equivalent diagrams of Fig.3.18 (a) and (b). Although the actual display uses a concave mirror for projecting the images of the LCDs on to the Fresnel lens, this component is shown as a convex lens for the purpose of ease of explanation – the function performed is the same in each case.

The optics can be considered as having two imaging functions, i.e. the one governing the illumination, and the one relating to the formation of the images seen by the viewer. In Fig.3.18 (a) the source is positioned in such a way that it forms a real image only on the lower half of the projection lens. The SLM is divided into two linear arrays, one above the other. The field lens projects a real image of the trans-

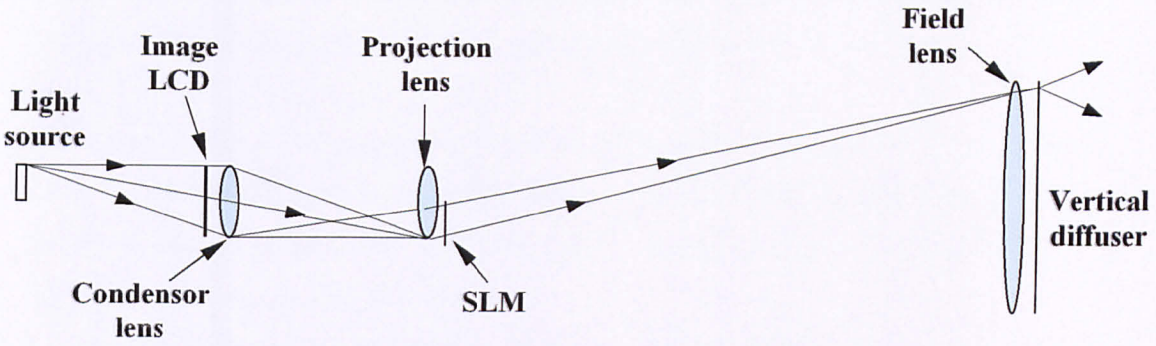

(a) Equivalent of Right Image Formation Optics

SIDE VIEWS

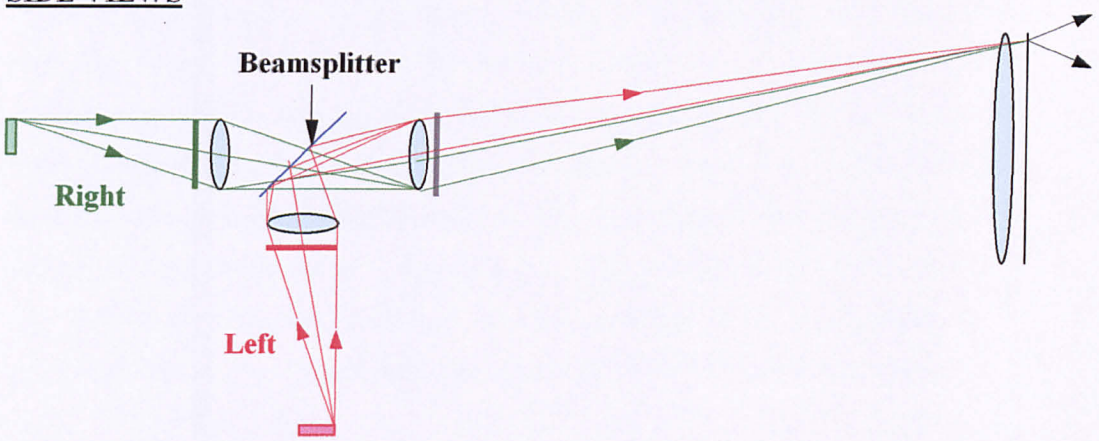

(b) Equivalent of Right and Left Image Formation Optics

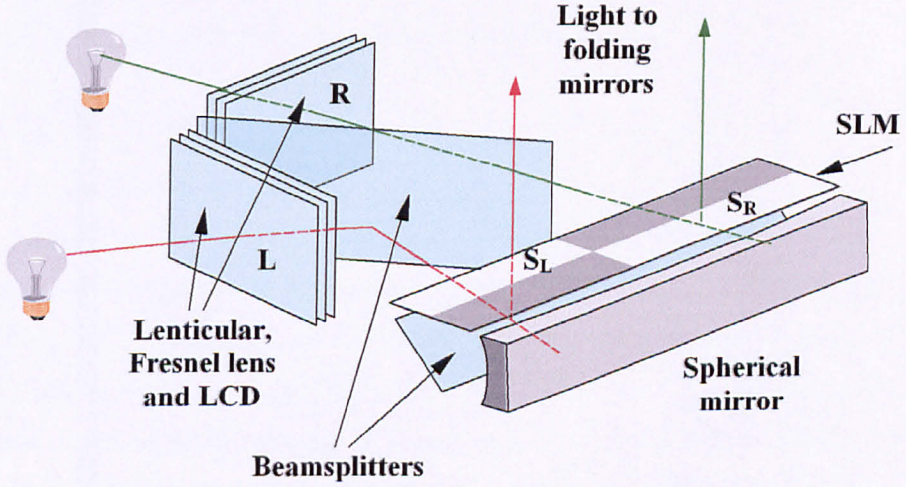

(c) Actual Configuration of Projection Region

FIG.3.18 KIST SINGLE-USER DISPLAY

mission area the SLM (S_R in Fig 3.18 (c)) into the viewing field. This image is extended into a vertical exit pupil by a lenticular vertical diffuser.

The image of the LCD is projected on to the field lens by the projection lens. The SLM is located sufficiently close to the projection lens for it to be effectively in the Fourier transform plane of the lens. Therefore, its image is not resolved on the field lens, and hence is not visible to the viewer.

In Fig.3.18 (b) the left and right light paths are shown. The right illumination source produces a real image on the lower part of the SLM, and the left source on the upper half. The images of the two LCDs are combined by the beamsplitter The actual configuration used in the display is shown in Fig.3.18. (c). Lenticular screens with vertically aligned lenses are used between the light sources and the LCDs in order to spread the light over the width of the LCD. The paper does not explain the reason for using a mirror as opposed to a projection lens. The possible reasons could be ease of manufacture, or reduction of aberrations. One drawback of this configuration is the loss of light at the beamsplitter, which is in addition to the left / right beamsplitter.

As the viewer moves, the boundary between S_R and S_L moves so that the image of this is formed between the viewer's eyes. The complete display consists of the assembly shown in Fig.3.18 (c), plus two folding mirrors and a Fresnel lens.

3.4.2 Lenticular Screen Displays

Lenticular screens can be used in various ways in order to produce exit pupils. The easiest method is simply to place a lenticular screen, with its lenses running vertically, in front of an LCD. If the pitch of the lenses is slightly less than double the LCD horizontal pitch, left and right exit pupils are formed when left and right images are displayed on alternate pixel columns. The exit pupils can be steered by changing effectively the relative lateral position between the lenticular screen and the LCD.

Simply swapping the images on the pixel rows can alter the relative positions between the pixel columns. This method is used in a display developed by the Nippon

Telegraph and Telephone Corporation (NTT) [ICHI89]. It is historically interesting as it the first use of a flat panel display for stereo that the author has found. The way in which this operates is illustrated in Fig.3.19. When the head tracker detects the centre of an eye-pair within the smaller diamond-shaped regions indicated in Fig.3.19 (a), left and right images are displayed on the columns as shown in the left-hand figure. This produces the exit pupils that are the larger diamond-shaped regions marked 'L' and 'R'.

When the viewer's eye-centre position moves into the zones shown in the right-hand figure in Fig.3.19 (b), the left and right images are swapped. This ensures that the eyes are never positioned in such a way that a pseudoscopic image is seen, as can happen in a fixed exit pupil display. Although this method is a vast improvement over fixed exit pupil displays, degraded images will still be seen when eyes are located near the exit pupil boundaries. Another drawback of this method is that the LCD must be used in the portrait orientation.

The problem of the eyes falling within these boundary regions has been solved by Sharp where a novel LCD mask structure called PIXCON provides contiguous light across the viewing field [WOOD97]. The pitch of the lenticular screen is set to provide exit pupils whose width is around 2 / 3 the average interocular separation. This arrangement reduced the observed intensity fluctuation at the exit pupil boundaries.

The exit pupils can be made to move continuously by actually moving the lenticular screen laterally. This approach is used by the Heinrich Hertz Institut (HHI) in Berlin [HHI02]. The display will also have the capability of tracking the viewer in the z-direction by moving the screen along both the x and z-axes. This uses a 21" display in the portrait orientation and will enable 300 millimetres of movement as this is considered to be sufficient for comfortable viewing of a monitor. The amount of movement of the lenticular screen is only in the order of one millimetre. Although the information given in this reference implies that the Z tracking display has been built, this is still under development and will be built within the ATTEST project.

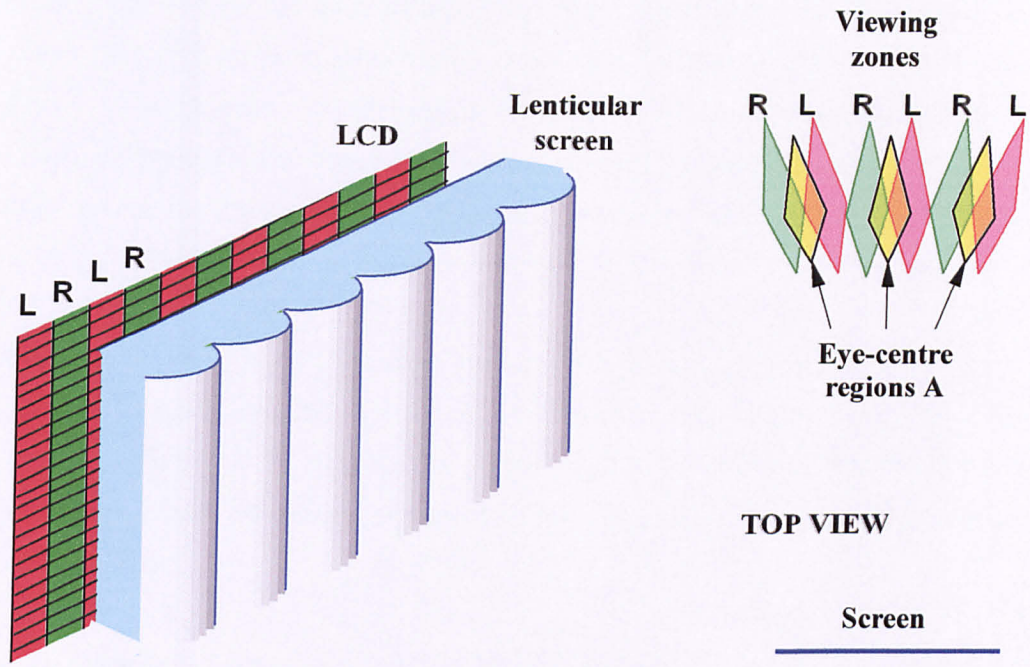

(a) Eyes centred in Regions A

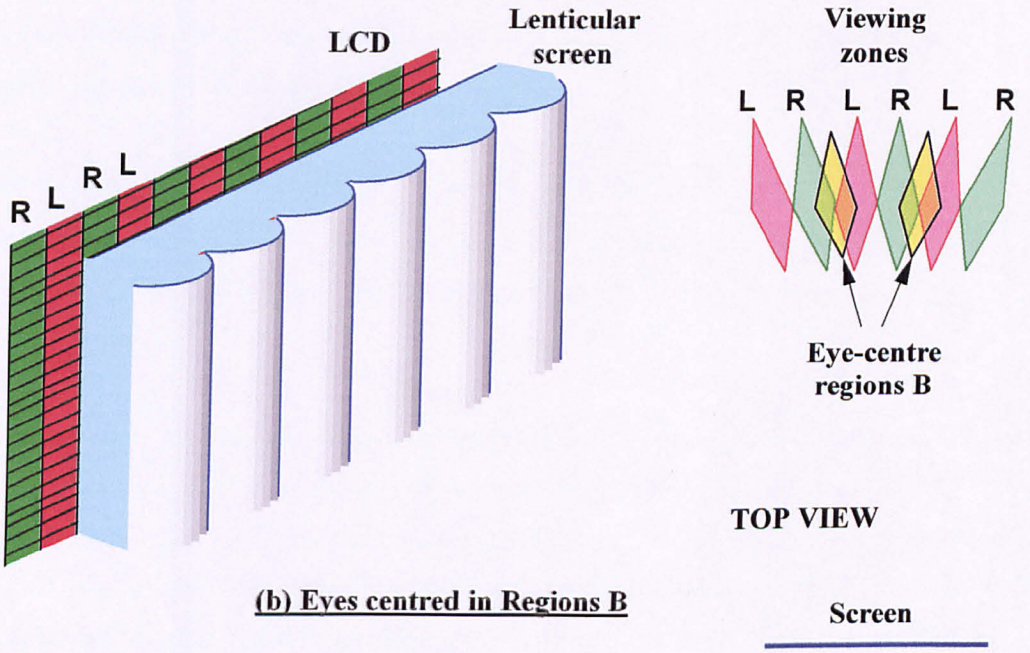

(b) Eyes centred in Regions B

FIG.3.19 NTT LENTICULAR DISPLAY

Another embodiment of this technique, mentioned in the same report, is the replacing of the LCD with a diffusing screen. Pixel columns are produced by focusing the output of a pair of projectors through a vertically aligned lenticular screen whose pitch is slightly greater than the *steering* lenticular screen. The projectors are located behind, and enable a 40" screen to be produced with exit pupils that are steered by a small mechanical movement. This compares favourably with projection techniques described in Section **3.4.3)** where large movement of the projector-pairs is necessary.

Steering exit pupils in the z-direction can also be achieved by using tapered lenticular optics in conjunction with an infrared retroreflective head tracker [STRE98]. The methods described so far steer the exit pupils by operating on the light emerging from the display. Lenticular screens can also be employed to operate on the light entering the LCD pixels.

In the Dimension Technologies Inc. (DTI) display, a lenticular sheet is used to form a series of vertical illumination lines on a diffusing layer located behind the LCD [EICH93] [EICH94] [EICH95]. These lines are images of narrow vertical sources situated behind the diffuser as illustrated in Fig.3.20. The exit pupils are produced by parallax as can be seen in the figure.

The head tracking version of the display has three sets of light sources so that three sets of overlapping exit pupils are formed. As the viewer's head moves, the appropriate lamps are lit so that the eyes always fall completely within a left and a right exit pupil.

Exit pupils are formed in a similar way in the display described by Sharp [WOOD97]. In this case the light lines are an array of vertical slits that are moved laterally by mechanical means, and have an illumination source behind them. This is located behind a lenticular screen and the assembly *effectively* forms a large lens with a vertical light source behind it as illustrated in Fig.3.1. A small movement of the slit array has the same effect as a large movement of a light source behind a lens. The assembly is mounted behind an LCD so that its image can be directed to an exit pupil.

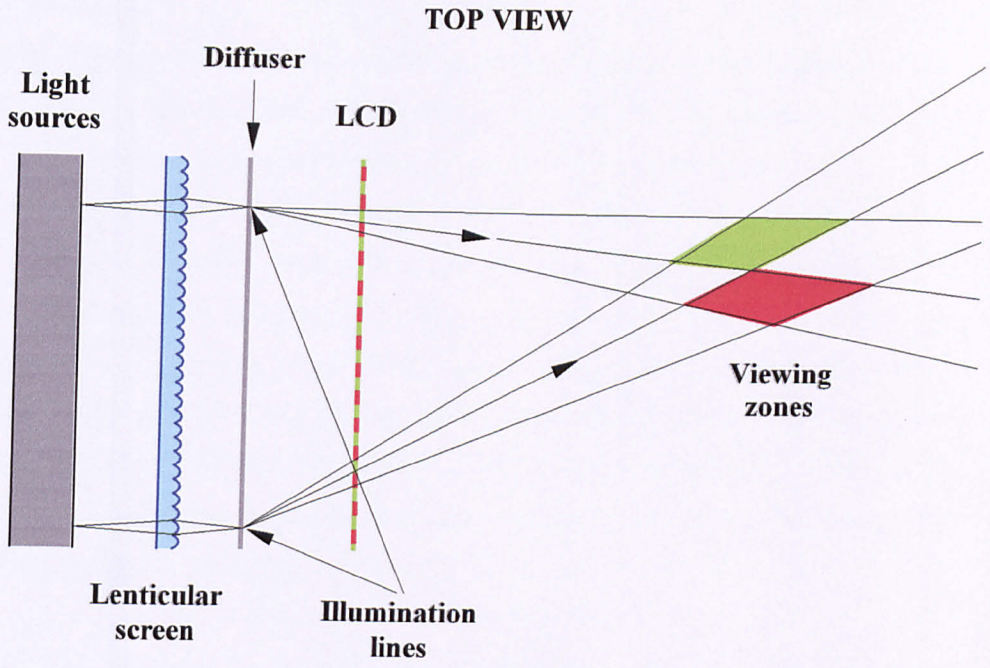

FIG.3.20 DTI DISPLAY

In order to produce a pair of exit pupils, with full horizontal resolution on the LCDs, the images of two LCD / steering optics assemblies are combined with a semi-silvered mirror. Sharp refer to this display as the 'micro-optic' version, as opposed to the 'macro-optic' display described in Section **3.4.1)** that uses lenses around the same size as the LCDs.

The use of polarized light to perform a similar function to the DTI and Sharp displays has been proposed [TSAI01]. In this display, the effective 'light lines' for the right exit pupils are vertical strips of one polarization on a 'micro tracking device', and the 'light lines' for the left exit pupils are strips with orthogonal polarization. The positions of these regions are controlled by a head tracker. A lenticular screen that forms the exit pupils is located in front of this. A micropolarizer array with its elements running horizontally allows light from the right light line to pass only through the LCD pixel rows displaying the right image, and vice versa. It is doubtful whether this approach can ever be very effective due to the high resolution required for the 'micro-tracking device' in order for the pupils to be directed in sufficiently small increments.

3.4.3) Projection

All projection stereo displays operate on the same principle, i.e. they form real images of the projector lenses in the viewing field. These are the exit pupils in which the viewers' eyes are located. If an array of projectors is used, the resulting display is in the multi-view category. The same optical configurations that are used for the multi-view displays can also be used with a pair, or with several pairs, of projectors to provide head tracking displays. The four main classes of projection display are determined by the screen type. These are all mentioned in 'Three-dimensional Imaging Techniques' by Okoshi and are: retroreflecting [OKOS76(a)], double lenticular screen [OKOS76(b)], mirror [OKOS76(c)] and lens [OKOS76(d)]. Although the book refers to non-head tracked displays, the optics are the same as the head tracking displays described in this section.

In retroreflecting screen displays, the projector illuminates the screen from the front, and the light is reflected back in the same vertical plane. In the early display of NTT [TETS89], projectors in an array are switched on selectively under the control of a head tracker in order to allow a single viewer a degree of lateral freedom of movement. The retroreflecting screen consists of a vertically orientated lenticular sheet. This has a diffuser on its flat back face, which is in the focal plane of the lenses. The screen has the added advantage of diffusing the light in the vertical direction only. Side lobes are also produced where this diffused light exits through adjacent lenses, but these are located outside the viewing region.

A variant of this has been developed by an Australian company, Xenotech [HARM96] [HARM97] [HARM00]. In this display, light from two projectors is directed on to the screen via a semi-silvered mirror and two folding mirrors as shown in Fig.3.21. This enables the projectors to be located behind the screen. The screen options are glass bead or prismatic. The prismatic screen consists of an array of corner cube elements where reflection takes place on three orthogonal surfaces. This type of display can provide screen sizes of 50" or more.

Exit pupils can be formed in the viewing field by using a pair of lenticular screens with a diffusing layer between them. If the lenses of the screens run vertically and are outermost, and the diffusing layer is located between the two inner flat surfaces, the

assembly acts as a one-dimensional version of the Gabor superlens [HEMB97]. The superlens consists of two microlens arrays that exhibit different imaging properties to conventional lenses. The action of the diffuser is to produce a vertical exit pupil, therefore giving the viewer more freedom of vertical movement.

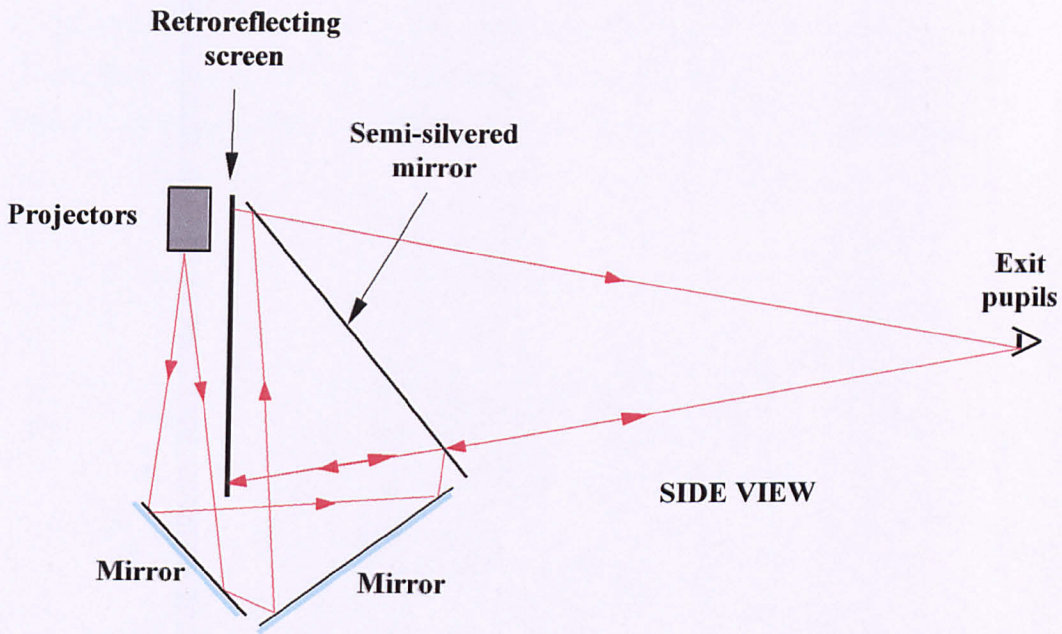

FIG.3.21 XENOTECH PROJECTION DISPLAY

Fig.3.22 (a) shows the top view of a small section of the screen. Unlike conventional lenses, the emergent angle increases as angle of incidence increases. Where the sheets have the same focal lengths, the object and image (in this case projector and viewer) positions are as in Fig.3.22 (b). The real images occupy the 'mirror image' positions of the object positions. Side lobes are produced where light passes through adjacent lenses, however, these will not extend as far as neighbouring viewers.

In an early paper relating to this method, the use of lenticular screens with different pitches is proposed [TETS94]. If the screen on the emergent light side of the screen has a slightly larger pitch than the other, the arrangement has the ability to magnify the movement of the projectors. It is not clear whether this was ever produced as a later paper by the same research group [OMUR98] describes a display where the

projectors are spaced at the interocular distance, therefore implying that magnification is not taking place. The magnifying version may never have been constructed, as large custom-built lenticular screens are extremely expensive. The same paper describes a 100" diagonal display where several viewers are served by the use of a projector-pair for each viewer located behind the screen. Movement of the projectors in both the x and z-directions, under the control of an infrared retroreflecting head tracker, allows the viewers a high degree of freedom-of-movement. NEC have developed a method of effectively moving stationary projectors by using a moving image-shifting piece of glass in front of them [IMAI96]. This type of display can support only one viewer.

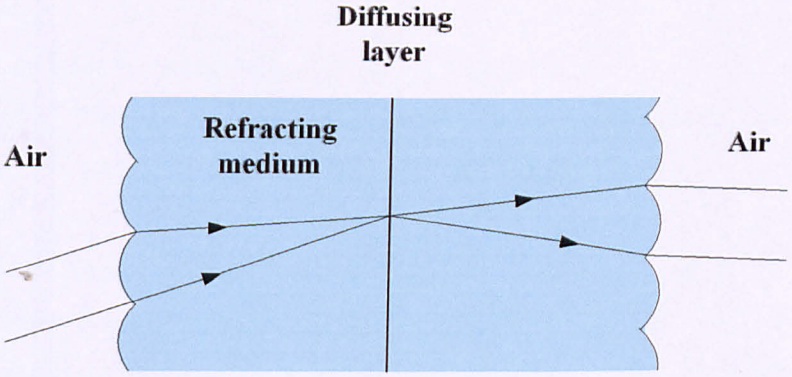

(a) Operation of Double Lenticular Screen

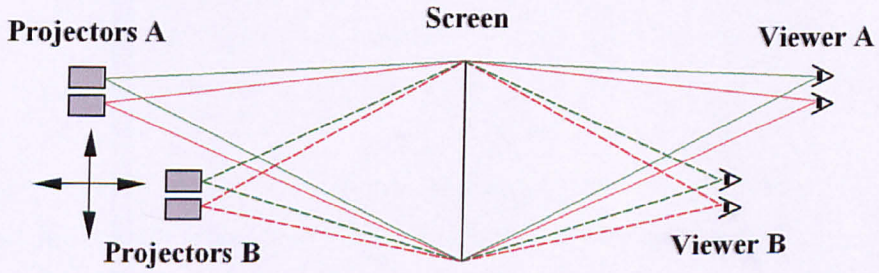

(b) Positions of Projector-pairs and Viewers

TOP VIEWS

FIG.3.22 ATR PROJECTION DISPLAY

A system using a large mirror to produce exit pupils has been developed by Hitachi [ARIM98]. Although moving projectors *could* be used in this configuration, the Hitachi display increases the viewing zone width by employing an array of four projectors, therefore making the display a multi-view type.

Fresnel lens displays operate on the principle of the display described in Section **3.4.1)** [SCHW85]. Hattori describes another Fresnel lens display in a paper where several mechanically driven projector-pairs are located behind a large lens [HATT93]. This display was probably never built and the complete paper seems rather speculative.

3.4.4) Parallax

Parallax can be used in various ways in a headtracking display. In a method proposed by Hattori [HATT94b], a parallax barrier is used to block the light from a pair of projectors that form exit pupils by utilising a large convex mirror.

In the Varrier™ display of the University of Illinois, a physical parallax barrier with vertical apertures is located in front of the screen [SAND01]. The complete system can be considered as comprising two parts. These are: the *real* part, consisting of the display, a barrier and the viewer's eyes; and the *virtual* part consisting of the image on the screen, a *virtual* barrier and a *virtual* projection point for each eye. In this system, the only object that is effectively fixed is the barrier. The eyes of the viewer move, and the image on the screen is controlled to direct a left and a right image to the appropriate eyes, by the output of a head tracker.

The image simulates the effect of two *virtual* projection points behind the screen passing through a *virtual* fixed barrier that is effectively just behind the screen. The system has the disadvantages that the horizontal resolution is reduced, only one viewer can be served and the display must have the RGB sub-pixels running horizontally (which means almost certainly it will be in the portrait orientation).

In the parallax display of New York University (NYU) a dynamic parallax barrier is located 100 millimetres in front of the display [PERL99] [PERL00] [PERL01]. The barrier is a fast SLM array that consists of a one-dimensional array of elements that

can block the light in selected vertical strips. Fig.3.23 shows the way in which a viewer in two different positions can see parts of left and right images from each eye. The appearance of the barrier transmission structure is eliminated by rapidly cycling the barrier through three different positional phases for every frame. The image on the screen is changed at the same rate in order to present the appropriate image to each eye.

The fast frame rate required by the image is obtained by using Texas Instruments' Digital Light Processor (DLP) that can handle sequential RGB. This is a projection system that incorporates a Digital Micromirror Device and enables monochrome images to be presented at three times the normal frame rate. A ferroelectric shutter in front of the projector lens blocks the light in the period the barrier is switching. The barrier is a custom-built pi-cell liquid crystal screen.

An IBM BlueEyes tracker, that uses infrared reflection from the viewer's retina, controls the barrier. Future versions of the display will use full-colour CRT monitors. The display can only support one viewer.

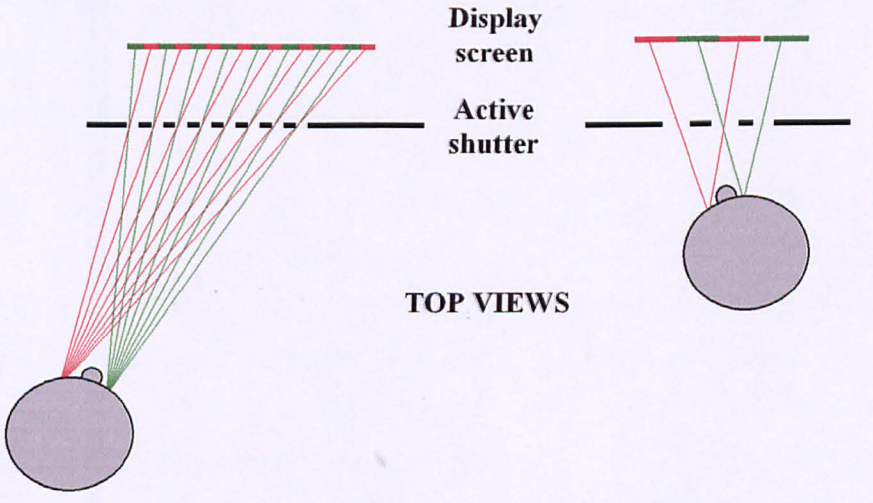

FIG.3.23 NYU PARALLAX BARRIER DISPLAY

3.4.5) Other Methods

There are several methods of producing a head tracking display, amongst these are prismatic arrays, macro-lens arrays and holographic optical elements (HOEs). Dresden University have developed a display that replaces a parallax barrier with a prism array [SCHW98]. Tracking is achieved by switching the images on the RGB sub-pixels. This enables the display to be used in the normal landscape orientation. In order to prevent crosstalk, four sub-pixels are allocated to each image pixel. The prism is designed to present all of two sub-pixels, for instance the G and B, and parts of two R pixels. This arrangement enables the pixel positions to be shifted in increments of one sub-pixel pitch, but lowers the horizontal resolution by a factor of 3 / 8. The prism pitch is slightly less than 8 / 3 of the pixel pitch. The display is a compact method of providing a single viewer with stereo, with no moving parts required. Also, the prism array allows more light throughput than a parallax barrier.

A method using an array of convex lenses has been proposed by Hattori [HATT95]. The drawings in the paper show an array of 100 convex spherical lenses with a monochrome panel behind it. Exit pupils are formed by selectively illuminating regions on the monochrome panel in accordance with the viewer's head position. Field sequential and spatially multiplexed versions are proposed. The field sequential version utilises a fast LCD and the spatially multiplexed display, a micropolarizer array. No further references to this technique have been found by the author, so it is probable these were never built.

Exit pupils can also be produced by HOEs. The method used by RealityVision has the advantage that a single HOE performs both the exit pupil formation and the image multiplexing [TRAY96] [TRAY97]. The HOE produces the left exit pupil by passing the light through the left rows of LCD pixels, and the right exit pupil through the right lines as shown in Fig.3.24. A vertical plane is formed in front of the screen where a left image can be seen to the left, and vice versa. When this plane lies between the viewer's eyes, stereo is seen, When both eyes are outside of the zone shown in the figure, either a left image, or a right image only is seen. The stereoscopic viewing zone can be made to follow the viewer's head position by moving the light source. The use of white LED array for this purpose is under investigation.

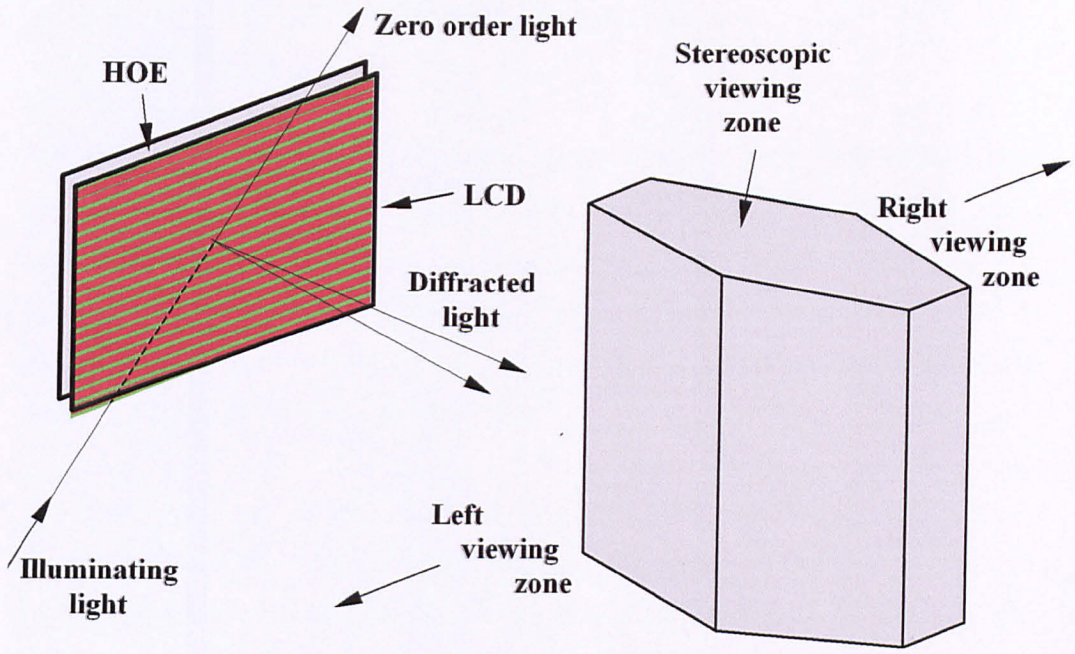

FIG.3.24 REALITY VISION HOE DISPLAY

3.4.6) Summary of Head Tracking Methods

Although there is a large amount of research into head tracked 3D displays, there are very few methods that have the potential to be developed into a multiple viewer display suitable for television. Any display that uses a Fresnel lens has a limited area over which exit pupils can be formed. This is due to spherical aberration of what is essentially a single refracting surface. Although some of these displays are *claimed* to be multiple-viewer [BENT99] [HATT00a], the author's experience with large Fresnel lenses suggests that the viewing area is unlikely to be sufficiently large to comfortably support even two viewers. Similarly, any method utilising a lenticular screen will suffer from the same problem. The geometry of the parallax methods described does not allow any of them to serve more than one viewer.

Some projection methods have the potential for multiple viewer operation, but these would require extremely large housings. The HOE method of RealityVision could possibly used for more than one viewer provided the pupils can be formed over a sufficiently wide angle. The inventor of this display, David Trayner, says that pupils can be formed up to 30° off-axis, but no multiple-viewer version has yet been built.

CHAPTER 4
FOLDING MIRRORS

4.1) Preface

The optics of the prototype 3D display requires the illumination to be positioned some distance behind the screen. In the case of the simple single-viewer prototypes under construction, Fresnel lenses form the exit pupils. The focal lengths of these cannot be too short as this will cause excessive spherical aberration. In order for the housing to be kept to a reasonable size, folding is carried out by using a series of horizontally aligned mirrors that fold the light vertically.

The more advanced steering optics of the multiple-viewer version that will be constructed under the ATTEST programme are, in effect, a large lens located behind the LCD and in the position indicated in Fig.4.1. The width of the optics would need to be in the region of around three times the screen width in order to provide the large viewing area necessary. This width can be reduced by the use of two additional vertical mirrors that are on either side of vertically folding mirrors, and in contact with their edges. In this chapter the procedure for the folding design is described, and the effectiveness of this folding – the folding efficacy – is discussed. The mirror assemblies that have been constructed are also described.

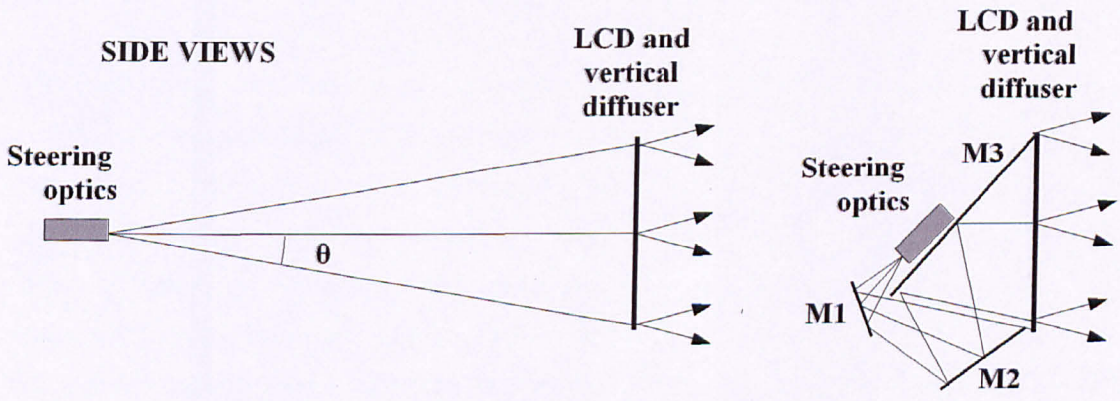

(a) Without Folding (b) With Folding

FIG.4.1 REDUCTION IN HOUSING DEPTH

In Fig.4.1 the effect of vertical folding is illustrated. In this case, the angle θ is 10°. It can be seen that the depth of the region that contains the optical path is reduced by a factor of around three. Another advantage of this configuration is that it allows the steering optics to have considerable depth, and still be accommodated above the mirror **M3**.

4.2) Vertical Folding Design Procedure

The folding operates by producing the series of virtual images as illustrated in Fig.4.2. **V1** is the virtual image of the steering optics in mirror **MI**, **V2** is the virtual image of **V1** in mirror **M2** and **V3** is the image of **V2** in mirror **M3**. As optics software was not available for this research, a graphical solution for the design was sought. Initially, the positions of the mirrors were drawn full size on a sheet of graph paper, and ray tracing used to determine the light paths. This process proved to be both tedious and inaccurate.

A simpler method is to simulate the folding of the light by actually folding a sheet of paper. If a triangular sheet of paper, whose apex is at **V3**, is attached to the figure at the position of the screen, it can be seen that by folding it at the position of **M3** will move the apex to **V2**, therefore simulating the function of the mirror. This procedure is repeated for **M2** then **M1**, therefore giving the position of the steering optics.

The method is used to find the steering optics and mirror positions for a given screen height and emergent angle from the optics. In practice, the light will exit from the optics over a height in the order of several centimetres in order to allow for image multiplexing – the reason for this will be made clear in Chapter 5. This means the shape of the paper will actually be trapezoidal, not triangular. Allowance has to be made for glass thickness and inaccuracies in construction. When this method is used to design a mirror layout, optimum mirror positions could be obtained in around fifteen minutes. The technique can be used for any number of mirrors.

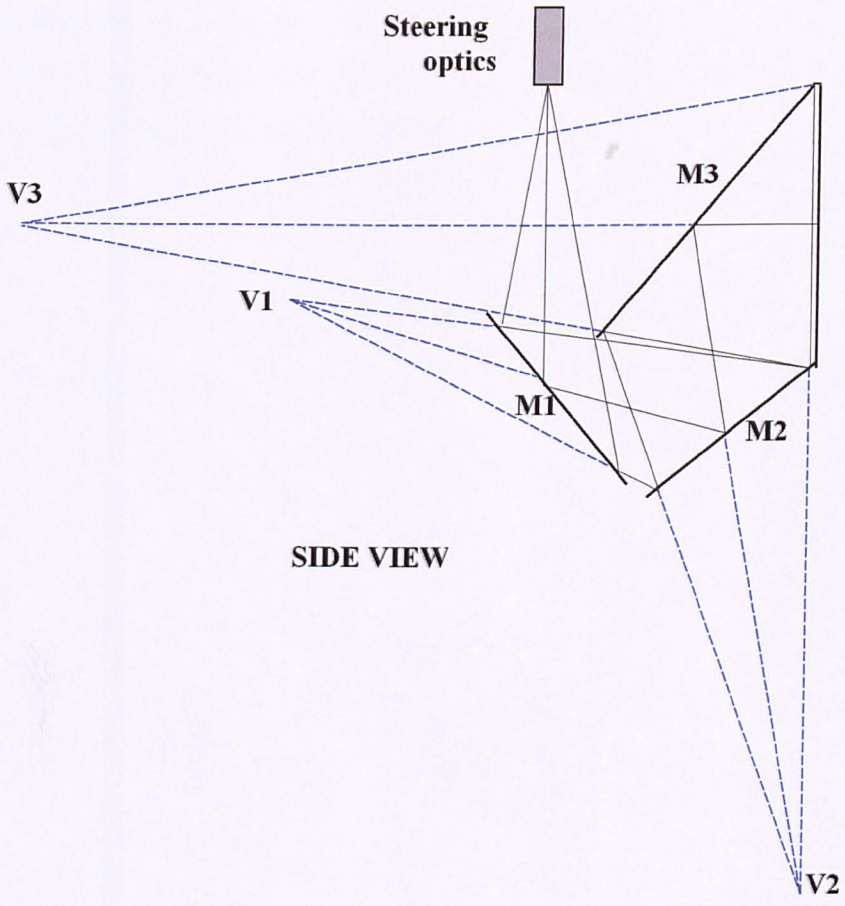

FIG.4.2 VIRTUAL IMAGES IN FOLDED OPTICS

4.3) Folding Efficacy

The effectiveness of the folding can be determined by assessing the total area of the cross-section where the rays are overlapping. In a set-up such as this, it is not possible to have light travelling in more than two different directions at any one point. Although it is not possible to achieve in practice, the maximum possible efficacy is 100%.

In Fig.4.3 the simple case of folding with one mirror is considered. The total area of the light path is the trapezium ABCD is denoted by A_{ABCD}. The area over which the light is folded most effectively is the area within EFGH, which is A_{EFGH}. The efficacy E_F is given by –

$E_F = A_{EFGH} / A_{ABCD}$

This is the ratio the area over which the optimum folding occurs, to the total cross-sectional area of the light path between the steering optics and the screen. The triangle EFH is a mirror-image of the triangle FGH.

Therefore -

$A_{EFGH} = 2.A_{FGH}$

And –

$E_F = 2.A_{FGH} / A_{ABCD}$ .....(4.1)

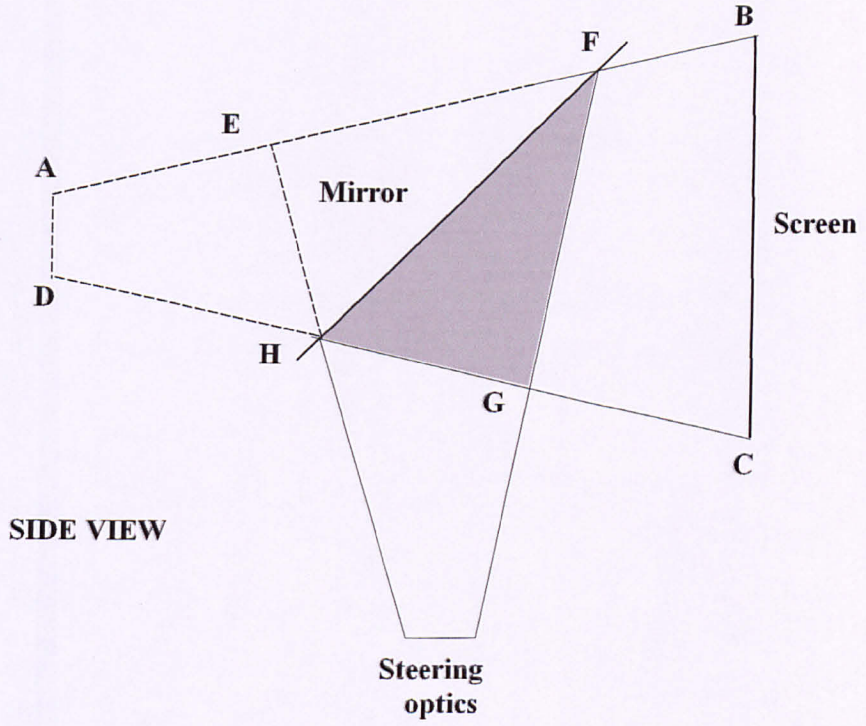

FIG.4.3 FOLDING EFFICACY WITH SINGLE MIRROR

Equation (3.1) shows that E_F is given by multiplying the shaded area by two, and dividing this the area of the trapezium enclosing the total light path area. When there is more than one reflection, as in Fig.4.2, double the sum of the shaded areas is divided by the total area A_{ABCD} in order to obtain E_F. This can be conveniently calculated by summing the products of the heights and base widths of the overlap triangles and dividing this sum by A_{ABCD}.

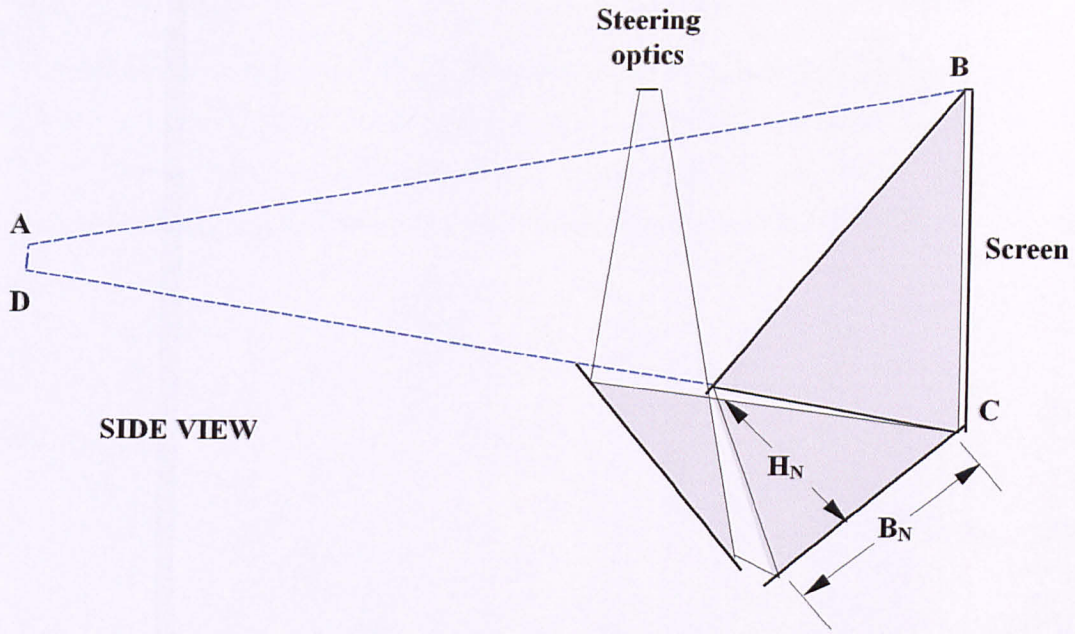

FIG.4.4 FOLDING EFFICACY WITH 3 MIRRORS

If H_N and B_N are respectively the height and base lengths of the overlap triangle adjacent to the N^{th} mirror then in a system with M mirrors, the total area of the triangles is -

$$\text{Total area} = \sum_{N=1}^{N=M} H_N B_N / 2$$

Substituting this into equation (4.1) gives –

$$E_F = \frac{\sum_{N=1}^{N=M} H_N B_N}{A_{ABCD}} \quad \ldots\ldots\ldots (4.2)$$

4.4) 12" Prototype Folding

The 12" prototype uses a Fresnel lens to form a pair of exit pupils seen by a single viewer who has limited lateral head movement. In the first version, the light source consists of a pair of 150-watt linear halogen lamps that are positioned by a mechanism driven by a stepper motor. As the movement of these lamps is limited, the light source can be contained within the width of the housing so that horizontal folding mirrors are not necessary.

The focal length of the lens is 457, millimetres and the optimum viewing distance is 1.11 metres from the screen. This requires the lamps to be 777 millimetres behind the lens. The screen height of 213 millimetres gives an angle θ of only 8°. In order to reduce the housing size for this small angle, six folding mirrors are used as in Fig.4.5.

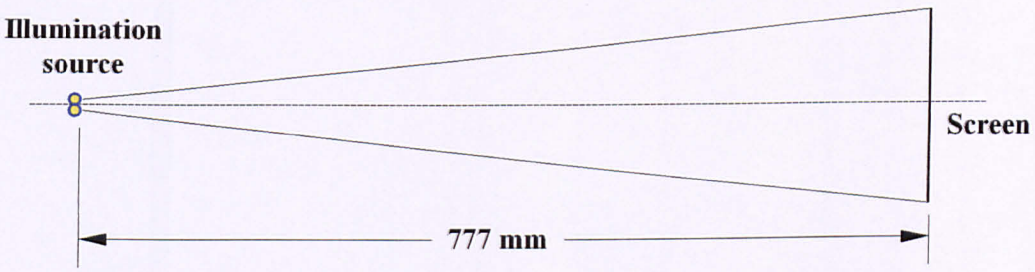

(a) Without Folding

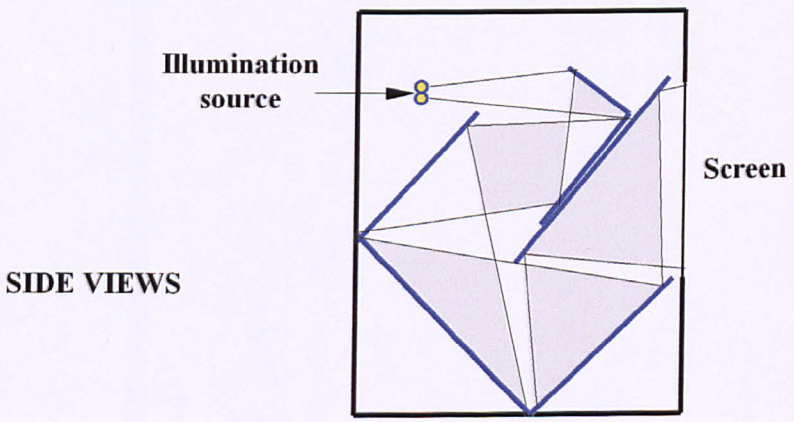

(b) With Folding

FIG.4.5 12" PROTOTYPE FOLDING

Measurements of areas made on the actual full-sized drawing used to design the prototype yielded a total area of overlap triangles of 34,500 square millimetres and a trapezium area of 82,080 square millimetres. This gives a value of E_F = 84%. This could be better but it does enable the display to fit into a housing that appears to be a reasonable size in relation to the screen dimensions.

In order for the prototype to be low-cost, ordinary mirror glass that is silvered on the back is used. As reflections off the front surfaces can affect the image multiplexing, and consequently possibly increase the crosstalk, it is worth carefully considering these reflections. Fig.4.6 is a simplified representation of the reflections. The thickness of the glass has been exaggerated in relation to the mirror separations, but this does not affect the result. Also, all the mirrors are shown as being at 45° to the horizontal, whereas they are slightly different to this in the actual display.

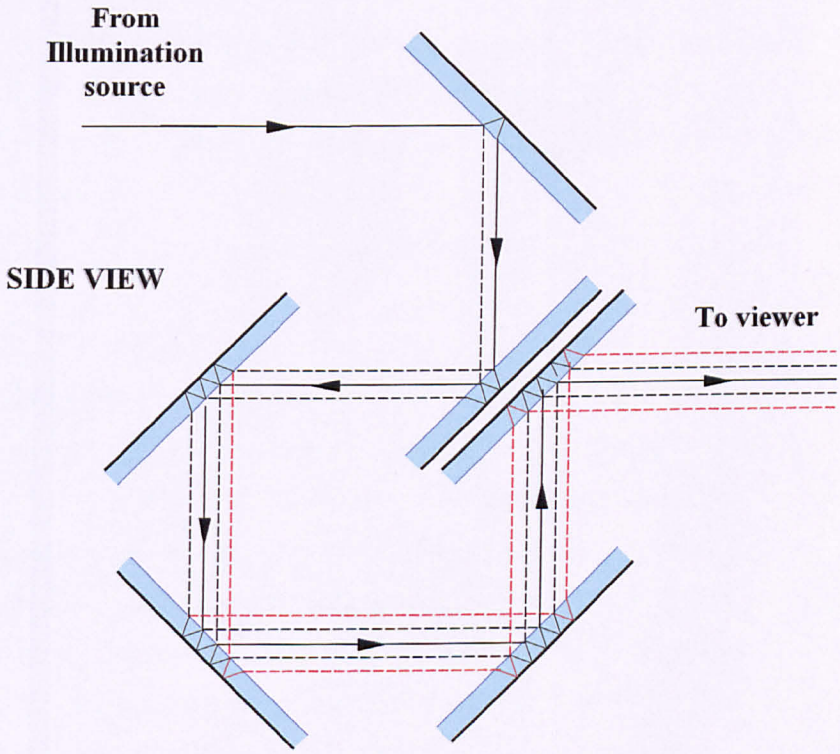

FIG.4.6 SURFACE REFLECTIONS IN 12" PROTOTYPE

In Fig.4.6, the unbroken line denotes the ray that is reflected only by the silvering. The broken lines adjacent to this are formed from either a single surface reflection, or by this ray being reflected by the silvering of the next mirror along. The broken lines that are the second out from the central unbroken line are formed by secondary reflection – that is by being reflected from two front surfaces. If, for example, 5% of

the light is reflected by the front surface, the secondary reflection will only be 0.25%. Reflection on the internal surfaces of the glass is assumed to be negligible in this application.

The secondary reflections are assumed to be sufficiently small to be neglected. However, when the primary front surface reflections are taken into account, the design of the image multiplexing parallax barrier will be affected. For a refractive index of 1.5 and a mirror angle of 45°, the surface reflection is displaced by 0.76 x T_M where T_M is the thickness of the mirror. The mirrors used are three millimetres thick, so that the images produced by the surface reflections are displaced 2.3 millimetres from the main images. The most important implication of this is the reduction of the value of R_A, the ratio of light passing with and without the barrier, of the parallax barrier due to the fact that the effective gap between the light sources G in Equation (5.5) is decreased.

4.5) Fully-folded Optics

A multiple-viewer 3D display requires the light to exit the screen over a wide angle, possibly up to 45° in a TV display. As the steering optics cannot be located immediately behind the screen, they have to be wide in relation to the screen as in Fig.4.7 (a). It is envisaged that the steering optics will be able to place any number of exit pupils over a large area. The viewer shown can either receive light from wide steering optics as in Fig.4.7 (a), or from narrower optics but with the light illuminating the right side of the screen originating from a virtual image of the optics as in Fig.4.7 (b). A vertical mirror, that is at right angles to the optics, produces this image. A mirror parallel to this is positioned on the other side of the display enabling a large viewing region from optics that are only slightly wider than the screen

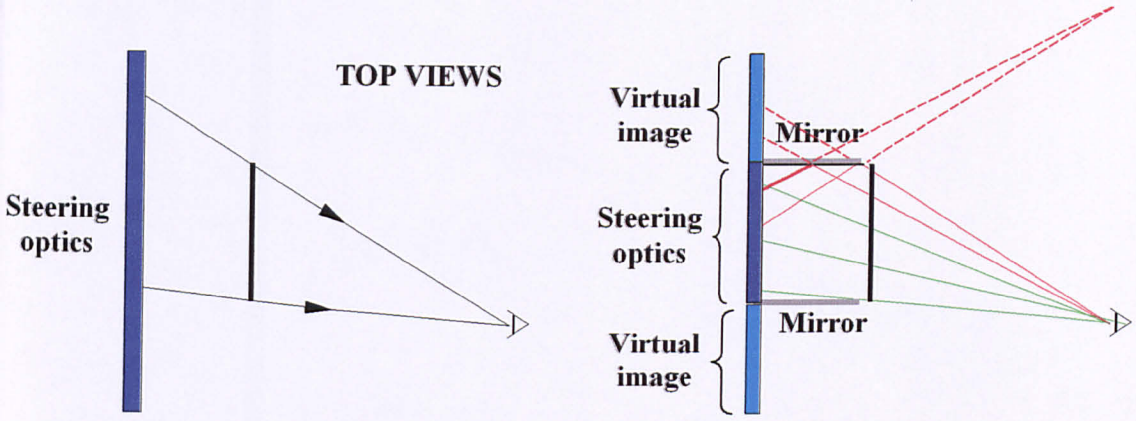

FIG.4.7 HORIZONTAL FOLDING

Given the fact that the steering has the ability to place multiple exit pupils over a large area, it can be seen that the use of side folding mirrors can be used to reduce the optics width. It is less obvious that side-folding mirrors can be used in combination with the vertically folding mirrors.

A convincing demonstration that this is possible can be given by positioning two mirrors as in Fig.4.8 where a mirror at 45° to the horizontal is mounted with one edge in contact with a vertical mirror. A series of numbers, placed underneath the mirror as shown, will produce the upper virtual image. The right portion of this image exhibits lateral inversion as the image is produced in only the angled mirror. The numbers '6' to '10' do not show inversion as they are formed by reflection from both mirrors.

Numbers '6' to '8' in the vertical image are formed by an image being reflected first from the angled mirror, and then by the vertical mirror: and numbers '9' and '10' formed by reflection from the vertical mirror being observed via the angled mirror. The net result of the two mirrors is of the numbers being in the position of the inverted image in M_A, with a vertical mirror being mounted to its left, and at right angles to it.

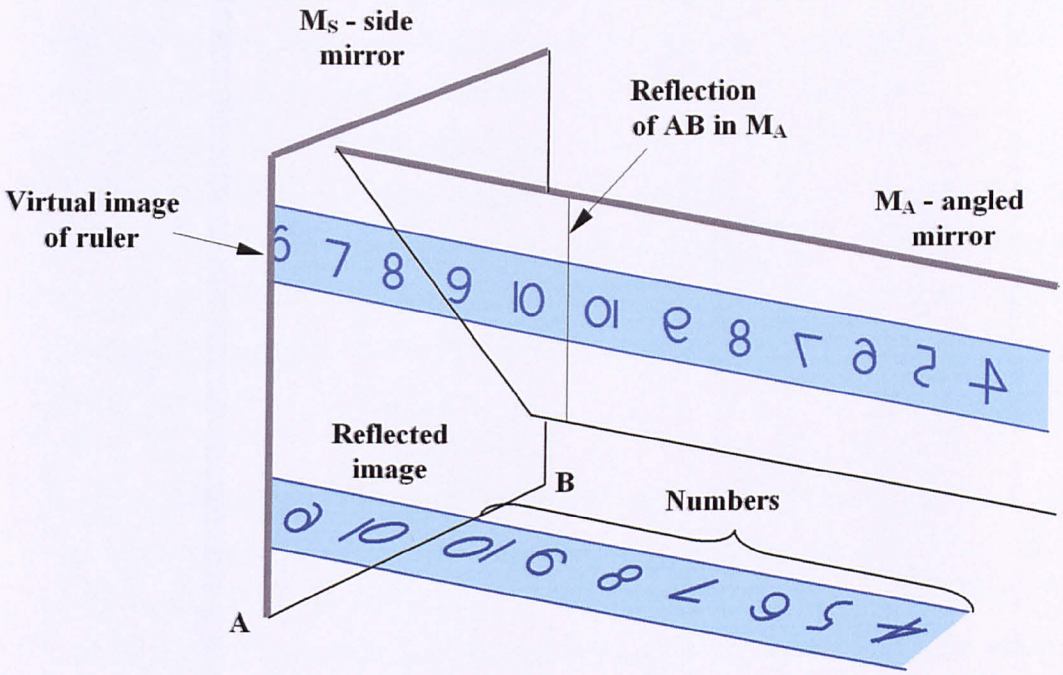

FIG.4.8 REFLECTION IN ORTHOGONAL MIRRORS

A demonstrator showing the operation of a five-mirror folding system was constructed with a 'screen' 43 millimetres square, and illumination supplied by a ten-watt bulb. The five-mirror configuration is the same as will be used for the ATTEST multiple-viewer prototype.

The steering optics are simulated by a strip of paper with the words 'LEFT' and 'RIGHT' printed on it. A bulb located behind the strip lights this, and the paper diffuses the light. The words are printed on the side of the paper that is illuminated so that they appear laterally inverted when viewed from the front. As there is an odd number of vertically folding mirrors, the words are laterally inverted in order to appear the right way round as Fig.4.9 shows. This is consistent with the lateral inversion produced with the single angled mirror in Fig.4.8. The central region, where the words appear the correct way round, is an image formed by reflection in the vertically folding mirrors only.

The images to either side of this, where the words are inverted, are formed by light being reflected by both the side mirrors and the vertically folding mirrors. As is the case with the two-mirror demonstration, the image has the appearance of a central region with a vertical mirror mounted at its edge and at right angles to it. Even though the image reaches the eye via several different paths, it has the appearance of having come from one mirror. A faint line can be seen between the 'T's of the 'RIGHT' and the inverted 'RIGHT' – this is the point of contact between the virtual central image and a virtual side mirror. Light to the left of this line reaches the eye via the vertically folding mirrors only.

As there is a mirror either side, the complete mirror assembly behaves in the same way as a mirror-pair. When the aperture is viewed from extreme left or right positions, a further non-inverted image is seen beyond the inverted one. However, this is not of any practical interest as the screen will not be viewed from such a large angle from the axis.

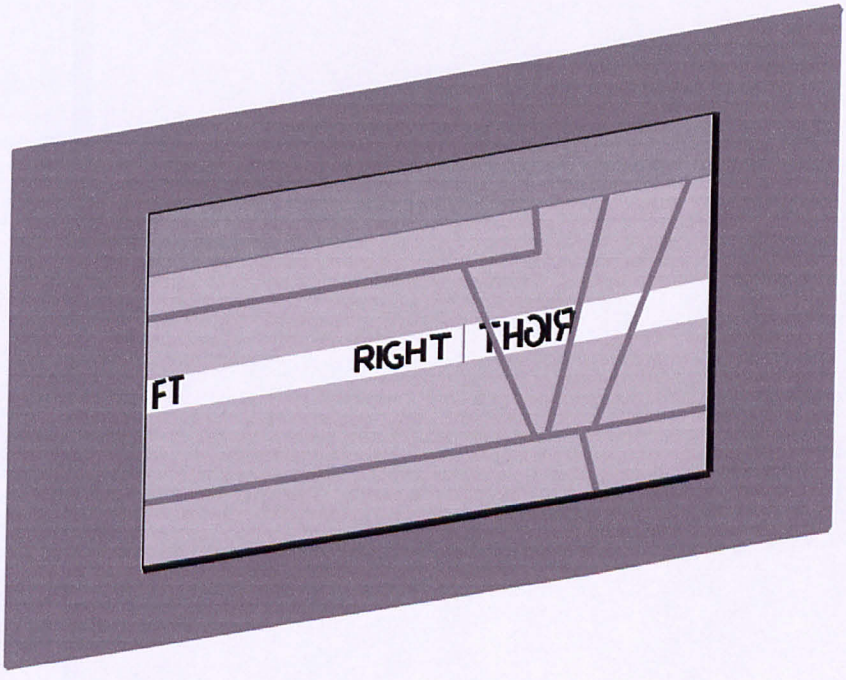

FIG.4.9 FOLDING DEMONSTRATOR WITHOUT DIFFUSER

Fig.4.10 illustrates the way in which unfolded optics can be developed into a compact display that is suitable for TV use. Fig.4.10 (b) shows how the width can be reduced. The separation between the mirrors must be greater than the width of the screen in order to prevent very oblique rays passing through the edges of the screen. Also, the steering optics will have to be wider than the mirror separation to allow for the formation of extreme off-axis exit pupils. No work has been carried out yet on the amount of increase in mirror separation over screen width, but some allowance will have to be made for this in future work.

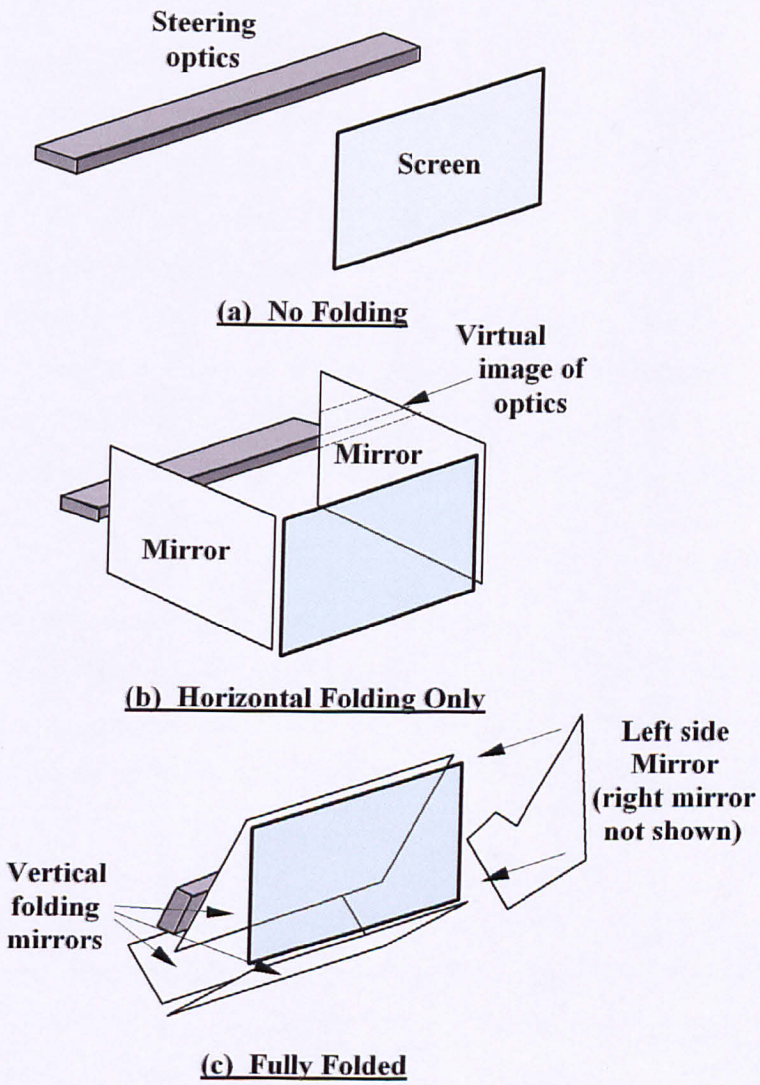

FIG.4.10 DEVELOPMENT OF FOLDING OPTICS

The three vertically folding mirrors of Fig.4.10 (c) enable the housing size to be reduced to a size that is comparable to current back projection TVs. The actual size of the housing is very dependent on the angle θ. Models have been constructed for θ = 12.5° and θ = 15°. These are very useful in visualising the appearance of the display. For θ = 15° the housing is compact, even though it is nowhere near 'hang-on-the-wall'. In the figure, the left side mirror is not shown and the right mirror is shown exploded.

4.6) 14" Prototype Platform

A folding optics assembly suitable for accommodating a 14" display has been constructed using surface-silvered mirrors. The mirrors are laid out as in Fig.4.11. This does not give the optimum folding for the most compact design, but at the time of its design it was envisaged that this layout would be convenient, as having the steering optics being mounted on top of the assembly allows easy access for experimentation. Also, the side mirrors are of an easily-constructed rectangular shape. The value of E_F obtained from the design drawing is only 0.623, but this is not really an issue with this model as the object of the design was to produce an assembly where the steering optics is easily accessible.

Although this platform will probably never be used in an actual display as a 21" version is being built under the ATTEST programme, it has proved very useful in determining potential problems and construction techniques. The assembly allows fine adjustment of mirror positions to be made. This is essential in order to eliminate the appearance of the mirror junctions.

A two-foot 36-watt fluorescent tube provides illumination for the platform and is contained in a housing that allows light to exit through a six-millimetre wide gap. The lamp assembly is detachable and merely rests on the top of the folding assembly. When the illuminated, a continuous band of light is observed that appears to be located 760 millimetres behind the screen

The mirrors used were cut to size using conventional glass cutting methods. This results in an edge that is not exactly at right angles to the mirror surface. The consequence of this is that there is a gap between the sides of the vertically folding mirrors and the side mirrors. This has not been measured accurately, but is variable and it is estimated that is that it is a maximum of around 200 microns.

The effect of this gap is not obvious until a horizontally aligned lenticular sheet is placed in the screen position. This performs the function of the vertical diffuser and gives the appearance of noticeable curved dark lines running across the screen. This would be unacceptable in a display application.

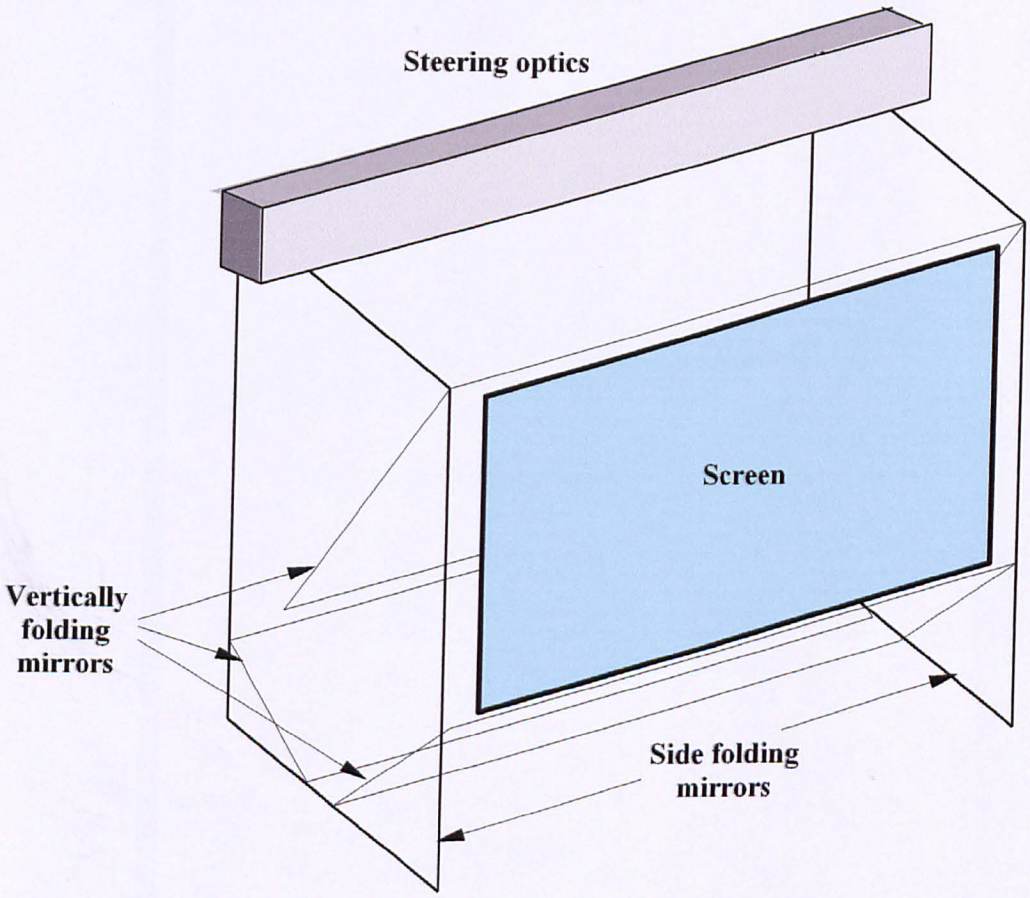

FIG.4.11 14" PROTOTYPE FOLDING

The importance of mirror alignment is also emphasised when the vertical diffuser is placed in position. Ideally, the illumination will have no discontinuities. Any slight discontinuities will show up as either dark or bright curved lines on the diffuser. In Fig.4.12, the effect of the right section of the image appearing to be higher is shown. A lenticular diffuser scatters light in the vertical direction only, therefore summing the light in any vertical plane.

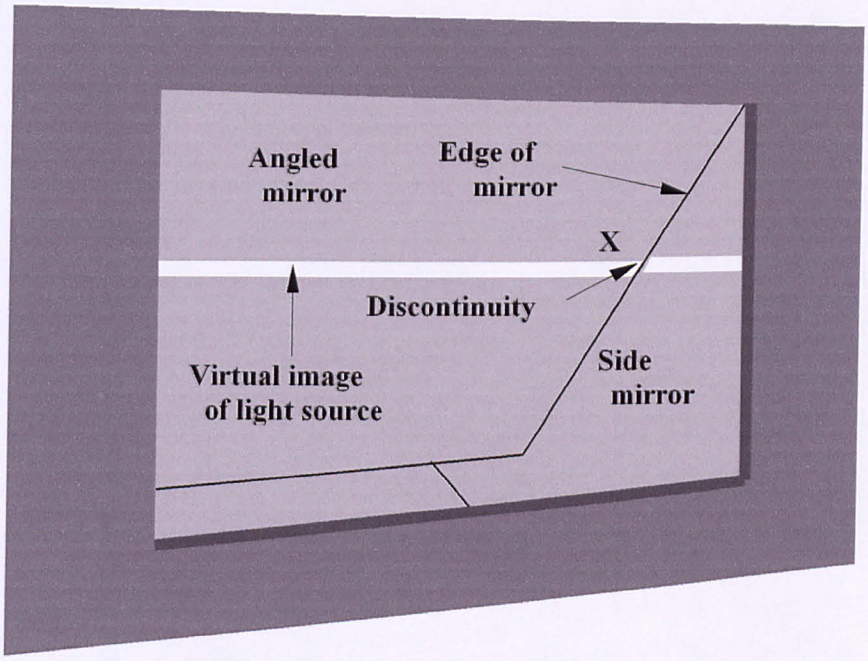

(a) 14" Folding Mirror Platform

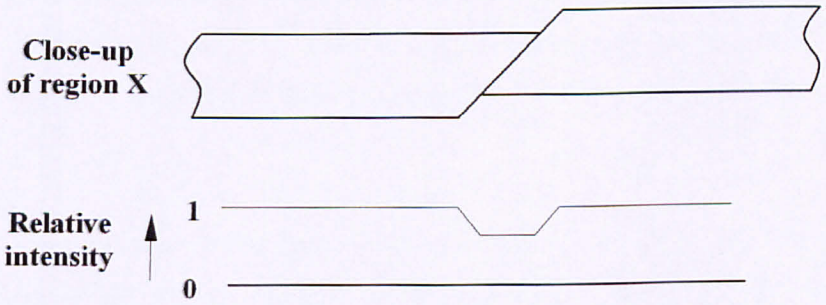

(b) Close-up and Intensity after Vertical Scattering

FIG.4.12 DISCONTINUITY AT MIRROR CORNERS

When the images are displaced, as Fig.4.12 (b) shows, the overlap gives rise to a dark region. When the total intensity in any vertical direction is summed as shown in the lower figure, it can be seen that there is a region of lower intensity. Conversely, when the right side of the image is displaced downwards, the opposite occurs and a bright line is formed. The images of the mirror-edge discontinuities appear curved as the lenticular sheet is not a perfect vertical diffuser and has some deviation in the horizontal direction when incident light light is not orthogonal to its surface (this is considered in detail in Chapter 7).

4.7) Conclusions

As the ultimate aim of this research is the design and construction of a 3D display that is suitable for TV use, it is desirable that it is contained within a housing that is compact. It is unlikely that the next generation of 3D TV is going to be 'hang-on-the-wall', however, it certainly must be no larger than current TV sets. Whilst it is not particularly important for the folding efficacy to be maximised in a prototype, it is essential in a consumer electronics product that will sell in millions of units. Careful design should yield an efficacy well in excess of 90% in a five-mirror folding assembly.

The precision that will be required in order to give an image of the steering optics with no visible discontinuities is possibly a cause for concern if this arrangement is going to be used in products that can be manufactured in high quantity at low cost. However, the problem is similar in nature to that of tiling two LCDs such that the join between the two is invisible. Several manufacturers have now solved this problem successfully.

Another anticipated problem that has not been covered within this research is that of the reflectivity of the mirrors being somewhat less than 100%. This will produce vertical banding in the image where the central region will be the brightest, and the regions to either side, where the inverted images of the steering optics are observed, appearing dimmer. The use of high reflectivity side mirrors should minimise this effect.

CHAPTER 5

IMAGE MULTIPLEXING BARRIER GEOMETRY

5.1) Preface

The prototypes described in Chapters 9 and 10 employ spatial multiplexing, where left and right images are presented on alternate rows of pixels. A left-image exit pupil is produced in the region of the viewer's left eye, and a right exit pupil at the viewer's right eye. This requires some means of separating the light from two sets of illumination sources on to the appropriate pixel rows.

The simplest method of achieving this is to place a screen with horizontal apertures between the steering optics and the LCD. Fig.5.1 shows that the light from the upper illumination source can only fall on the pixel rows marked L, and light from the lower source on those marked R. The light is then scattered in the vertical direction only by a vertical diffusing element. In this figure, the distance D has been exaggerated in relation to the distance A for the sake of clarity. In practice A will be in the order of hundreds of millimetres, and D, millimetres.

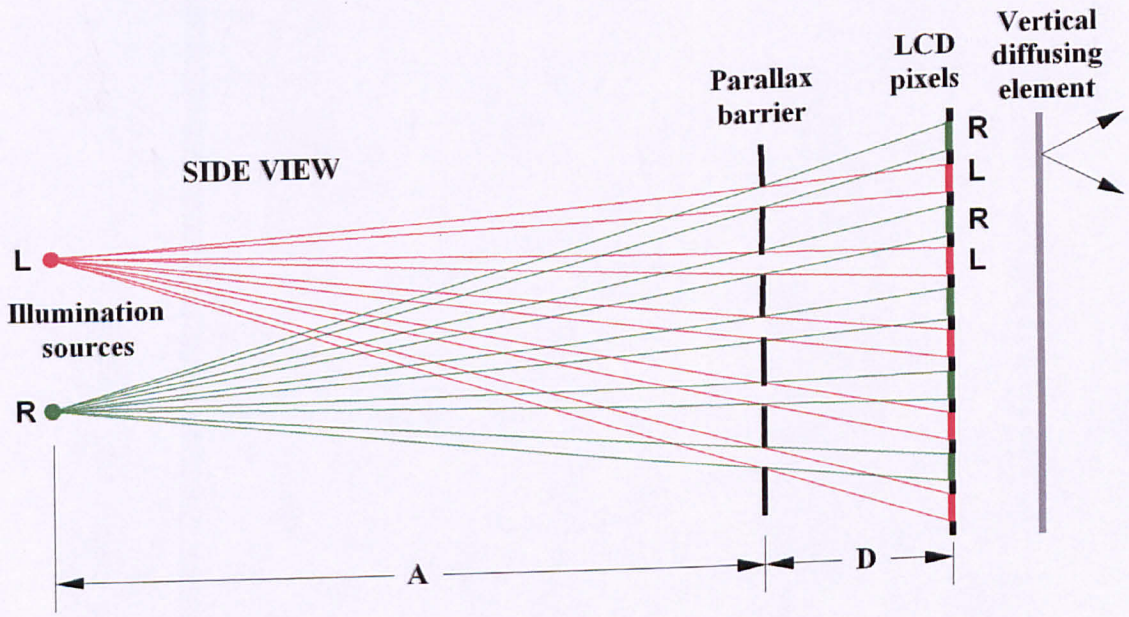

FIG.5.1 PARALLAX BARRIER IMAGE SEPARATION

The light throughput can never be more than 50% with a parallax barrier as light must be blocked to half the pixel rows. However, the reason for choosing this method of image multiplexing in the prototype is it that is inexpensive to produce, and is sufficient to prove the principle-of-operation. The geometry determining the dimensions and efficiency of the barrier is examined in this chapter.

5.2) Exit Pupil Formation

In Fig.5.2, if the L illumination source only is lit, it produces a real image at the centre of the L exit pupil if the Fresnel lens and LCD only are in place. When a viewer's eye is located in this position, it will see an image that is formed by every row of the LCD over the complete area of the screen. If left and right images are presented on alternate rows of pixels, both will be seen. With the addition of the vertical diffusing element, the images will be seen when the eye located in any position over the complete height of the pupil.

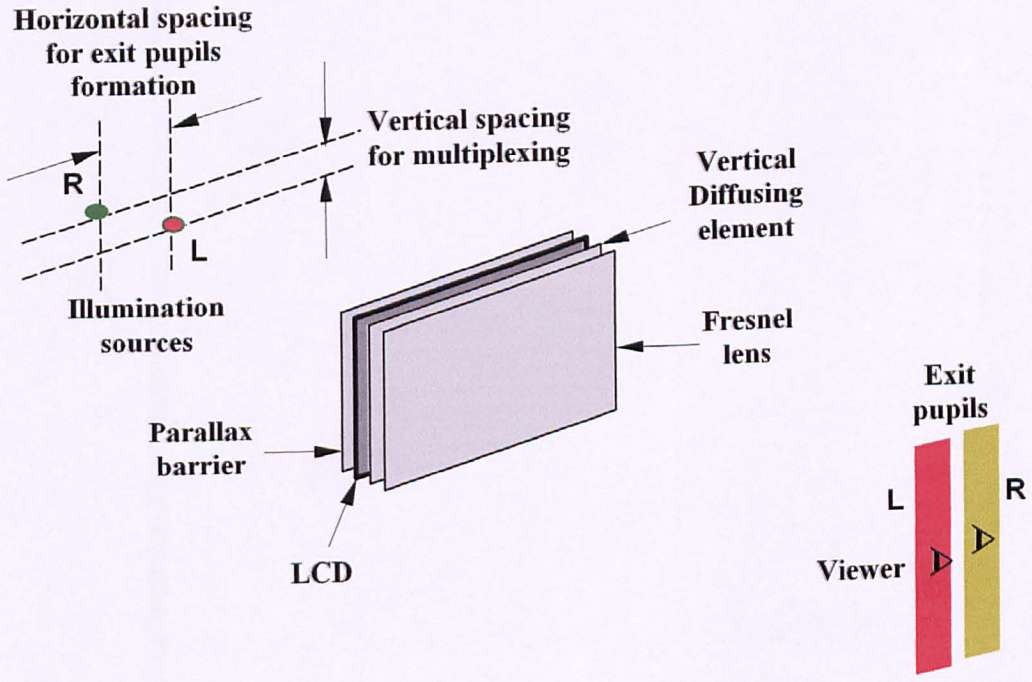

FIG.5.2 RELATIVE POSITIONS OF LIGHT SOURCES

When the multiplexing barrier is added, the left-image only will be seen over the complete area of the screen by an eye located in the L exit pupil region. When the R illumination source is also lit it will produce the vertical exit pupil R. As it is displaced to the left of the L source, this exit pupil is located to the right of exit pupil L. Being situated on a different vertical plane, the light from this source only falls on the rows of pixels that show the right image.

5.3) Aperture Height and Barrier / LCD Separation

Fig.5.1 shows the illumination sources as being small. In this case it can be seen that the height of the apertures could be as much as around half their pitch without light passing to adjacent rows of pixels. The small sources are also able to illustrate clearly the operation of the barrier. In the prototype, the height of the sources is not negligible in relation to their vertical separation, and this has to be taken into account when calculating the barrier dimensions. In Fig.5.3 the extreme rays determining the height of the apertures are shown.

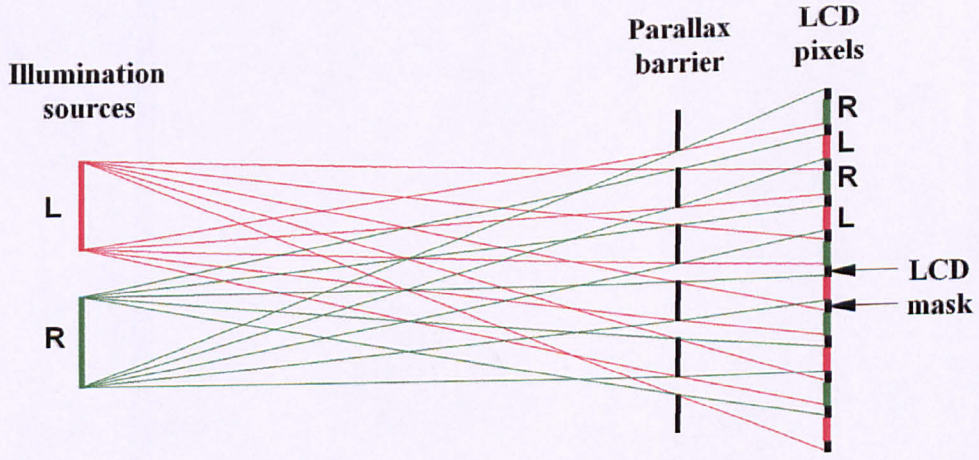

FIG.5.3 EXTREME RAYS IN PARALLAX BARRIER

As this figure shows all the extreme rays, the procedure for deriving the equations is not very apparent from this. It is made clearer by separating the two sets of limiting rays as in Fig.5.4. In Fig.5.4 (a), the rays from the inner edges of the sources are shown. Rays from the lower edge of source L are prevented from reaching the R pixels by the upper edges of the apertures. Conversely, rays from the upper edge of the source R are blocked from the L pixels by the lower edges of the apertures.

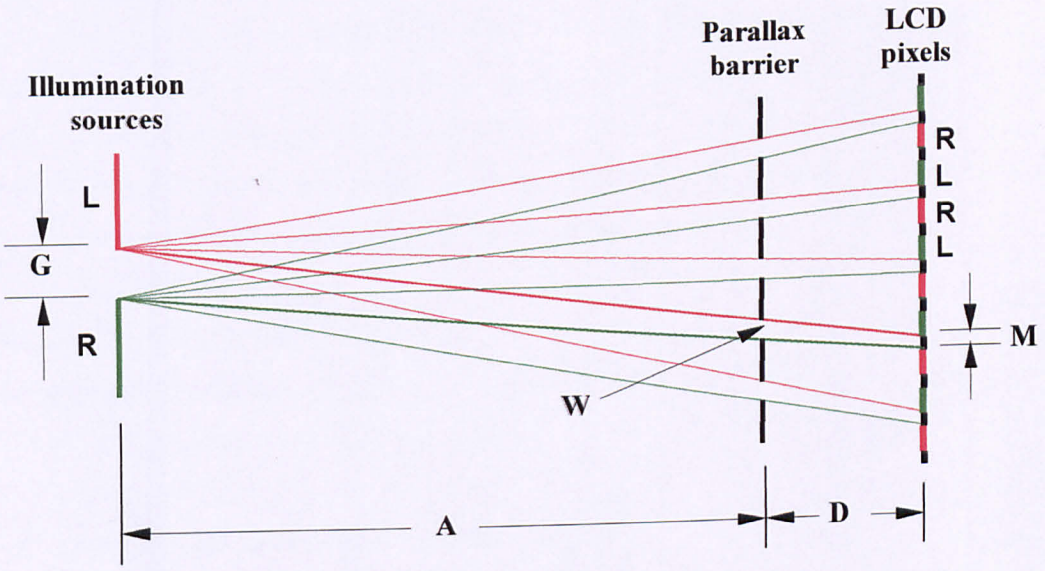

(a) Rays Determined by Illumination Spacing

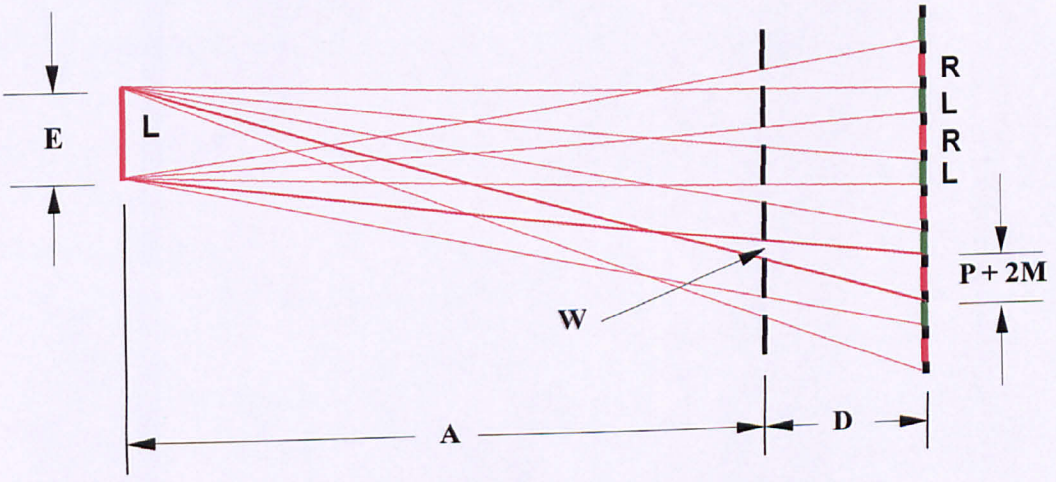

(b) Rays Determined by Illumination Height

FIG.5.4 LIMITING RAYS IN PARALLAX BARRIER

Referring to Fig.5.4 (b), where light from the edges of the left illumination source is shown, rays from the upper edge of the source L are prevented from reaching the R rows of pixels by the lower edges of the apertures. Also light from the lower edge of the L source blocked from the R rows by the upper edges of the apertures.

The geometry of the barrier is more clearly explained with the diagrams in Fig.5.5. In Fig.5.5 (a), the ray from the top of the right illumination source is shown as being horizontal for ease of explanation. However, the same principle of similar triangles applies to positions on the barrier where this ray is not horizontal - in these cases the similar triangles are not right-angled. Similarly, in Fig.5.5 (b) the light from the lower edge of the source to the upper edge of the aperture is shown as being horizontal, but the same geometry applies over the complete height of the barrier.

The dimensions are as follows –

E = height of illumination sources

G = vertical gap between illumination sources

W = aperture height

A = illumination sources to barrier horizontal distance

D = barrier to LCD spacing

P = pixel aperture height

M = LCD horizontal mask height

Referring to Fig. 5.5 (a), by similar triangles –

$$(G - W) / A = (W - M) / D$$

Solving for W gives –

$$W = (D\,G + A\,M) / (A + D) \quad .....(5.1)$$

In 5.5 (b), by similar triangles –

$$(E + W) / A = (P + 2\,M - W) / D$$

Solving for W gives –

$$W = (A\,P + 2\,A\,M - D\,E) / (A + D) \quad .....(5.2)$$

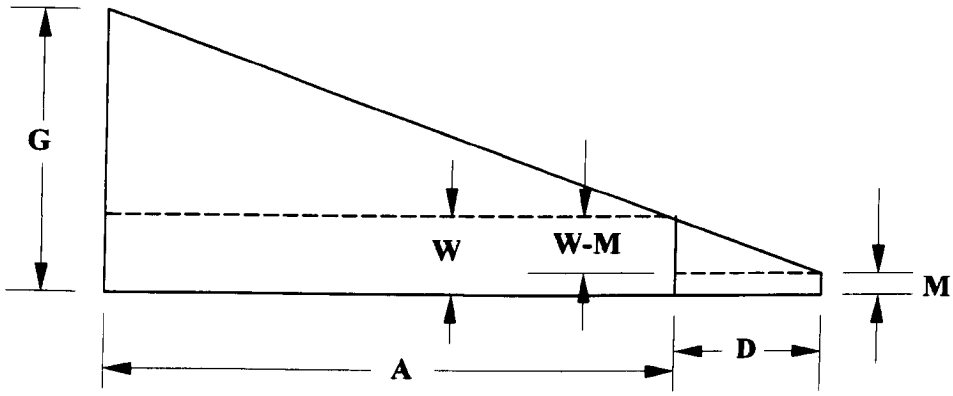

(a) Rays Determined by Illumination Spacing

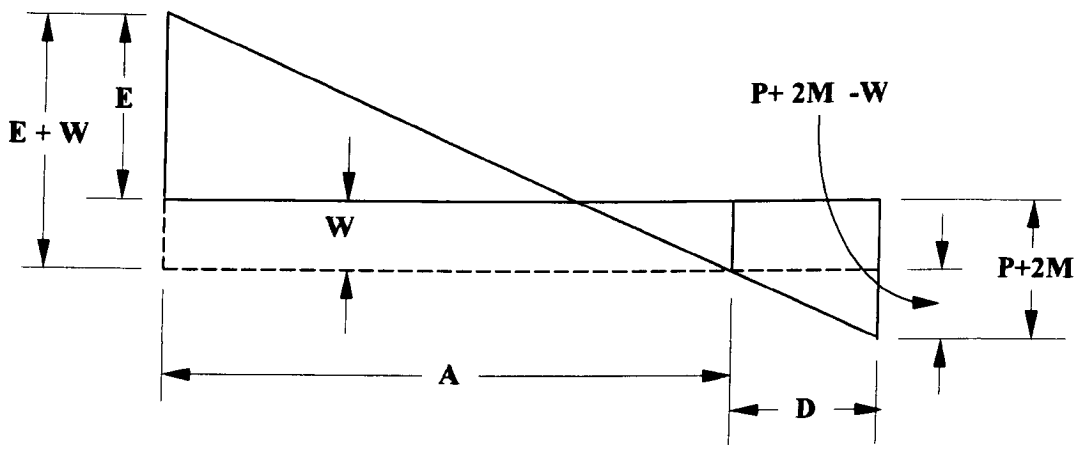

(b) Rays Determined by Illumination Height

FIG.5.5 GEOMETRY OF LIMITING RAYS

In Equations (5.1) and (5.2), the aperture height for two limiting cases is found. Equation (5.1) applies to height when it is determined by the vertical gap between the illumination sources, and Equation (5.2) by the height of the illumination sources. The values of P and M are set by the LCD dimensions. Although the dimensions of the illumination sources and their distance *can* be varied, in practice it is more convenient to keep them fixed. The one dimension that can conveniently be altered is the barrier to LCD spacing D.

The aperture height is optimised when the two methods of determining it are equal. The value of is found from this condition, i.e. when –

$$(D\,G + A\,M) / (A + D) = (A\,P + 2.A\,M - D\,E) / (A + D)$$

Solving for D gives –

$$D = A\,(P + M) / (G + E)$$

The pitch P_L of the LCD is equal to the height of the pixel aperture added to the horizontal mask height, i.e. –

$$P_L = P + M$$

Therefore, an approximate equation that does not allow for the LCD substrate thickness is -

$$D = A\,P_L / (G + E) \quad .....(5.3)$$

The distance of the illumination sources to the barrier is in the region of several hundred millimetres, and the barrier to LCD spacing only a few millimetres. Therefore $A >> D$. This simplifies Equation (5.1) to

$$W = D\,G / A + M$$

Substituting Equation (5.3) into this gives-

$$W = G\,P_L / (G + E) + M \quad .....(5.4)$$

This equation gives the absolute *maximum* value of aperture height before light from one of the illumination sources falls on the wrong pixel rows. If this occurs, crosstalk will result. In practice, the aperture height would have to be less than this. The most important factor determining this dimension would be the material used for the barrier. If it is made on a substrate glass that the same type as the LCD, the effect of differing thermal expansion coefficients should be negligible. In this case a relatively small allowance will be made and the aperture height closer to the value determined in Equation (5.4). This subject has not been investigated to date, but will be within the ATTEST programme.

Diffraction should not be a problem as the typical aperture height will be in the order of 0.2 millimetres. This height represents several hundred wavelengths, therefore the effect of diffraction at the barrier to LCD distance of a few millimetres will be negligible.

As the light throughput is reduced with the use of a parallax barrier, it is useful to know the amount of this reduction. An estimate of the relative throughput with, and without, the barrier can be determined as follows -

The proportion of light R_L passing through the LCD is given by –

$$R_L = P / (P + M) = P / P_L$$

Note that this does not allow for the light that is stopped by the vertical components of the LCD mask. However, this does not affect the *relative* light throughputs.

The barrier pitch is slightly less than double the LCD pitch, and is considered in detail in the next section. However, for the purposes of this analysis it can be considered as being equal to double the LCD pitch. Therefore, the light throughput R_B through the barrier is –

$$R_B = W / 2.P_L$$

The ratio R_A of light with and without the barrier is –

$$R_A = R_B / R_L$$
$$= (W / 2\,P_L) / (P / P_L)$$

Therefore

$$R_A = W / 2P \quad .....(5.5)$$

This applies when $R_B < 1$. R_A cannot be greater than 0.5 as light can only pass through half the pixel rows.

5.4) Barrier Pitch

As the barrier is located slightly closer to the illumination sources than the LCD, the aperture pitch will not be double the LCD vertical pitch, but slightly less. In Fig.5.6 the ray through the N^{th} aperture from the axis is shown. This passes through the barrier at a distance $N\,P_B$ from the axis, where P_B is the barrier pitch. Due to the separation D, it passes through the LCD at the slightly greater distance of $2\,N\,P_L$ from the axis. The distance D had been exaggerated in relation to A in order for the

difference to be visible on the figure. The difference between the centres of the N^{th} aperture and the 2 x N^{th} pixel from the centre is N (2 P_L – P_B).

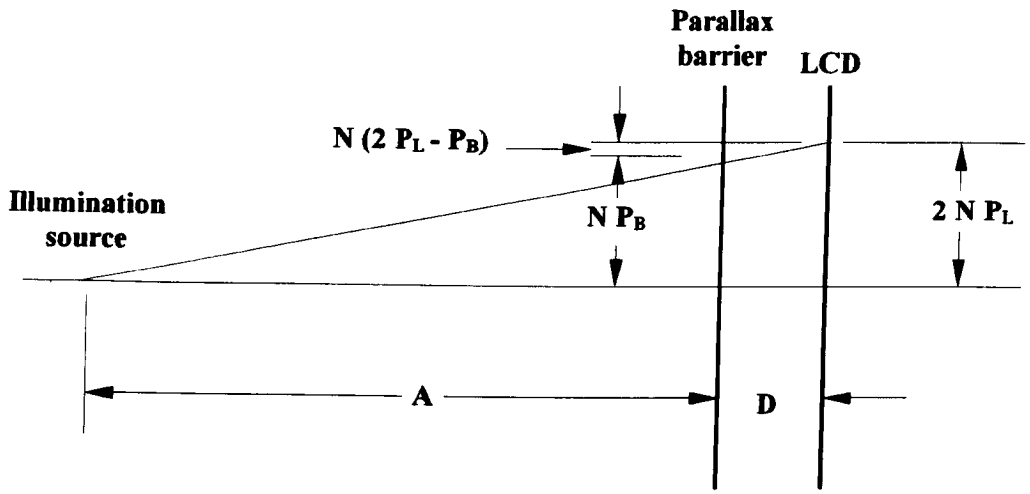

SIDE VIEW
(not to scale)

FIG.5.6 PARALLAX BARRIER PITCH

By similar triangles –

$$2 N P_L / (A+ D) = N P_B / A$$

Solving for P_B gives –

$$P_B = 2 P_L A / (A + D) \quad .....(5.6)$$

Equation (5.6) is derived on the assumption that the ray path between the barrier and the LCD is straight. In practice, the glass substrate of the LCD will deviate the path slightly as illustrated in Fig.5.7. As the barrier in the prototype might be printed on an acetate sheet, this may have to be sandwiched between two layers of glass as shown in the left of Fig.5.7. If the light were not deviated by the glass, it would follow the straight path HM. However, it *is* deviated by the glass layers, and actually follows the path HJKL. This deviation requires the barrier pitch to be slightly greater than that predicted from Equation (5.6).

In Fig.5.6 a different pair of similar triangles can be considered so that –

$$N P_B / A = N (2 P_L - P_B) / D$$

Rearranging gives –

$$2 P_L - P_B = P_B D / A$$

The value of the term $(2 P_L - P_B)$, when refraction by the glass is taken into account, can be found as follows –

In Fig.7 the total value of $(2 P_L - P_B)$ is found from the sum of three parts. These are the vertical components of the paths HJ, JK and KL. As the geometry for all the apertures is the same, the following calculation will be for N = 1. The slope of the path JK is the same as that of the incident light and is equal to P_B / A. The vertical component is equal to the slope multiplied by the horizontal path length $(D - T_B - T_L)$.

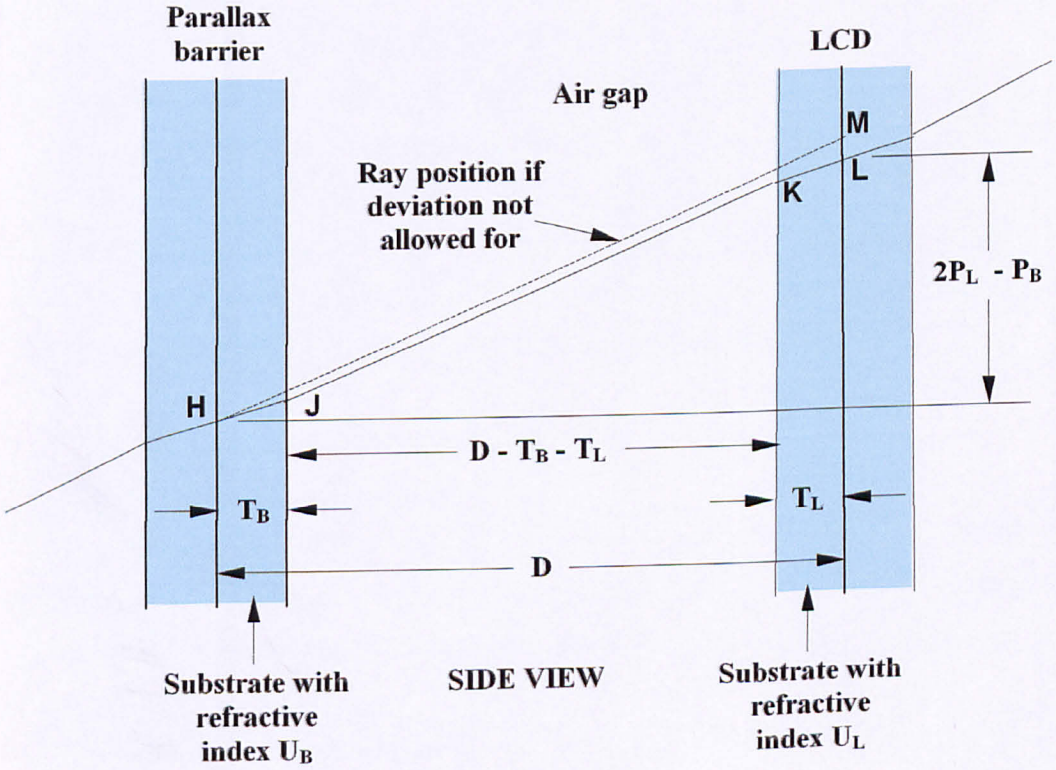

FIG.5.7 SUBSTRATE DEVIATION

The slope of the path HJ will be reduced by a factor of the refractive index of the barrier glass. This is an approximation but is close enough for the purposes of this examination, and, in fact, is the same assumption made for paraxial analysis of lenses. Over the region HJ the slope is P_B / U_B A, so the vertical component is $T_B P_B / U_B$ A, where U_B is the refractive index of the barrier support glass, and T_B its thickness.

Similarly, the vertical component of the path KL is $T_L P_L$ / U_L A, where U_L is the refractive index of the LCD substrate glass and T_L, its thickness.

Summing these products gives –

$$2 P_L - P_B = [T_B P_B / U_B A] + [P_B (D - T_B - T_L) / A] + [T_L P_L / U_L A]$$

Solving for P_B gives –

$$P_B = \frac{2 P_L A}{A + D + T_B\left(\frac{1}{U_B} - 1\right) + T_L\left(\frac{1}{U_L} - 1\right)} \quad \text{.....(5.7)}$$

Examination of Equation (5.7) reveals that if the glass layers are not taken into consideration, i.e. T_B and T_L are zero, the equation reverts back to (5.6). When the glass is accounted for, the third and fourth terms of the denominator are negative, hence making greater the value for P_B for a given P_L. This is consistent with the ray path positions of Fig.5.7. The deviation LM will have a small effect on Equations (5.1) to (5.5), but its effect can be considered negligible, and will be accommodated by the apertures being made narrower than the absolute maximum.

5.5) Practical Application of Equations

The effect of this deviation will now be considered. In the 12" prototype, described in Chapter 10, the effective value of A is 760 millimetres. A is the distance of the virtual image of the illumination sources after being reflected by six folding mirrors.

Two light sources have been used with this prototype. One of these consists of a pair of linear halogen lamps offset both horizontally and vertically. These are physically moved laterally by a stepper motor driving a rack-and-pinion mechanism. The output

of the lamps passes through the mask depicted in Fig.5.8 (b). This prevents stray light giving rise to crosstalk. The values of E and G are 7 and 10 millimetres respectively and the vertical pixel pitch P_L of the LCD is 0.307 millimetres. The LCD pixels were measured on a travelling microscope, and the value of M determined to be 0.06 millimetres to an estimated accuracy of ± 5 microns. Although the data was not given for the LCD, its back substrate thickness and refractive index are assumed to be one millimetre and 1.5 respectively.

This gives a value of P, the pixel aperture height, of 0.247 millimetres. These figures yield values of: D = 13.72 millimetres, W = 0.241, millimetres R_A = 0.488 millimetres and P_B = 0.6034 millimetres. This aperture ratio means that an absolute maximum of 48.8% of the light can pass through the barrier, in relation to the light that can pass without it. When allowance is made for differing thermal expansion coefficients and misalignment, this value is likely to be around 35-40% in practice.

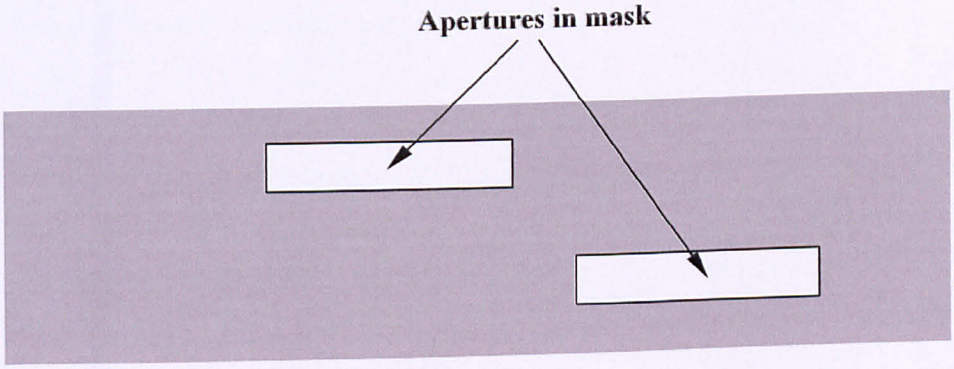

FRONT VIEW
Drawing to actual size

FIG.5.8 PROTOTYPE HALOGEN LAMP SOURCES

The effect of the LCD glass substrate will now be considered. Equation (5.7) yields a barrier pitch of 603.37 microns. If the glass is neglected, the final term in the denominator is not used, the value is 603.11 microns. The difference of 0.26 microns might not seem small, but it is not insignificant. The display used in the 12" prototype

has a resolution of 800 x 600 pixels, so that the barrier will require 300 horizontal apertures. This means the furthest aperture is the 150th out from the centre. If the barrier is aligned correctly at the centre, there will be an increasing error toward the upper and lower edges. 0.26 microns multiplied by 150 is 39 microns – this is around 13 % LCD pitch and could cause light passing to the adjacent rows, thereby causing crosstalk.

5.6) Conclusions

A parallax barrier provides an inexpensive method of providing image multiplexing for a simple prototype. It has the disadvantages of requiring two sets of illumination sources and having a relatively low light throughput. Although the low throughput is not desirable, it must be borne in mind that if, for instance, the barrier allows 30% of the light can pass, this light illuminates only half the pixel rows. Therefore the use of two sets of illumination enables the display to be 60% as bright as it would be without the barrier, and with only one illumination source.

This analysis has necessarily been fairly rigorous as positional differences between the barrier and the LCD pixels in the order of tens of microns can have a severe effect on crosstalk. Thermal coefficient effects have not been considered here as the prototypes will be kept within a reasonably narrow temperature range in the laboratory.

It should be noted that Equations (5.4) and (5.5) give the *maximum* values of W and R_A. In practice this will have to be less in order to allow for inaccuracies in alignment and dimensions, and differences in thermal effects.

The barrier pitch P_B is found rigorously in Equation (5.7). However, it can be seen that the deviation of the barrier and LCD substrates, covered by the last two terms in the denominator, can be compensated for by varying either the illumination source to barrier distance A, or the barrier to LCD spacing D.

5.7) Summary of Useful Equations

$$D = A P_L / (G + E) \quad \text{.....(5.3)}$$

$$W = G P_L / (G + E) + M \quad \text{.....(5.4)}$$

$$\left.\begin{array}{ll} R_A = W / 2P & \text{if } W / 2.P < 1 \\ R_A = 0.5 & \text{if } W / 2P > 1 \end{array}\right\} \quad \text{.....(5.5)}$$

$$P_B = \frac{2 P_L A}{A + D + T_B\left(\frac{1}{U_B} - 1\right) + T_L\left(\frac{1}{U_L} - 1\right)} \quad \text{.....(5.7)}$$

Where –

E = height of illumination sources

G = vertical gap between illumination sources

W = aperture height

A = illumination sources to barrier horizontal distance

D = barrier to LCD spacing

P_L = LCD vertical pixel pitch

P = pixel aperture height

M = LCD horizontal mask height

P_B = barrier pitch

R_A = the ratio of light with and without the barrier

T_B = thickness of barrier front substrate (where applicable)

U_B = refractive index of barrier front substrate (where applicable)

T_L = thickness of LCD back substrate

U_L = refractive index of LCD back substrate

CHAPTER 6
LCD SCATTERING

6.1) Preface

As the operation of the display depends on exit pupils being formed by light from behind a direct-view LCD, any scattering of light at the LCD will contribute to crosstalk. Experiments to determine this scattering were carried out by placing a small LCD screen in the Fourier transform plane of an optical system, and then photographing the results.

The test apparatus consists essentially of a light source providing a collimated beam of light, an LCD and a camera. Measurements were made indirectly by comparing the images of the scattering intensity against a reference. Dimensions and scattering angles were measured, but the necessary equipment to measure light levels was not available. However, the photographs provide strong evidence that the scattering of the screen is predominantly due to diffraction caused by the RGB sub-pixels.

6.2.) Apparatus

A light source, collimating lens, LCD, binoculars and a camera are mounted on an optical bench as illustrated in Fig.6.1. Collimated light is obtained from a 55-watt, 12-volt halogen car headlight bulb type H3. This is contained within a metal housing which allows the light to pass through a 0.5 mm diameter aperture. A concave lens with a focal length of –67 mm is mounted between the lamp and the LCD in order to give a reduced virtual image of the aperture.

The LCD is the screen of a Citizen 65 mm diagonal television type DD-T126 whose liquid crystal layer operates in the supertwist mode. The body of the television is separated from the screen and these are both mounted on a table that is fixed to a thrust bearing enabling it to be rotated 45° either side of the bench axis. The image-capture assembly consists of a pair of binoculars where only one half is used to magnify the image formed in a 35-millimetre camera.

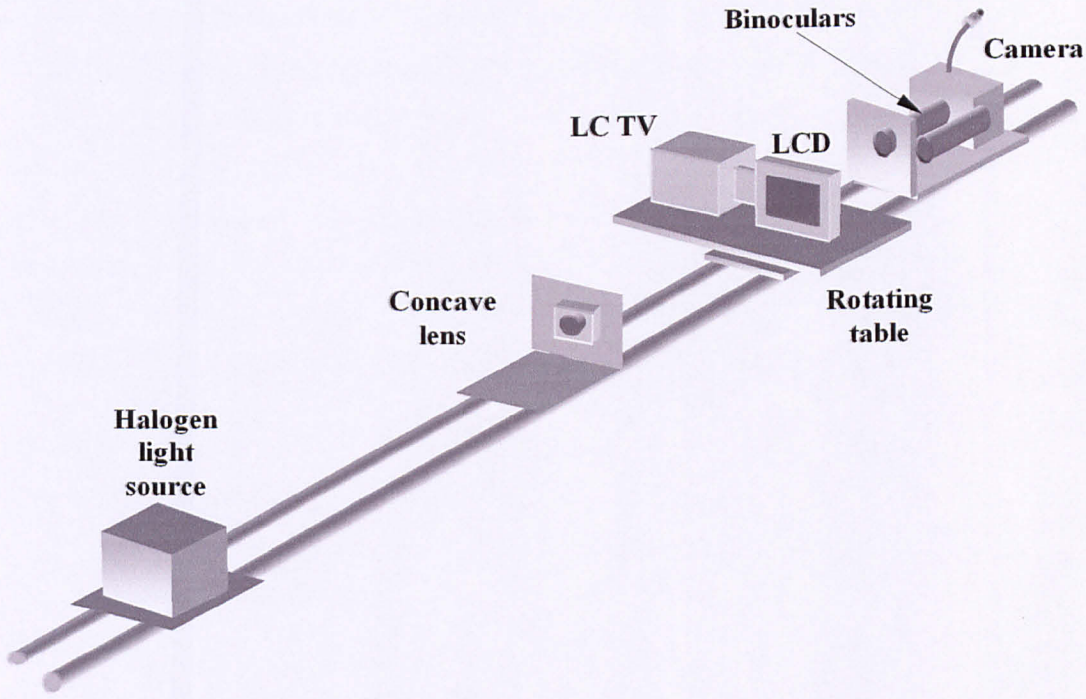

FIG.6.1 APPARATUS FOR PHOTOGRAPHING LCD SCATTERING PATTERN

6.3) Test Apparatus Optics

A white light source was chosen for its ability to simultaneously indicate the scattering at all wavelengths. Coherent laser light is not necessary to produce diffraction scattering, and, in fact, diffraction is encountered in everyday illumination situations. The small light source does enable a polychromatic semi-coherent collimated beam to be produced, and allows clear patterns to be photographed.

The effective size of the light source is reduced from 0.5 mm down to 35 microns by the use of the concave lens (the angle subtended is reduced from 0.46 milliradians to 0.13 milliradians). This reduction *could* be achieved by moving the light source further from the LCD but this would entail the use of a very long optical bench.

An advantage of using a virtual source that is relatively close to the LCD is that the system can be calibrated simply by removing the LCD and concave lens and placing a scale, in this case a clear plastic ruler, the position of this source. This enables angular measurements to be determined.

The Fourier transform lens comprises four components as Fig.6.2 shows. These components being, an additional 298-millimetre focal length lens placed in front of the binocular, the objective and eyepiece, and the camera lens. The effective aperture of the camera used is set by the binocular objective diameter and is fixed at f 11.4 .

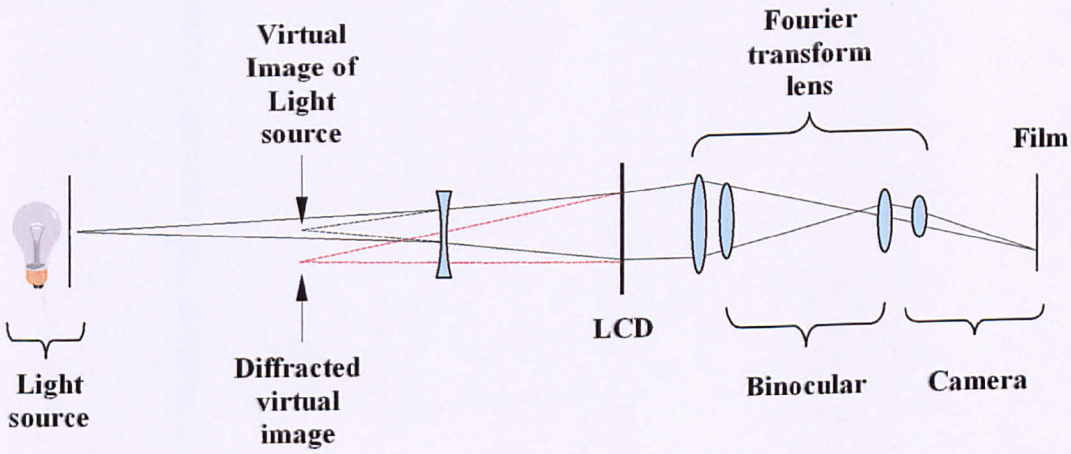

FIG.6.2 TEST APPARATUS OPTICS

6.4) Results

The results fall into two categories, these being the measurement of the LCD pixel dimensions, and photographing scattering patterns. All measurements were made by comparison of photographs of the pattern with those of the reference ruler – no direct observations were made.

6.4.1) LCD Dimensions

It was found that the halogen lamp yielded much sharper photographs than the LCD backlight. Fig.6.3 is one of the series of photographs taken. The horizontal and vertical pitches of the pixels were determined by measuring the total of fifteen pixels and comparing these distances with a photograph of the ruler in the same position.

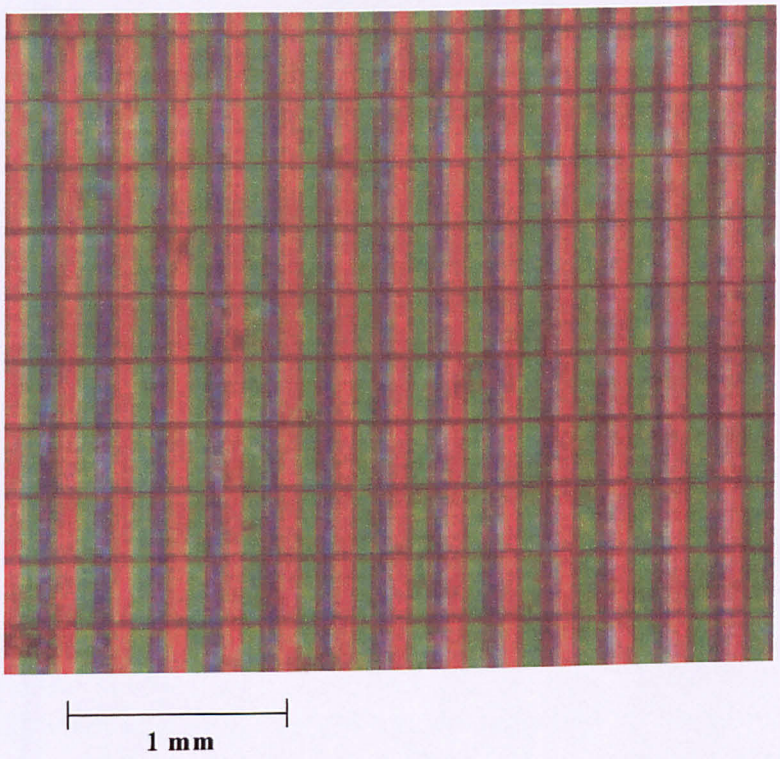

FIG.6.3 CITIZEN LCD TV PIXELS

The most convenient method of estimating the width of the conductors was to take a photograph of the pixel photograph itself. This increased magnification enabled the conductor widths to be determined to an estimated accuracy of ± 2.5 microns. The dimensions obtained are shown in Fig.6.4.

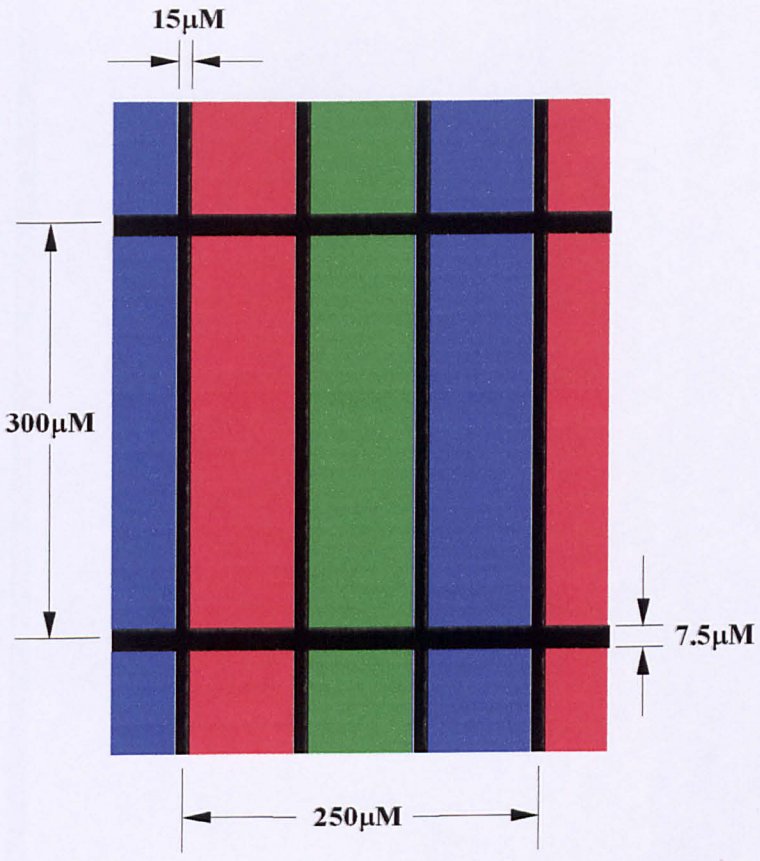

FIG.6.4 SUB-PIXEL DIMENSIONS

6.4.2) Scattering Pattern

With the LCD illuminated by the halogen light source, patterns as illustrated in Fig.6.5 were obtained. Their appearance was determined by the exposure time that was varied between four and sixty-four seconds. The optimum time was found by trial-and-error, with the aperture kept constant at the value of f 11.4 determined by the binocular objective.

Short exposure times showed clearly the elements of the central column, but with barely perceptible outer columns. As the times were lengthened, the central column became a blur but with more outer columns becoming visible.

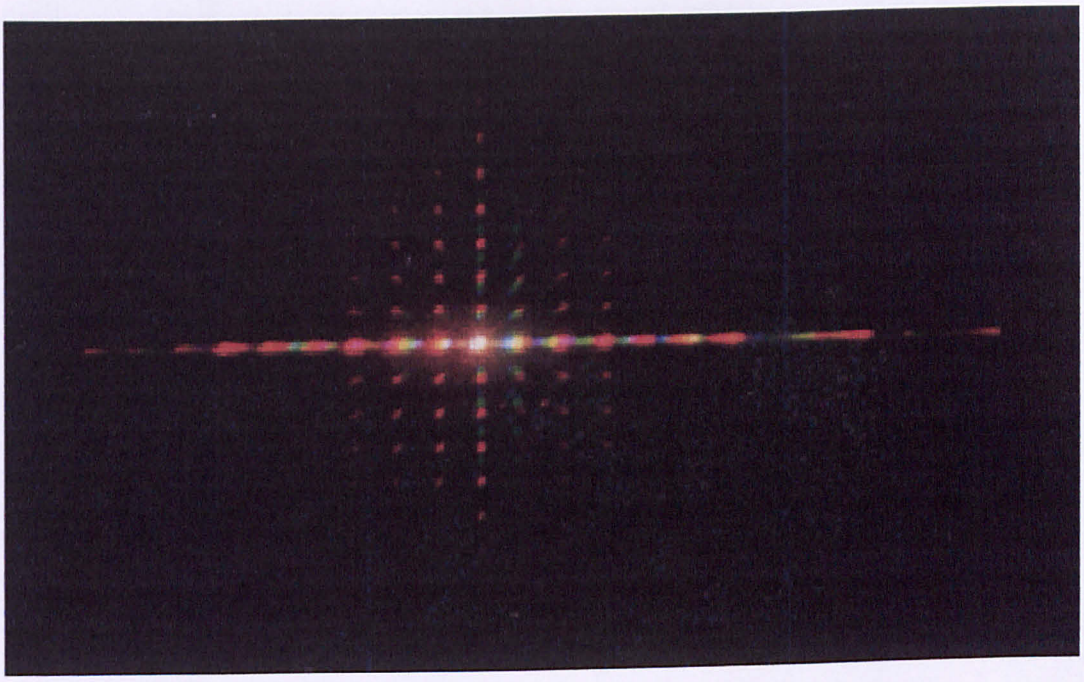

FIG.6.5 LCD SCATTERING PATTERN

Although intensity measurements could not be made, initial examination of the appearance of the scattering pattern indicated that it is almost certainly produced by diffraction. Measuring the pitch of the pattern further tests the validity of this assumption. Measurements of the photograph of the ruler when it is situated in the plane through the virtual light source show that the actual distances in this plane can be found by dividing distances on the photographs by a factor of 5.3.

It is shown in the following section that the relationship below applies to a diffraction pattern :-

$$\lambda = \frac{C\,L}{S} \quad \ldots\ldots\ldots (6.1)$$

Where –

λ = wavelength

C = pattern pitch in virtual image plane (plane in which the virtual light source lies)

L = pixel pitch

S = virtual image to LCD distance

The pitches of red and green patterns were measured for several values of virtual source to LCD distance. The average values obtained from this give values of 618 nanometres for red and 519 nanometres for green. Allowing for experimental error, these correspond reasonably closely to the typical LCD filter characteristics of Fig.5.6.

Another implication of equation (6.1) is that for a given wavelength and virtual image to LCD distance, the diffraction pattern pitch is inversely proportional to the pixel pitch. In other words, the ratio of pixel horizontal to vertical pitch equals the ratio of pattern vertical to horizontal pitch. In this case the ratio is 300 / 250 = 1.2. This is the same ratio as measured for similar coloured elements in all the photographs.

The pitch of the diffraction pattern is also determined by the angle of the screen to the incident beam as the pixel spacing is effectively reduced. If the LCD is rotated through angle θ then –

$$C = \frac{\lambda . S}{L} \sec \theta \quad \ldots\ldots\ldots\ldots (6.2)$$

When the LCD was rotated 22.5° and 45° around its normally vertical axis, the pattern pitch was reduced to a value within ± 4 % of the calculated value. Measurements were difficult to make with the screen rotated around its normally horizontal axis due to large intensity reductions with angle.

6.5) Theory

As there is sufficient evidence from the appearance and characteristics of the scattering patterns to indicate they are due to diffraction, an analysis of the observed effect of the scattering of the two-dimensional LCD transmission function will now be considered.

6.5.1) Pattern Formation with a Non-parallel Beam

When the diffraction of the LCD is observed , the actual pattern is resolved by it being focused by the lens of the eye on to the retina. This is a case of Fraunhofer diffraction, where the pattern is focused at infinity, and has to be resolved by a lens – it would not appear on a screen placed in front of the LCD as it would with Fresnel diffraction.

It is most common for Fraunhofer diffraction to be both produced experimentally, and analysed, with plane wavefront light from an infinitely distant source, known as far-field illumination, for example from a source such as a laser. However, this is not necessary and Fraunhofer diffraction can also be produced with either cylindrical or spherical wavefronts, as opposed to just a plane wavefront [STEW83a]. When the maximum diffraction order produces a wavefront at a sufficiently small angle to the zero-order wavefront, the same analysis can be applied. This is due to the sines and tangents of small angles having, for practical purposes, the same value as the angle expressed in radians.

6.5.2) Diffraction Grating

The diffraction pattern of a two-dimensional mask is a two-dimensional Fourier transform of the mask, this is also referred to as an optical transform. The analysis of this can be quite complex. However, examination of Fig.6.4 shows that there are ways in which the analysis can be simplified. It must be borne in mind that the test LCD is a simple supertwist type, without the driver transistors of an active-matrix LCD.

In Fig,6.5 the diffraction pattern can be seen to form a two-dimensional matrix, When the LCD is used in the 3D display, the vertical diffuser used in conjunction with it (described in Chapter 3), has the effect of summing the columns of this pattern.

When an LCD pixel is displaying part of an image, generally there will be some transmission through all three RGB sub-pixels. However the worst-case should be considered – this is where only one colour sub-pixel is transmitting light, and the other two are opaque. In the case of the supertwist test LCD, it can be considered as a simple diffraction grating with a pitch of 250 microns and a aperture width of 76 microns.

Worst-case conditions also occur at certain wavelengths. This is due to the spectral characteristics of the RGB colour-filters, typical of which are plotted in Fig.6.6 [KNAP90]. Consider, for example, a wavelength of 450 nanometres, where the transmittance of the blue filter is around 70 %, but is just a few percent for the red and blue filters. The LCD will behave in very much the same manner as a grating at this wavelength.

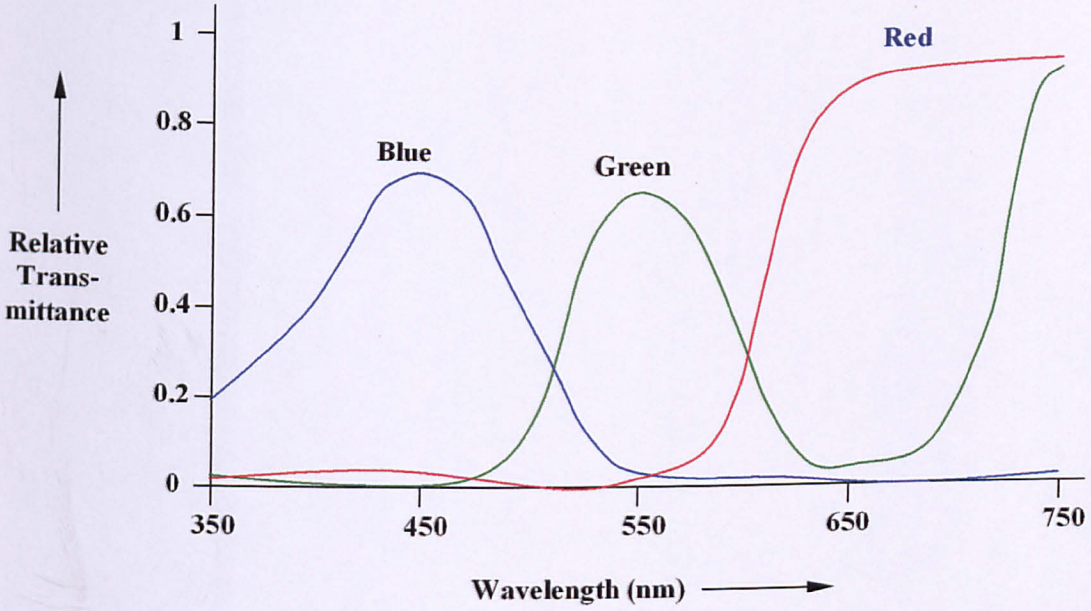

FIG.6.6 LCD COLOUR FILTER CHARACTERISTICS

Having established that diffraction grating theory can be applied to the LCD, this will be examined, and the simplifications that apply will be determined. The complete equation for the intensity from a grating [FINC80a] is –

$$I = \left(\frac{\sin\left[\frac{\pi\, b \sin\alpha}{\lambda}\right]}{\frac{\pi.b.\sin\alpha}{\lambda}} \right)^2 \times \left(\frac{\sin\left[\frac{\pi\, n\,(b+c)\sin\alpha}{\lambda}\right]}{\sin\left[\frac{\pi\,(b+c)\sin\alpha}{\lambda}\right]} \right)^2 \quad \ldots\ldots\ldots (6.3)$$

Where –

I = intensity

b = width of slit

α =angle from normal

n = number of slits

(b + c) = grating interval

λ = wavelength

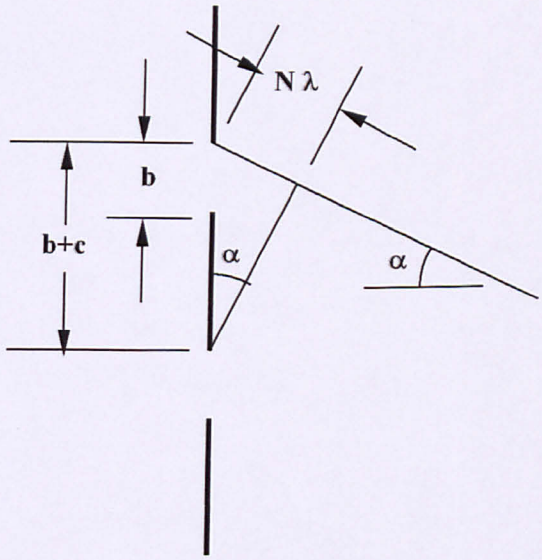

FIG.6.7 DIFFRACTION GRATING

The envelope of the intensity maxima is given by the first term of the equation, and the sharpening of the fringes by the second term. Fig.6.7 is the diagram of a section of grating with the vertical scale exaggerated.

If the beam through the grating had infinite width, i.e. if n was infinity, the intensity function would consist of a series of lines whose values were given by the first term. In practice, the beam is of course finite, but for the purpose of these calculations it is assumed to be sufficiently wide, in relation to the grating width, to produce fringes of negligible width.

Maxima occur when corresponding points on adjacent slits are in phase. This is when –

$$\text{Sin}\,\alpha = \frac{N\lambda}{b+c}$$

Where N is an integer and is the order of the pattern element. If this is substituted into Equation (6.3) then –

$$I = \left(\frac{\sin\left[\pi b \left[\frac{N\lambda}{b+c}\right]\right]}{\pi b \left[\frac{N\lambda}{b+c}\right]} \right)^2 \quad \ldots\ldots\ldots\ldots \quad (6.4)$$

Let the ratio of grating width to grating interval be P –

$$P = \frac{b}{b+c}$$

Then substituting this into Equation (6.4) gives the simplified equation –

$$I = \frac{\text{Sin}^2(\pi N P)}{(\pi N P)^2} \quad \ldots\ldots\ldots\ldots \quad (6.5)$$

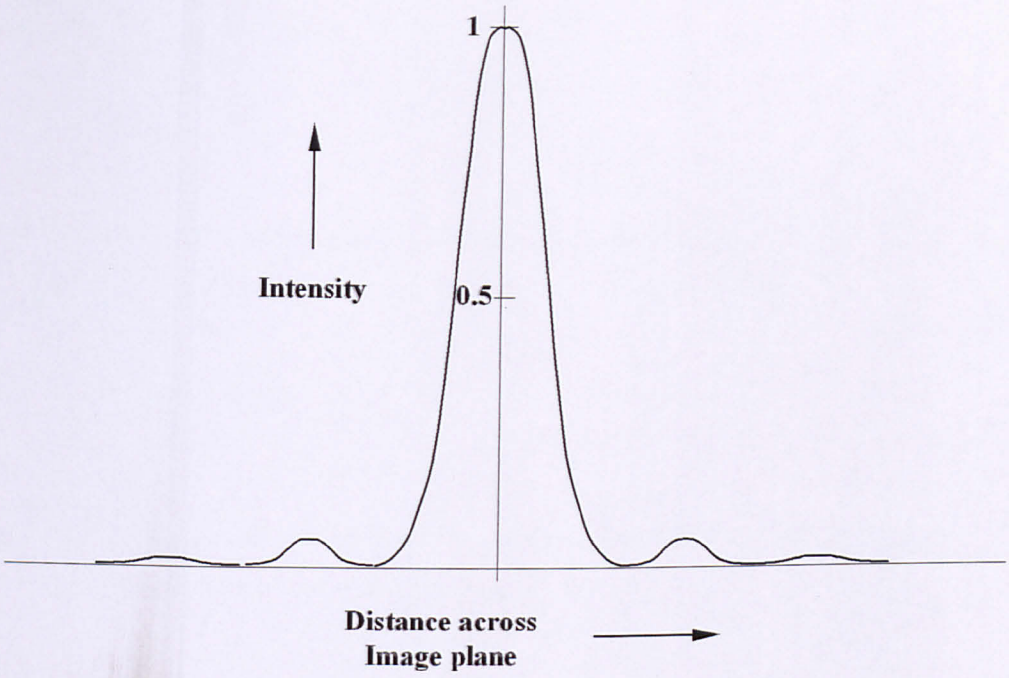

FIG.6.8 SINC^2 FUNCTION – ENVELOPE OF IMPULSE FUNCTIONS

Therefore the intensity is only dependent on the grating ratio and the order of the fringe, and is independent of wavelength. Equation (6.5) is called the sinc squared function so that the equation can also be written as –

$$I = \text{sinc}^2 (\pi N P) \ldots\ldots\ldots (6.6)$$

The form of the sinc squared function can be seen in Fig.6.8 where there is a central maximum which is shown as having a relative value of 1. The relative intensities of the second, third and fourth maxima are 1/21, 1/61 and 1/120 respectively [HOUS38a]. This is a continuous function and is the envelope of the impulse functions shown in Fig.6.9. These impulse functions correspond to the pattern elements and only occur when N is an integer.

Equation (6.7) is derived as follows –

Referring to Fig.6.7 –

$$\text{Sin}\,\alpha = \frac{N\lambda}{b+c}$$

If α is small then the pattern pitch is constant across the viewing field, also sin α = tan α = α (expressed in radians). In the test setup, tan α = C / S, therefore –

$$C/S = \frac{N\lambda}{b+c}$$

As the pitch between all pattern elements is the same as for N = 1, and the pixel pitch L = (b+c), rearranging the above equation gives –

$$\lambda = \frac{CL}{S} \qquad \ldots\ldots\ldots (6.7)$$

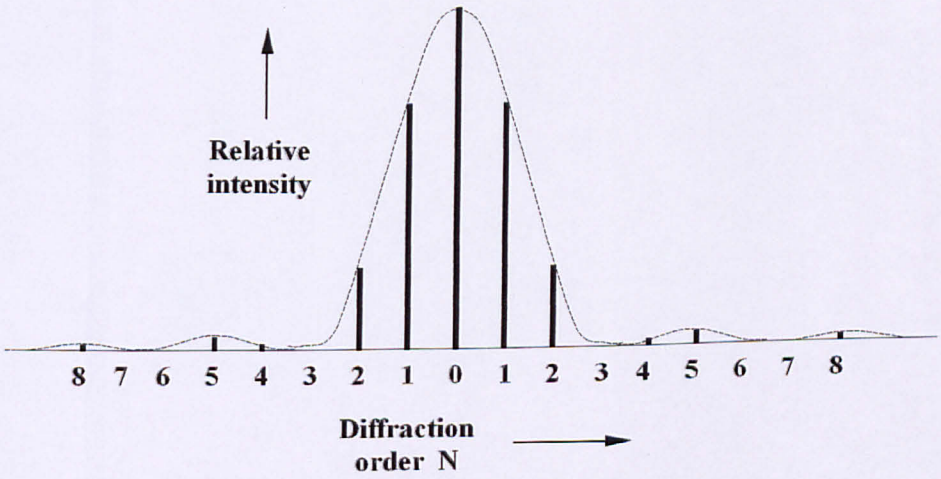

FIG.6.9 CALCULATED INTENSITIES FOR P = 0.303

6.5.3) LCD with Driver Transistors

The majority of active matrix LCDs (AMLCDs) have a mask as shown in Fig.6.10, where the driver transistors are located in one corner of each colour sub-pixel. In this case, the summation of the pattern elements cannot be obtained by simply considering the LCD as a diffraction grating. The diffraction pattern is obtained by evaluating its two-dimensional Fourier transform, and then summing the columns.

A two-dimensional transform is obtained by first calculating the Fourier transforms in the horizontal direction. This resultant has the dimensions of spatial frequency in the x-direction, and distance in the y-direction. Transformsof this, performed in the y-direction, then yield the 2D transform.

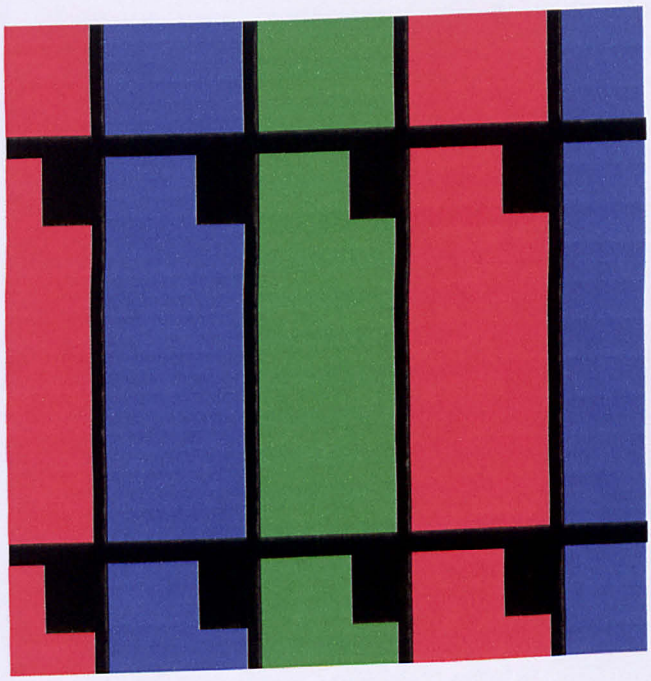

FIG.6.10 SUB-PIXELS IN A TYPICAL TFTLCD

Consider monochromatic light, and only one colour of the RGB sub-pixels transmitting. The position of the columns in the x-direction is determined by the wavelength and the diffraction order. Taking transforms across the LCD produces three types of region running across this intermediate stage which is not shown in Fig.6.11.

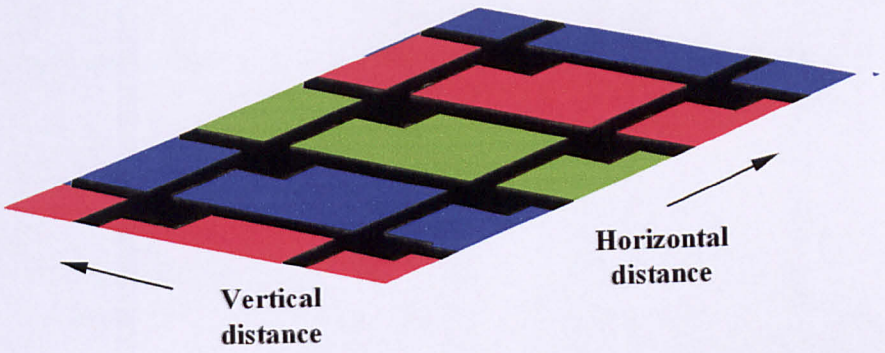

(a) LCD Sub-pixels

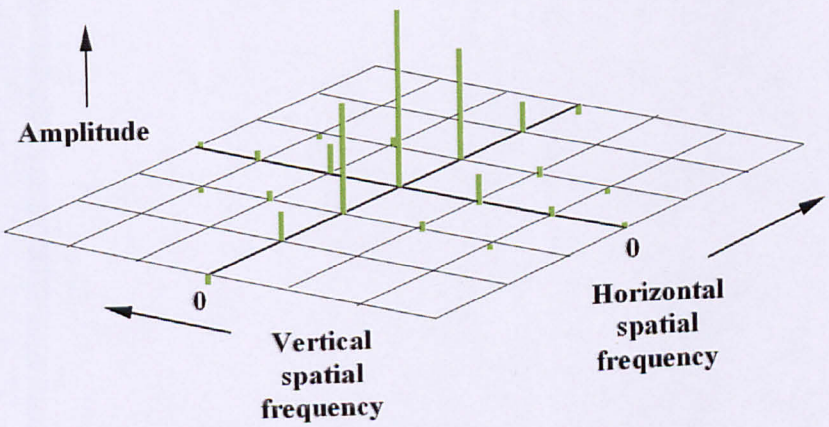

(b) Fourier Transform

FIG.6.11 LCD FOURIER TRANSFORM

The regions that line up with the horizontal conductors have zero amplitude, those in line with the driver transistors have the largest amplitude, and those lining up with the remainder of the pixel have smaller amplitude. These values are also complex so their

phase angle has to be considered. As the centres of the driver transistors are displaced from the centres of the vertical conductors their transform components will have a different phase angle to those of the conductors.

Taking transforms of the columns produces a transform which is the 'bed of nails' function shown in Fig.6.11 (b). For monochromatic light this transform will be a series of impulse functions as in the figure. In practice, polychromatic light will give planes radiating from the centre. This effect can be seen in Fig.6.5.

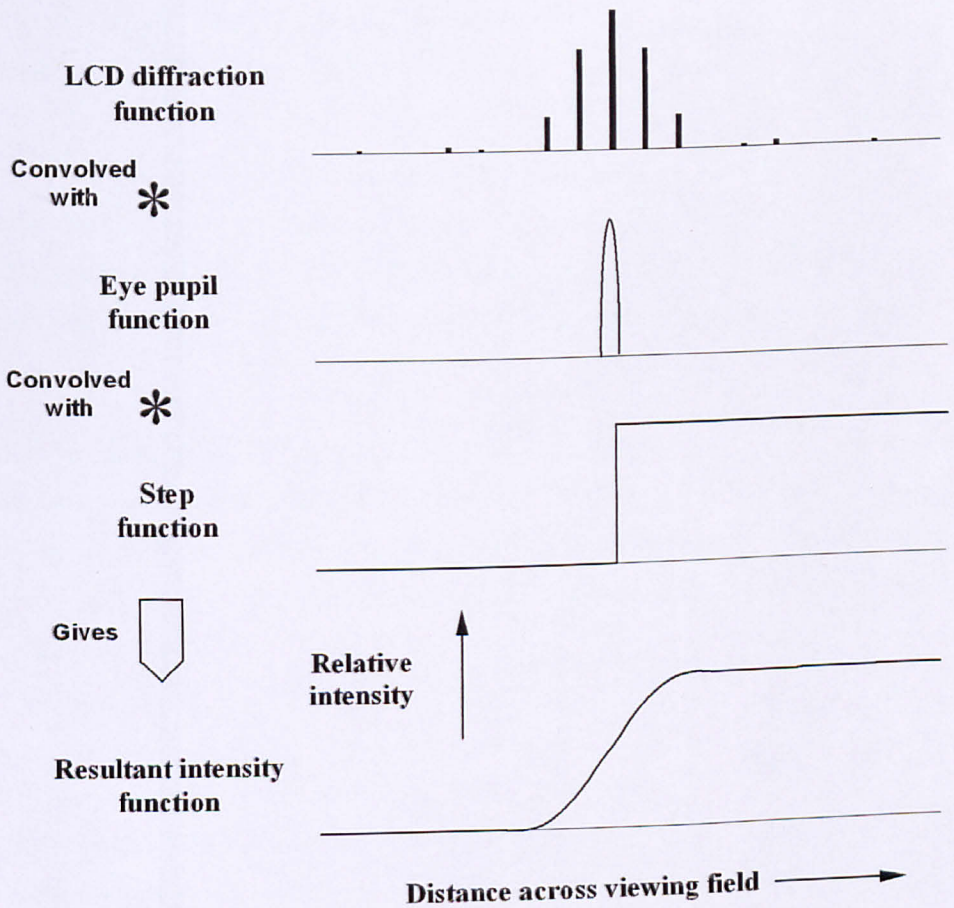

FIG.6.12 INTENSITY ON RETINA

The intensities are determined by the squares of the amplitude, and the observed effect is obtained by summing the columns in Fig.6.11 (b). This is due to the vertical scattering required for the 3D display.

6.5.4) Image Formation in the Eye

As mentioned in section 6.4.1) the pattern is formed by Fraunhofer diffraction and so can only be resolved by a lens. In the case of a viewer observing the pattern, the lens of the eye acts as the Fourier transform lens that resolves the image on the retina.

As it is the image on the retina that is of interest in the case of a display, the effect of the size of the pupil of the eye must also be taken into account. This is in the order of a few millimeters in diameter and will give the semi-elliptic function as shown in Fig.6.12.

The horizontal scale in Fig.6.12 gives actual typical values where the pupil diameter is 3 millimetres, and the pattern spacing is 5 millimetres. The pattern spacing is proportional to the distance of the viewer from the screen. In this case the pattern spacing is larger than the pupil diameter, but if the viewer was closer to the screen it could possibly be less.

The resultant intensity shown is obtained by convolving the diffraction and pupil functions with a step function. In practice this would not be a step function, but one whose width is determined by the steering optics. However, the lower curve provides a useful indication of the contribution of exit pupil boundary-zone width due to LCD diffraction.

6.6) Summary

Although the simple apparatus used did not enable intensity measurements to be made, the photographs obtained were sufficient to indicate that the scattering of the LCD is due to diffraction. The use of a Fourier transform lens does not imply that a diffraction pattern was expected before the experiment was carried out. The action of this is to resolve

angular scattering, from whatever cause, into positional information on the photographic film.

As the LCDs used in the prototypes are active matrix types with driver transistors, a thorough analysis of its performance would require the calculation of the 2D Fourier transform of one set of sub-pixels. Also, in a conversation with IBM, the author was informed that the performance of the LCD cannot be modeled with complete accuracy merely by considering its mask pattern. For these reasons, it will be easier, and probably more accurate, to measure the scattering directly on the actual LCD used. Nevertheless, a first approximation, and an insight into the expected performance, can be obtained by neglecting the driver transistors and treating the display as a straight grating.

Another effect on the diffraction that is not immediately obvious is the contribution of the 'softness' of the edges of the mask. This is described in a paper by Sharp [MONT01], where the LCD is used in a parallax display to produce a 3D image. The level of crosstalk produced by diffraction is less than predicted from simple theory that does not account for the apodised, or 'soft', edges.

CHAPTER 7
VERTICAL DIFFUSER

7.1) Preface

As the illumination source is situated some way behind the LCD, and only around a few centimetres high, light must be scattered at the screen in the vertical direction in order for illumination to cover its complete height. Ideally, this would be performed without any deviation of the light in the horizontal direction as this will contribute to crosstalk. The diffuser can be a lenticular screen, a light shaping diffuser (LSD) or a holographic optical element (HOE). The vertical light distribution and the horizontal deviation caused by the screen, are considered in this chapter. The designation of the angles of the rays, and the convention adopted for their signs, is given in Fig.7.1. V_{in} and H_{in} are respectively the vertical and horizontal components of the input ray, and V_{out} and H_{out} the components of the output ray. The calculations and measurements in Sections **7.2)** to **7.5)** are for a lenticular screen.

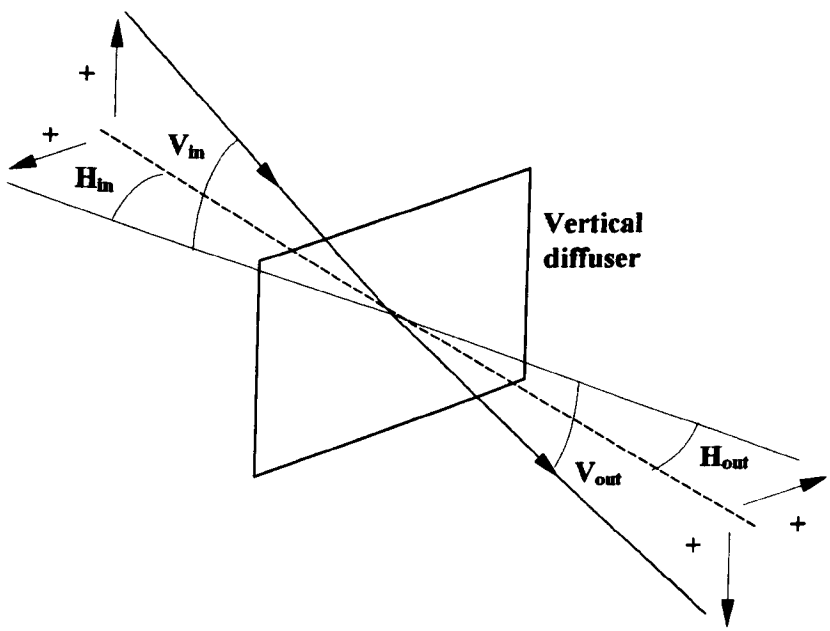

FIG.7.1 DESIGNATION OF ANGLES IN CHAPTER 7

7.2) Intensity Variation in Vertical Direction

The observed intensity in the viewing field is determined solely by the F-number of the lenses, and on the vertical position of the viewer in relation to the central axis. The observed intensity is approximately proportional to the F-number, as the higher this is, the less the light is spread. The effect of increasing the focal length of the lenses in order to increase the observed intensity is discussed in Section **9.8)**.

The variation of intensity with vertical position is calculated by considering the variation dV_{out} in the output angle over an elemental strip of illumination of height dD within the lens. V_{out} is calculated from the variables U, the refractive index of the lens material; R, the lens radius; V_R, the vertical angle of the ray within the lens; and D, the distance from the axis. The height dD is exaggerated in Fig.2 which illustrates the variables.

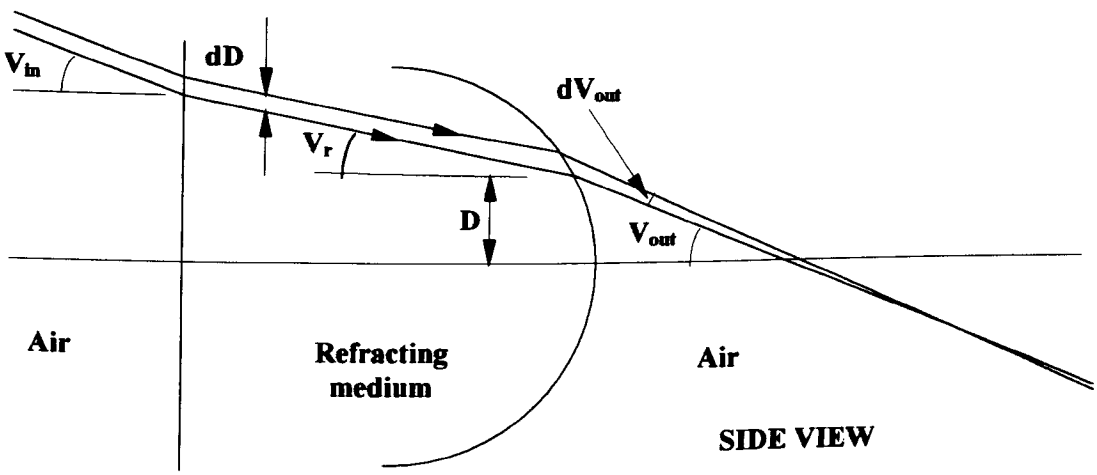

FIG.7.2 VARIABLES FOR DETERMINING INTENSITY

The observed intensity is proportional to the ratio dD / dV_{out}, as this is a measure of concentration of light for a given elemental beam height. Another factor that must be taken into account is the ratio of the input beam to the width of the beam within the refracting medium. This is independent of the refractive index as it is only the vertical component dD which is of interest. This is unaffected by the angle through which the beam is refracted and is compensated for by multiplying by the factor cos V_{in}.

The observed intensity is therefore proportional to $(dD / dV_{out}) \cos V_{in}$. The ratio dD / dV_{out} is calculated in a BASIC program. dD has the value of 0.0001 millimetres in order for the calculations of V_{out} for values of D and (D + dD) to be used to effectively differentiate the function. This is then multiplied by $\cos V_{in}$. The relative intensity is determined from this by dividing the result by the maximum value obtained.

The results for a refractive index of 1.5 and a lens radius of one millimetre are plotted for two values of V_{in} in Fig.7.3. There is no allowance in the program for an individual lens width of less than double its radius, therefore the results are limited by either the extreme of the semicircular profile, or by total internal reflection. When $V_{in} = 0°$, the relative intensity curve is centred at $V_{out} = 0°$ as might be expected, and the limits of the curve are at the positions K that are determined by the outer extremes of the refracting surface. When the input vertical angle is 10°, the curve has the same shape, but is displaced by 10°. Also, at $V_{out} > L$, light cannot pass through the lens due to total internal reflection. The locus of these points is a straight line as shown in Fig.7.3. Other curves plotted for other values of V_{in} follow the same pattern.

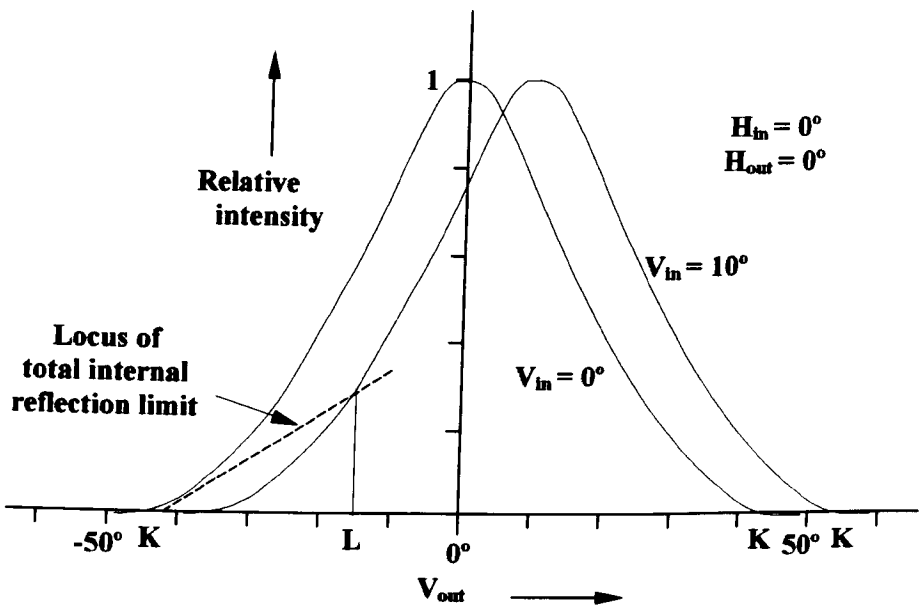

FIG.7.3 INTENSITY VARIATION WITH VERTICAL ANGLE

7.3) Measured Horizontal Deviation for $V_{in} = 0°$

As a selection of lenticular sheets was readily available, horizontal deviation was determined by empirically, as opposed to ray tracing. A simplified diagram of the experimental apparatus is shown in Fig.7.4. The lenticular screen under test is mounted on a rotating table that is attached to a ball bearing thrust race.

The illumination source consists of a 3-milliwatt laser, with a wavelength of 645 nanometres, that is mounted 150 millimetres behind the lenticular screen. The deviation pattern is curved and is formed on a screen as shown in the figure. The screen is exactly one metre from the test piece and only displays the top half of the deviation pattern: only the upper half is necessary as the pattern is symmetrical about its centre.

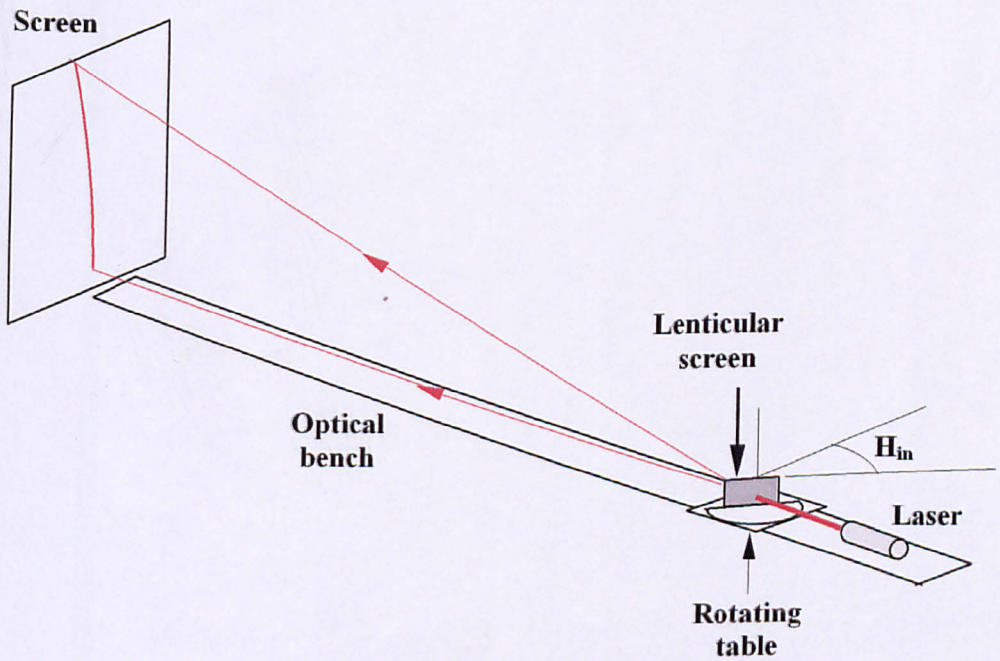

FIG.7.4 DEVIATION MEASUREMENTS APPARATUS

The lenticular screen has a pitch of 0.4 millimetres and is 1.25 millimetres thick, with a focal length of 1.67 millimetres. This gives it an F-number of 4.2. The flat surface of the screen is towards the light source.

The screen is sufficiently large to allow for deviations for a maximum V_{out} of 30° to be plotted on it. When the lenticular screen is perpendicular to the laser beam, that is for $H_{in} = 0°$, the pattern is a vertical line, as might be expected. The position of the line is then plotted for the test piece being rotated 5° clockwise, that is $H_{in} = 5°$. A curved line, with its top to the left of the central axis, is formed. No deviation occurs at the bottom of it where $V_{out} = 0°$. The procedure is repeated for H_{in} up to 45° in 5° increments. A series of curves with increasing curvature is produced.

A polynomial equation that gives the deviation D from the central axis has been determined. This fits the measured results to an accuracy better than ± one millimetre, and is as follows –

$$D = \mathbf{f}(V_{out}) \,.\, \mathbf{g}(H_{in}) / 0.54 \quad \text{.....(7.1)}$$

Where

$$\mathbf{f}(V_{out}) = (5.5.10^{-3} . V_{out}^{\,2}) + (4 .10^{-4} . V_{out}^{\,3}) - (2 . 10^{-9} . V_{out}^{\,6}) \quad \text{.....(7.2)}$$

and

$$\mathbf{g}(H_{in}) = (0.08 . H_{in}) + (4 . 10^{-4} . H_{in}^{\,2}) + (0.4 . (H_{in} / 45)^6) \quad \text{.....(7.3)}$$

The angles V_{out} and H_{in} are in degrees and D is the deviation in millimetres at a distance of one metre.

This deviation is more conveniently expressed in terms of angle H_{dev}, which is the change in H_{out}.

$$H_{dev} = \tan^{-1}(D / 1000)$$

therefore-

$$H_{dev} = \tan^{-1}[\mathbf{f}(V_{out}) \,.\, \mathbf{g}(H_{in}) / 540)] \quad \text{.....(7.4)}$$

The family of curves for H_{out} in terms of H_{in} and V_{out} is plotted in Fig.7.5. In equation (7.2) the first term of the polynomial is dominant. This conforms to the rule-of-thumb often encountered with the display optics that problems increase approximately in proportion to the square of distances or angles.

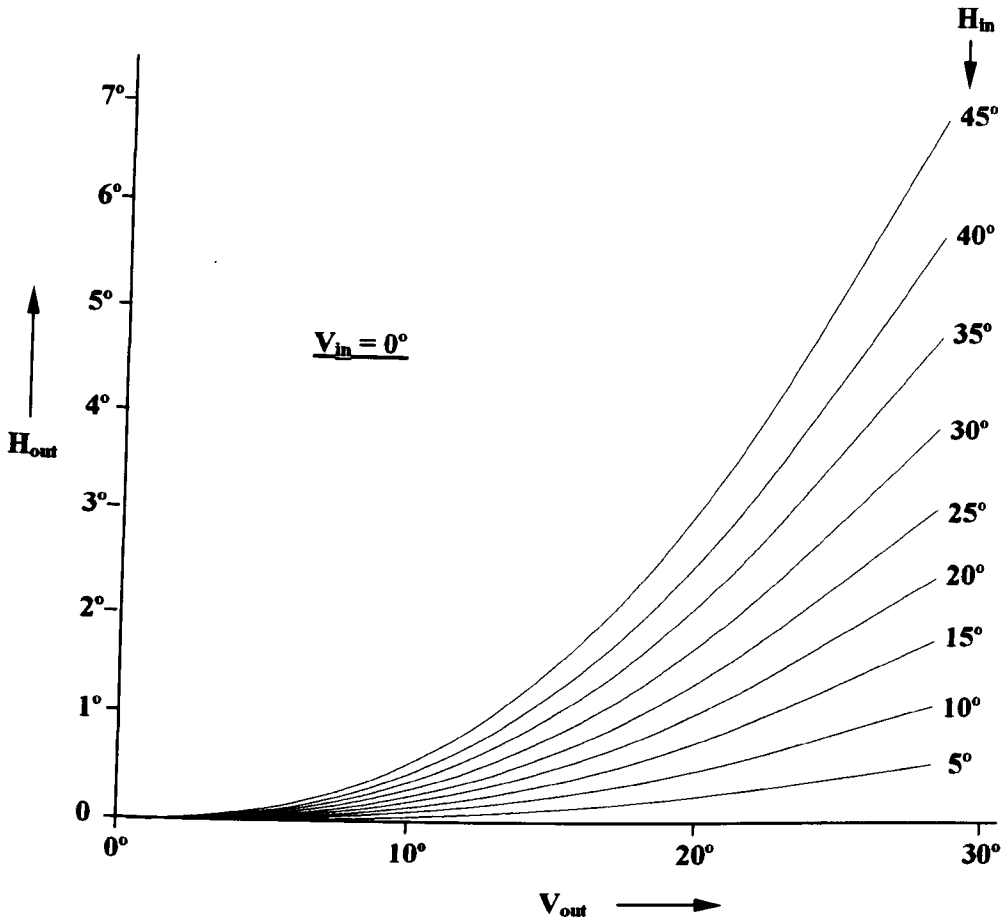

FIG.7.5 DEVIATION CURVES

A lenticular screen can be completely specified by the focal length and pitch of its lenses, its thickness and its refractive index. The thickness does not affect the direction of the emergent light. The refractive index of all the sheets tested is around 1.49, so this is not going to cause appreciable differences in deviation between samples. The refractive index of the screen material, and the horizontal and vertical components of the angles of the surface and of the internal ray incident on it, govern the direction of the emergent ray. These variables are independent of scale, so deviation is only determined by V_{in} and H_{in} .

This conclusion is demonstrated by measurements on various samples of lenticular sheet where they all exhibit the same deviation characteristics. For example, a five-millimetre thick sheet, with 0.5 millimetre pitch and 6.7 millimetre focal length lenses, has the same shape characteristics. The difference in this case is that the pattern is only around 120 millimetres high due to the high F-number of 12.7.

The measured deviations are the same when the lens surface is towards the light source as when it is away from the source.

An interesting point observed with all the samples is that at very oblique angles, the reflection from the front of the lenses when these are towards the source *appears* to fall on the same ellipse as the refracted pattern. The left-hand side of the major axis is the central point on the deviation curve, where the deviation is zero. In addition to being an interesting curiosity, the possibility that the deviation curves are partial ellipses could provide a more satisfactory equation than the polynomial, was investigated. Unfortunately, the best-fit ellipses cannot provide results that approach the accuracy obtained from the polynomial. This indicates that the deviation curve is not, in fact, part of an ellipse.

7.4) Measured Horizontal Deviation for a variable V_{in}

In the previous section, the input beam from the laser is horizontal so that $V_{in} = 0°$. With the apparatus modified, the deviation curves for various values of V_{in} can be determined as shown in Fig.7.6. For a given value of H_{in}, it was found that the shapes of the patterns appear to remain unaltered, and are displaced in the horizontal direction. The amount of displacement is determined by the angle V_{in}. When $V_{out} = V_{in}$, there is no deviation. This has the effect of displacing the curve to the right as shown in Fig.7.6.

This result is interesting in that when V_{in} is not equal to zero, there will be two points where the deviation is zero. These are marked X and Y on Fig.7.6. As the deviation is either side of the zero deviation line, the maximum deviation within a given range of V_{out} is actually a maximum for $V_{in} = 0°$.

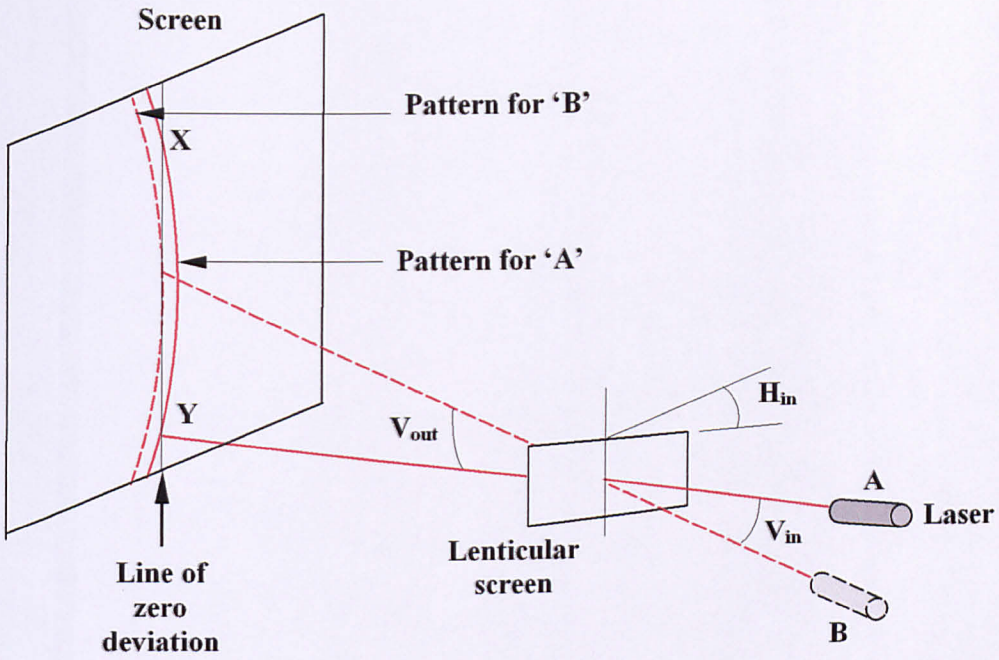

FIG.7.6 DEVIATION FOR VARIABLE H_{in} AND V_{in}

This information can now be used to determine the complete characteristics of any lenticular screen. The effect of deviation on crosstalk is determined by the product of the deviation angle and the distance of the viewer from the screen.

As the deviation for any particular curve is zero when $V_{out} = V_{in}$ it can be seen that the curve for any particular value of H_{in} passes through the x-axis at $V_{in} = V_{out}$. Fig.7.7 shows the deviation angle as a function of the variables H_{out} and V_{out} for $H_{in} = 30°$ and $V_{in} = 20°$. This curve is obtained by extracting the curve for $H_{in} = 30°$ in Fig.7.5, and moving it down, in order to pass through the x-axis at $V_{out} = 20°$. This is effectively simulating the displacement obtained in the experiment. Expressed algebraically this is –

$$H_{dev} = \tan^{-1} [\mathbf{f}(V_{out}) \times \mathbf{g}(H_{in}) / 540)] - \tan^{-1} [\mathbf{f}(V_{in}) \times \mathbf{g}(H_{in}) / 540)] \quad .....(7.5)$$

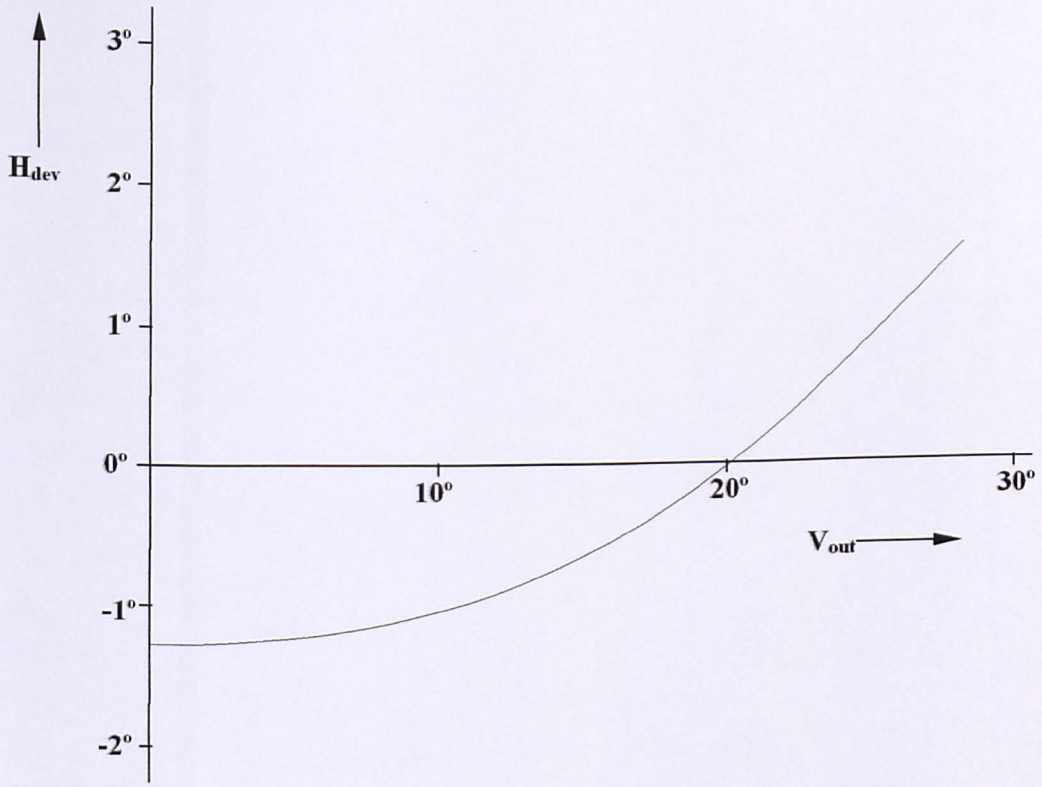

FIG.7.7 DEVIATION CURVE FOR $H_{in} = 30°$, $V_{in} = 20°$

For an angle θ: as $\theta \longrightarrow 0$

$\tan^{-1}\theta \longrightarrow \theta$ when θ is expressed in radians.

Therefore, as $H_{dev} \longrightarrow 0$, from equation (7.5)

$$H_{dev}\text{ (radians)} \sim [\mathbf{f}(V_{out}) \times \mathbf{g}(H_{in}) / 540)] - [\mathbf{f}(V_{in}) \times \mathbf{g}(H_{in}) / 540)]$$

$$= \mathbf{g}(H_{in})\,[\mathbf{f}(V_{out}) - \mathbf{f}(V_{in})] / 540$$

Radians are converted to degrees by the factor $180 / \pi$, therefore -

$$H_{dev}\text{ (degrees)} = 180 \times \mathbf{g}(H_{in}) \times [\mathbf{f}(V_{out}) - \mathbf{f}(V_{in})] / [540 \times \pi]$$

$$H_{dev} = 1.061 \times 10^{-1} \times \mathbf{g}(H_{in}) \times [\mathbf{f}(V_{out}) - \mathbf{f}(V_{in})] \quad \text{.....(7.6)}$$

We now have a simple general equation that can be applied to *any* lenticular screen. It must be borne in mind that this applies to light of a wavelength of 645 nanometres. Use of a green laser would provide an equation more representative of behaviour over

the complete visible spectrum, but unfortunately one was not available for this research. However, it is the author's opinion that this equation should prove sufficiently accurate for preliminary design work on the display.

7.5) Direct-viewing Measurements

Although the work carried out so far gives a useful insight into the deviation characteristics of lenticular sheets, it is quite difficult to determine how these will affect the exit pupil boundaries. In any event, there is no substitute for actual direct measurements as there are invariably unforeseen problems that will not have been allowed for.

7.5.1) Apparatus

Fig.7.8 illustrates the apparatus used for direct measurements. The items are mounted on an optical bench that allows them to be moved in relation to each other. The steering optics is simulated by the laser and vertical diffuser. This diffuser is the same screen that was used to obtain the results in Sections **7.3)** and **7.4)**. This produces a fan of rays illuminating a vertical line on the lenticular screen that simulates the screen diffuser. This screen is mounted to the rotating table on the optical bench in order to vary the angle H_{in}.

Measurements are made on the apparatus by observing the pattern on the screen, and then relating these observations to head positions. Head position is determined by referring its position to a plumb line attached to the ceiling. This technique has an estimated accuracy of ± five millimetres. Note that there is no danger associated with looking at the laser through the vertical diffuser as this is equivalent to looking at the light from a bar code reader where a laser beam is also scattered in one direction only.

The lenticular screen used has a lens pitch and focal length of 0.179 and 0.254 millimetres respectively. Two sets of measurements were taken. Firstly the screen was masked top and bottom to simulate a 14" screen, and then the full height of the sheet was used.

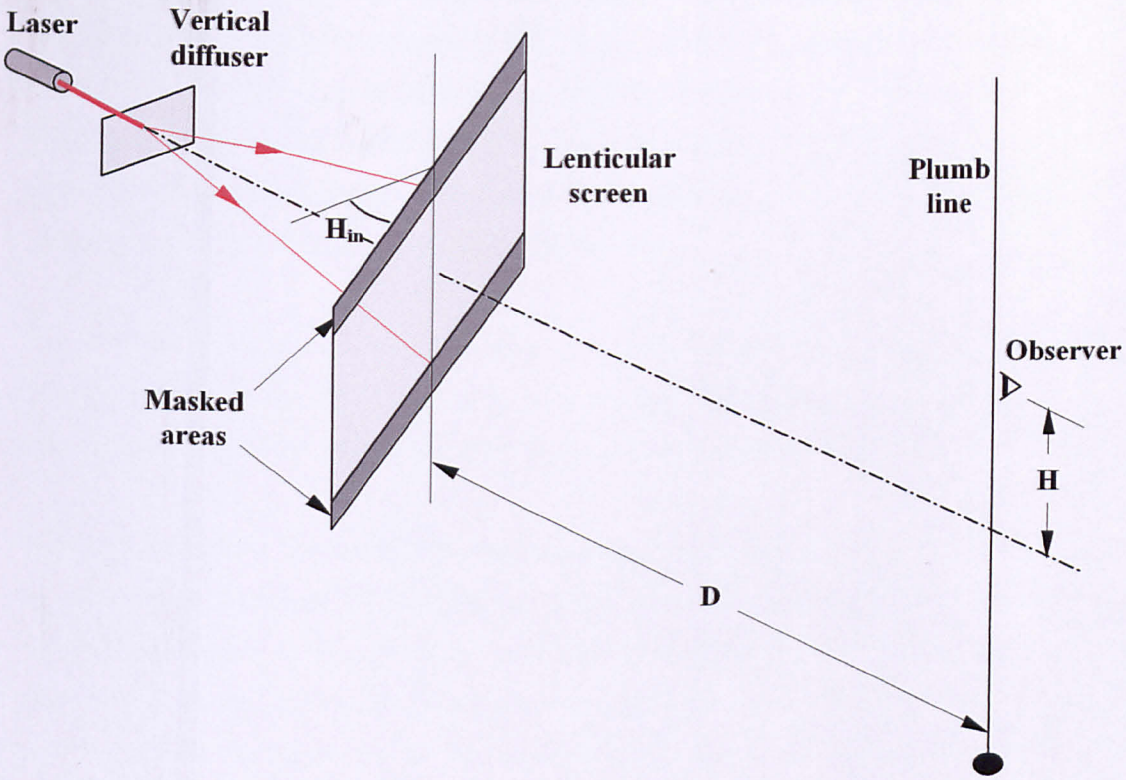

FIG.7.8 OBSERVED DEVIATION TEST SETUP

7.5.2) Direct-viewing Observations

There is a difference between the appearance on the diffuser in the apparatus and the diffuser in a display. The reason for this is that the laser and its diffuser produce a narrow fan of light, whereas in a display a beam with a width in the order of tens of centimetres passes through. The light from the laser can be considered as the edge of this beam and in fact makes the measurements easier to make.

The screen is observed both on the horizontal axis, and above it. Due to the vertical symmetry, it is not necessary to take measurements below the axis. When viewed from above the axis, the screen appears as in Fig7.9 (a). The vertical broken line is the region of the screen where the main beam falls. As there is some light scattered horizontally by the vertical diffuser for the laser, a small amount of light is incident across the complete width of the lenticular screen under observation. This produces the faint curved line shown.

When observed from directly ahead, a central bright region, lying on the dim line, is seen as shown in the centre figure in Fig.7.9 (a). As the eye traverses from left to right, the bright region appears to move upward. The broken line indicates the part of the screen on which the fan of light falls. The bright region always lies on this line. The dim line appears to move to the right as the head moves to the right, and a bright section appears where this line crosses the broken line.

The exit pupil boundary zone width caused by the deviation is determined by the lateral distance the head has to travel in order for the bright region to start to appear above the bottom of the screen, and for it to disappear completely at the top.

When seen from the horizontal axis, the screen has the appearance of Fig.7.9 (b). As the observer moves from left to right, the centre of the dim line appears bright as in the left-hand figure. It then parts in the middle, and finally the two bright regions disappear at the top and bottom. The boundary zone width is the distance between the position where the bright region just appears in the centre, and where the bright regions completely disappear.

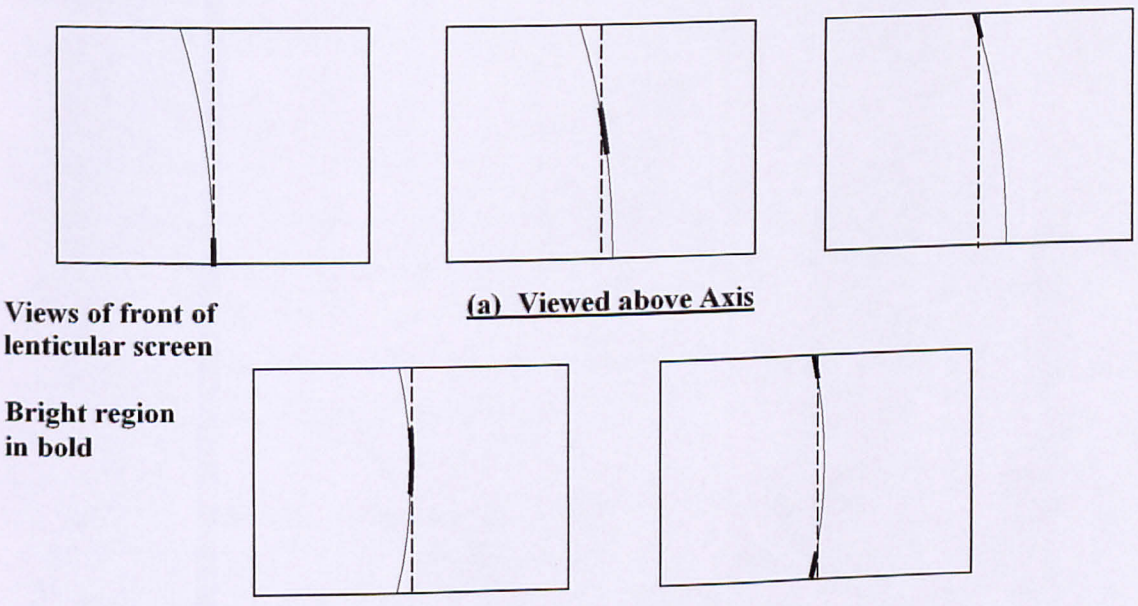

FIG.7.9 APPEARANCE OF DEVIATION

Whilst the apparatus was set up, it was considered worth examining the assumption that the deviation is independent of the sheet lens dimensions. One simple way of determining this is to place another smaller lenticular screen in front of the main screen as in Fig.7.10. With the screen viewed under a range of off-axis conditions, the scattering line and the bright region never alter position over the area of the extra lenticular sheet.

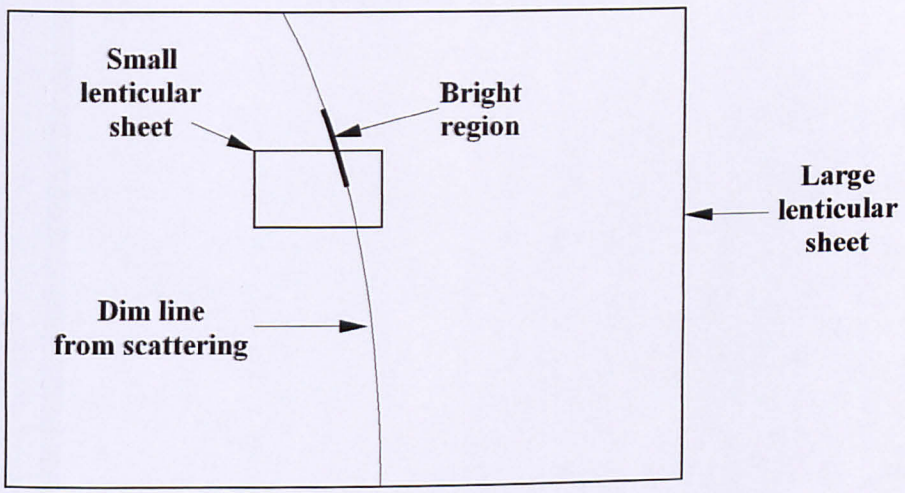

FIG.7.10 EFFECT OF CASCADED LENTICULAR SHEETS

7.5.3) Results

The screen was masked as shown in Fig.7.8 to give a height of 213 millimetres in order to simulate a 14" display. Measurements were made for angles of H_{in} of 30° and 45°. D is the distance from the screen in metres from the screen, and H the height above the axis in millimetres. The laser diffuser was 760 millimetres behind the screen giving an emergent angle of ± 8°.

Table 7.1 - Deviation Range for H_{in} = 30° ; Screen Height = 213 mm.

D (metres)	H (millimeters)		
	0	700	1050
1.25	0	28	-
3.5	10	15	26
5	10	10	10

Table 7.2 - Deviation Range for H_{in} = 45° , Screen Height = 213 mm.

D (metres)	H (millimeters)		
	0	350	700
1.25	0	50	70
3.5	10	20	30
5	15	-	20

The above tables show the deviation range, but give no indication of the central position of that range. The table below was obtained for H_{in} = 30° and gives the position of the centre of the zone in relation to its position on the horizontal axis. The estimated accuracy of the results is ± 10 millimeters.

Table 7.3 - Mean Deviation for H_{in} = 30° ; Screen Height = 213 mm.

D (metres)	H (millimetres)		
	0	350	700
1.25	0	65	-
3.5	0	25	65

The next measurements used the full 305-millimeter height of the screen. The laser diffuser was moved to 865 millimetres behind the screen to give an emergent angle of ± 10°.

Table 7.4 - Deviation Range for H_{in} = 30° ; Screen Height = 305 mm.

D (metres)	H (millimetres)	
	0	650
3	20	20
5	30	30

Table 7.5 - Deviation Range for H_{in} = 45° ; Screen Height = 305 mm.

D (metres)	H (millimetres)	
	0	650
1.5	5	65
2.5	5	45
3.5	25	35

Note that the above results are for the observer facing the screen, so the eyes are not parallel with the screen. At first sight it might appear that allowance will have to be made for this by dividing the results by cos H_{in}. However this correction is not necessary for television viewing where the screen subtends a relatively small angle. It can be safely assumed that the viewer's head faces the centre of the screen so the measurements are made under real viewing conditions. This assumption is also made in Chapter 8 where image space geometry is examined.

7.6) Holographic Light Shaping Diffuser (LSD)

One possible alternative to a lenticular screen as a vertical diffuser is the LSD manufactured by the Physical Optics Corporation in the USA. These have a surface that is replicated from a holographically produced master. The structure of the surface is random, not periodic as in a lenticular sheet. This has the advantage that there are no fringing effects with the LCD pixels.

This company offers a range of elliptical diffusers that have a range of major and minor axis diffusing angles that are stated in terms of their full-width half-maximum (FWHM) values. These are the inclusive angles over which the power is in excess of the half of the maximum value. Two standard products that appear to be suitable for vertical diffusing are the 0.2° x 10° and the 0.2° x 40° versions.

Tests carried out by passing a laser beam through the 0.2° x 40° sheet show that it is an effective vertical diffuser, as it forms a narrow vertical image on a screen. When the sheet was put in to the test set-up shown in Fig.7.4, the same deviations were obtained as for the lenticular diffuser.

Although these diffusers are described as 'holographic', it is interesting to note that the same phenomenon, of the reflected and transmitted images appearing to fall on a common ellipse also occurs. This, along with the fact that the surface has a noticeable roughness, indicates that the action *could* be possibly refractive, not holographic. However, this does not make any difference to its potential usefulness in a 3D display.

7.7) Conclusions

The derivation of an empirical equation for determining the deviation of a lenticular screen might not, at first sight, seem to be the optimum method. However, it provides a fast and accurate method yielding results that give a useful insight into the behaviour of lenticular screens.

The results in Tables 7.1 and 7.2 for the 313 millimetre high screen are encouraging as they indicate that a lenticular screen could possibly be used as a diffuser for a reasonably large viewing field. There is no set limit on the maximum tolerable deviation range, as this has to be added on to other factors such as steering optics aberrations, and diffraction by the LCD. However, a value less than 20 millimetres, for example, allows 45 millimetres for the other factors.

Comparison of the results of Tables 7.1 and 7.3, where the screen height and H_{in} are the same, shows that the mean deviations are far in excess of the deviation range that contributes to the exit pupil boundary width. The implication of this is that the exit pupils are effectively curved, and tracking in the vertical direction will also be required if a lenticular screen is used as a diffuser. However, the accuracy requirement of this will be considerably less than for the horizontal direction.

The results in Tables 7.4 and 7.5 are useful as they relate to a diffuser that is a comparable size to that proposed in the forthcoming ATTEST project where a 21" LCD will be used. The lenticular screen height of 305 millimetres is only slightly less than the LCD height of 317 millimetres. The viewing field of the ATTEST prototype will be 30° either side of the axis so Table 7.4 is relevant. At the maximum viewing

distance of 3 metres, the deviation contribution to the viewing field boundary will be 20 millimetres both on the axis, and 650 millimetres above and below the axis. More accurate and extensive measurements will need to be made, but these results show that the use of a lenticular diffuser need not be ruled out.

The other method of vertical diffusing considered is the use of a holographic optical element (HOE). A holographic vertical diffuser is mentioned in one of the 3D 'Bibles', 'Three Dimensional Imaging Techniques' by Okoshi [OKOS76e], but no mention is made of its performance.

A simple experiment was carried out where the lenticular screen was replaced by an HOE on a compact disc (CD) that was obtained from Chalmers University of Technology in Sweden. This has several HOEs on it, and the most suitable one features a logo that produces an image 118 millimetres high at a distance of 800 millimetres. When the CD is rotated through 45°, the image exhibited a curvature slightly in excess of two millimetres at its centre. This is comparable to the two millimetres produced by a lenticular screen at this angle.

Within the ATTEST project, it is anticipated that a custom-built holographic diffuser will be built and evaluated. As a full-sized version will be extremely expensive, a smaller one will be constructed in order to compare its performance with a lenticular screen.

A company in the UK, and an Institute in Russia, have been approached regarding this. The Physico-Technical Institute in St Petersburg have experience in this area [DENI98] as they have constructed a holographic diffuser for a 3D display where horizontal only parallax is presented. The author has been in correspondence with the Institute and has ascertained that the requirement for the diffuser is different to De Montfort's as they are not concerned with rays that are away from the axis. However, Yuri Denisyuk, the author of the paper, has an understanding of our requirements and is of the opinion that the deviation is inevitable with *any* form of diffuser.

CHAPTER 8
3D IMAGE CONSIDERATIONS

8.1) Preface

Although the current research is concerned only with the hardware to produce a 3D television display, certain **human factors** considerations, such as crosstalk and critical flicker frequency (CFF), have some bearing on the design. Section **8.2)** is a brief survey of work in this area. Crosstalk is the limiting factor determining the extent of the useable viewing field as this increases with distance from the screen and with angle from the axis. The field is small in the single-viewer prototypes under construction, but in the final television version it will cover a large region in front of the screen. The choice of image multiplexing method is decided by the speed of the display in relation to the CFF. Viewing 3D displays for prolonged periods can possibly induce nausea and headaches. Although the subject of human factors is beyond the scope of the current research, it is a problem that will need to be addressed if head tracking binocular television is going to be widely adopted.

Image-space geometry is considered in the following section. This is an analysis of the way in which the apparent 3D image varies with viewer position. This will not have any bearing on the display design, but the results can be used to predict the distortions produced from a given apparent depth of image field. This could be an important consideration where the viewing field covers a large area, as would be the case with a television display.

In the final section of this chapter, the subjective effect of **screen intensity variation** is described. The single-viewer prototypes use Fresnel lenses to produce the exit pupil-pairs. This gives a backlight that has substantially the same intensity across the width of the screen. However, the more complex optics necessary to form the multiple exit pupils required for a television is likely to give the appearance of vertical bright and dark bands. The subjective effect of these is determined.

8.2) Human Factors

The proposed television display will be binocular, i.e. it will provide only two images to the viewers. The same images will be directed to every viewer, so motion parallax

is not available. As mentioned in Section **2.5.1)** (p41), unless a display can give around two views or more per pupil width, the eyes will focus at the screen, but will converge at the apparent image distance. This problem occurs with all multi-view and binocular displays and means of combating this are considered in Section **8.2.4)**.

Two important aspects regarding the viewing of television are that it is a casually-watched, non-immersive medium, and also that the brain is probably much more adaptable than we normally give it credit for. It can make corrections for stereo distortions [SPOT53b]. There are undoubtedly undesirable psychovisual effects caused by viewing stereo displays, but when it is borne in mind that television is generally only intermittently watched, the question is raised as to whether these effects are as important as is commonly thought. It is interesting to note that we quite happily watch a two-dimensional picture, where the perceived image can be very distorted under certain viewing conditions, without this really bothering us. Many experienced stereo users can tolerate a high degree of stereo inconsistency; unfortunately novice users do not have this ability [MULK01]. Hopefully, with increased general usage of 3D, the majority of the population will become stereo-tolerant. However, one aspect of 3D displays is that of possible damage to young developing eyes. Although it is the author's experience that children are generally very enthusiastic about 3D, and have little difficulty in fusing stereo pairs, some concern has been expressed on the effect of stereo viewing on the growth of the eyeball [MAYE00].

The improvement afforded by 3D over monoscopic images has been widely reported by leading workers in the field, For example: Pastoor states that the overall psychological impact of a 3D screen is equal to flat images twice their size [PAST91b]. The consensus is that the wearing of special glasses in unacceptable, and in some viewing situations this can be especially important [FHM98].

8.2.1) Image-space Distortions

Two important artefacts of two-image stereo displays are: points in the image appear to rotate as they follow the viewer's head position, and the image can appear to 'pivot' around the vertical axis as the viewer moves laterally. These effects were

described as long ago as 1953 [SPOT53a] and are considered in detail in Section **8.3)** Lack of motion parallax means that the 'look-around' facility is lost. When viewers first see stereo, they have a tendency to try to look behind objects in the foreground. However, when the novelty wears off, they usually stop doing this. As television viewers are generally fairly static [PALE92], none of these effects should be particularly detrimental to viewing quality.

8.2.2) Picture Size

For the presentation of a completely realistic image, the angles subtended by objects in the image should be the same as in real life so that the image is orthoscopic. This condition is difficult to achieve if the display is not very large. It has been suggested [PAST91c] that the optimum viewing distance for television is three times the picture height. Another phenomenon, that is a consequence of the lack of orthoscopy, is the 'puppet theatre' effect [PAST91c]. This is the unrealistic quality that is the result of the objects in the image occupying a smaller region on the retina than they would for a natural scene. It has been pointed out that this is intrinsically no more disturbing than viewing the miniaturised two-dimensional images that we currently seem to find acceptable [SMIT88d].

This 'puppet theatre' effect can be reduced by the way in which the images are captured [YAMA95] [YAMA98]. When a pair of cameras are used to captute they are usually 'toed-in' so that their axes cross at the distance of the subject of the scene. This gives zero disparity, and the subject appears to be in the plane of the screen when the image is reproduced. It has been found that if the cameras have parallel axes - the orthostereoscopic condition - the effect is less.

It has been observed that when viewed at four times the picture height, there is an imperceptible difference between the perceived image sharpness between an 825 line and 1125-line images [WILC92]. This finding could be useful as the spatial image multiplexing used in the prototypes halves the number of lines. Progressive scanning, as opposed to interlaced scanning, improves perceived image quality. It has been reported that at a field rate of 50 Hz an interlaced scan only appears to have a resolution of 1.2 times that of a progressive scan with half the number of lines

[SCHW90]. It is only when the frame rate approaches 100Hz. that the two scanning modes have the same subjective appearance. This is important as LCDs are operated in the progressive scanning mode.

An image that has relatively low definition will benefit from the addition of stereo. This can be demonstrated in the following ways; for someone with unimpaired stereo vision, the appearance of a natural scene does not appear to be much less realistic if one eye is closed. On the other hand, if television is being watched through Pulfrich glasses, the picture will suddenly appear to 'come alive' when the camera carries out a tracking shot. This is due to some of the monoscopic depth cues not being particularly strong due to the low definition. This benefit of adding stereo to a relatively poor quality image is mentioned in Spotiswoode [SPOT53c].

8.2.3) Implications for Coding

In his book 'Stereoscopy', Valyus states that if a pair of stereo images is of differing quality, the subjective quality of the fused pair is determined by the better image [VALY66d]. In 'Vision', Marr mentions that if the high-frequency spatial components in a pair are in rivalry, and the low-frequency components are not, the image-pair can be fused readily [MARR80]. The stereo pairs of Fig.8.1 are taken from the book. When the images are fused, the dark details give the appearance of being in

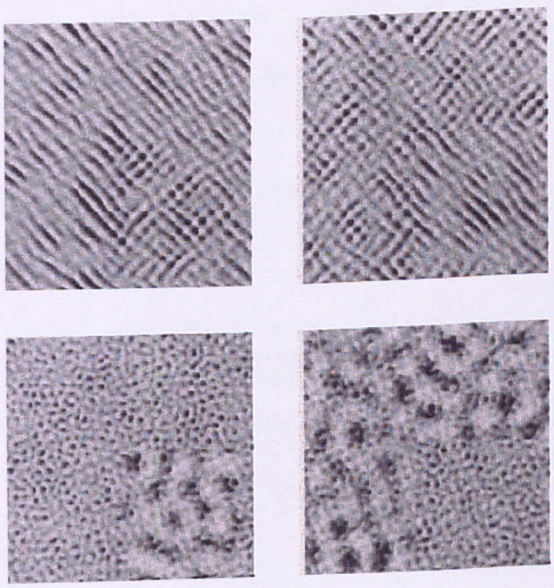

FIG.8.1 STEREO PAIRS WITH TEXTURE DIFFERENCES

both images.

These effects have important implications for stereo image coding. It is quite possible that, due to the large proportion on information common to both images, coding will be achieved by synthesising the second image from the first by the transmission of a small amount of additional information. This will undoubtedly create some artefacts, but these may possibly not be too apparent.

8.2.4) Accommodation / Convergence Difference

It is inevitable with any display showing a different image to each eye, that the eyes will focus at the screen, and converge at the apparent image distance. The Heinrich-Hertz Institut has investigated controlling the amount of disparity in order to keep it within a 'comfortably viewable' range [PAST92]. This will also reduce excessive depth discontinuity at the border of the screen that can also put stress on the visual system.

A solution to the problem has been offered where the synthesis of an intermediate view reduces the effective camera separation [KONR99]. This approach has the advantage that the virtual separation can be chosen after the images have been captured. The method is limited by the quality of the algorithms used to synthesise the image. Comparison is made between block-based and pixel-based methods and the latter was found to be superior. One interesting point made was that there could be 'depthness' control, so the apparent depth could be selected by the viewer. This facility will also be investigated within the ATTEST project. However, individual selection by each viewer will obviously not be an option in the multiple-viewer prototype to be built as every viewer sees the same image-pair.

8.2.5) Crosstalk

Crosstalk will arguably be the most important factor concerning the design of a 3D television. Lipscomb suggests that reduction in disparity reduces crosstalk, also that colour selection can help [LIPS94]. However, it is not clear whether the findings only refer to CRT-based 3D displays where phosphor decay times are an issue.

A useful means of reducing the effects of crosstalk is afforded by the 'kinder, gentler approach' that aims at 'just enough reality' [SIEG01]. The image pairs are generated

from a pair of cameras with separations of millimetres. The effect of this to produce images that appear to exhibit blurring at high crosstalk levels, as opposed to objectionable 'ghosting' where double images are perceived. As high levels of crosstalk might be encountered in the multiple-viewer prototype with its large viewing field, a useful area of research will be an investigation into the trade-off between disparity limitation and crosstalk, and its effect on the overall subjective quality of the image.

8.2.6) Flicker

Flicker is an important consideration as it determines the method of image multiplexing, and hence the display-type. The critical flicker frequency (CFF) – the frequency at which flicker just becomes visible – increases with luminance [KING83]. The CFF varies from 13Hz. at a luminance of 3.4×10^{-3} nits, to 51 Hz. at 343 nits. However, there are many other factors determining the CFF, for example age, foveal or peripheral vision, and luminance of screen surround amongst many others [MAXW92]. TFT LCDs will exhibit flicker at half the field frequency. Driving the display in such a way that the phase of the flicker is inverted on alternate rows can eliminate this [KNAP90]. TFT LCDs are far too slow to operate in the field-sequential mode where left and right images are presented in succession, therefore spatial multiplexing is adopted for the prototypes.

8.2.7) Depth Plane Quantization

Depth plane quantization is the separating of the image into discrete planes, due to the effect of the horizontal pitch of the display pixels giving disparity quantization. The suggested threshold for this to become apparent is 0.8 minutes of arc [BARD95c]. Disparity quantization is doubled in simple lenticular 3-D displays where left and right images are displayed on alternate pixel columns. However, it is not altered when spatial multiplexing is carried out on alternate rows as in the author's display. In one of the displays proposed for the ATTEST prototypes, the horizontal pitch of the RGB triads is 0.207 millimetres. At the minimun viewing distance of one metre, this corresponds to a quantization error of 0.7 minutes of arc.

8.3) Image-Space Geometry

An ideal 3D display would exhibit motion parallax, i.e. where the image changes continuously with movement of the viewer across the viewing field. However, in the real world, this is a luxury that is unlikely to be achieved in the first generation of 3D television due to the large amount of image information content required. Also, motion parallax would need a capture camera in the order of two to three metres wide, and a higher transmission bandwidth. Additionally, there are image field geometry factors that favour the use of a two-image 3D system.

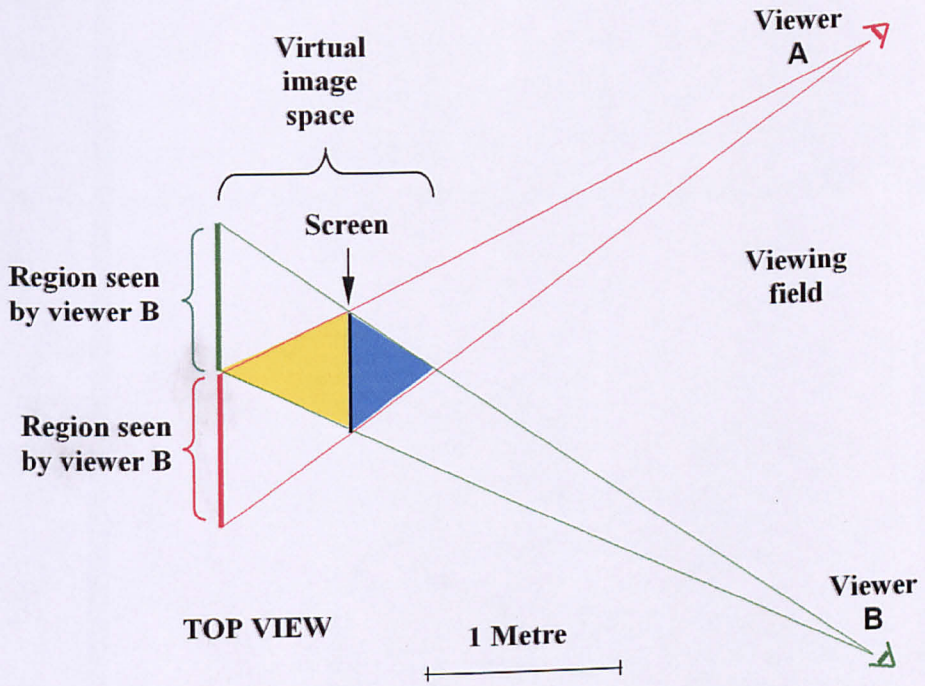

FIG.8.2 'WINDOW' EFFECT OF SCREEN SIDES

Consider a typical viewing situation shown in Fig.8.2 where the viewers A and B are 2.75 metres away from a 28" diagonal screen. It can be seen from the figure that if the image consists of a plane located 650 millimetres behind the screen, completely different regions of the plane are seen by each viewer. In fact the prism-shaped volume, whose apex is 650 millimetres behind the screen, is the only region seen by both viewers.

Similarly, the viewing region in front of the screen is also limited. It is unnatural for objects to be cut off in mid-air, consequently images will be confined to the prism-shaped region that only extends to 440 millimetres from the screen. This fact is contrary to popular, but misleading, depictions of 3D displays where the image is shown popping out of the screen and appearing outside its boundary.

When the screen is considered to be, in effect, a small window, it is obvious that an actual window the size of a television screen would present a very restricted view of the real world existing the other side of it. This 'window' effect could possibly be acceptable in a larger, say 40", display if the image space is reduced to around half a metre from the screen. Also, the effect will be reduced in any two-image 3D display as the apparent depth of the image will have to be restricted in order to reduce the conflict between the difference in accommodation and convergence of the viewers' eyes.

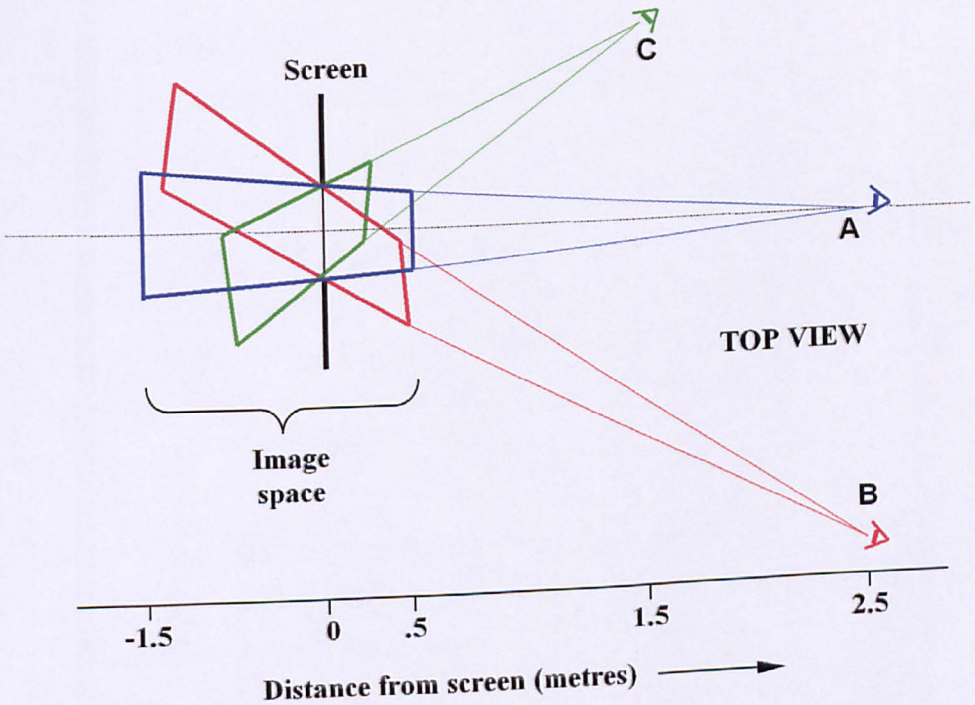

FIG.8.3 VARIATION OF IMAGE SPACE WITH VIEWPOINT

Possibly, in the future, the screen will become large enough to occupy the complete wall of a room so that the 'window' effect will not be an issue. However, this is unlikely to happen in the foreseeable future. In addition to requiring only two-camera image capture, it can also be advantageous from the picture-content point of view to have all viewers seeing the same image-pair [KLEI90].

The first generation of 3D television, whether or not it will be our method of multiple steerable exit pupils controlled by a head tracker, will almost certainly be a two-image system with its attendant stereo distortions that arise from the lack of motion parallax. Fig.8.3 shows the way in which the image varies with viewing position. There are three effects produced; these are false rotation or 'pivoting' of the image around the screen as the viewer moves, variation of apparent image distance with viewing distance, and image plane rotation.

8.3.1) False Rotation

False rotation is the effect where the image appears to move with movement of the viewer's head. This is inevitable in any two-image stereo as an image point must always lie on the axis between the centre of the two image-points on the screen, and the mid-point between the viewer's eyes. Fig.8.4 indicates how this effect arises. As the viewer moves from position P_1 to P_2, the image moves from M_1 to M_2. Although the figure shows virtual images in front of the screen, the same considerations apply to images behind the screen where the images appear on the axis extended into this region.

The effect is usually most noticeable when stereo is first seen, and is consequently still a novelty. Viewers, especially children, tend to try to look round images when first confronted with stereo. However, when this novelty wears off, they tend to remain fairly static, as do most television viewers.

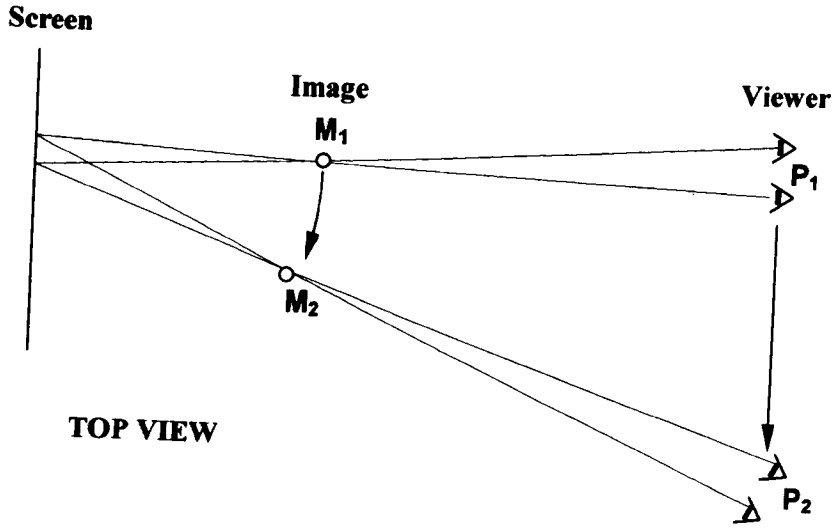

FIG.8.4 FALSE ROTATION

8.3.2) Image Distance Variation

The distance of the viewer from the screen also determines the virtual image position. Consider the reference viewer in Fig.8.5 (g). By applying similar triangles it can be seen that –

$$A_r / (V_r - A_r) = D / I$$

Where –

A_r = distance of reference virtual image from screen

V_r = distance of reference viewer from screen

D = disparity

I = interocular distance

If the viewing distance is changed to V, as in Fig.8.5 (b), the image distance A is –

$$A = A_r V / V_r \quad \text{.....(8.1)}$$

This means the virtual image distance from the screen is proportional to the viewing distance. This relationship also applies to images with uncrossed disparity that appear behind the screen, or when the viewer if further away than the reference distance, i.e. when $V > V_r$.

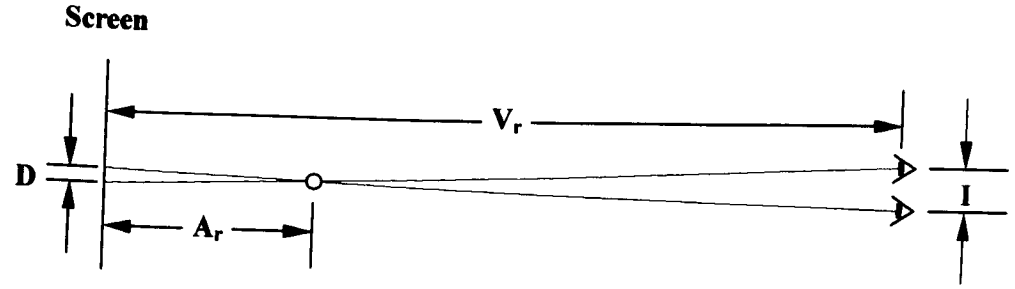

(a) Reference Viewer Geometry

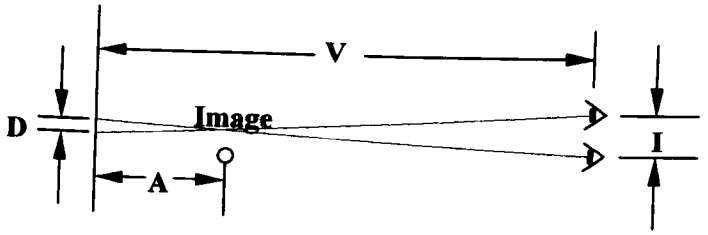

TOP VIEWS

(b) Other Viewer Geometry

FIG.8.5 IMAGE DISTANCE VARIATION

8.3.3) Image Plane Rotation

As the viewer moves away from the axis, image planes that are parallel to the screen appear to rotate around the vertical axis in the manner shown in Fig.8.3. The cause of this is the rotation of the head in order to face the screen - which subtends a fairly small angle in the case of television - as the viewer moves away from the axis. If the viewer's head remained facing straight ahead, viewing would be uncomfortable.

If the head always faced straight ahead, the geometry would be as in Fig.8.6. JKL and JR_xL_x are similar triangles so that –

$$A / (A+V) = KL / R_xL_x.$$

Therefore:

$$A = V \times KL / (R_xL_x - KL).$$

Similarly, HKL and HR_yL_y are similar triangles and

$$A = V \times KL / (R_yL_y - KL).$$

R_xL_x and R_yL_y have the same value as they are both the interocular distance, therefore it can be seen that A is the same in each case so that the image plane does not change position. Image plane rotation is mentioned in Spotiswoode and Spotiswoode [SPOT53b] as a curiousity due to their analysis of image geometry assuming that the viewers' heads remain facing ahead. This assumption is based on cinema screen

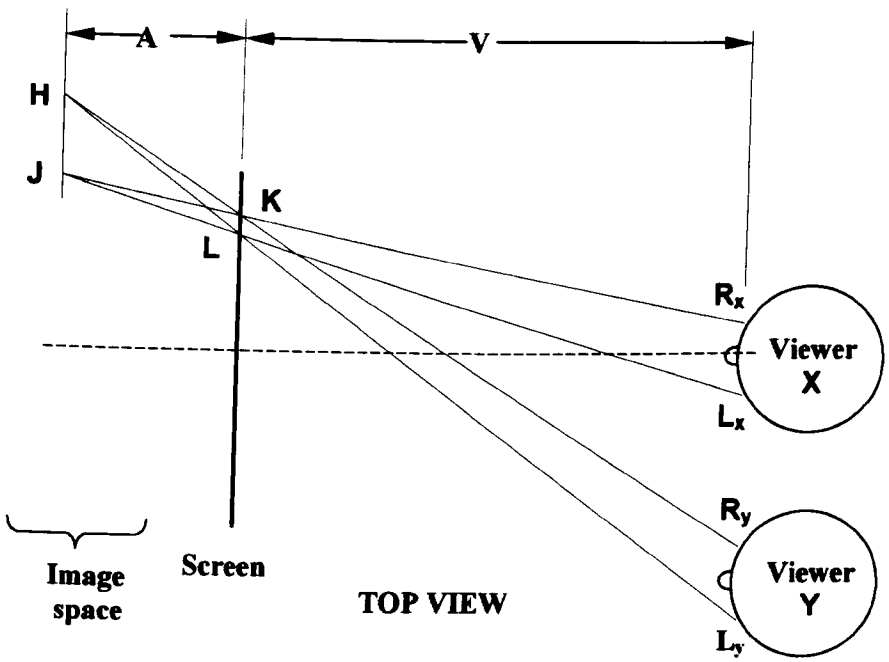

FIG.8.6 IMAGE GEOMETRY WITH VIEWERS' HEADS FACING AHEAD

viewing but is not applicable to television with its much smaller screen.

As the head is rotated in order to face the screen, the effective interocular distance I_1 in the plane parallel to the screen is increased as Fig.8.7 shows, therefore moving the image closer to the screen. I_1 is given by applying the sine rule to the triangle –

$$I_1 = I \cos(\beta-\alpha) / \cos\beta \quad \ldots\ldots\ldots\ldots(8.2)$$

Where -

I = interocular distance

α = angle between eye-centre to screen-centre axis and normal to screen

β = angle between left-eye to left image-point axis and normal to screen

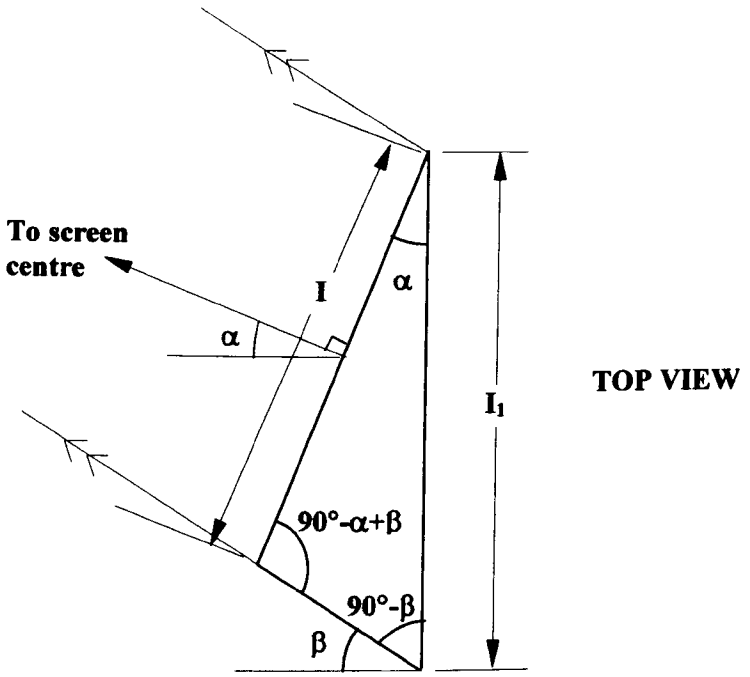

FIG.8.7 EFFECT OF HEAD ROTATION

In Fig.8.8, where the image is behind the screen, it can be seen that the that the disparity D is -

$$D = I A / (V + A)$$

And $D = I_1 A_1 / (V + A_1)$

Which gives -

$$A_1 = \frac{I A V}{I_1 (V + A) - I A}$$

Substituting equation (8.2) into this gives –

$$A_1 = \frac{A V \cos\beta}{(V+A) \cos(\beta-\alpha) - A \cos\beta} \quad \text{.....(8.3)}$$

As the angle (β-α) is only a few degrees, the term cos(β-α), for all practical purposes, can be considered as having the value of one. This produces a negligible difference, and reduces the equation to –

$$A_1 = \frac{A\,V\cos\beta}{V + A\,(1 - \cos\beta)} \qquad \ldots\ldots\ldots(8.4)$$

This simplification corresponds to a slight rotation of the head, that is from facing directly towards the centre of the screen to facing the area under consideration.

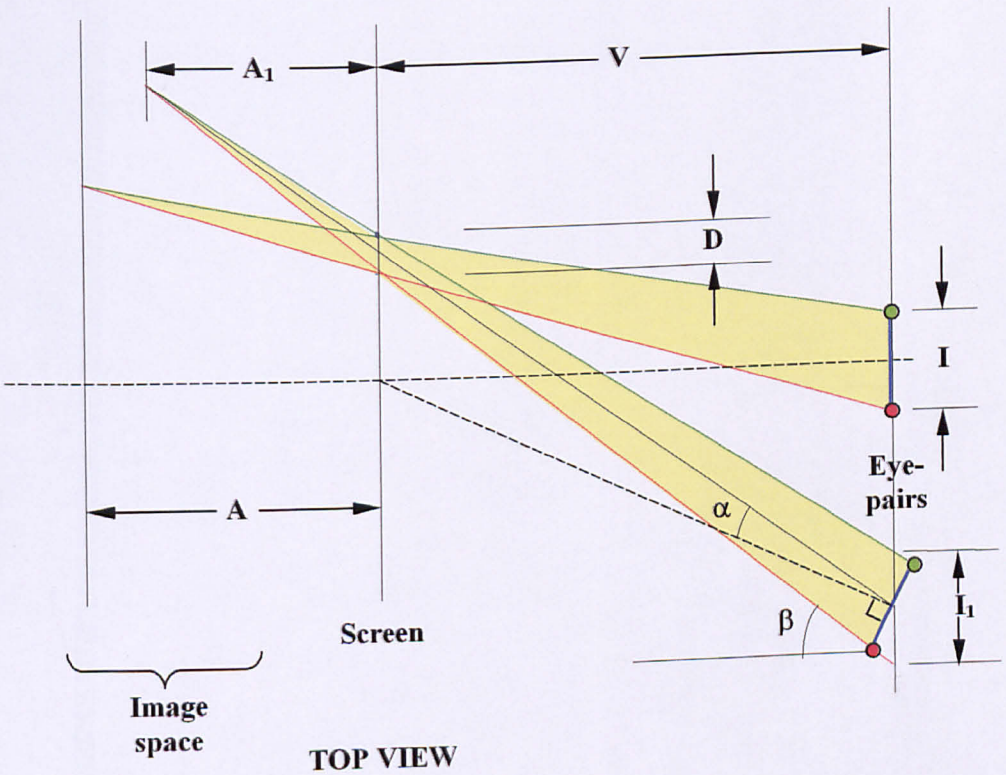

FIG.8.8 APPARENT DISTANCE BEHIND SCREEN

When the image is in front of the screen, the geometry is as in Fig.8.9.

In this case the equations are –

$$D = I\,A\,/\,(V - A)$$

$$D = I_I\,A_I\,/\,(V - A_I)$$

$$A_I = \frac{I\,A\,V}{I_I\,(V - A) + A}$$

$$A_I = \frac{-\,A\,V\cos\beta}{(V - A)\cos(\beta - \alpha) + A\cos\beta} \qquad \text{.....(8.5)}$$

As expected, equation (8.5) is the same as equation (8.3), but with the distances A and A_I considered as being negative.

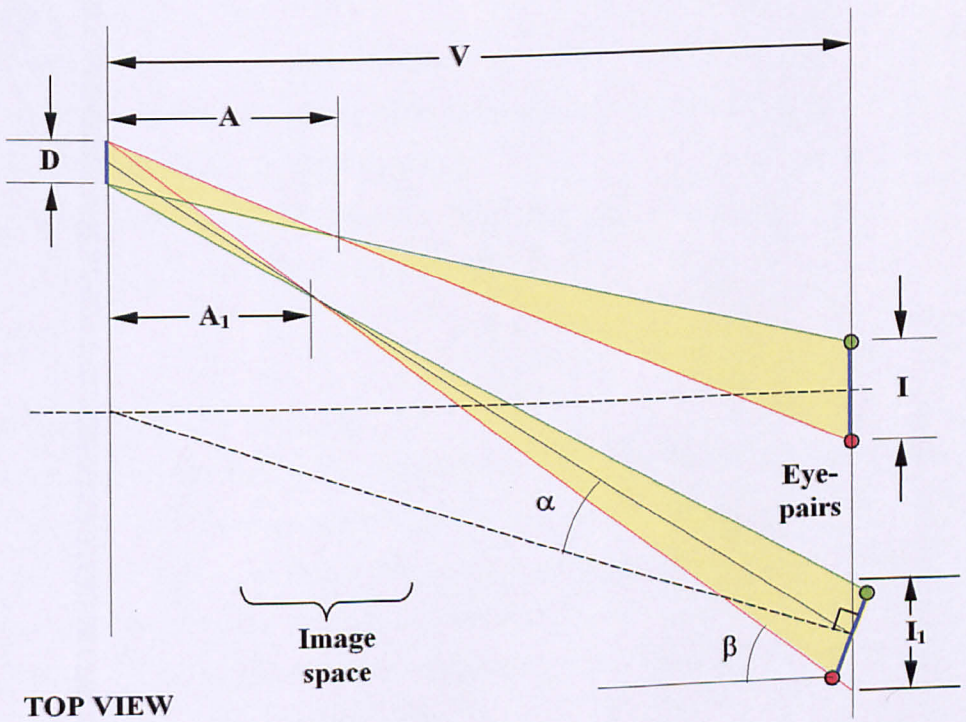

FIG.8.9 APPARENT DISTANCE IN FRONT OF SCREEN

8.3.4) Summary

These distortions can be considered as being the price paid for having the image space 'follow' the viewer around. It is beyond the scope of this research to investigate the psychovisual implications of this, but it should be borne in mind that distortions are tolerated in 2D images, for example those of extreme off-axis viewing.

The combined effect of distance and off-axis viewing can be found by first applying equation (8.1) to give A, and then applying this value of A in Equation (8.4). This gives the rotations shown in Fig.8.3, where planes in front of the screen rotate anti-clockwise as the viewer moves to the left, and vice versa; and planes behind the screen rotate clockwise as the viewer moves to the left, and vice versa.

Substituting equation (8.1) into Equation (8.4) gives –

$$A_I = \frac{A_r V \cos\beta}{V_r + A_r (1 - \cos\beta)}$$

Where –

V_r = distance of reference viewer from screen

A_r = distance of reference virtual image from screen when viewed from axis

V = y-axis component of viewer's distance

β = angle between viewers' left-eye to left image-point axis and normal to screen

A_I = y-axis component of observed image distance

8.4) Screen Intensity Variation

It is anticipated that the steering optics of the ATTEST muptiple-viewer prototype may possibly take the form a series of illumination sources, as opposed to a single source. As the light from these sources might originate from a region that is only a few centimetres high, and situated some distance behind the LCD, illumination must be made to fill the complete height of the LCD. This is achieved by using a diffuser that scatters light in the vertical direction.

The light sources will possibly be arranged so that they form a contiguous region of light in the horizontal direction. Aberrations and assembly inaccuracy may cause overlaps or gaps in this region and would create the appearance bright and dim

vertical bands when the light is scattered vertically. The appearance of these is illustrated in the top figures Fig.8.14. When the sources are narrower than the pitch, a dark vertical band is formed as in the top left-hand figure, and when they are wider, a bright band is formed as in the top right-hand figure.

As this illumination effectively forms the backlight of an LCD, these visible bands will be unacceptable. This section describes an experiment to determine the amount of spreading, and hence lowering of contrast of these bands, that is necessary for them to become imperceptible. If these bands can be made wider, but with less variation from the general illumination, there will be a point where the bands become imperceptible. This will be achieved by modifying the steering optics, and can be simulated by using a lenticular sheet with its lenses running vertically. This causes the bands to be wider, but with less variation from the background.

8.4.1) Theory

The light from the left aperture has the form of Fig.8.10 (a) where the right edge is sharp. When it is viewed through a lenticular screen with vertically aligned lenses, the edge will appear 'soft' and have the intensity distribution as shown in Fig.8.10 (b). The screen simulates the action of fading components that might be incorporated into the steering optics.

Fig.8.10 (c) illustrates the effect of the lenticular screen on a pair of apertures that have positive overlap as shown in Fig.12 (a). The narrow band, where the intensity is approximately doubled, is replaced by a wider region where slightly increased intensity is observed, as in Fig.8.10 (d).

The intensity increases over the overlap distance as shown in Fig.8.10 (d). The increase in intensity I_B over the central region is proportional to the overlap o/l, but inversely proportional to the fading width F. Therefore, for a given overlap, increasing the fading width will reduce the intensity increase. The object is to reduce this increase to the point of imperceptibility. Similarly, when there is a gap between the apertures, the intensity decreases over the central region.

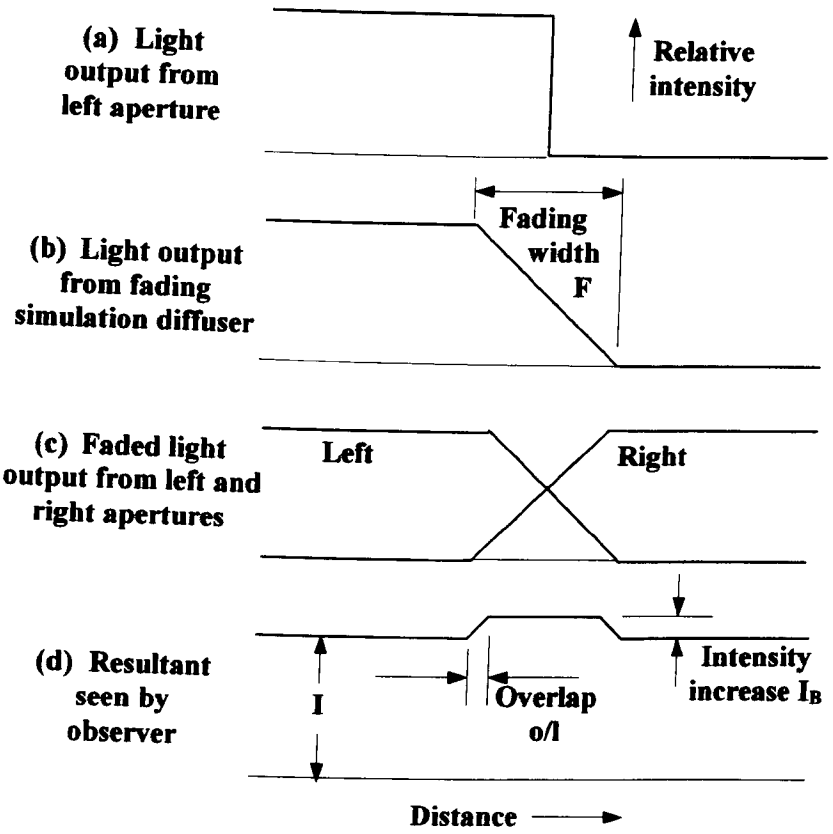

FIG.8.10 INTENSITY VARIATION

8.4.2) Experimental Apparatus

The experimental apparatus consists of a pair of apertures that simulate a boundary in the steering optics, with a 3-watt fluorescent light source mounted behind them. These are mounted on an optical bench as shown in Fig.8.11. The widening of the bands, or fading, is achieved with the lenticular having with vertically aligned lenses, and is mounted in front of it. This screen has a pitch of 0.6 mm, with lenses of 6 mm focal length. This can be moved longitudinally in order to give different fading widths; the further it is away from the apertures, the greater the fading width. The position of this is measured on the scale shown.

After the light has passed through this, it then passes through a larger lenticular screen whose lenses run horizontally in order to provide vertical scattering. The distance between the apertures and the vertical diffuser is 500 mm, and the observer is situated

two metres in front of the vertical diffuser. These are typical distances likely to be encountered in a display.

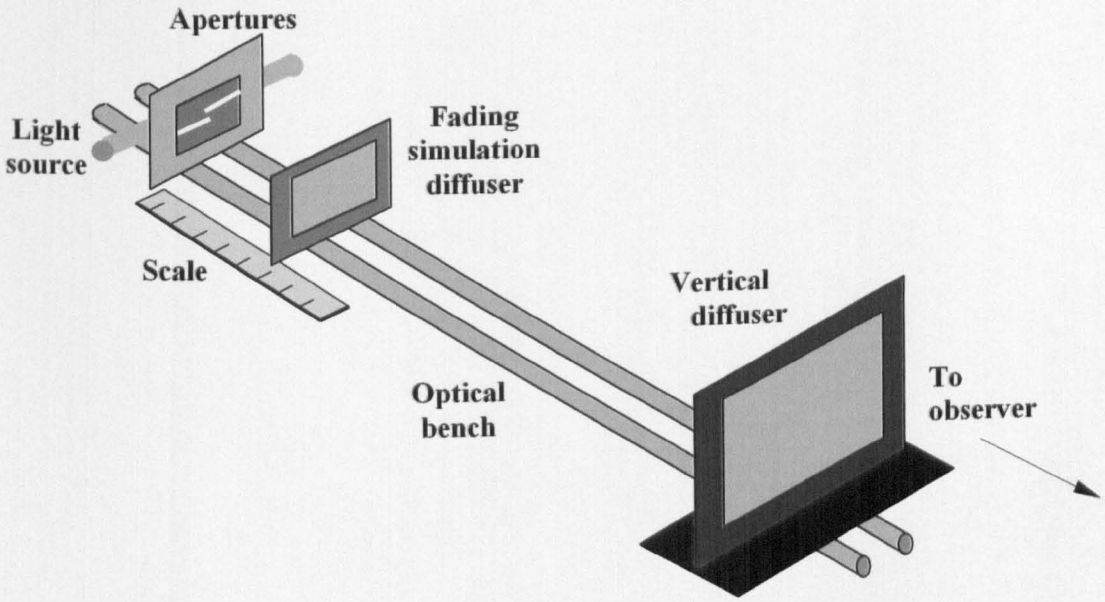

FIG.8.11 EXPERIMENTAL APPARATUS

As the apparent fading width is dependent on the distance of the lenticular screen from the apertures, the relationship between the screen position and fading width was established. This was achieved by mounting a ruler against the horizontal diffuser, and removing the vertical diffuser. The spread width was measured through a monocular` located at the observation position used for the experiment. The diffuser was moved longitudinally and the scale was calibrated according to the observations. It was found that an increase of one centimetre distance between the apertures and the diffuser gave an increase of one millimetre in the spread.

A series of seven masks was constructed which had overlaps ranging from –1.5 mm to 1.5 millimetre overlap in 0.5 millimetre increments. These included one with zero overlap that was not used in the experiments on the subjects. The diagram, to actual size, of two of these is shown in Fig.8.12. The masks were constructed by sticking black vinyl tape on to Perspex sheets.

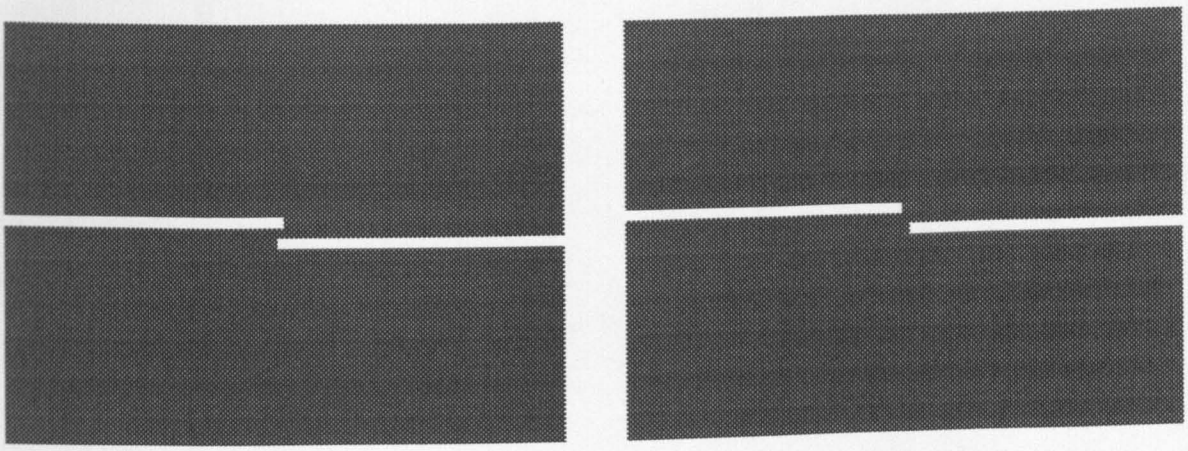

(a) 1 mm overlap **(b) -1 mm overlap**

FIG.8.12 MASKS TO ACTUAL SIZE

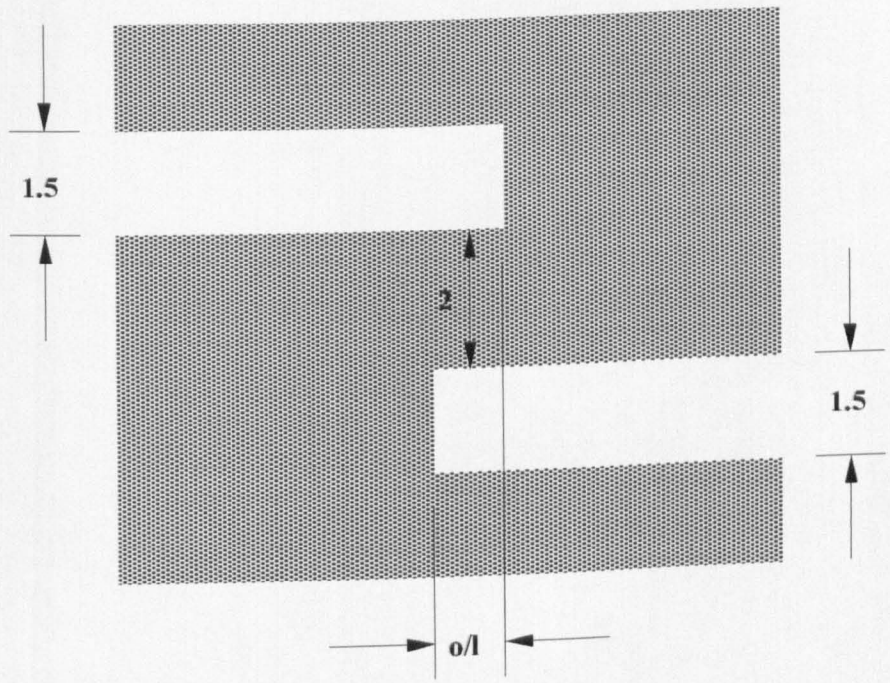

Dimensions in mm

FIG.8.13 CLOSE-UP OF OVERLAP REGION

A close-up of the overlap region is illustrated in Fig.8.13. In this case, where the overlap is one millimetre, it can be seen that a vertical line through the central region passes through two apertures, and through one aperture only either side of this. A vertical diffuser has the effect of summing the light, therefore the central region has

double the intensity of the rest of the screen. When there is negative overlap, the central region has zero intensity.

8.4.3) Experimental Procedure

When the scale had been calibrated, the vertical diffuser was replaced and a seat placed in front of the apparatus to enable observers to view the screen two metres away from it. Lighting in the room was kept at normal ambient levels as this represents typical television viewing conditions.

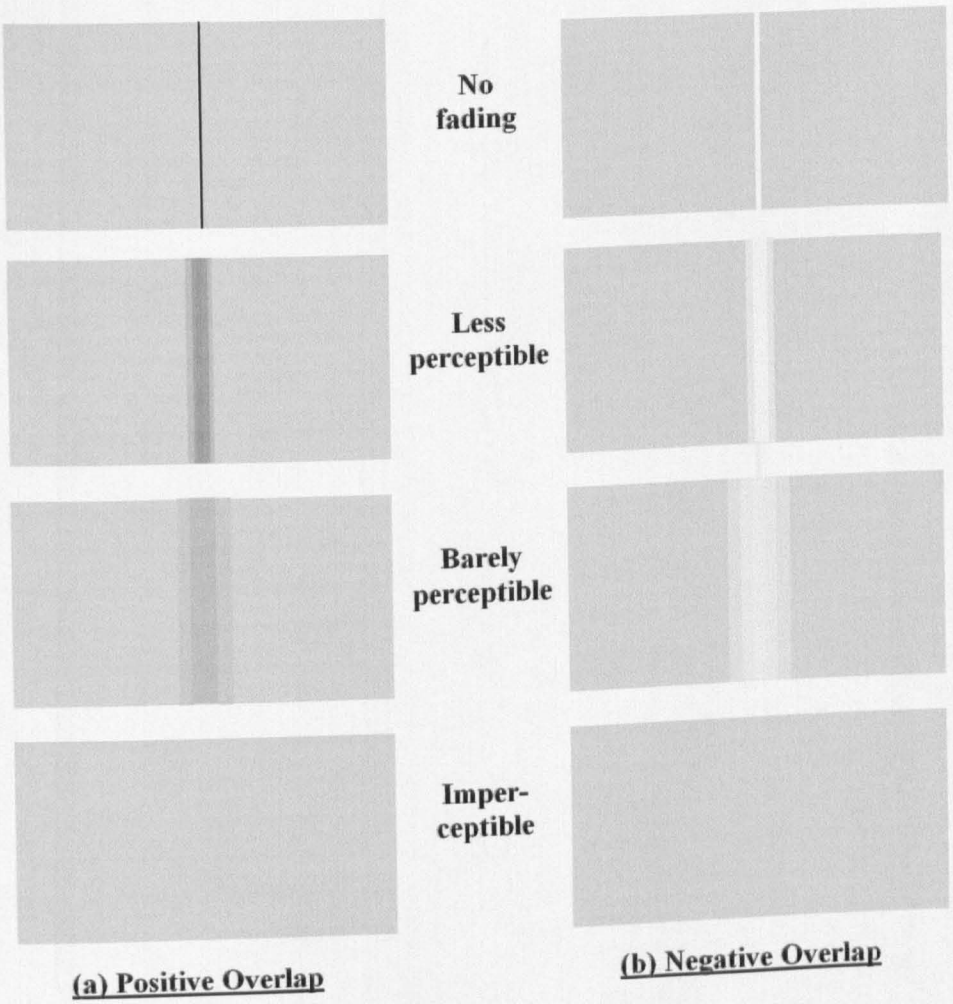

FIG.8.14 APPEARANCE OF DIFFUSED APERTURES

With the observer in position, the mask with 1.5 mm overlap was placed in front of the illumination source, and the fading simulation diffuser located close to the mask. A dark band as illustrated in Fig.8.14 (a) 'Less perceptible' was seen. As the diffuser is slid gradually along the optical bench away from the apertures the appearance changed to Fig.8.14 (a) 'Barely perceptible' and finally to Fig.8.14 (a) 'Imperceptible'. The reading at which the appearance became imperceptible is noted. This procedure was repeated for the masks with 1, 0.5, -0.5, -1 and – 1.5 mm overlaps.

8.4.4) Results

The measurements were carried out on nineteen subjects of widely differing ages and are given in the table below. Histograms derived from this are plotted in Fig.8.15 and clearly show the spread of results.

Table 8.1 Screen Intensity Variation Threshold Experimental Results

SUBJECT	AGE	-1.5 mm o/l	-1 mm o/l	-.5 mm o/l	.5 mm o/l	1 mm o/l	1.5 mm o/l
AS	**21**	19	14	8	6	12	24
CB	**20**	26	21	12	10	16	23
CS	**6**	19	17	8	6	11	17
ES	**46**	26	19	10	9	12	22
IS	**36**	24	17	11	10	14	23
JB	**32**	17	13	7	7	10	15
JB	**33**	20	17	9	7	14	19
JB	**44**	20	14	10	9	11	15
JC	**30**	17	14	9	8	14	17
KB	**7**	18	15	7	7	13	15
LW	**42**	20	15	9	7	12	14
MG	**10**	18	13	10	7	11	14
MJ	**26**	22	16	10	8	11	15
PS	**51**	26	16	12	9	14	23
RS	**10**	18	17	9	11	15	18

SP	**34**	19	15	8	7	12	16
SS	**18**	18	14	8	10	11	20
TP	**84**	17	15	8	8	11	17
VL	**76**	19	15	7	7	12	19
	Ave.	**20.16**	**15.63**	**9.05**	**8.05**	**12.42**	**18.21**

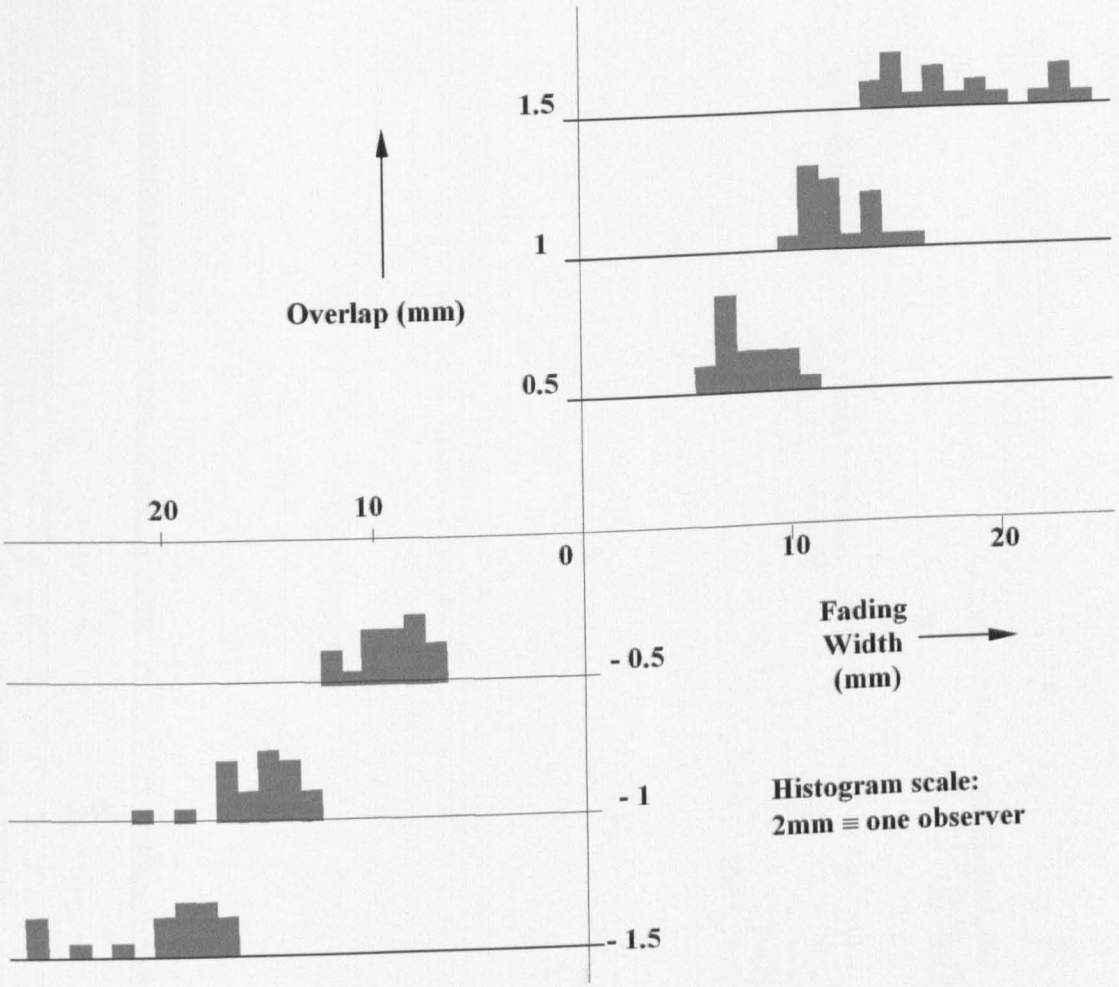

FIG.8.15 HISTOGRAMS OF FADING RESULTS

The average fading widths for each of the six overlaps in Table 8.1 are plotted in Fig.8.16. The straight line 'best fit' to these is taken as that where the sum of the square of the differences in fading width is a minimum. Table 8.2 shows that this is the straight line passing through the point: overlap = 1.5 millimetres, fading width = 20 millimetres

Table 8.2 Results for Obtaining 'Best Fit' Fading Width Plot

Fading width at 0/l = 1.5 mm	Σdifference^2
19	14.67
19.5	11.93
19.9	11.61
20	11.31
20.1	11.51
20.5	12.77
21	14.03

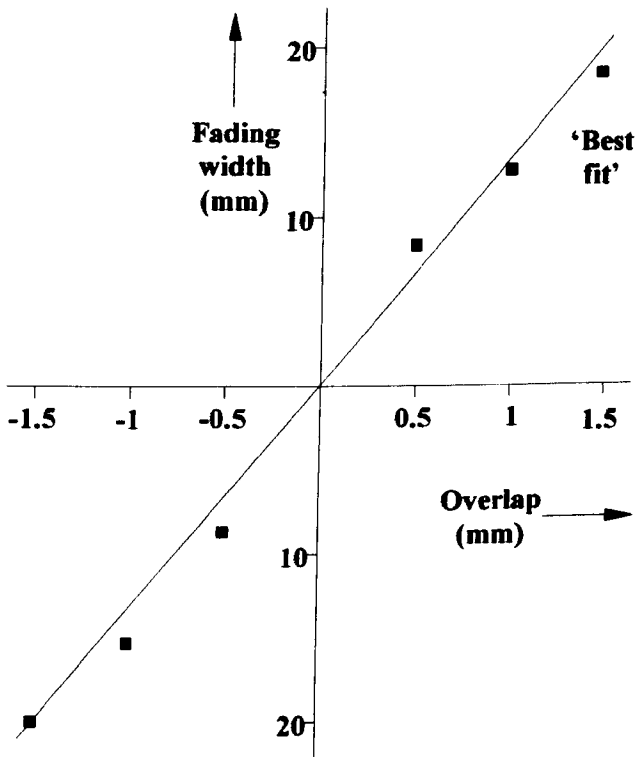

FIG.8.16 'BEST FIT' TO RESULTS

8.4.5) Screen Intensity Variation Conclusions

The results in Fig.8.14 indicate that a fading width of 20.0 mm is necessary to remove the appearance of dark or bright bands formed by positive or negative overlap of the apertures of 1.5 millimetres.

In obtaining this result certain assumptions have been made. The 'best fit' is assumed to be linear. This is probably reasonable as the perceptibility is most likely to be determined by the difference in intensity between the boundary region and the surroundings, not on the actual width. As can be seen in Fig.8.10 (a) the intensity increase I_B over the boundary region is given by $I_B = I \times o/l / F$, where I is the unfaded intensity, o/l is the overlap and F is the fading width. I_B is assumed to be the threshold for visibility of the band AND the equation can be rewritten as $F = o/l \times (I / I_B)$. As the term (I / I_B) is a constant, fading is proportional to the overlap as assumed. The line will pass through the origin as there will obviously be no variation in intensity, even with no fading, when the aperture sides line up exactly.

The experimental results represent worst-case conditions, for two reasons. Firstly, the bands were observed on an otherwise blank screen that had no picture content on it. It is probable that the bands will be less noticeable when superimposed on a picture. Secondly, the method of reducing a visible band to imperceptibility, as opposed to the observer noting the onset of its visibility, is likely to give higher readings.

The subjects for the experiment were non-expert and were taken from a wide range of age groups. Experiments that use mainly students as subjects tend to have a narrow age band that is not necessarily representative of the general population.

It should be borne in mind that these results would only be used as a guide as to the dimensions of fading elements possibly employed in the steering optics to be used in a prototype. The final optimisation of the fading dimensions will be carried on the actual prototype when it has been constructed.

CHAPTER 9
5.6 INCH PROTOTYPE

9.1) Preface

At an earlier stage of the current research, the construction of an extremely inexpensive prototype was commenced. This incorporates a small 5.6" diagonal LCD, and the Fresnel lens forming the exit pupils also acting as a magnifier. The display is designed to serve stereo to a single viewer who has limited lateral and fore-and-aft head movement. Illumination is supplied by two arrays of white LEDs, and image multiplexing achieved using a simple inexpensive parallax barrier. The head tracker is the same as is used on the 12" prototype and utilises reflection of infrared from a retroreflector located behind the viewer's head. This is described in Chapter 12.

9.2) General Description of Optics

The display operates by producing a pair of exit pupils in the viewing field as illustrated in Fig.9.1. If the optics consisted of a Fresnel lens, mirrors and white LED arrays only, a pair of real images would be formed in the darker regions marked R and L. The thicker lines indicate the lit regions of the LED arrays. When an eye is situated in one of these regions, intense illumination is seen across the complete lens area. As these regions are too small to allow for sufficient freedom of movement of the viewer, they are expanded to the exit pupils denoted by the lighter regions.

As both left and right images are presented on alternate rows on single LCD, the light from each of the LED arrays must be separated in order for the correct image to be formed in the appropriate exit pupils. This is achieved by the use of a parallax barrier located a short distance behind the LCD, as described in Chapter 5. This is a sheet that has horizontal apertures whose pitch is slightly less than double the LCD vertical pixel pitch. The vertical displacement of the two arrays ensures that the light from the L array falls only on the LCD pixels showing the left image, and the light from the R array on to the right image pixels.

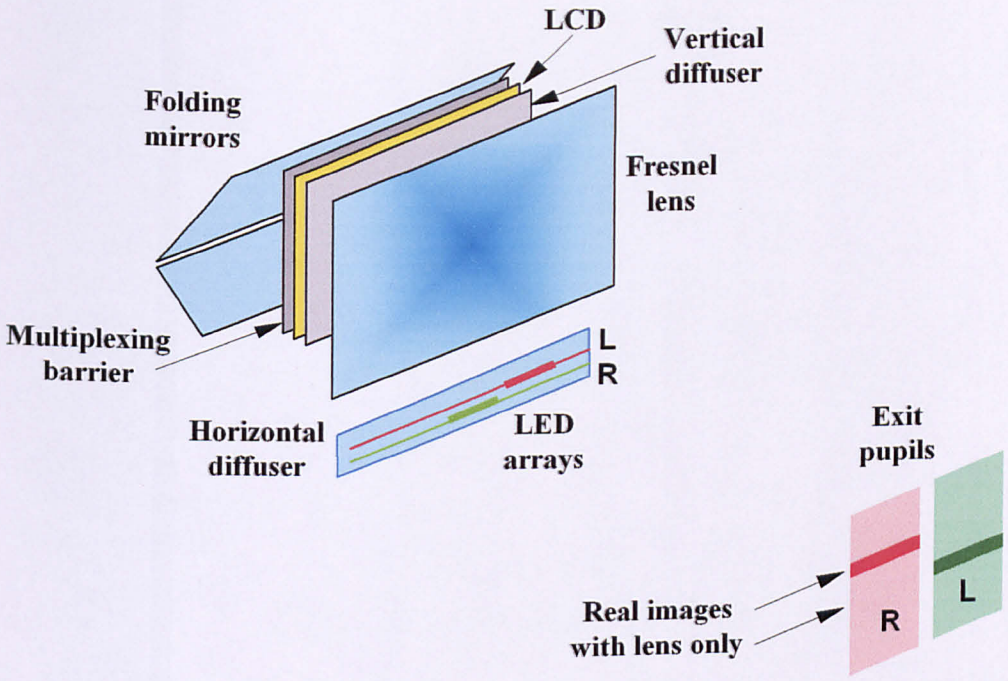

FIG.9.1 5.6" PROTOTYPE SCHEMATIC DIAGRAM

The LED arrays consist of discrete devices that cause uneven illumination to appear across the screen. Mounting a lenticular sheet, with vertically aligned lenses, in front of the arrays eliminates this effect. The two folding mirrors are used to keep the housing size down to a compact cube with 240 millimetre sides.

9.3) Magnifying Optics

When work on this prototype commenced, LCDs were still relatively expensive. For this reason a small 5.6" panel was chosen. As the optics of this design of display requires the use of a Fresnel lens, simply mounting the lens some distance in front of the LCD enables it to be used for both exit pupil formation and as a magnifier. Another advantage of the small screen was that an extremely inexpensive Fresnel lens can be used. The lens used in this prototype is a magnifying sheet costing less than two pounds and its optical quality is sufficiently good for this application.

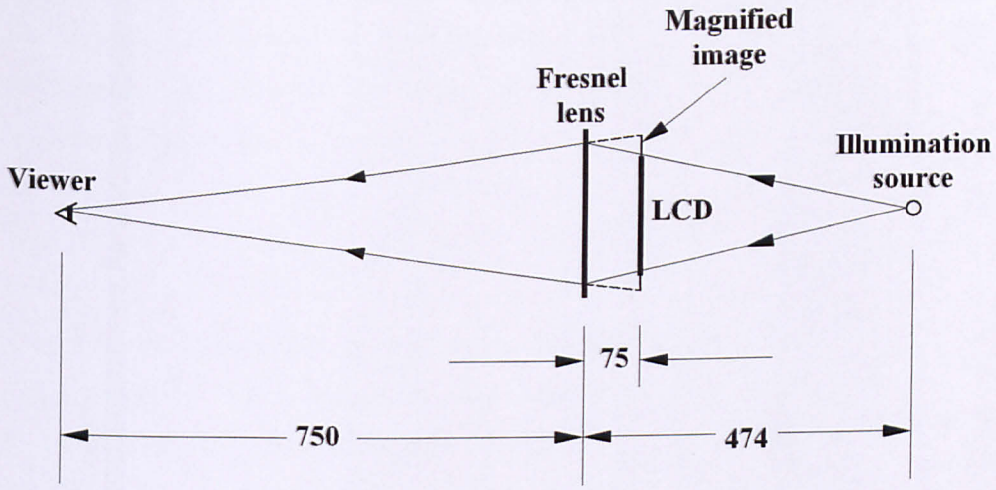

SIDE VIEW
Dimensions in millimetres
Vertical scale X 2

FIG.9.2 5.6" PROTOTYPE OPTICS

The focal length of the lens is 291 millimetres, which gives the viewer and illumination source distances as in Fig.9.2. With the lens 75 millimetres in front of the

LCD, the magnification M_S is given by –

$$M_S = 474 / (474 - 75) = 1.188$$

This makes the image equivalent to a 6.65" display. The image subtends the same angle as a 21" display at 2.37 metres and is therefore similar to typical TV viewing conditions.

9.4) LED Arrays

The illumination is supplied from two 36-element arrays of white LEDs. Fig.9.3 is a full-size diagram of these. They are mounted diagonally on standard 0.1" stripboard, so the pitch is 0.1" x 1.414, which is 3.6 millimetres. This allows three-millimeter LEDs to be used with a minimum gap between them. The arrays are displaced laterally by 11 LED pitches, and each LED in the upper array is connected in series to

its corresponding element on the lower array. Namely, the two LEDs at the left end are in series, the second in from the left connected in series, and so on. The magnification M_I between the array and its image in the viewing field at 750 millimetres is given by

$M_I = 750 / 474 = 1.582$

Therefore the displacement of 11 pitches corresponds to 11 x 3.592 x 1.582, which is 62.5 millimetres. This is around the same value as the typical interocular distance of 65 millimetres. The illumination shown, with two sets of 11 adjacent LEDs lit, will form two exit pupils that are 62.5 millimetres wide, with centres 62.5 millimetres apart.

The figure shows that the position of the boundary between the two lit regions is able to move by 25 LED positions. This is 142 millimetres in the viewing field and is the lateral distance over which the head is able to move.

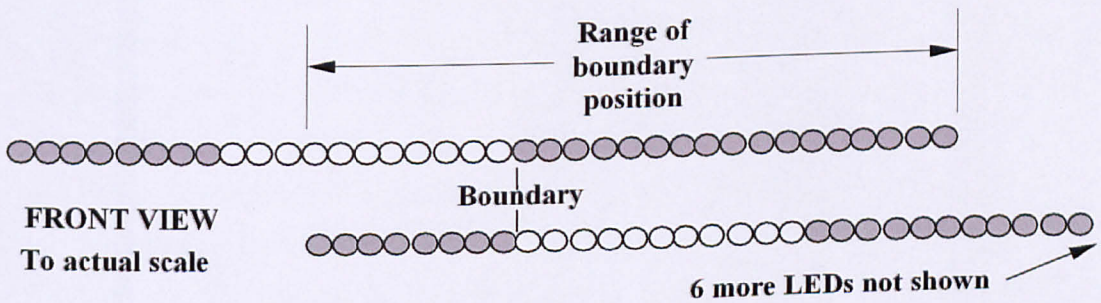

FIG.9.3 WHITE LED ILLUMINATION SOURCE

The LEDs chosen for the array are Nichia type NSPW310AS with a typical luminous intensity of 900 millicandelas at 30 mA. Other devices are available with a luminous intensity of 3000 millicandelas, but these were considerably more expensive. The reason for the Nichia LEDs having a lower intensity is their larger viewing angle of 120°. The problem is overcome by placing ten-millimetre Perspex rods in front of the arrays. These act as a cylindrical condensor lenses whose action is shown in Fig.9.4.

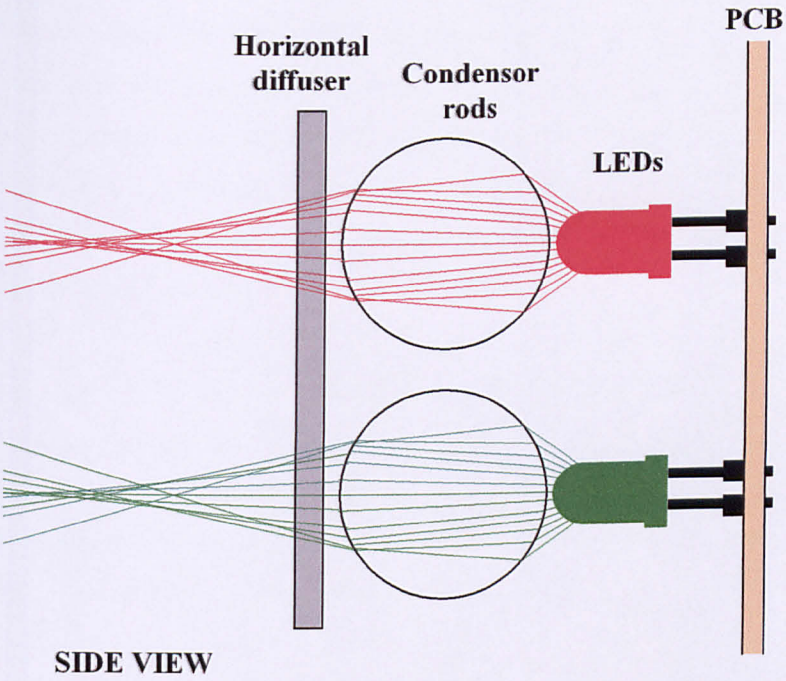

FIG.9.4 SECTION THROUGH LED ARRAY ASSEMBLY

In order to quickly ascertain the luminous intensity improvement obtained with the rods, comparative measurements were made using a flicker photometer. Light from a 10-element arrays of similar LEDs was shone directly on to both sides of the photometer. The procedure was then repeated with a 10-millimetre Perspex rod mounted in front of the test array. With no Perspex rod, the illumination was the same on both sides of the photometer when the arrays were each 140 millimetres away. With the rod, the illumination was the same on both sides with the LEDs 240.5 millimetres away. The measurements were carried out in a darkened room and the intensity of the LEDs was sufficiently high for the results to be unaffected by ambient light. The inverse square law determines the light intensity on the spot so that the increase is proportional to the ratio of the squares of the distances.

Therefore the increase in luminous intensity I_R is given by –

$I_R = 240.5^2 \ / \ 140^2 = 2.95$

The effective luminous intensity becomes 2655 millicandelas, which compares favourably with the 3000 millicandelas of more expensive devices with a 20° viewing angle. Measurements were only taken on the axis, however, when the illumination assembly is mounted in the display, the illumination across the screen appears even. It is envisaged that the technique of using a rod as a condensor lens will prove to be very useful when applied to more advanced versions of the display where surface-mount LEDs might be used.

Mounting a horizontal diffuser in front of the condensors can eliminate the effect of the LEDs being discrete light sources. The design was not carried out rigorously, but a small piece of the lenticular sheet used for the vertical diffuser was mounted in front of the condensors and its optimum position determined. This was found to be when the lenticular sheet is around one millimetre in front of the rods.

One area of concern, when white LEDs are used with LCD displays, is the spectral distribution of the LED output. The LEDs produce white light by exciting a phosphor located in front of a blue LED. The phosphor emits a broad spectrum of light that is centred in the yellow region. The resultant is the spectrum shown in Fig.9.5 (b). The effect of this is to produce a bluish-appearing light with a colour temperature of around 8000° K. The peak at 460 nanometres is produced by the blue output of the LED leaking through the phosphor.

Although subjectively the white light produced is acceptable, albeit rather blue, when viewed directly, this will cause colour distortions when used either for indirect lighting, or in this case, through the RGB colour filters of the LCD.

Typical LCD colour filter characteristics are shown in Fig.9.5 (a) for comparison. Although compensation for this spectrum is beyond the scope of the present work, solutions to this problem are likely to be by either the use of a bandstop filter at around 460 nanometres, or by adjusting the drive to the LCD.

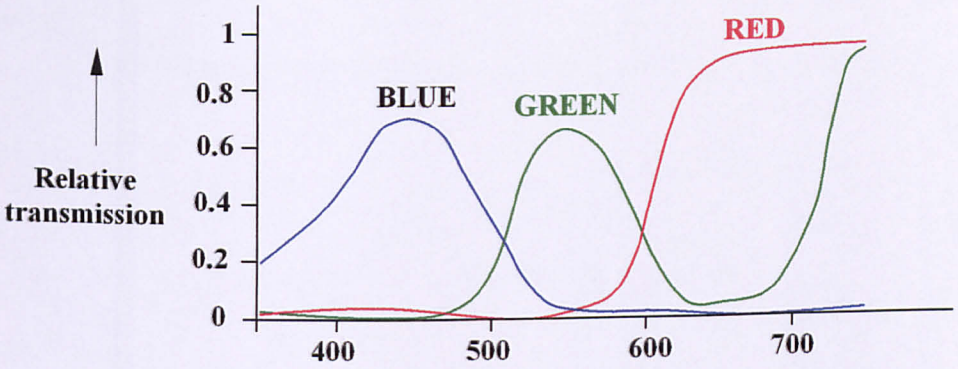

(a) Typical LCD Filter Characteristics

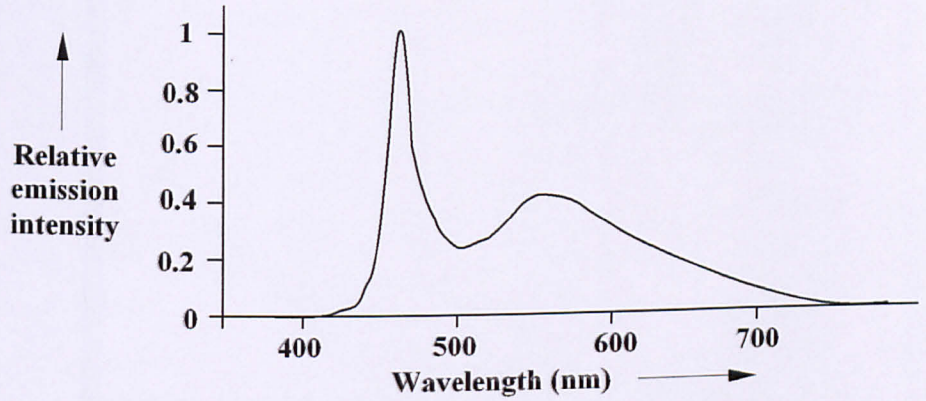

(b) White LED Relative Intensity Spectrum

FIG.9.5 SPECTRAL RESPONSES OF WHITE LED & LCD FILTERS

9.5) Folding Mirrors

In order to keep the housing size down to a compact 240-millimetre side cube, the light from the LED arrays is folded by two mirrors as illustrated in Fig.9.6. This subject is covered in detail in Chapter 4. The mirrors are at 45° to the horizontal and enable the depth of the housing to be halved. The virtual images of the arrays lie 474 millimetres behind the LCD. From the arrays, the LCD subtends an included of angle of 20°. This angle is necessarily small as it corresponds to tolerable spherical aberration in the Fresnel lens. It can be seen that the light from the upper array R approaches the multiplexing barrier from a virtual image that is beneath that of the L array. This enables the barrier to separate the rays to the appropriate rows of pixels.

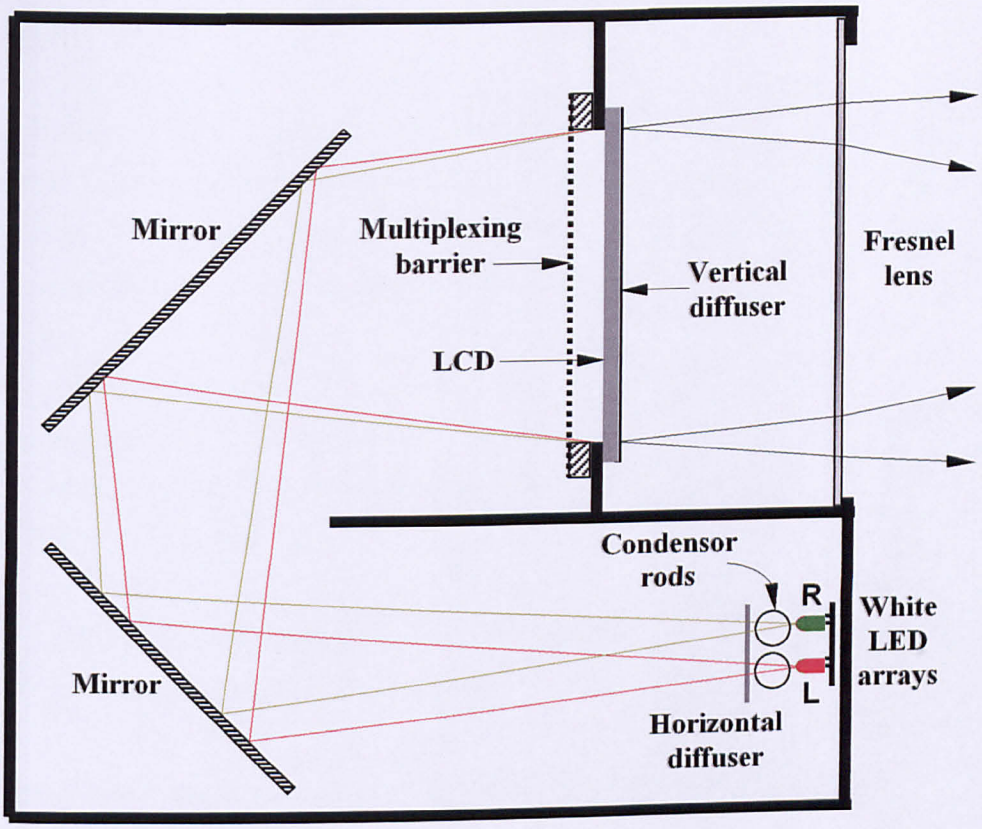

SIDE VIEW
Figure to half actual size

FIG.9.6 SECTION THROUGH 5.6" PROTOTYPE

9.6) Multiplexing Barrier

After being reflected by the folding mirrors, light from the arrays then enters the multiplexing barrier. This allows the light from the lower array to fall on the pixel rows displaying the left image, and light from the upper array on to the right-image rows. Originally it was planned to use an acetate sheet, with the mask printed by an image setter, for the barrier. However, funding has now become available that will enable the barrier to be made on a glass substrate.

As mentioned in section **9.2),** the barrier consists of horizontally aligned apertures that run across the width of the screen. The equations determining the barrier aperture

dimensions, and its spacing from the LCD, are derived in Chapter 5. The variables in these equations are as follows (all dimensions in millimetres) –

E = 10 E is the height of the illumination sources. This is the diameter of the virtual image of the LED phosphor when viewed through the spherical front surface of the device. When a Perspex rod is used as a condensor lens, the light appears to originate from the complete height of the rod, making E the diameter of the rod.

G = 7.57 The use of a standard 0.1" stripboard at an angle of 45° determines the array centre spacing of 12.57 millimetres. Therefore, if the width of the array light sources is effectively ten millimetres with a condensor rod, the gap between the arrays is 7.57 millimetres.

A = 391 A is the distance between the illumination array and the barrier. Subtracting 8 from 399 millimetres GIVES the illumination source to barrier distance.

P_L = 0.3733 P_L is the vertical pitch of the LCD. The active area of the LCD is 85 millimetres high and the vertical resolution is 225 pixels.

M = 0.07 The LCD horizontal mask measured, on a travelling microscope, to an estimated accuracy of ± 5 microns. This was achieved by comparison of the mask width with the known LCD vertical pitch.

P = 0.303 This is obtained by subtracting the mask width from the pixel vertical pitch.

T_B = 0 If the barrier on a glass substrate is used, and the barrier layer is on the front surface, this value is zero.

U_B is N/A The value does not apply as the barrier has no front substrate.

T_L = 1 T_L is the thickness of the LCD substrate. This is not given on the LCD data sheet, but it will probably be around one millimetre

$U_L = 1.5$ Is the refractive index of the LCD substrate glass. Again, this information is not given the data sheet, but it will be sufficiently close 1.5 for this value to be used.

Applying these values to Equations 5(3), 5(4), 5(5) and 5(7), derived in Chapter 5, gives the following values –

$D = 8.22$
$W = 0.231$
$R_A = 0.38$
$P_B = 0.7317$

Where W is the height of the barrier aperture, D is the barrier to LCD spacing, R_A is the ratio of light throughput with and without the barrier and P_B is the barrier pitch.

9.7) LCD

The LCD used is a Sharp 5.6" device that is 225 x 300 pixels and has an active area of 84 x 115 millimetres. There are two important aspects of the LCD construction that affect its use in a direct-view 3D display with steering optics replacing the conventional backlight. The first problem is that the column driver PCB lies in the light path when the backlight is removed. In its normal configuration in the monitor, the backlight illumination sheets lie between the drivers and the LCD itself. When the display was dismantled, it was found that the column drivers, which are connected to the top of the LCD via a flexible PCB, could not simply be folded out of the way without disconnecting the input. This is a problem that is encountered with many LCDs. As the input is through a flexible PCB and connector with 0.5 millimetre pitch, it is difficult to extend this. At the time of writing this has not been done as a previous attempt led to the failure of the device.

Another potential problem is that of scattering caused by the anti-reflection (A/R) surface on the front of the display. Fortunately, this particular device does not have one

9.8) Vertical Diffuser

When the light has exited the LCD, it has to be scattered in the vertical direction in order for the complete height of the screen to be illuminated. This can be achieved using a lenticular sheet. In Fig.9.7 it can be seen that the parallel light falling on the inner surface of the sheet is focused a short distance in front of it causing it to be effectively scattered. As the lenses are cylindrical, light is only scattered in the vertical direction.

The most suitable readily available lenticular sheet is one with a lens height of 0.179 millimetres, and a focal length of 0.254. This gives an F-number of F 1.42. This is rather small for this application as the extreme rays will be as shown in Fig.9.7 (a). It can be seen that this angle at a viewing distance of 750 millimetres (825 millimetres from the actual sheet) will give an exit pupil which is much larger than is necessary for this display that is only intended to provide a small usable viewing region. The result of this is a dim image as the light is spread over a large vertical region.

In order to increase observed intensity, longer focal length lenses will be required. As there is only a small range of sheets available, the easiest solution appeared to be to modify the focal length of the lenses. This can be achieved by placing a refracting medium in contact with the lenses which reduces the effective refractive index at the lens surfaces and gives a longer focal length as illustrated in Fig.9.7 (b). The effect of the refractive index of the medium is as follows –

Let:

F_A = focal length in air

F_M = focal length with medium

N = factor of focal length increase

R = lens radius

U_L = refractive index of lenticular sheet

U_M = refractive index of medium

U_E =effective refractive index at lens surface

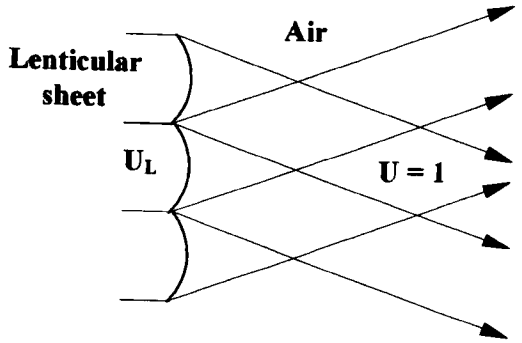

(a) Sheet in Air

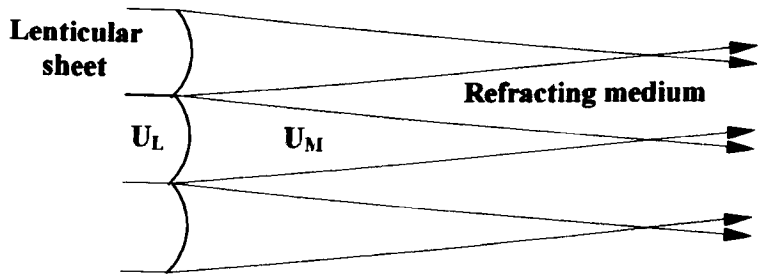

(b) Sheet in Contact With Refracting Medium

FIG.9.7 INCREASING LENTICULAR SHEET FOCAL LENGTH

Applying the equation for the focal length of a single refracting surface -

$$F_A = R / (U_L - 1)$$

$$F_M = R / (U_E - 1)$$

Therefore:

$$F_M \cdot (U_E - 1) = F_A \ (U_L - 1)$$

As

$$F_M = N F_A$$

$$N F_A (U_E - 1) = F_A (U_L - 1)$$

Solving for U_E :

$$U_E = 1 + (U_L - 1) / N$$

The effective refractive index between two media is given by-

$$U_E = U_L / U_m$$

Therefore:

$$1 + (U_L - 1) / N = U_L / U_m$$

Solving for U_m gives:

$$U_m = U_L N / (N + U_L - 1) \quad \text{.....(9.1)}$$

And solving for N gives:

$$N = U_m (U_L - 1) / (U_L - U_m) \quad \text{.....(9.2)}$$

Equation (9.2) is useful as the value of N is the ratio by which the observed intensity is increased for a given medium. For example, if the medium is water then $U_m = 1.333$ at 589 nanometres. The refractive index of the lenticular sheet is 1.49. These refractive indices give a value of N of 4.16. This represents a considerable increase in brightness.

However, it is possible to increase the brightness by a greater amount, as the height of the exit pupil, which is inversely proportional to N, can be further reduced. A convenient method of adjusting the refractive index to accommodate a given value of N is to make the medium from a mixture of glycerine and water. If, for example, the value of N is 6 and $U_L = 1.49$, then equation (9.1) gives a refractive index of 1.37.

The refracting medium in contact with the lenses of the lenticular sheet requires a layer to retain it. This is a two-millimetre thick acrylic sheet that is sealed round the edge with two-millimetre thick, 10 millimetre wide, tape used for general plumbing purposes. Fig.9.8 is the exploded view of the complete screen assembly. The void between the lenticular screen and the acrylic sheet is filled through the two-millimetre filling hole using a syringe. When filled, the hole is covered with a short length of the sealing tape.

The water must be boiled first in order to kill off any living organisms. One test piece was assembled without the water being boiled first. In this sample grey patches appeared over the whole area of the sheet within two months. The actual

glycerine/water mix was not calculated rigorously, but found by trial-and-error. The optimum, for a reasonable height viewing field of around 150 millimetres with good brightness, is around one part glycerine to three parts water.

A striking demonstration of the increase in brightness can be given by half-filling the assembly with the mixture. This makes the lower half of the screen appear to be

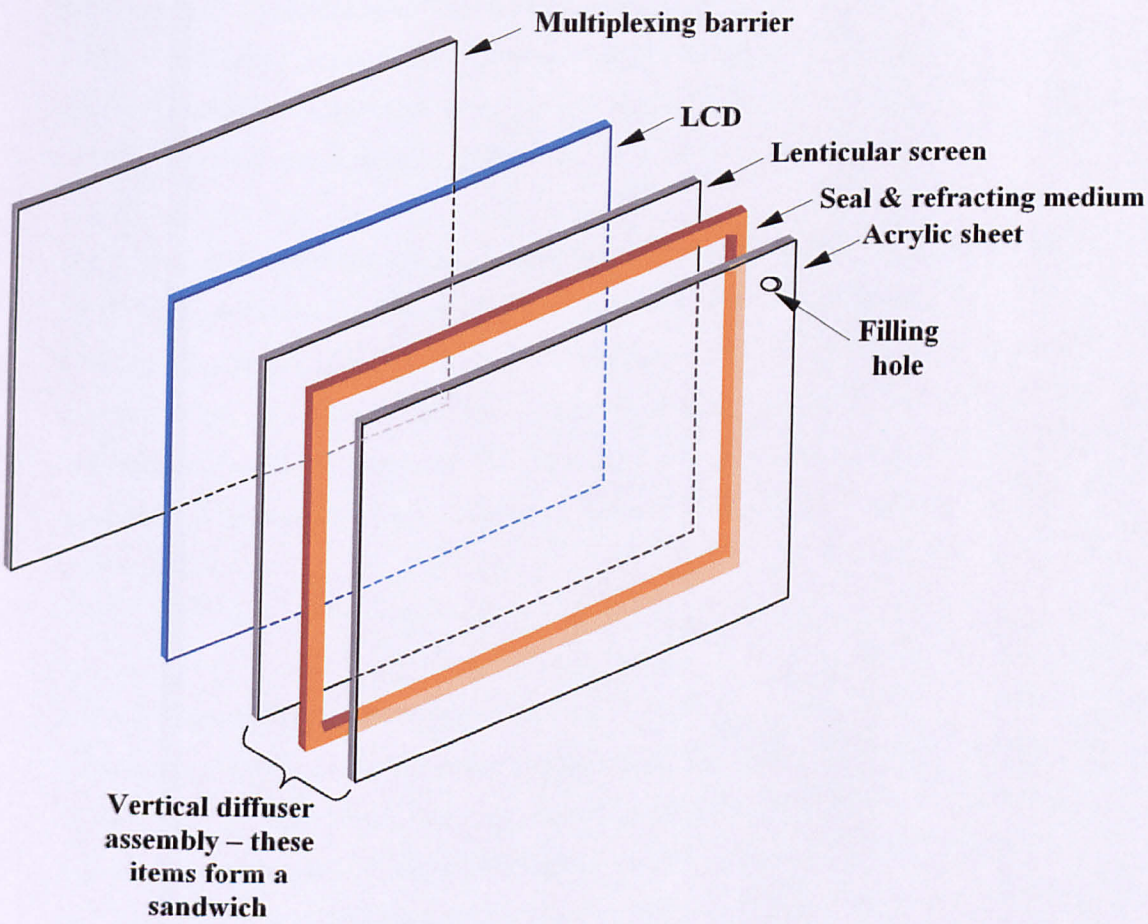

FIG.9.8 EXPLODED VIEW OF SCREEN LAYERS

extremely bright in comparison to the upper half.

9.9) Head Tracker

The head tracker camera consists of a 128-element CCD linear array housed within a plastic box. The array was adjusted in order for the complete length of 128 elements

to correspond to 400 millimetres across the viewing field at 750 millimetres distance from the lens. Around the lens is a ring of 24 near infrared LEDs whose peak output is at 900 nanometres. As the array is sensitive in the visible range also, an infrared filter is mounted in front of it. This virtually eliminates the effect of ambient light and the set-up operates reliably even in sunlight.

A retroreflector consisting of a sheet of 3M Scotchlite film is placed around 1.2 metres in front of the camera. This is the material used for traffic signs and it provides a very well defined 'shadow' of the viewer's head around the region of the eyes. The eye-centre position is assumed to be at the centre of the shadow. The principle-of-operation is discussed in detail in Chapter 12

The white LED arrays allow a head movement of 142 millimetres, and a typical head 'shadow' is around 200 millimetres wide. This means that the CCD array must cover a width in excess of 342 millimetres. The 400 millimetres allowed for by the camera is considerably more than this. The resolution of the array is 400 / 128 = 3.125 millimetres. This is only around 5% of the interocular distance and therefore the resolution is sufficiently high. The head tracker is described in greater detail in Chapter 12.

9.10) Current State of Prototype

At present, this version is still under construction. The LCD requires modification in order for the column drivers to be moved out of the light path. This modification had previously been carried out on a 12" display, and this subsequently failed. As funding has now become available, it might not be worthwhile continuing with the 5.6" prototype. One of the prototypes being built is a 21" version that operate on the same principle. The larger LCDs have the advantage that the driver boards can be more easily removed from the light path.

CHAPTER 10
12 INCH / 10 INCH PROTOTYPE

10.1) Preface

During the time the 5.6" prototype was under contructiion, the cost of 12" TFT LCDs fell to a reasonable level and the author decided to construct a single-viewer prototype based on a 12.1" TFT monitor. The display chosen is a Phantom type 400AH SVGA panel (800 x 600 pixels). The prototype is housed within a nine-millimetre thick medium density fibreboard (MDF) case. Initially, illumination was provided from a pair of 150-watt linear halogen lamps, but this assembly was removed in order for it to be replaced by arrays of white LEDs. This prototype is still under construction, but may superseded by A 21" version. The 48-element array infrared camera described in Chapter 12 was designed to be mounted above the display housing and be an integral part of its construction. This has been replaced by a more compact version using a 128-element integrated array on a single chip. The LED head 'shadow' indicator, described in Chapter 12, remains in use as a demonstrator of the principle of infrared retroflection head tracking.

As there were some problems encountered with the use of the 12" LCD, the housing built for this version was modified in order for it to be used for a 10" LCD that would not suffer with the same difficulties. The 10" version also has a simple parallax range-finder added that enables the viewer to be situated at the optimum viewing distance.

10.2) 12" Prototype

10.2.1) 12" Prototype Optics

The exit pupil pair for the single viewer are formed by a Fresnel lens with a focal length of 460 millimetres. This requires the lamps to be 770 millimetres behind the lens for a viewing distance of 1.1 metres. The six-mirror folding shown in Fig.10.1 enables the housing to be contained within a depth of 290 millimetres. This allows ample space above mirror M3 for the light sources. Also, power supplies and electronics can be fitted in the voids below the mirrors M4 and M5.

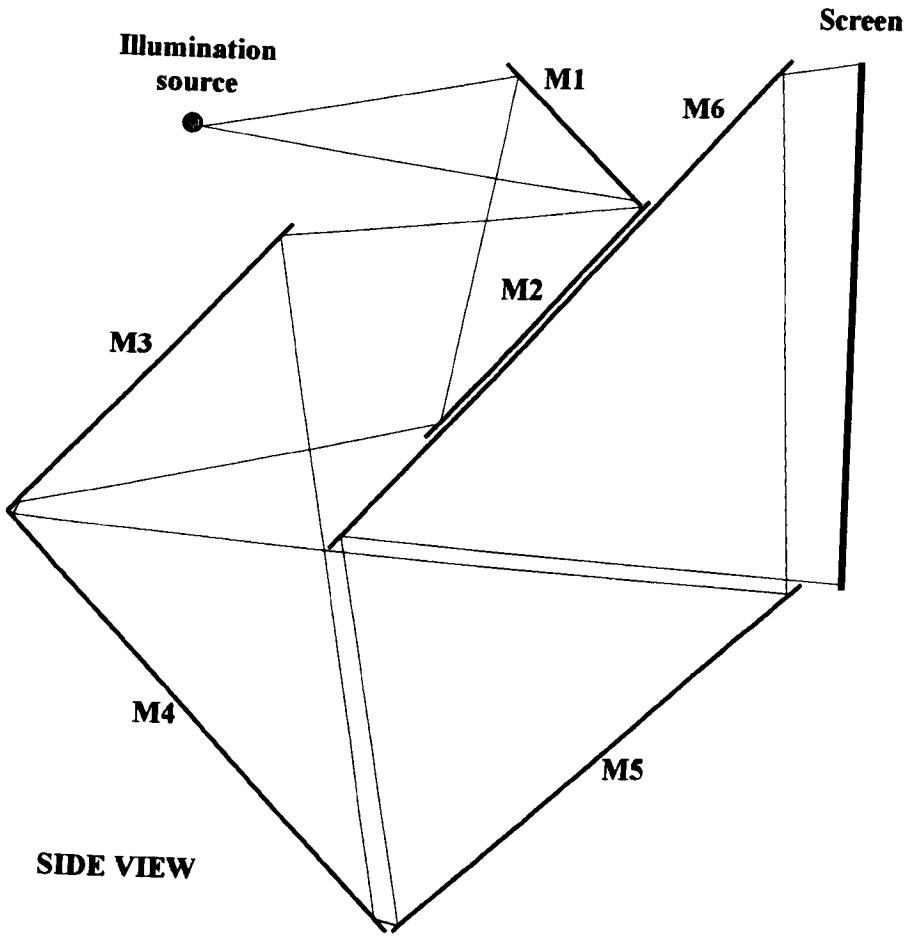

FIG.10.1 12" PROTOTYPE FOLDING

The folding path is determined by the graphical method described in Chapter 4, and this particular folding configuration allows M2 to be conveniently mounted on the back of M6, therefore simplifying the construction. The mirrors are three-millimetre thick back-silvered glass.

As in the 5.6" prototype described in Chapter 9, the light has to be scattered in the vertical direction only. The same technique of using a water / glycerine mixture in contact with the lenticular sheet lens surface is used to increase the observed brightness. In this case the lenticular sheet is adjacent to the Fresnel lens so that these two components are joined together with a seal around their edge, and the gap filled with the mixture. The flat surface of the Fresnel lens is in contact with the mixture. Again, the optimum mix is around one part glycerine to three parts water.

One effect of the lenticular sheet characteristic likely to cause problems is that of a visibly brighter band across the screen in line with the illumination sources. This is due to the region between the lenses passing light through without vertical deviation. The lenticular sheet was obtained from Edmund Optical as this was easily available. In future, a light shaping diffuser (LSD) sheet will be used as a vertical diffiser. This does not exhibit this artefact.

10.2.2) 12" Prototype Illumination Sources

Halogen lamps were chosen originally for the light sources as white LEDs were expensive at that time. Linear halogen lamps provide a high light output over a small region. The filaments, which are 36 millimetres long and around one-millimetre diameter, provide a very convenient light source for operation with the parallax multiplexing barrier. As the light is scattered by the envelopes of the bulbs, apertures are placed in front of them as shown in Fig.10.2. These are 35 millimetres wide by seven millimetres high, and their centres are spaced 17 millimetres in the vertical direction.

The halogen bulbs are not shown on this figure as they are located behind the screen with the apertures. There is also a reflecting screen behind the halogens, which is also not shown, that serves to keep heat away from the stepper motor. Heat is a considerable problem where a total of 300 watts is dissipated within a relatively small volume. The most effective barrier was obtained by using a layer of aluminium foil backed with a layer of asbestos matting.. This heat shield is mounted on both on the carriage platform below the lamps, and on the fixed housing above the lamps.

Heat is carried away from the unit by a cooling fan located behind the stepper motor. The combination of reflecting surfaces and cooling fan ensures that the illumination assembly is able to operate in complete safety. The lamps are mounted on a carriage that uses four 12.5 millimetre ball-races that act as wheels. The fore-and-aft position of the carriage is maintained by two plastic L-sections that act as a track. Lateral position is controlled by a stepper motor whose rotation is transmitted to a rack on the carriage by a pinion.

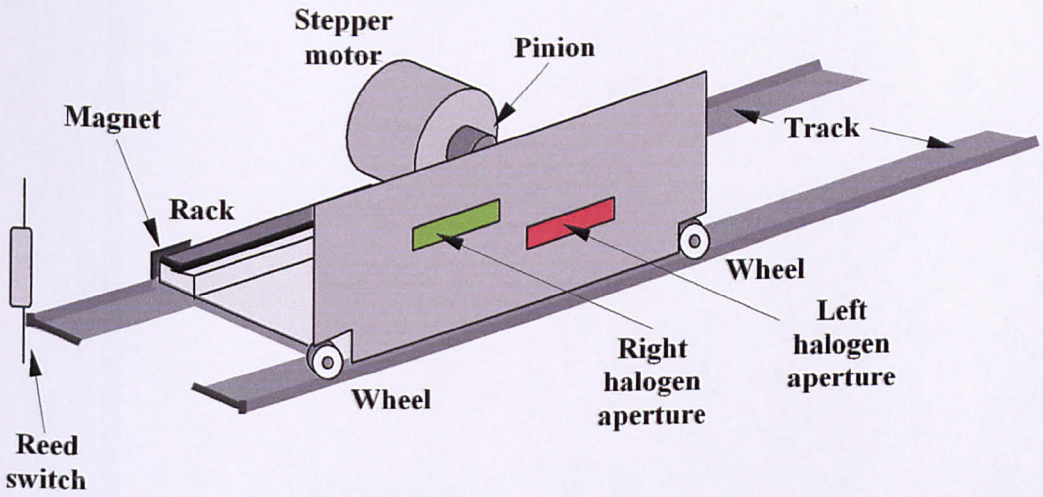

FIG.10.2 HALOGEN LAMP ILLUMINATION ASSEMBLY

The stepper motor and driver are provided in inexpensive kit form and the motor has a step angle of 7.5°. The output of this is connected to the lamp carriage by a rack and pinion that moves it 0.667 millimetres for each pulse to the stepper driver. The sides of the housing limit the total lateral movement to 160 millimetres.

A magnet is attached to the left-hand side of the carriage in order to close the contacts of a reed switch just before the carriage reaches the extent if its travel. This information is fed to the tracking processor in order to determine absolute position each time the apparatus is switched on.

The appearance of the images of the halogen lamps when focused by the Fresnel lens only (without the addition of the vertical diffuser) gives a useful indication of the performance of the optics. Fig.10.3 is a full-scale drawing of the images. Note that the drawing is in negative form with the brightest regions being depicted by the darkest regions on the figure. It can be seen that the centres of the regions are 65 millimetres apart – the average interocular spacing. The lenticular sheet extends these images into regions around 200 millimetres high.

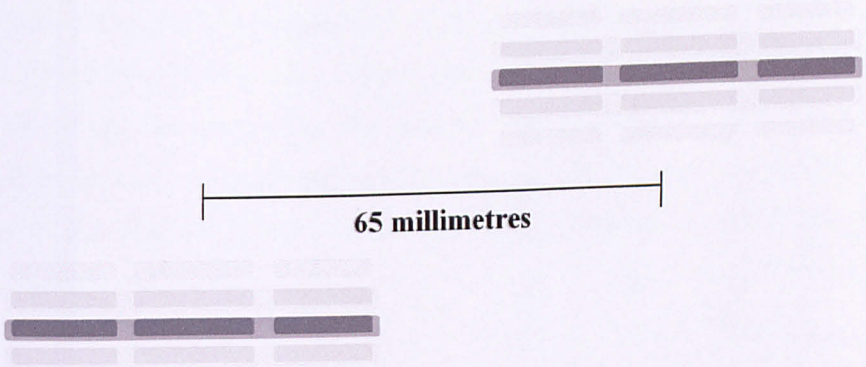

FIG.10.3 IMAGES OF HALOGEN LAMPS

Two useful results can be obtained from these images, Firstly, the effect of gaps produced by the two filament supports can clearly be seen. The selection of lamps makes a considerable difference and it was found that some bulbs (those supplied by Homebase) produced virtually imperceptible gaps. Secondly, multiple images produced by reflections from the mirror surfaces are visible. This confirms the assumption, made in Section **4.4)**, that only the primary reflections need to be accounted for, is valid. The secondary reflections` can be seen, but are barely perceptible.

10.2.3) 12" Prototype LCD

When used in this application there are two modifications that must be made to the LCD. As the backlight of the LCD is replaced by steering optics, light must be able to pass through the LCD over its complete area. When used in the monitor application, light enters the back of the LCD from a series of sheets that allow that light to exit uniformly over the complete area of their front surface. A 1.5-millimetre diameter fluorescent tube mounted below their lower edge illuminates these sheets, which are manufactured by 3M. A flexible PCB that has 800 tracks on it connects the column driver board to the top of the LCD. This board needs to be folded out of the light path as shown in Fig.10.4 (a).

Unfortunately, this is not straightforward, as the column drivers are connected to the line drivers by a 16-way and a 24-way connector as shown in Fig.10.4 (b). In order to move the column drivers into the position shown in Fig.10.4 (a), these connections must be broken and extended. As the connections are made by flexible PCBs that have tracks with a 0.5 millimetre pitch, folding the column drivers out of the way is not a simple matter.

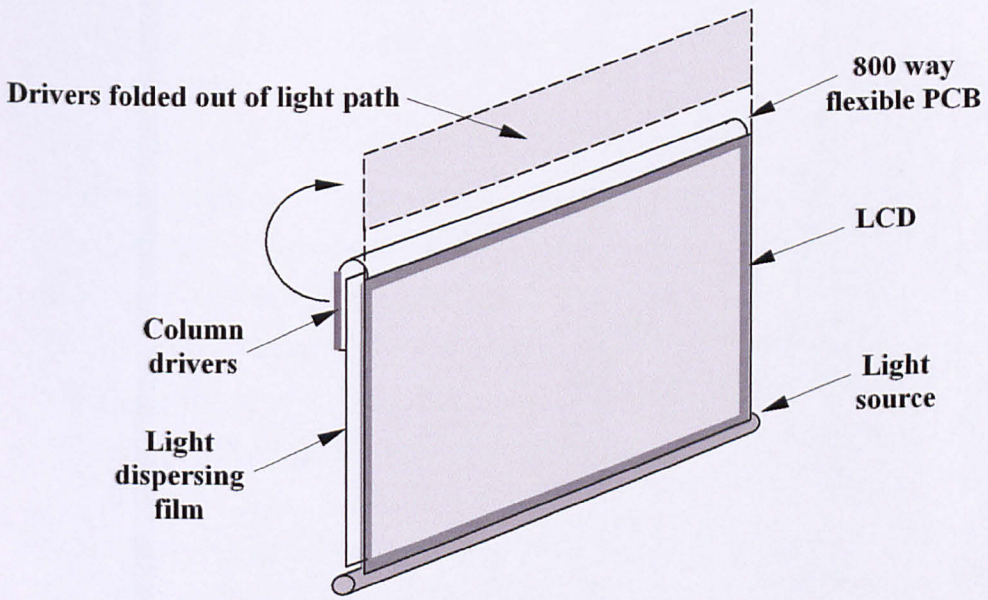

(a) LCD Layout

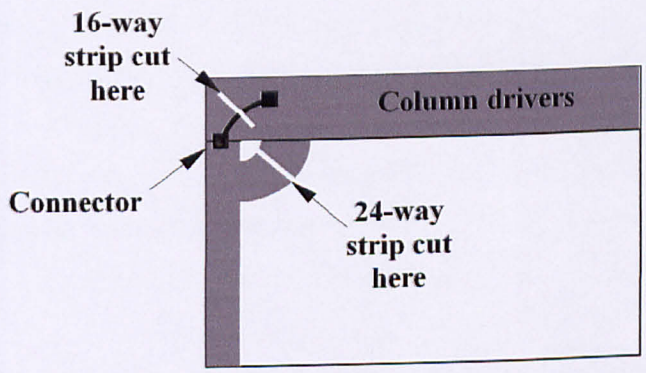

(b) Back of LCD

FIG.10.4 LCD COLUMN DRIVERS

Due to the difficulty of this work, it was put out to a technician with experience of work of this nature. Unfortunately, the display did not function after being modified. The fault appeared to be caused by two adjacent tracks short-circuiting.

The second problem to be addressed is that of scattering caused by the antireflection surface on the front face of the LCD. The operation of the display in a 3D application depends on light passing through it with negligible deviation in the horizontal direction. The surface irregularity of the antireflection surface causes an unacceptably high degree of scattering that must be eliminated.

In the particular LCD used, the antireflection property is produced by the LCD front substrate having an uneven surface. The same principle used to modify the focal length of the lenticular sheet can also be used to eliminate the scattering. In this case, however, the refractive index of the medium in contact with the irregular surface must be the *same* as that of the surface material. As the use of a liquid in contact with the LCD appeared to be a risky solution due to the possibility of leakage, the possibility of bonding the front surface of the LCD to a sheet of glass was investigated.

Although its refractive index was not known, the effectiveness of Glass Bond™, manufactured by Loctite, was assessed. In order not to possibly ruin an expensive LCD, the adhesive was tested on two sheets of three-millimetre thick pieces of glass of dimensions 200 x 250 millimetres. Five tubes of adhesive were required to cover the central area of one of the sheets. The second sheet was pressed on to this so that the adhesive covered the complete area between the sheets. This operation proved difficult, and even after several attempts, it was found impossible to cover the complete area without air bubbles forming. The final best attempt was placed in strong sunlight in order for ultraviolet to cure the adhesive.

It appears that the viscosity of the adhesive is rather too high for this operation to be successful. Even when heated up, the adhesive did not appear to have a noticeably reduced viscosity. As this technique is liable to destroy the LCD it was not pursued, however, the use of glass adhesive performing the same purpose has been successfully carried out in the 3D display of Reality vision [TRAY97].

One option that would not destroy the LCD would be the use of a layer of glycerine in contact with the antireflection coating. The refractive index of 1.463 is probably sufficiently close to that of the LCD layer for the scattering to be negligible. This technique is currently being investigated on a 21" prototype.

10.3) 10" Prototype

After the 12" LCD was damaged, it was decided to use a panel that did not need modification in order to pass light from an external source over its complete area.. There are very few off-the-shelf LCDs that are suitable, and the only one found at the EID 2000 exhibition is a 10.4" NEC panel which is a backlight-less unit intended for high ambient light applications where a standard backlight would be insufficient. It has VGA resolution (640 x 480 pixels). Another advantage of this device is that it does not have an antireflection coating.

As this panel is smaller, the same strategy as is used in the 5.6" prototype is used here to increase the apparent screen size. The 12" prototype housing was modified as shown in Fig.10.5 to enable the Fresnel lens to magnify the LCD image. The lens is mounted 100 millimetres in front of the LCD. It is therefore separated from the lenticular sheet diffuser as this needs to be located immediately in front of the LCD.

The distance between the LCD and the light sources is still 0.78 metres as in the 12" version. With an object distance of 0.88 x (0.78 + 0.10) metres, and a lens focal length of 0.46 metres, the images of the light sources are focused 0.95 metres in front the lens.

The magnification M is given by –

$$M = (0.78 + 0.10) / 0.78$$
$$= 1.13$$

This magnification makes the 10.4" LCD appear to be the same size as an equivalent 11.7" panel at 1.05 x (0.95 + 0.10) metres from the viewer. When allowance is made for the slightly smaller viewing distance, the image subtends the same angle as a 12.3" panel at 1.11 metres viewing distance. Therefore the use of the 10.4" LCD

overcomes the practical problems of the 12.1" unit, and also gives a slightly increased apparent size.

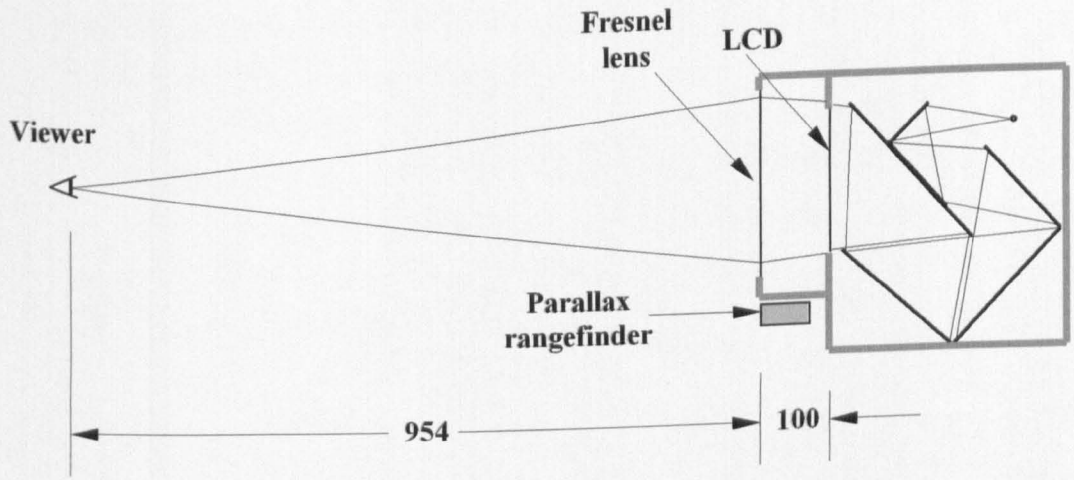

SIDE VIEW
Dimensions in millimetres

FIG.10.5 10" PROTOTYPE OPTICS

As the viewing field depth over which stereo can be observed is limited, a parallax range-finder was constructed. This simply consists of two small plastic boxes attached to the underside of the extension housing for the Fresnel lens. The right-hand box consists of a red LED that has a one-millimetre wide aperture marked on its front surface with paint. This is mounted 40 millimetres behind a three-millimetre wide aperture in the front of the box. The left-hand box is of the same construction, but with a green LED. The boxes are each mounted with a single screw in order to allow them to be rotated. With the axes adjusted to cross at 600 millimetres in front of them, the geometry of Fig.10.6 is formed.

If the viewer's head moves towards the optimum viewing distance of 954 millimetres, and is moved from side to side, the position is reached when the red LED in box R is seen by the left eye, and the green LED in box L by the right eye. This will occur

when the eye-centre position is located at the furthest part of the shaded diamond-shaped region. This is a simple and quick procedure.

Red is seen by the left eye, and green by the right eye, when the eye-centre position is anywhere within the furthest shaded region. When the viewer's head is located here, it should be moved back until the red and green LEDs just disappear.

The other shaded regions are where both LED are seen by either one, or by both eyes. As it is difficult to determine which eye is seeing which LED, these regions could potentially cause confusion. However, as they are obviously too close to the screen, they do not cause any problems in practice.

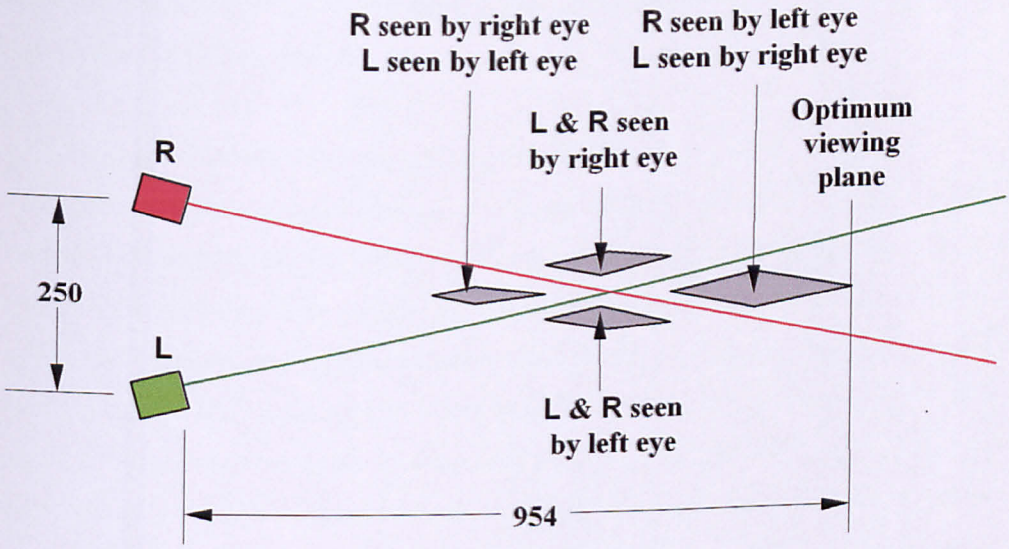

TOP VIEW
Dimensions in millimetres

FIG.10.6 PARALLAX RANGE-FINDER GEOMETRY

CHAPTER 11
HEAD TRACKING – SURVEY OF METHODS; ACCURACY REQUIREMENTS

11.1) Survey of Head Tracking Methods

Apart from the electromagnetic Polhemus head position tracker, there are various optical means by which the position of the head can be determined. The simplest method is the use of an infrared retroreflector attached to the viewer's head. The head tracking displays of Dimension Technologies [TOUR94] and Graham Street [STRE98] mention the use retroreflectors, but do not describe the apparatus. Sharp Laboratories of Europe also used this method in their display demonstrated to the author in 1995. This required a small retroreflector attached to the forehead. In the ATR Research Laboratories lenticular display [OMUR98] a retroreflector attached to the viewer's chin is described.

11.1.1) Infrared Reflection from Complete Head

The earliest head tracking displays use infrared reflected off the viewer's head. In the Fresnel lens single viewer display of Alfred Schwartz [SCHW85] the head detector moves with the lens. The observer's head is illuminated with a cluster of infrared LEDs and its image is captured with another lens whose image is segmented into two halves through the vertical axis. When the head is directly in front of the tracker, equal illumination is received by each half of the image. As the head moves, more information is received on one half of the image. This information is used in feedback system with a servo-motor that keeps the lenses aimed at the viewer. This simple system does not require any processing of the image. An interesting feature is that it can be easily adjusted to compensate for tonsorial assymmetry.

It appears that a single detector is used to track the head in the early lenticular display of Ichinose [ICHI89] as the brief description of the tracker says that the light source and detector are packaged as one unit that is located above the display. This description does not explain the way the tracking is actually carried out.

11.1.2) Infrared Reflection from Each Side of the Head

A development of this is the use of illumination of each side of the viewer's head by two bands of infrared wavelengths. A display using a large format convex lens [NISH95] illuminates the left side of the viewer's head with infrared in the 830 – 870 nanometre range, and the right side of the head in the 930 - 970 nanometre band. The outputs of a pair of cameras with matching filters are used to control the illumination from a monochrome 2D display directly without the use of any additional processing. The use of different bands of infrared to light either side of the head is utilised in other displays by the same researchers [HATT93] [NISH94].

A variant of this tracker is used in the display produced by the Sea Phone company [HATT00]. In this display a Fresnel lens produces the exit pupils. In order to eliminate parallax errors, the same lens is also used to capture the infrared images.

11.1.3) Retinal Reflection

Reflection off the retinas of the eyes is used in some head trackers. This is the 'red-eye' effect seen in some photographs taken with flash. When this occurs, the eye is acting in the same manner as a 'cats eye' in the road where light from the source, which is located close to the observer, is focused on the back surface of the device and then retroreflected back along the same path by the lens.

An Australian company, Dynamic Digital Depth Pty. Ltd. [HARM00], reports use of three reflection methods. They found that significant retinal reflection occurred with the infrared source on the axis. An alternative technique is also described where an off-axis illumination is reflected off the corneas. Apparently, when spectacles are worn, scattering from the front of the lenses is sufficient to cause the retinal reflection technique to fail. In this case, strong reflections from the boundary of the spectacles and the viewer's face are used to implement a reliable tracking system.

The Media Research Lab of New York University have developed a single-viewer prototype that allows a wide degree of head movement [PERL01] and this also utilises 'Red-eye' reflection. They use an IBM BlueEyes tracker [MORI00] that compares the difference between the image formed from on-axis illumination, where

the retinal reflection is strong, and the image formed from off-axis illumination, where the this reflection is considerably less. The sources of illumination are a ring of infrared LEDs close to the camera lens for the on-axis illumination, and a ring of LEDs further away for the off-axis illumination. These are switched so that the head receives on and off-axis illumination on alternate frames of the capture camera. As the reflection is greatest from the fovea region of the retina, best results are obtained by locating the tracker as close as possible to the region being viewed.

In another system being developed by NEC [IMAI99], allowances are made for the time during which the viewer blinks, and for the size of the pupil. For a typical viewing situation, where the screen subtends a relatively small angle to the eye, it is unlikely that screen luminance will be the dominant factor in determining pupil size as is implied in this paper – ambient lighting levels will probably have a greater effect. Movement prediction vectors are used to estimate the position of the pupils during the 200 milliseconds or so the eyes are closed during blinking.

11.1.4) Image Processing

Eye position can also be determined by image processing. A system of this type was demonstrated to the author at Sharp Laboratories of Europe in 1997, but no papers appear to have been published on it. There are various means of separating the eyes and the head regions from those areas in the scene that are not of interest. Amongst these are segmentation of the face region by its colour, the blinking of the eyes, matching the eyes to a template and to each other, synchronous movement of eye-pairs and use of a reference image where no heads are present.

The University of Dresden describe a method for the tracking of a single viewer for an autostereoscopic display [HEID00]. This involves the use of a pair of cameras and a feature-based stereo algorithm, not specified in the paper, in order to extract interest points in the images. Points represent the eyes of the viewer are determined by various means such as stereo correlation, template matching and detection of synchronously moving pairs. As the viewer is assumed to be the closest object to the camera, and is assumed to lie within a given separation on the images, the distance between the points of interest will be within a given range. This can be used to

distinguish between the eyes of the viewer, and the eyes of other people in view of the cameras.

The head tracker being developed by the Heinrich-Hertz Institut in Berlin [HHI02] determines the eye positions in two stages. First the face region is segmented, and then the eyes are located within this region. Regions of the image that are skin colour are extracted by comparing each pixel with a region in RGB colour space held on a look-up table. A reference image, with no head in it, is captured before the viewer is in place. Regions of the image that are not background can then be identified. This background is updated during the tracking process. The facial region is then determined by some further processing. The eyes are located within this region by the detection of blinking where two regions chance shape simultaneously, and also by taking into account the geometric relationship of the eyes. After matching has been successfully completed, allowances are made for variations in average luminance values with time.

Although the work was not undertaken with head tracking in mind, the effect of viewer concentration on blink rate has been studied [NHK96]. The studies show that the blink frequency is reduced during periods of concentration when 3D-HDTV is being viewed, however this happens to a much lesser extent with 2D-HDTV.

The effectiveness of skin-colour segmentation has been examined by a group at Chiba University in Japan [SANG95]. In this study, images were initially captured on colour reversal film, then scanned and processed electronically. Some results printed in the paper appear to segment the skin areas very effectively. One factor that could affect this method is that of racial skin colour variations. No mention of this is made in the HHI paper but conversations by the author with workers in this field have indicated that although racial variations may give some differences in luminance, the region in RGB space will not change considerably.

11.1.5) Summary of Head Trackers

In work carried out on a head tracked monitor [PALE92] it was observed that after the initial novelty of viewing 3D wears off, viewers are inclined to adopt a more settled pattern. There is typically around one to two inches of movement from side to side

and up and down. Additionally, there are occasional shifts of several inches due to changes in body position. The amount of movement of a television viewer is likely to be small as they tend to be 'couch potatoes'. Also, unlike the display in the paper, the proposed television to be developed from this research will not have motion parallax so there is no need for viewers to attempt to look round objects in the image.

Retinal reflection is one method the author considered might be a useful candidate for a head tracker for the prototypes. However, the report from New York University indicates that there could problems associated with this method if multiple viewers, who might be up to several metres distance, are to be tracked. The human eye lacks the highly reflecting tapetum of night hunting animals such as cats.

One point regarding terminology is that the term 'head tracking' will be continue to be used within this research, even though this has been replaced with 'eye tracking' frequently in recent reports. Use of 'head tracking' avoids confusion with the detection of what the viewer is actually looking at - often referred to as 'eye tracking'.

11.2) Head Tracking Accuracy Requirements

Although head tracking accuracy is not critical in the single-viewer prototypes, it will be an important issue in the proposed multiple-viewer prototype, and in a production television, as the viewing distances are greater. The accuracy requirements, with special regard to quantization, are considered in this section.

11.2.1) Exit Pupil Boundary Zone

The boundaries of the exit pupils must fall between the viewer's eyes if crosstalk is to be avoided. The solid line in Fig.11.1 is the intensity characteristic across the viewing field at an exit pupil boundary. It is envisaged that the stering optics of a multiple-viewer 3D display could possibly incorporate optical elements spatial light modulators (SLMs). The intensity characteristic is then determined by four factors, these are the point spread function (PSF) of the steering optics, the boundary characteristic of the SLMs, the diffraction function of the LCD and the eye pupil function. S is the distance between the positions for zero intensity and full intensity.

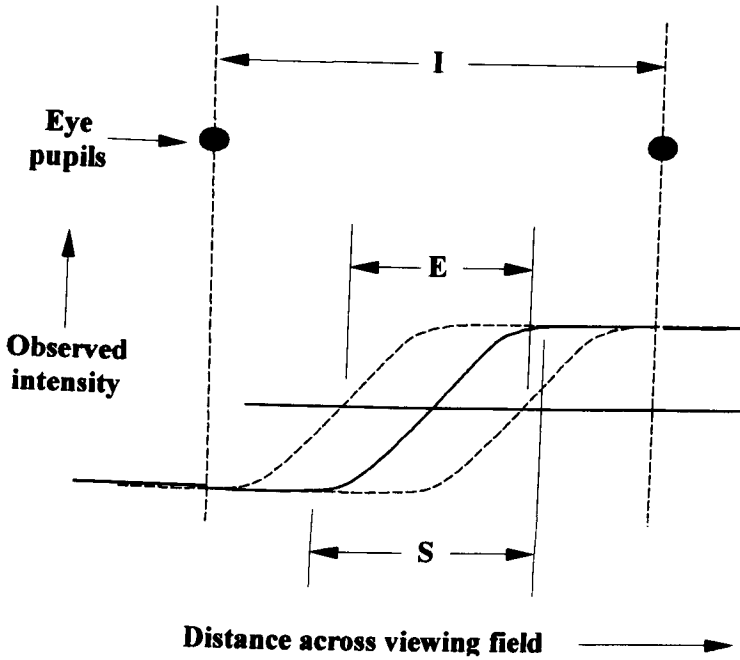

FIG.11.1 EXIT PUPIL BOUNDARY ZONE

The broken curves are the limits of the intensity characteristic when tracking error and the positional uncertainty of the SLM boundaries in relation to the viewing field are allowed for. The spacing of these is the distance E. The position of the intensity characteristic in relation to the eye pupil positions might lie anywhere between the broken lines. I is the interocular distance and is typically 65 millimetres.

11.2.2) Components of Boundary Zone Characteristic

The characteristics shown in Fig.11.2 are those that might typically be expected and are drawn to actual horizontal scale. The overall boundary intensity function 11.2 (e) is obtained by performing a convolution on four functions 11.2 (a), (b), (c) and (d).

The design of the steering optics for a multiple-viewer display has not been completed yet, but it may possibly utilise components that exhibit aberrations. A typical aberration characteristic is shown in 11.2 (a). It is anticipated that the light will be controlled by an SLM and the boundary between light from adjacent elements could be of the form illustrated in 11.2 (b).

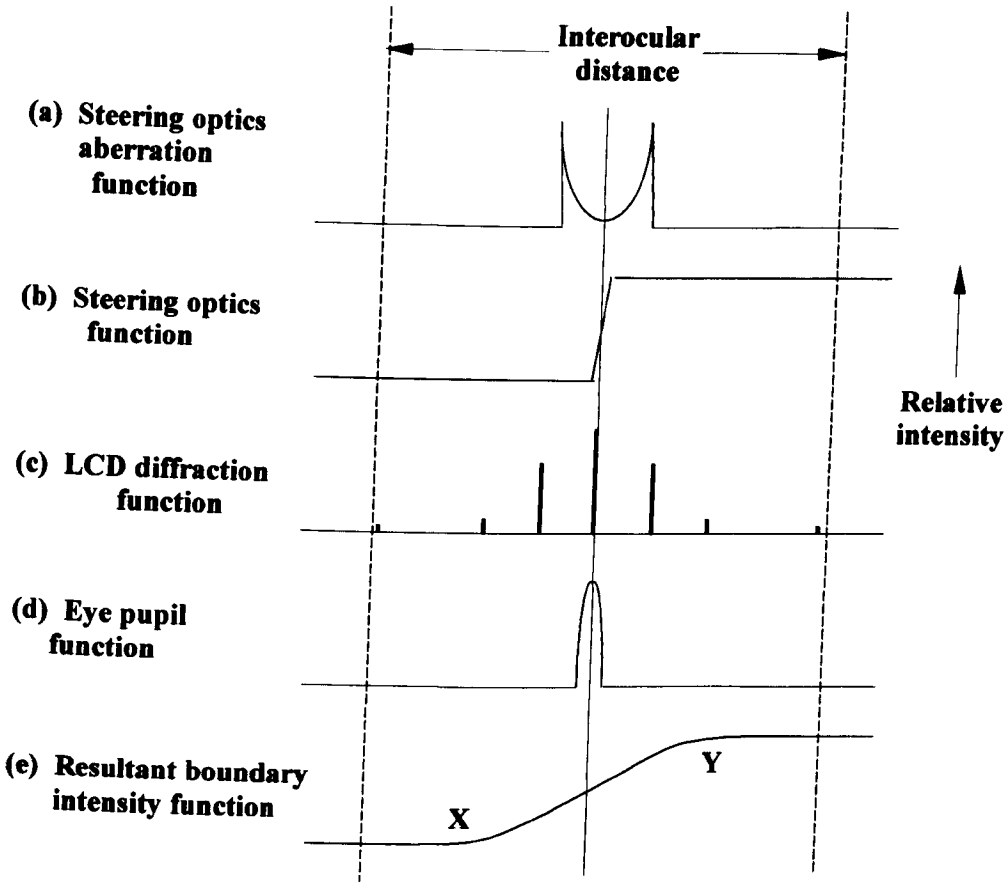

FIG.11.2 EXIT PUPIL BOUNDARY COMPONENTS

The majority of LCDs have a vertical stripe RGB sub-pixel configuration and these behave in a similar way to a diffraction grating. The worst-case occurs when only one set of sub-pixels transmits light. This will happen when only one of the stripes is transmitting, with the other two fully off, but this is an exceptional case. However, examination of the spectral characteristics of typical RGB filters (Fig.9.5) shows that at around 550 nanometres the green has peak transmission, whilst the red and blue filters barely transmit any light. Therefore, at the maximum response wavelength of the eye, the worst-case always occurs, irrespective of the colour actually being displayed.

At any given wavelength, the diffraction function will be a series of narrow lines whose envelope is a sinc-squared function. The spacing of the lines is inversely proportional to the wavelength and proportional to the distance from the screen.

The eye pupil diameter is not negligible and must be accounted for in any rigorous analysis of the intensity across the viewing field. Although the *eye* pupils can be considered static in relation to the *exit* pupils that are steered across the viewing field, combining their characteristic together with those of the others in the convolution yields the same result.

Another point regarding the eye is that the LCD scattering is treated as Fraunhofer diffraction as the pattern is resolved on the retina by the lens of the eye - it is not what would be seen on a screen placed in the viewing field. Crosstalk is dependent on what is actually perceived.

The widths of functions 11.2 (a), (b) and (c) are proportional to distance from the screen, and the eye pupil function 11.2 (d) obviously has a constant width. As head tracking ensures that this boundary lies around the centre point between the eyes, the only parts of the characteristic that are of interest are the ends of the curve where an eye pupil could be possibly situated.

11.2.3) Quantization Errors

The head tracking system determines the range and direction of the mid-point between the viewers' eyes in order to place the exit pupils in the correct positions. Quanitzation error is the maximum difference between the actual eye-centre position and exit pupil centre position. This is caused by the pixels of the tracking camera and the elements in the SLM. The combined positional uncertainty produced by the cameras and the tracking processor is denoted by U_P in Fig.11.3. An eye-centre position anywhere in the viewing field between points A and B will give an output at P_1, and between points B and C at P_2 and so on. P_1, P_2 etc. are separate outputs and are effectively quantized eye-centre positions.

The SLM is a linear light valve whose elements effectively form images in the viewing field. The pitch of the array images is denoted by U_S. Referring to Fig.11.4 (a), imagine the input to array element S_1 is set to give no transmission, and the other inputs set for full transmission, the boundary will be at W. The head might be in any position in relation in the viewing field. Assuming that the head tracking ensures that

the closest boundary is chosen, the eye-centre may be up to $U_S / 2$ away from W. This gives the effective uncertainty of the spread function position of U_S in relation to the pupils as shown in Fig.11.4 (b).

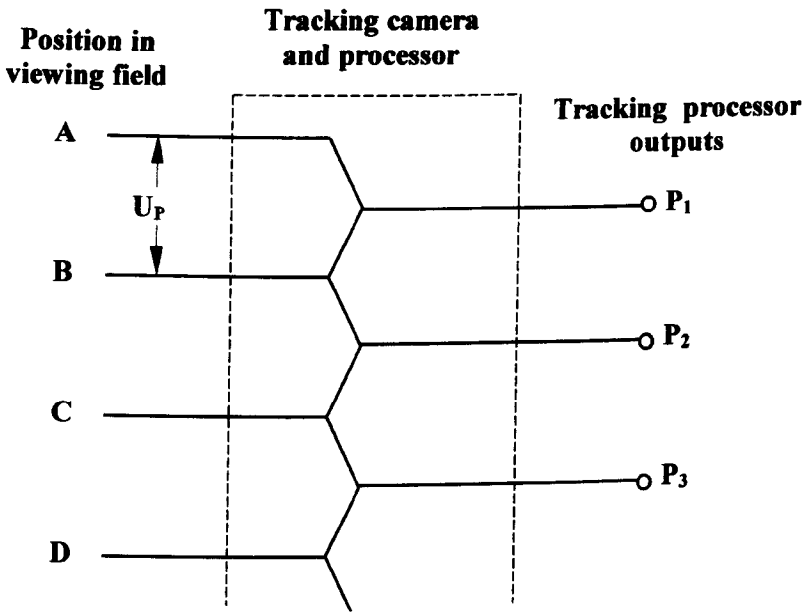

FIG.11.3 TRACKING PROCESSOR QUANTIZATION

So far, the total error is the $\pm U_P /2$ contribution from the tracking processor plus $U_S / 2$ from the SLM array. However, this not the end of the story. The tracking processor outputs must be connected to the appropriate SLM elements by another processor that allows for the overall geometry of the system. This introduces an error of $\pm$ G. As this processor chooses the SLM input closest to the tracking output, and its error is assumed to be negligible for all practical purposes, the maximum value of G is $U_S / 2$. This yields a total error of $\pm (U_P / 2 + U_S)$.

Therefore:-

$$E = E_T + U_S$$

where- E = Total error

$E_T = U_P / 2$ = Tracking error

U_S = SLM array image pitch in viewing field

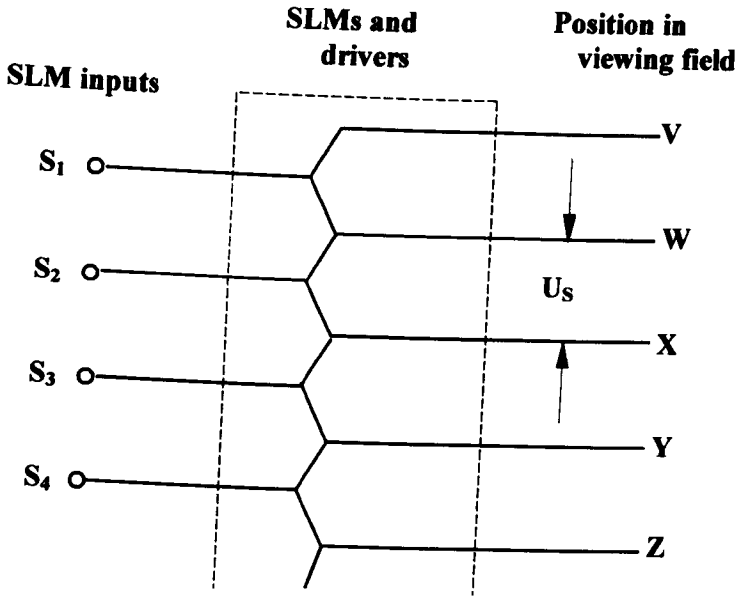

(a) SLM Array Quantization

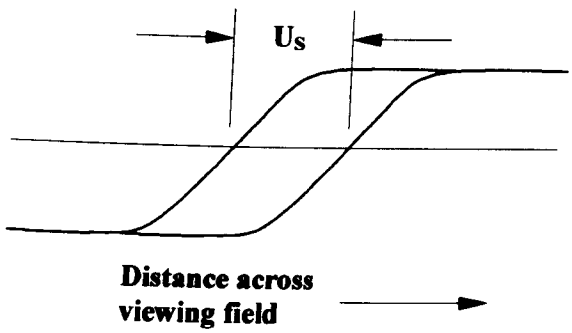

(b) Boundary Function Displacement

FIG.11.4 SLM ARRAY QUANTIZATION

11.2.4) Summary of Tracking Errors

The design of the steering optics for a multiple-vIewer prototype has not yet been finalised, but preliminary investigation has indicated that the aberration function is likely to be in the order of 10 to 20 millimetres at 3 metres viewing distance.

With the SLM that might be used in one of the ATTEST prototypes, function 11.2 (b) will effectively be a step function, and the quantization increments only about four

millimetres at 3-metres distance. However, one option that might be considered in the future is the use of white LEDs as both the light sources and the light control elements. If this is the case, then the boundary region and quantization increments could be appreciable in relation to the interocular distance.

The diffraction function will be dependent on the horizontal pitch of the LCD. If, for example, this pitch is 0.207 millimetres, the first order diffraction pattern will be eight millimetres away for a viewing distance of 3 metres and a wavelength of 550 nanometres. The worst-case intensities for green light are shown in Fig.11.2 (c). As mentioned in Chapter 6, this occurs when only the green sub-pixels transmit light. 0.207 millimetres is the pitch of the 20.8" QXGA panel whose use is proposed in one of the ATTEST prototypes.

The intensities in Fig.11.2 (c) are based on the width of the LCD mask being negligible in the horizontal direction giving an aperture ratio P of 0.333. By applying equation (6.5) in section **6.4.2)** intensities can be calculated. The third and sixth order intensities are zero. Examination of Fig.11.2 (c) shows that the fifth or sixth, and higher orders will all fall within the adjacent exit pupil. This happens, irrespective of the accuracy of the head tracker. Summation of the intensities shows that the total of these higher orders is around 3.5% the sum of the central orders. This figure fits in with the fact that the maxima of the *envelopes* containing these higher orders are 1/21 and 1/61 of zero-order value [HOUS38a].

The eye pupil function is semi-elliptical, and its width is that of the pupil. This function can be considered as the intensity received at a point on the retina by an eye that traverses a field illuminated with a step function.

Functions 11.2 (c) and (d) relate to the image formed on the retina, not what would be formed on a screen. However, as it is the effect on the retina that is relevant, they can be used in a convolution with functions 11.2 (a) and (b) to obtain the resultant 11.2 (e). The width of the boundary zone will be equal to the sum of the individual functions, provided these are finite. In this case, the diffraction function in not finite. However, it is the zero, and the first and second order components that largely determine the contribution of diffraction, therefore making it *effectively* finite.

The important regions of function 11.2 (e) are X and Y as these are where the eyes are likely to lie. If an eye is located in region Y the brightness of the image will be reduced, with the possible consequence of giving an uneven appearance. Crosstalk will occur when the eye is located in region X. This will be the subject of considerable investigation in the ATTEST project. The object of the prototypes produced will be to provide stereo over a large viewing volume, and the boundaries of this volume will be determined by the limits of acceptable crosstalk.

CHAPTER 12
RETROREFLECTING INFRARED HEAD TRACKER

12.1) Preface

As the principle purpose of this research is to design and evaluate the *optics* of a prototype 3D display, the head tracker under development is simple and inexpensive. It is also preferable, but not absolutely essential for proof-of-principle purposes, that the tracker is non-intrusive, i.e. it will not need attachments to the head. Previous 3D-display work within the group has employed the use of a Polhemus electromagnetic head tracker. This suffers from the disadvantages of being affected by magnetic objects within the immediate environment, and of the necessity of wearing a special headband.

The first prototypes under construction are single-viewer 3D displays, but future work will be on developing these into a multiple- viewer version. It will be useful if the tracker can be also be used in this application. This is the rationale behind the design of the infrared head tracker described in this chapter. The head tracker accuracy in relation to other factors contributing to crosstalk is also considered in this chapter.

12.2) Principle of Operation

The object of the head tracker is to determine the centre point between the viewer's eyes as this is the boundary between the left and right exit pupils. Various possibilities exist: for example a machine vision-based system, or maybe one reflecting infrared light off the viewer's head or eyes. However, the simplest method is probably to determine the effective 'shadow' of the viewers head position against a background, and then estimate the eye-centre position from this.

When the problem was first considered, the obvious solution appeared to be an infrared source located above the centre of the display screen, and a linear array of detectors placed behind the viewer's head. However, this suffers from the disadvantages of requiring the array to be connected to the display, and the necessity for positional calibration. A more effective method is to mount an infrared source and camera above the centre of the display, and place a reflector behind the viewer's head.

If the camera incorporates a horizontal linear array, it can be set up to detect the 'shadow' in the plane of the viewer's eyes. In the prototype, the viewer's head will be constrained to occupying a small range of vertical positions. This would not be acceptable in a television display, but the prototype is designed only to provide stereo over a limited viewing volume.

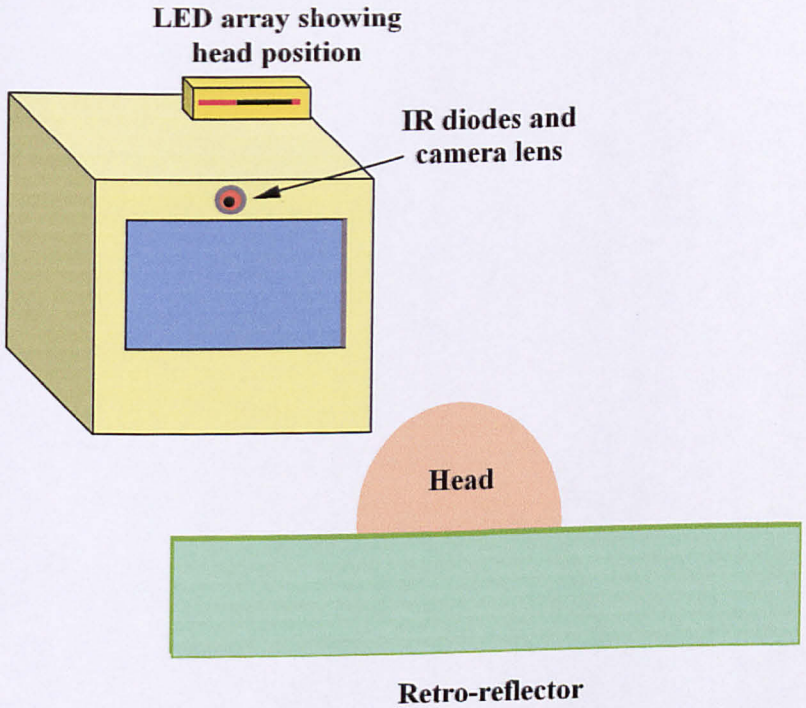

FIG.12.1 HEAD TRACKING SET-UP

Fig.12.1 illustrates the configuration of the display, viewer and reflector. It can be seen that the position of the reflector is not critical, it merely has to cover the region imaged by the camera. In order to increase the amount of infrared light reflected to the camera, the reflector consists of a retro-reflector where reflected light is returned along its entry path. The illumination source consists of 28 infrared LEDs located around the camera lens.

The display shown here incorporates an array of red LEDs. This shows the position of the head, and is not necessary for the operation of the display. However, it does provide a very useful demonstration of the operation of the tracker.

The view of the viewer's head and retroreflector is shown in Fig.12.2 (a). In the version of the tracker that incorporates the red LED array, the width of the region imaged by the camera is 510 millimetres at the optimum viewing distance of 1.11 metres. The retro-reflector is 930 millimetres wide by 230 millimetres high. This is located behind the viewer's head at a distance of around 1.5 metres from the camera.

The red LED array consists of 24 elements giving a resolution of around 22 millimetres. It is wired to give a 'shadow' image of unlit LEDs that moves in the same direction as the head. Typically, ten to twelve LEDs are unlit when a head is in front of the camera.

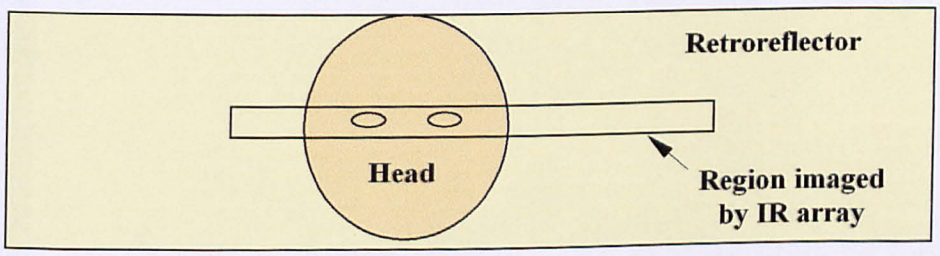

(a) View from Camera Lens

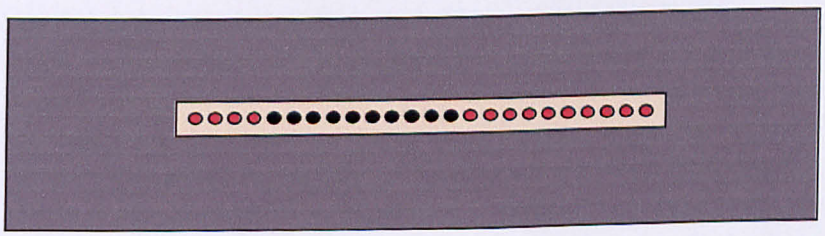

(b) Red LED Array

FIG.12.2 HEAD 'SHADOW'

The geometry of the tracker is shown in Fig.12.3 where rays of both the tracker and the exit pupil forming optics are indicated. The line passing through the centre of the head and camera lens, also passes through the centre of the image on the detector array and the boundary between the light sources producing the exit pupils. It can be seen that if the light source positions are made to follow the image on the array, the left and right exit pupils will follow the viewer's left and right eye positions.

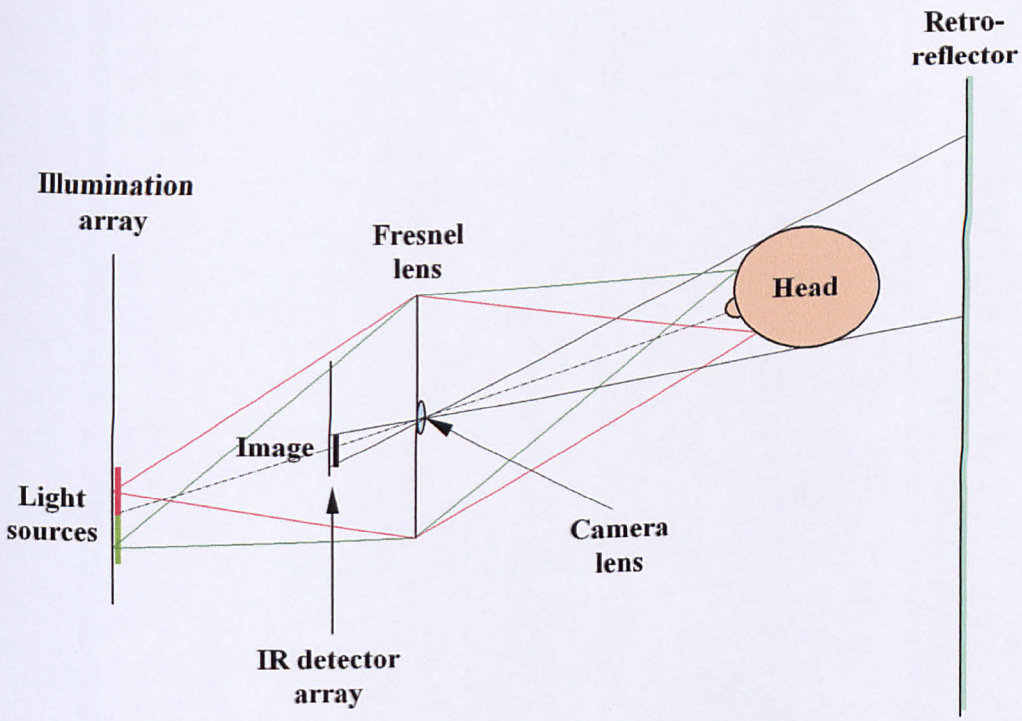

FIG.12.3 OPERATION OF HEAD TRACKER

12.3) Illumination

The infrared LEDs are arranged in a ring around the camera lens as shown in Fig.12.5 (b). In order to ensure that they are located sufficiently close to the camera lens, it is necessary to know the reflection characteristic of the retro-reflecting film. Although absolute measurements of this were not obtained, a good estimation can be obtained visually. The peak output of the LEDs is at 950 nanometres and their viewing angle is 120°.

The spread of the reflected light was determined by shining a laser pointer through a hole in a white card. With the laser 1.5 metres from the reflector, a pattern as depicted in Fig.12.4 was obtained. This is a fairly accurate full-scale representation of the pattern observed, with the exception of the effect of speckle that gives the pattern a shimmering and speckled appearance. The reflector is manufactured by 3M Traffic Control Products, and is intended for traffic sign purposes, where light from the vehicle headlight beam is reflected back to the driver's eyes. The reflection sheet operates on the cube corner principle where three orthogonal reflecting surfaces return light back along its original direction. The product is VIP Diamond Grade™ Reflective Sheeting type 3990 White.

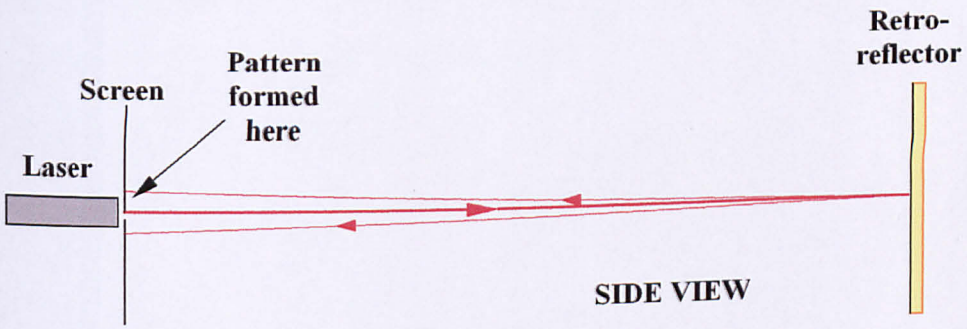

(a) Reflection Pattern Test Set-up

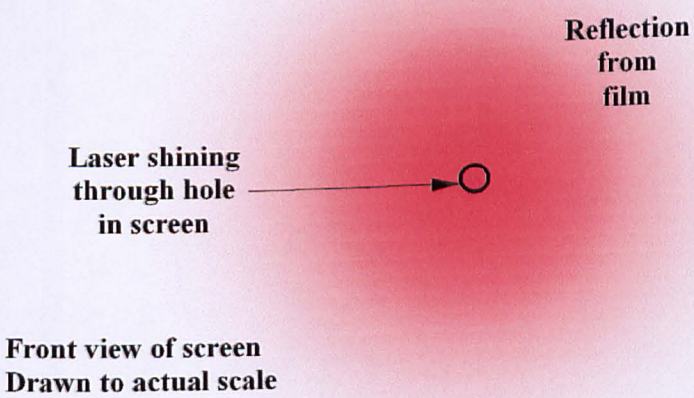

(b) Reflection Pattern at 1.5 Metres

FIG.12.4 RETROFLECTOR

The suitability of the reflection characteristic will now be determined. In Fig.12.5, both the infrared LEDs and the reflection at 1.5 metres are drawn to their actual size. Each LED produces the pattern shown in Fig.12.5 (b), giving a resultant that is the summation of 28 of these patterns whose centres coincide with those of the LEDs. This is difficult to analyse but can be simplified by considering the illumination domain where the pattern is shown in Fig.12.5 (b). This pattern has the same shape as the retro-reflection from a single LED. The contribution over the aperture region from LED X can be represented on the lower figure by the aperture X_A where the relationship between the aperture and the pattern remains unaltered. This is achieved by the simple transformation where the aperture centre is transferred to the point opposite the centre of LED X. The same procedure can be applied to all the LEDs with the same intensity characteristic being used for all apertures.

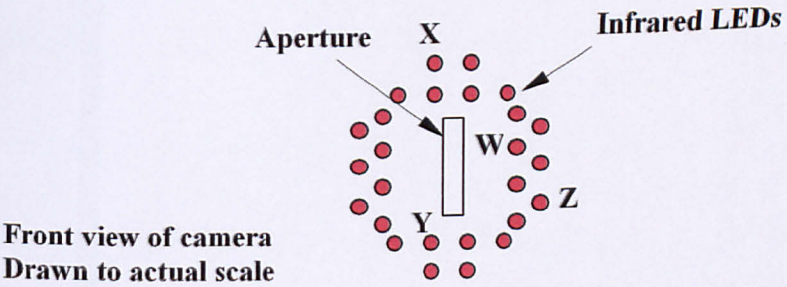

(a) Infrared LEDs and Aperture

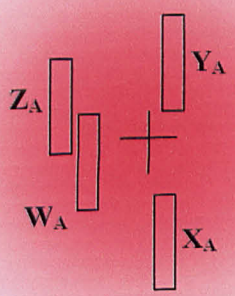

(b) Transformations into the Reflection Domain

FIG.12.5 48-ELEMENT ARRAY CAMERA INFRARED CAPTURE

When the pattern consists of a decreasing intensity that is only dependent on the distance from the centre, transformations need not be carried out - the aperture can be considered as being located around the LED centre.

Fig.12.5 (b) shows the transformations for various LEDs, from the closest at W to the furthest at X. It can be seen that all lie within an area with strong reflection. The retro-reflection characteristic is well matched to the dimensions of the LED array.

Initially the camera was used with a blank vehicle 'number-plate' as the retroreflector, the aperture size was set at fifteen-millimetres square in order to capture sufficient light. The aperture was square as this was simple to construct from a section of plastic Fresnel lens. With the increased amount of reflection from the retroreflective sheet, better performance, both optically and electrically, is obtained by keeping the same height, but narrowing the width to 2.5 millimetres.

As only the horizontal resolution is of interest, the reduction in the aperture width reduces spherical aberration in the horizontal direction whilst maintaining the aberration in the vertical direction. Interestingly, this could be the reason that some predatory animals such as cats and snakes have pupils that are horizontal slits when not fully open. The anatomical reason for the pupils being that shape is, possibly, not clear. However, for daytime hunting, the narrowing of the pupil in order to let less light through - as opposed to keeping its shape circular - aids horizontal resolution,.

The discrete components in the 48-element array, which was the first to be constructed, performed better when the aperture width was decreased. With the square aperture, there are high levels of hysteresis in photodetector outputs, the reason for this is not clear. This is effectively a *positional* hysteresis and can be observed on the red LED array. When a target was moved across the field in one direction, there could be a difference of up to 20 millimetres for red LED switching when it was moved back in the other direction. This hysteresis is in the order of one to two millimetres with the narrower aperture.

The second camera being built utilises a 128-element linear sensor array on an eight-pin chip and requires only a conventional double convex lens that is five millimetres diameter. It would be possible to use a more compact infrared LED assembly but it was not felt that this would be necessary for the evaluation of the camera. The infrared capture can be determined by simply superimposing a set of five-millimetre circles, in the same layout as the LEDs, on the reflection pattern.

A laser was used in order to provide a bright reflection pattern. As the beam from this is only a few millimetres wide at the reflector, the effect is not exactly the same as that from an LED where the light is spread over an angle in excess of 120°. Scattering the light from the LED can be used to assess the suitability of a laser to simulate the performance of an LED. A ten millimetre diameter Perspex rod mounted immediately in front of the laser was used to scatter the beam in the vertical direction only, and gave a spread greater than the 230 millimetre height of the reflector. The scattering pattern did not display any discernible difference, therefore indicating that the method used here is adequate for determining the suitability of the reflector characteristics.

When the camera was tested indoors, the shadow on the red LED array showed that the camera provides reliable positional determination. The camera also operates in sunlight and only becomes unreliable when sunlight shines directly into the lens. This robust performance indicates that the camera would probably operate reliably with fewer LEDs. However, as this type of head tracker will be used only in prototypes, it is safer to use more LEDs than is necessary in order to guarantee good reliability.

12.4) 48-Element Array

The camera with a 48-element array incorporates discrete photodetectors as a suitable integrated device was unavailable at the time of its construction. Also there was some concern as to whether ambient infrared might necessitate the use of discrete components in conjunction with amplitude modulation.

12.4.1) Camera Optics

The optical design is based on the array dimensions, which is in turn determined by device dimensions. The photodetector type is a TSL260 manufactured by Texas

instruments. This is a combined photodiode and amplifier that has a response in the near-infrared 820 to 1050 nanometer range. It is housed in an infrared transmissive three-pin package, and it is this package size that determines the length of the array.

Fig.12.6 is the front view of the array looking from the lens. The devices are mounted on standard 0.1" pitch stripboard. Each board has two rows of photodetectors where one row is 0.2" in front of the other. The lighter grey devices in Fig.5 denote the rows closest to the lens. The pitch of each row is 0.4", giving a combined pitch of 0.2". A second board of similar construction is mounted above the lower board, but displaced 0.1" to the right so that the effective overall pitch is 0.1". This rather difficult construction arose from the fact that originally, the use of one board only was envisaged in order to drive the red LED indicator. However, this had insufficient resolution for the head tracker. In any event, it is difficult to see the way in which a 0.1" pitch can be achieved by any other means with these devices. The effect of the vertical separation of five millimetres between the upper and lower layers is assumed to be negligible.

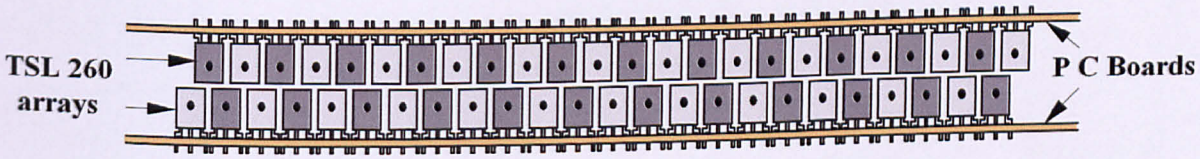

Front view from lens
Drawing to actual scale

FIG.12.6 48-ELEMENT ARRAY

The distance between the centres of the extreme elements is 119.4 millimetres. The size of the housing limits the maximum lens to array distance to a maximum of 260 millimetres. With an optimum viewing distance of 1.11 metres, the magnification

between the array and the viewing field is 1110 / 260 = 4.27. Therefore an array length of 119.4 millimetres corresponds to 510 millimetres at the viewing distance. For a head 200 millimetres wide, this will give head movement detection of 310 millimetres. The positional accuracy is 0.1 x 2.54 x 4.27 = 10.8 millimetres.

Object and image distances of 1.11 metres and 260 millimetres yield a *focal length* requirement of 211 millimetres. The focal length of the Fresnel lens used is 291 millimetres. From the equation for cascaded lenses, an additional lens with a focal length of 767 millimetres will be required. This is 1.30 diopters which is close to the standard spectacle focal length of 1.5 diopters. The combined focal length of 202 millimetres with the spectacle lens is sufficiently close to 213 millimetres for this application.

Fig.12.7 is a cross-sectional view of the camera. Stray infrared light is prevented from entering the lens by a fifteen-millimetre square mask indicated in the figure. The LEDs and the mask are contained within an open plastic box that is attached to the body of the camera simply with the use of double-sided tape - as are many of the components of the camera.

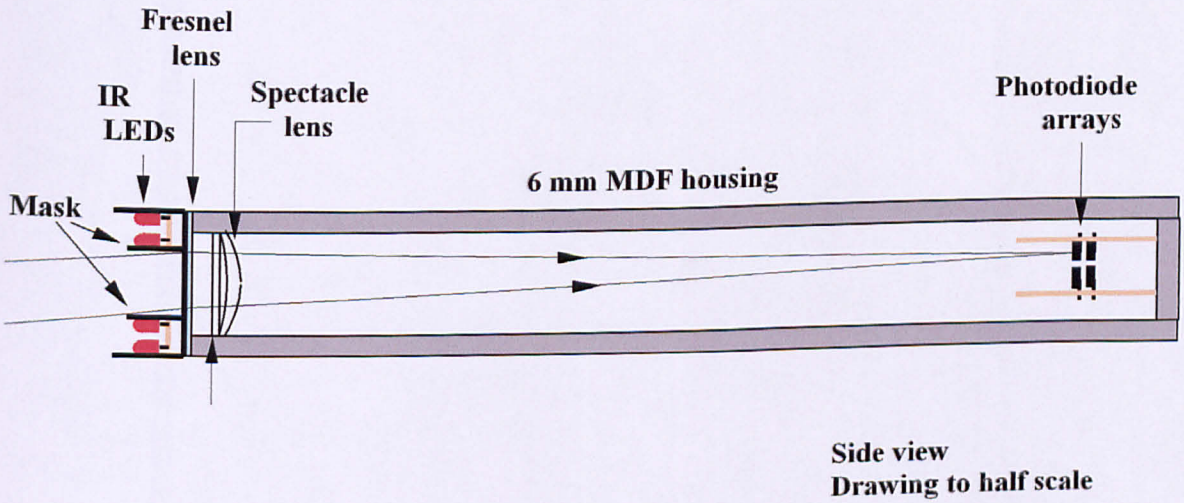

FIG.12.7 SECTION OF 48-ELEMENT ARRAY CAMERA

Note that the axis of the rays changes as it passes through the lens. As the camera is relatively large, it is preferable that it is not angled towards the viewer's eyes. If it were angled, the back of the camera would be around 40 millimetres higher than the front. This would not look particularly elegant and also it would also be more difficult to construct. Fortunately, the bending of the axis is simple to perform with the use of a Fresnel lens.

The geometry of the camera optics is shown in Fig.12.8 where the vertical scale is x 1/5, and the horizontal scale x 1/10. The Fresnel lens is depicted as a conventional lens for ease of explanation. If there were no restrictions on the lens size or on the light path, a large lens, with light passing through its centre, could be used. However, as the lens occupies the region indicated by the bold lines, only this portion needs to be used. As the aperture lies in the Fourier transform plane of the lens, the image is unaffected apart from an increase in aberrations.

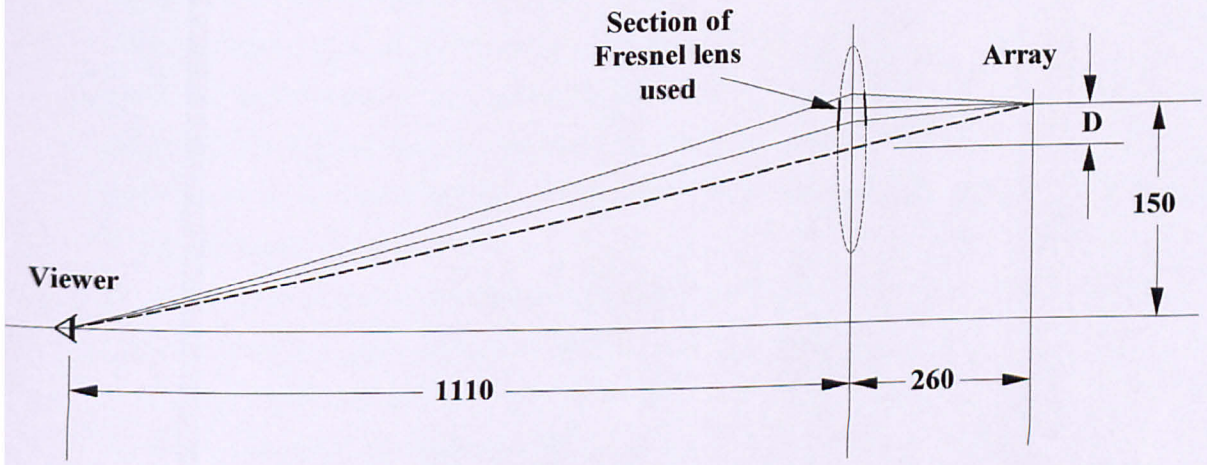

Side View
Dimensions in millimetres
D = 28.5

FIG.12.8 48-ELEMENT ARRAY CAMERA GEOMETRY

The particular Fresnel lens used lends itself to this application as it is the inexpensive magnifier used for the 5.6" prototype described in Chapter 9, and is made of a soft plastic material that can easily be cut with scissors. The section of lens is effectively a combination of a focusing lens and a prism that bends the light.

The position of the area of lens used is found as follows. Let the distance between the centre of the complete lens and the centre of the section used in the camera be D. By similar triangles it can be seen in Fig.12.8 that-

$(150 - D) / 1110 = D / 260$

This gives D = 28.5 millimetres.

12.4.2) Camera Electronics

The outputs of the 48 array elements are connected in parallel to 48 buffer amplifiers as there as there is no straightforward method of multiplexing their analogue outputs - multiplexing is best carried out when the information has been converted to levels suitable for logic circuitry. For ease of construction, the buffers are on the same circuit boards as the photodetectors. The circuit boards are mounted within the camera housing as shown in Fig.12.9, and are connected by ribbon cables and header plugs. This method enables all the circuitry to be contained within the same box. In any event, the buffers have to be kept in the dark as they are on the same boards as the detectors. The original camera contained only the lower board at the back as this was sufficient to drive the 24-indicator LED array. The functions of the regions of the boards numbered are as follows –

1) Odd numbered photodetector elements nos. 1 – 47 inclusive.
2) Even numbered photodetector elements nos. 2 – 48 inclusive.
3) Odd numbered buffers nos. 1 – 47 inclusive.
4) Even numbered buffers nos. 2 – 48 inclusive.
5) Multiplexer for odd nos. 1 – 47 inclusive.
6) Multiplexer for even nos. 2 – 48 inclusive.
7) Multiplexer controller.
8) Processor
9) Stepper motor drive buffer.
10) Infrared LED series resistors.

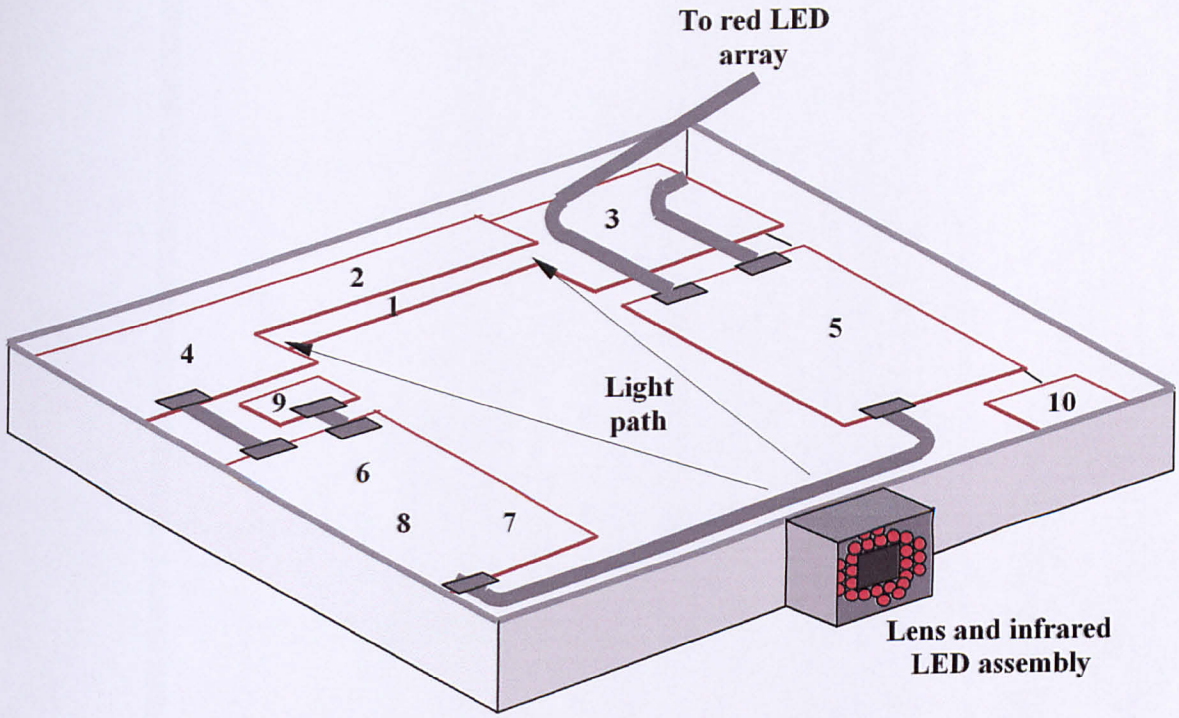

FIG.12.9 48-ELEMENT ARRAY CAMERA LAYOUT

The 48 buffer amplifiers convert the low analogue output levels of the photodetectors into levels suitable for logic. When the aperture was reduced to 2.5 millimetres width the output voltage of the various detectors varied between 40 and 98 millivolts when they received reflected infrared light, and less than 6 millivolts when in the image of the shadow. Referring to Fig.12.10, optimum performance is obtained when the bias voltage on the ´-` inputs on the LM324 operational amplifiers is around 29 millivolts. This is obtained from the resistors $R_1$ and $R_2$ that are connected to all the ´-` inputs of the 24 amplifiers on the board. In this application, these act as an effective constant voltage source as their Thevenin equivalent circuit is a 29-millivolt constant voltage source with a 3.3 Ω series resistor.

Resistor R_3 and diode D_1 protect the logic. D_i is a Schottky diode that ensures the output cannot go below – 0.3 volts, and R_3 limits the current through the diode. The gain of the amplifier ensures the output voltage is above 66% of the supply voltage for a logic ´1`, and 33% of supply voltage for ´0`.

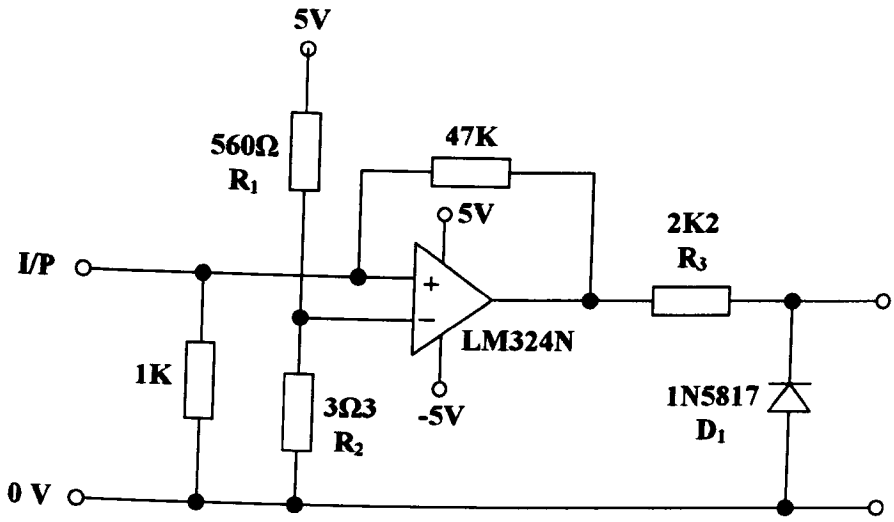

FIG.12.10 BUFFER FOR TL260 TO LOGIC

The functional diagram of the complete circuit is shown in Fig.12.11. As the processor can accept only eight inputs, the 48 array outputs must be multiplexed. The information is presented sequentially to the 6805 processor as six sets of eight-bit parallel data. The data is selected by six octal buffer/drivers type 541 whose function table is given below.

Table12.1 - 541 Function Table

INPUTS			OUTPUT Y
$\overline{OE1}$	$\overline{OE2}$	A	
L	L	L	L
L	L	H	H
H	X	X	Z
X	H	X	Z

When the control inputs OE1 bar and OE2 bar are low, the data on inputs A1 – A7 is transferred to the Y1-Y7 outputs. When either of the control inputs are high, the outputs are in the high-impedance state (Z).

The three-state outputs enable the outputs of the six 541s to be connected together as in Fig.12.12. The data on the PA0 – PA6 inputs of the processor is determined by the 541 that has a low on the control inputs. The control is obtained from a 1 x 8 decoder type 138 whose input is a three-bit code from the PB3 – PB5 outputs on the processor.

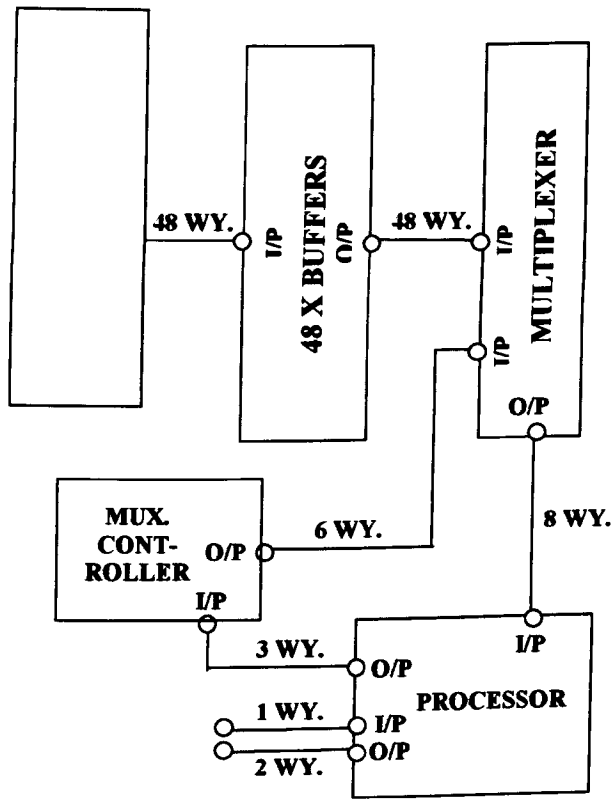

FIG.12.11 48-ELEMENT ARRAY CIRCUIT - SCHEMATIC

Table 12.2 – Multiplexer Operation

OUTPUT TO CONTROLLER			INPUTS TO PA0 – PA 5
PB3	PB4	PB5	
0	0	0	1 – 15 ODD
1	0	0	17 – 31 ODD
0	1	0	33 – 47 ODD
1	1	0	2 – 16 EVEN
0	0	1	18 – 32 EVEN
1	0	1	34 – 48 EVEN

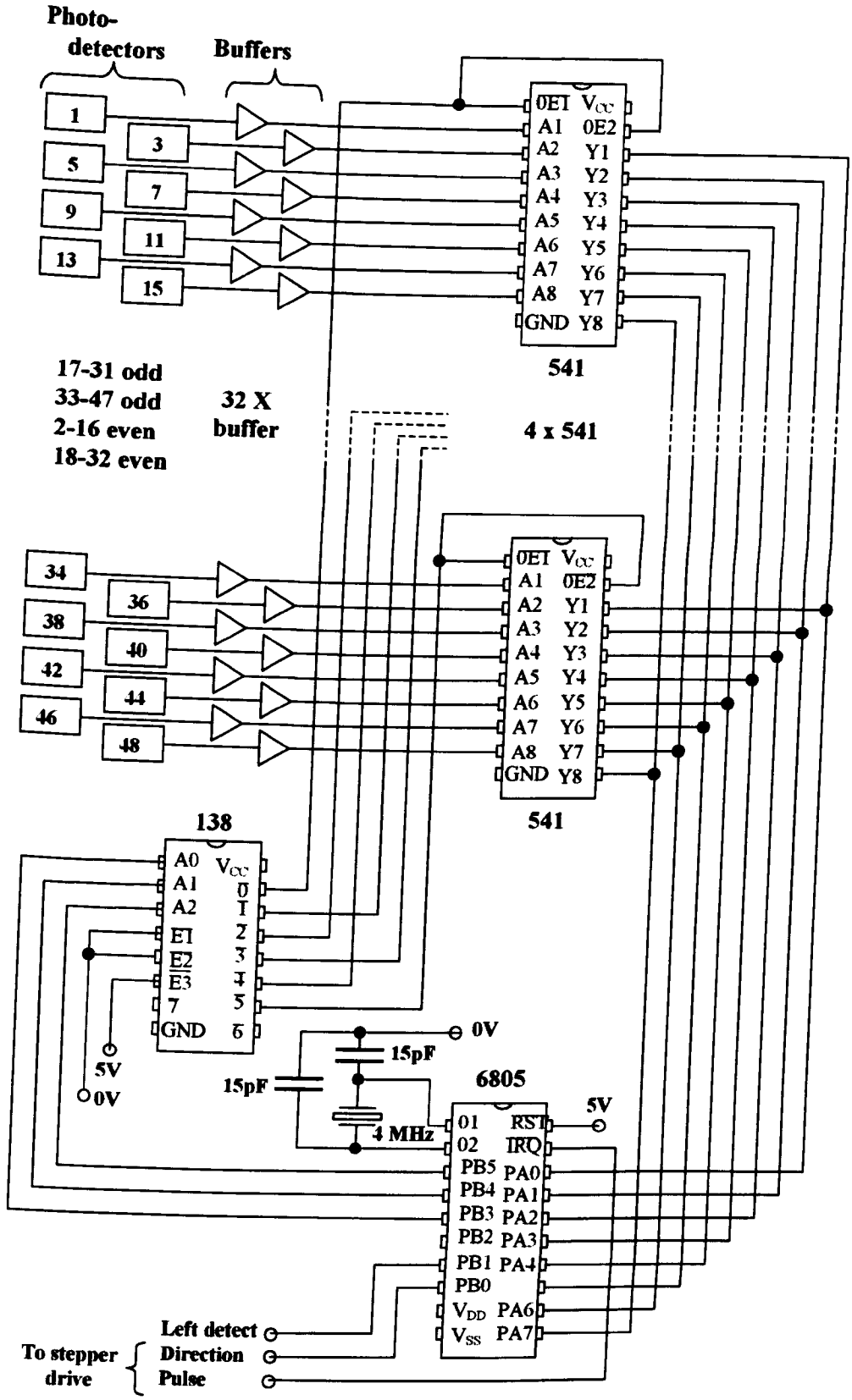

FIG.12.12 48-ELEMENT ARRAY CIRCUIT

The outputs PB0 and PB1 of the processor are used to control a stepper motor driver. This controls the lateral position of a pair of linear halogen lamps as described in Chapter 10. The stepper motor driver requires a 'pulse' input to move the motor by one increment, and a 'direction' input to determine its direction of rotation. As the driver needs 0 and 12 volts, there is a buffer after the processor output. This both inverts and amplifies the voltages. When the output from PB0 on the processor is low, the output from the buffer is around 12 volts and the stepper motor runs anticlockwise. This causes the carriage, on which the lights are mounted, to move from left to right, and the exit pupils from right to left. The motor moves a step when the driver input changes from 0 to 12 volts.

Each pulse rotates the stepper motor shaft by 7.5°. This drives a rack-and-pinion, where one revolution of the pinion gives 31 millimetres lateral rack movement. Therefore each pulse to the motor moves the lamps 0.667 millimetres. When magnified by the Fresnel lens, this corresponds to 2.85 millimetres in the viewing field.

The processor needs to know the lamp assembly position. Although this could be achieved using a position sensing encoder, this is not necessary with a stepper motor system. As a stepper motor moves by a predetermined amount for each pulse, no feedback is necessary once the initial position of the lamps has been determined – dead reckoning alone is sufficient. This is achieved by sending the lamp assembly to the extreme left of its travel when the tracker is first switched on. A magnet on the assembly actuates a reed switch that is connected to the processor. When the contacts on the switch close, the motor stops turning. The position of the lamps is now known.

The processor estimates the centre of the 'shadow' region with the information from the array outputs, then sends pulses to the stepper drive to move the lamp assembly to the left in order to produce exit pupils either side of this position. Thereafter, the stepper drive is provided with pulses and direction information in order to follow the movements of the viewer's head.

12.5) 128-Element Array

The use of discrete components made the 48-element array rather complex to build. During the time of its construction, a suitable single-chip array was found. This is the TSL1401 manufactured by Texas Advanced *Optoelectronic* Solutions Inc. This device incorporates a linear array of 128 photodiodes. Each photodiode has an associated amplifier and a data hold function that integrates the light energy over a sampling period that is the same for all the elements. During the integration period, a sampling capacitor connects the output of the integrator through an analogue switch. The amount of charge accumulated at each pixel is directly proportional to the product of the light intensity and the integration time.

When the integration period has finished, the sampling capacitors are disconnected from their respective integrators. The charges on the sampling capacitors are sequentially connected to an amplifier by a 128-bit shift register that has a rising edge on input S1 clocked through it. The output *A0* requires a 330 Ω pulldown resistor.

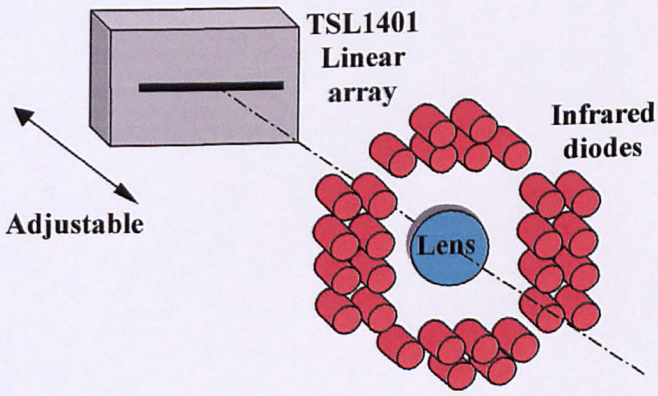

FIG.12.11 128-ELEMENT ARRAY CAMERA

The TSL1401 is an eight-pin dual-in-line package, and the array has a 63.5 micron pitch. This enables the camera to be very compact in comparison to the discrete component version. It is housed in a 48 x 70 x 26 millimetre plastic box with a 15-millimetre focal length lens mounted in one side. This is 4.5-millimetre diameter and is glued into a hole of the same diameter. The TSL1401 is mounted on a small piece

of stripboard on which two nuts are soldered. The board is fixed to the box by two screws that allow it to be moved longitudinally for focusing purposes. The infrared diode assembly used for the 48-element array is also used for this camera. Fig.12.11 is a simplified drawing of the camera.

The array pitch of 63.5 microns gives an array length of 8.06 millimetres between the centres of the first and 128th elements. With a 15-millimetre focal length lens, the capture width is 596 millimetres at 1.11 metres viewer distance. This is sufficiently wide to allow for adequate head movement.

As the TSL1401 is a white light device, a near-infrared filter is used to make it less susceptible to interference from stray visible light. The response characteristic in Fig.12.12 shows that the peak output is at around 770 nanometres. In order to eliminate light from the visible spectrum reaching the array, a near infrared filter is attached to the front of the lens. This does not allow light with a wavelength less than 760 nanometres to pass through it.

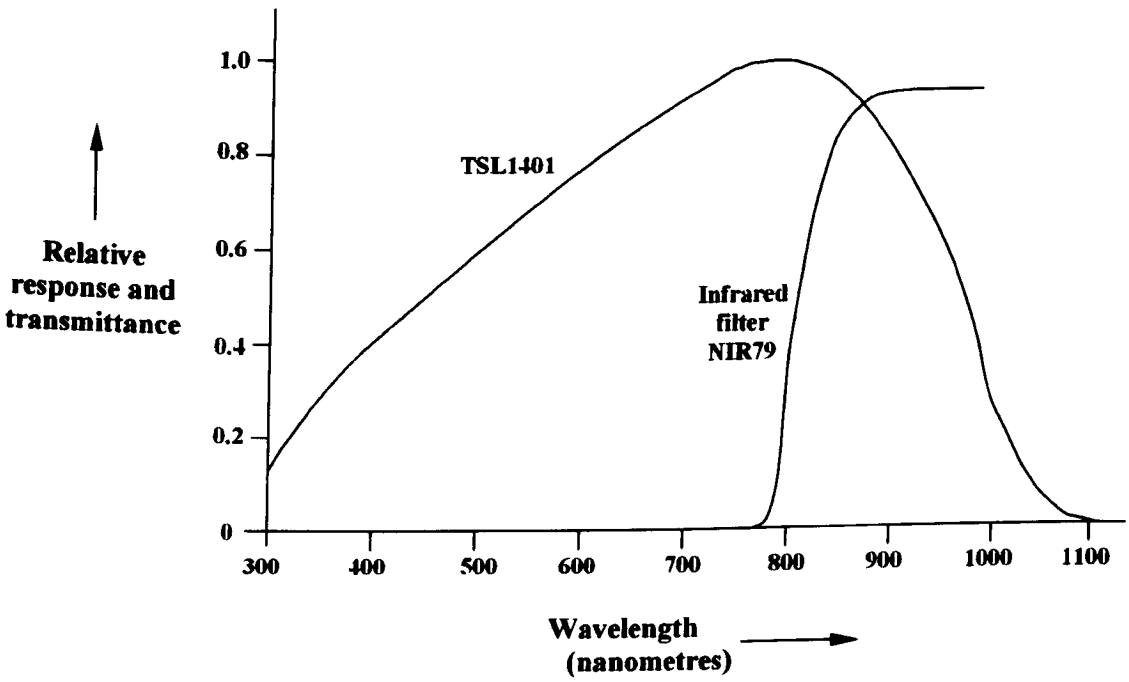

FIG.12.12 PHOTODETECTOR AND INFRARED FILTER RESPONSE

The filter type NIR79 is one of a range of near infrared filters manufactured by Nitto Jushi Kogyo Co. Ltd. The '79' component in the type number refers to the wavelength at which the transmittance is around 0.3. Other designations in the range are '81', '83', '84' and '86'. Inspection of the spectral characteristics indicates that the NIR79 is the most suitable for matching the camera to the infrared LEDs.

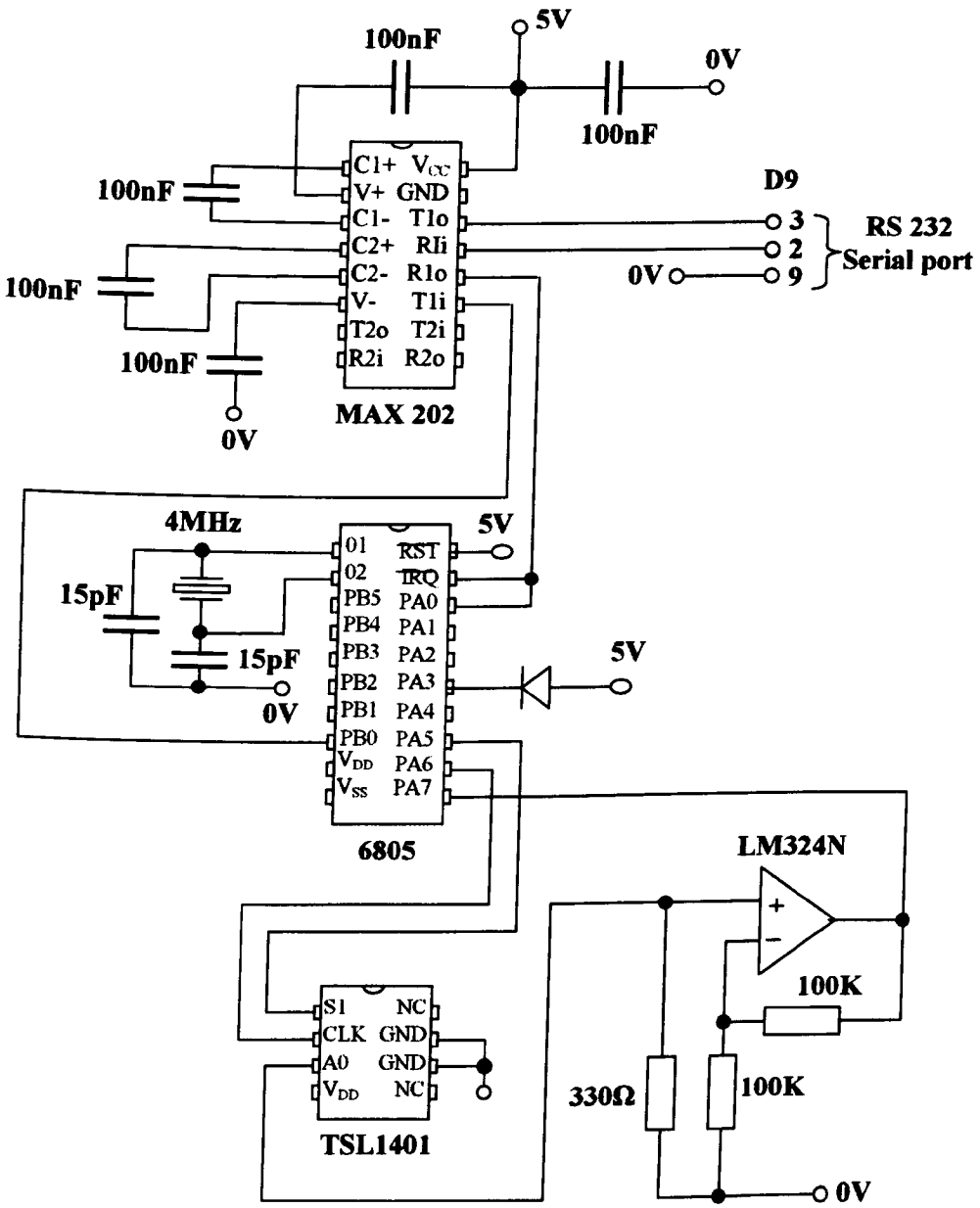

FIG.12.13 128-ELEMENT ARRAY CIRCUIT

Referring to Fig.12.13, the signal from the A0 output of the TSL1401 is connected to an operational amplifier that has a gain of two. This information is fed to a PC via the processor, and a MAX202 tranceiver that provides the correct voltage levels. The clock pulses and the output cycle initiation pulse are generated by the processor.

In this case, the processing is simpler as the 128-element array is only intended for use with the white LED array illumination sources. The geometry in Fig.12.3 shows that the illumination on the LEDs only has to follow the centre of the 'shadow'. This mode of operation only requires allowance for the scaling between the sensor pixel pitch, and the white LED pitch, when these are transferred to the viewing field via the lenses.

The output of the processor is displayed on an array of white LEDs. This is for test purposes only and consists of inexpensive devices that are too dim to be suitable for use in the display illumination. The LEDs are driven from the outputs of eight octal buffer drivers type 2803. The inputs of these are connected to the outputs of eight serial in / parallel out shift registers type 164. These are cascaded, with the output of the first connected to the input of the second, and so on. The clock rate is sufficiently fast for the outputs not to require inhibiting whilst the data is being shifted through the register. The LEDs, drivers and shift registers are all mounted on one circuit board to provide a convenient means of visualising the output of the processor.

12.6) Current State of Head Tracker

It is unlikely that work will continue on the 48-element tracker with discrete photodetectors as the construction is complex and bulky. Although the processor is programmed to operate a stepper motor mechanism, it would not be difficult to reprogram it for white LED operation. However, the camera will remain in use for demonstrating the principle of the infrared 'shadow' method of head tracking. When used only for this purpose, most of the circuitry, including one of the arrays, is redundant. Evaluation has not been carried out on the complete tracker as the program for the processor was not perfected before the decision to use a single-chip array.

Work is continuing on the 128-element array, but the complete tracker incorporating white LED arrays mounted in the display has not yet been completed. As funding is now available for a multiple-viewer prototype, the work carried out so far may be used as the basis for a multiple-viewer tracker. The viewing field for this version will be large, with viewing distances up to three metres, and both the range and direction of several viewers will need to be determined. Two cameras will be required in order to obtain this information.

CHAPTER 13
ACOUSTIC HEAD TRACKING

13.1) Preface

At an early stage of this research, various possibilities for head tracking were considered, one of these being ultrasonic head and eye detection and ranging. Certainly ultrasonic *ranging* would be a very useful technique. Inexpensive ultrasonic tape measures are available off-the-shelf. These use the time-of-flight of the reflected sound and are accurate to around ±10 cm, which is well within the accuracy required for head tracking. Ultrasonic ranging could be used in conjunction with other methods of determining head directions. As ranging is so easily achieved, the use of reflected sound to also obtain the horizontal positions of the viewers' heads is considered in this chapter.

13.2) Acoustic Array

The top views of the sound wavefronts for range determination are shown in Fig.13.1. The size of the sound source is assumed to be negligible so that the wavefront from a notional vertical line source is cylindrical. It should be noted that the analysis given here is two-dimensional as the calculations for this are relatively simple, and the results can be used to give a general indication of the viability of acoustic methods. The distance of an object is simply determined by the time-of-flight (Fig.13.2), however, the determination of an object's shape requires the *amplitude* and *phase* information of the reflected pulse from an array of receivers.

In the two-dimensional analysis, the outputs of a linear array of sound detectors will be as shown in Fig.13.3. Consider the simple case of an object situated on the axis. When the received signal at two central array elements is taken as the reference, the vector outputs of the other elements will be as in Fig.13.3, where the phase angle decreases with the distance from the centre due to the increasing path length. When the outputs of the elements are summed in complex form, the resultant is as shown in the figure.

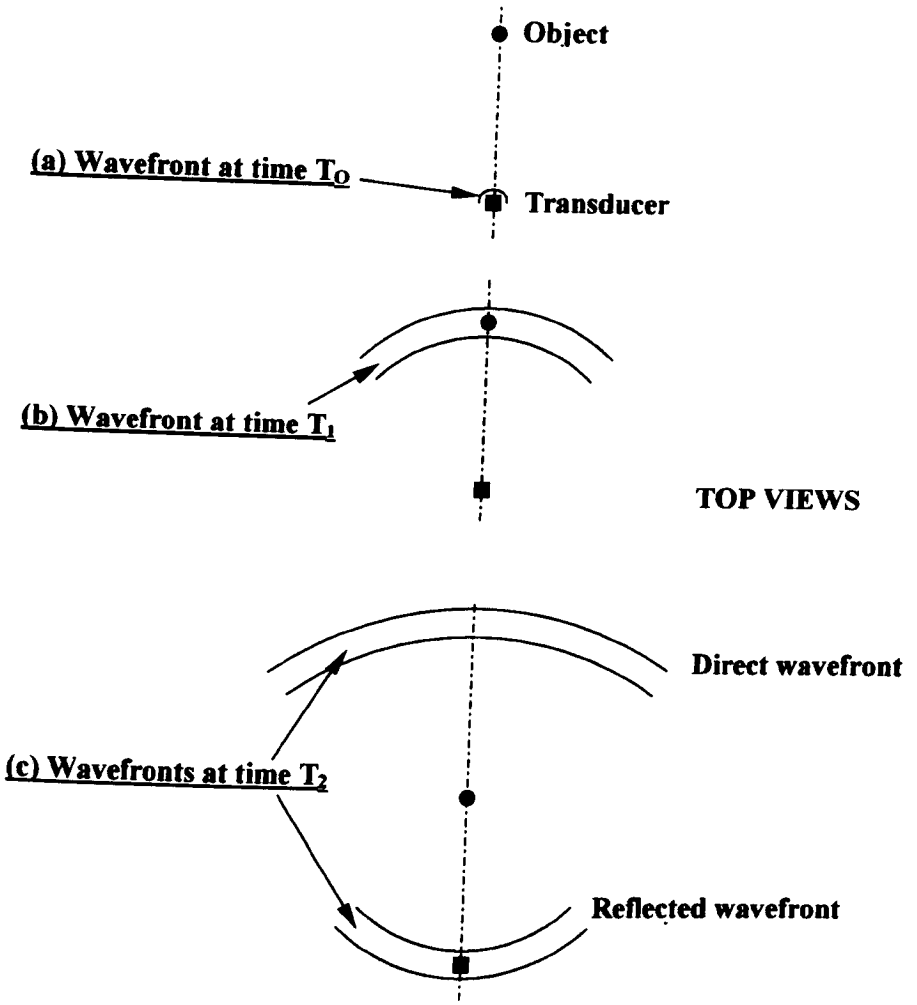

FIG.13.1 WAVEFRONTS AT TIMES T_1, T_2 & T_3

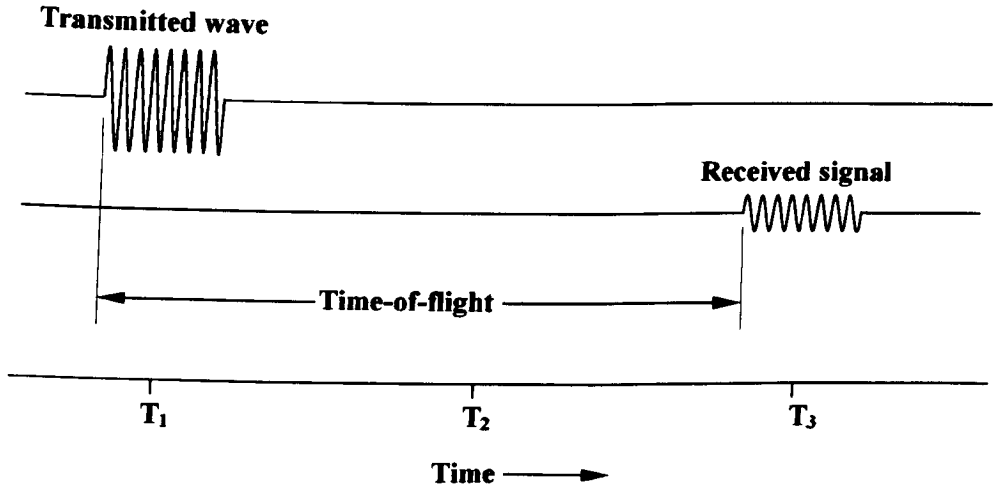

FIG.13.2 ACOUSTIC WAVEFORMS

The optical analogue of this is Fresnel diffraction of a cylindrical wavefront. When light is diffracted at an edge, the intensity of the light at a given point on a surface in front of the edge is determined by the contribution of the complete wavefront from the edge to infinity. The amplitude and phase of this contribution can be found by applying the Cornu spiral [HECH89a]. In Fig.13.4, the central section of the complete curve is shown. The complete curve starts at the asymptotic point B, passes through the origin, and finishes at the asymptotic point A. Points A and B correspond to contributions of the wavefront at infinity.

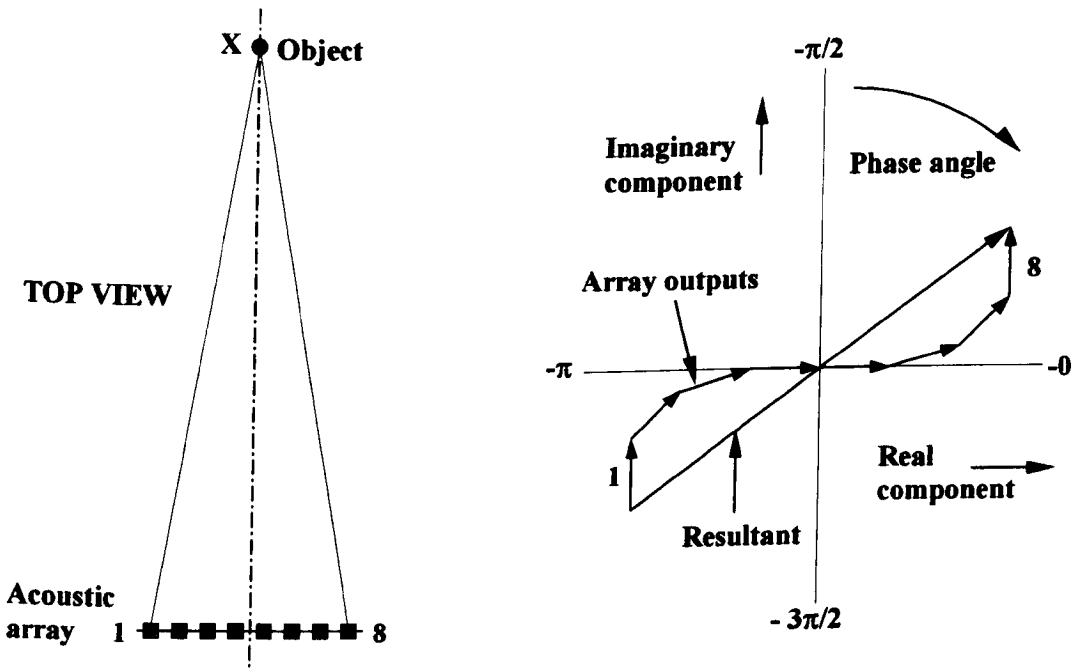

(a) Array Configuration

(b) Vector Addition of Array Outputs

FIG.13.3 ACOUSTIC ARRAY

The outputs of the eight-element array shown in Fig.13.3 (a) can be seen to approximate to the central portion of the spiral. In the case of the acoustic array shown, the sound is *received* by the array elements, as opposed to being transmitted from these regions as in the consideration of light diffraction. However, the phase and

amplitudes of the vectors are the same for each condition so that reversibility applies. Also, the output of the array consists of discrete vectors as opposed to the continuous contribution of the Cornu spiral. The more elements the array has, the closer the vectors become to being a continuous curve.

The optical equivalent of Fig.13.3 would be diffraction at a slit where the object at X corresponds to a point on a screen that lies on the normal to the centre of the slit. The resultant vector passes through the origin in Fig.13.3 (b), as it would also do on the Cornu spiral. When the object is not on this central line, the resultant does not pass through the origin and also diminishes in amplitude.

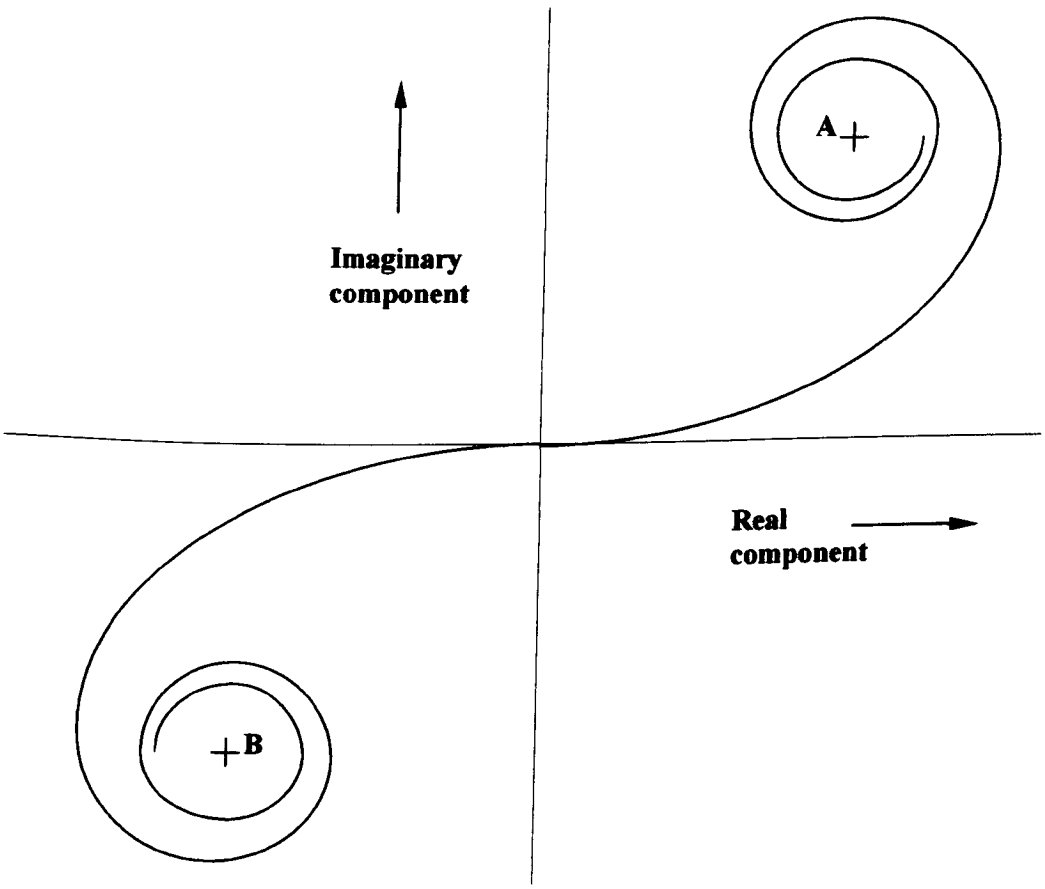

FIG.13.4 CORNU SPIRAL

13.2.1) Array Focusing

If the outputs of the array in Fig.13.3 (a) are summed in complex form, so that the resultant of Fig.13.3 (b) is obtained, the array is effectively focused at infinity. A sound source at infinity will give a plane wavefront and all the array outputs are in phase. In this case, all the individual output vectors will lie along the horizontal axis, and the magnitude of the resultant will be the sum of their magnitudes. As the point X approaches the array, the outputs form a more pronounced s-shape, as shown in Fig.13.3 (b). The resultant then becomes less than the sum of the individual components.

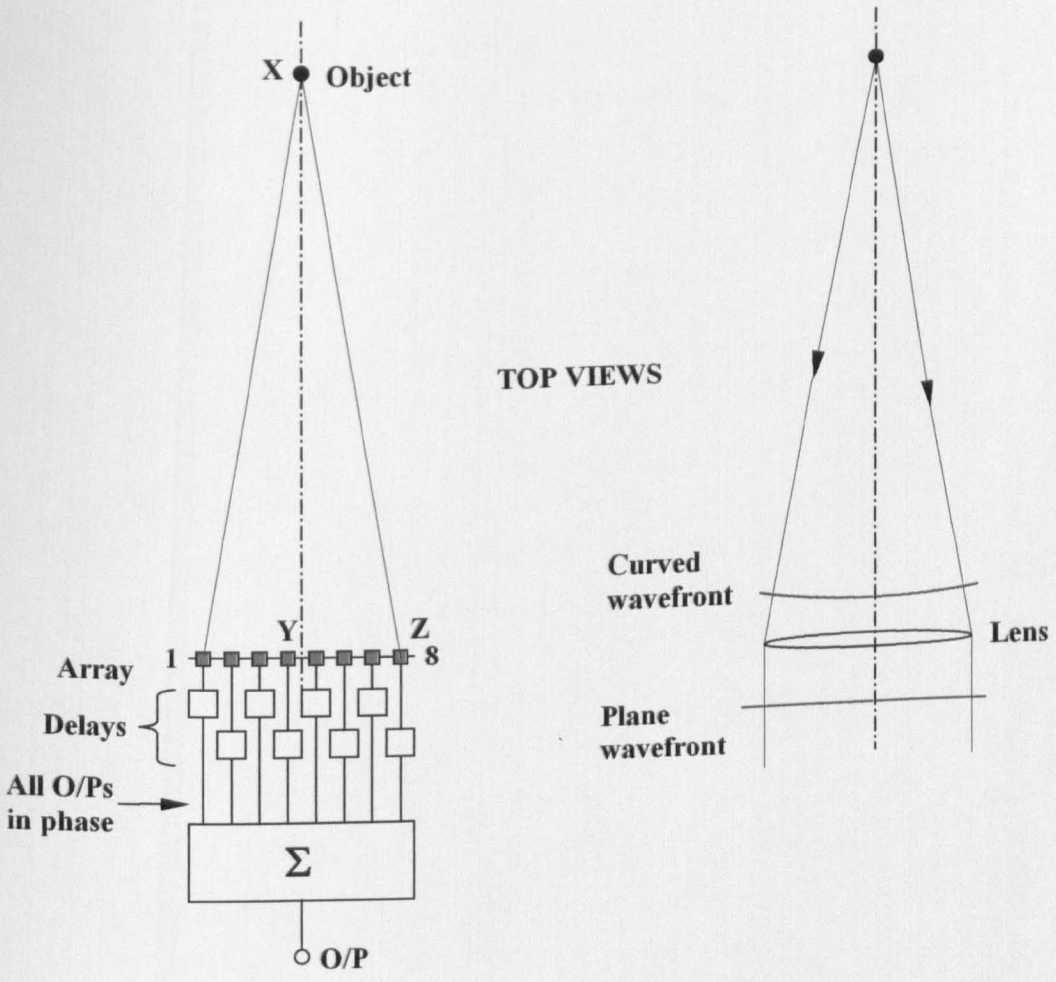

(a) Acoustic Configuration

(b) Optical Equivalent

FIG.13.5 FOCUSED ACOUSTIC ARRAY

Optimum performance in terms of sensitivity and resolution will be obtained if the array can be focused. This will be considered in detail in Section **13.2.4)**, It can be achieved by applying delays to the outputs as in Fig.13.5 (a). As the sound reaches the centre of the array first, these outputs will need to be delayed the most. If the delay on elements 1 and 8 is zero, then the delay on 4 and 5 will need to be equal to the time taken to travel the distance (XY – XZ). When delays based on this principle are applied to the other outputs, a virtual curved array whose centre is located at X is produced. All the inputs to the summation processor will be in phase from a source at X.

13.2.2) Array Steering and Focusing

As it is not practicable to physically rotate the array, it must be steered in another way. Again, delays can be applied to achieve this. Consider Fig.13.6 (a), where the object is to the right of its previous position. If there is zero delay on element 1, increasing linearly to maximum delay on 8, the delays can be adjusted in order to give the maximum sensitivity in the direction of the object. The optical equivalent of this is the prism shown in Fig.13.6 (b). Again, the resolving optics for the emergent waveform is not shown.

The way in which a linear array is converted into a virtual array that can be focused on an object that is neither at infinity, nor on the axis, can be seen in Fig.13.7. The *actual* positions of the array elements lie on the line AF. In order produce the virtual array situated on the curve AEG, the delays in Fig.13.7 (b) are required. The focusing and steering delays are shown separately as the focusing element of each delay can be the same for all lateral positions of X, provided the object is sufficiently close to the axis. A series of linearly increasing delays as shown in the middle figure of Fig.13.7 (b) provide both the steering and the focusing delays and enable the arc of the virtual array to be centred at X. The envelope of amplitudes lies on an ellipse. The two delays are added to give the total delay times shown in the lower figure in Fig.13.7 (b).

When the array is beamed in the direction of the axis, every element of the steering array has the same delay. This is equal to the delay of the central two elements which

is always the same irrespective of direction. This has the effect of effectively rotating the virtual array around the point B.

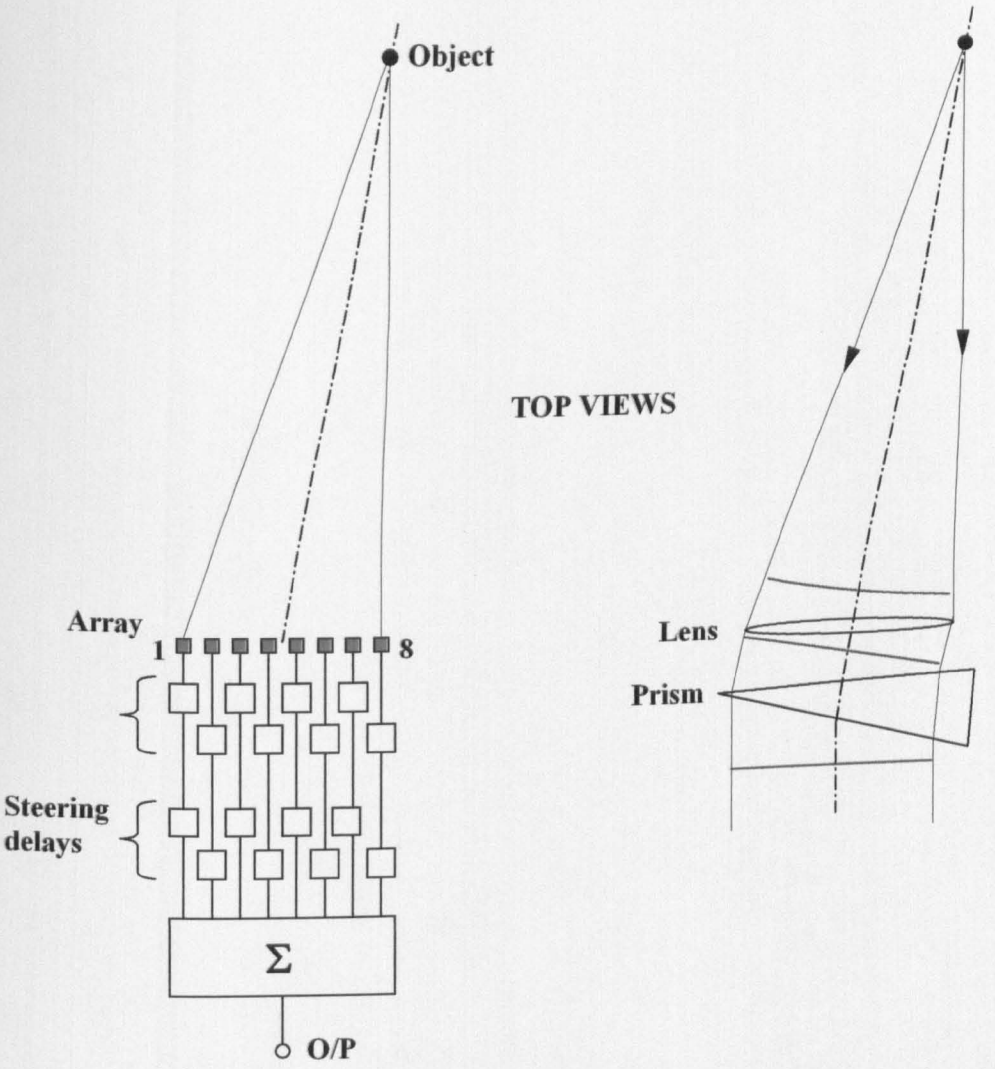

(a) Acoustic Configuration

(b) Optical Equivalent

FIG.13.6 ACOUSTIC ARRAY WITH FOCUSING AND STEERING

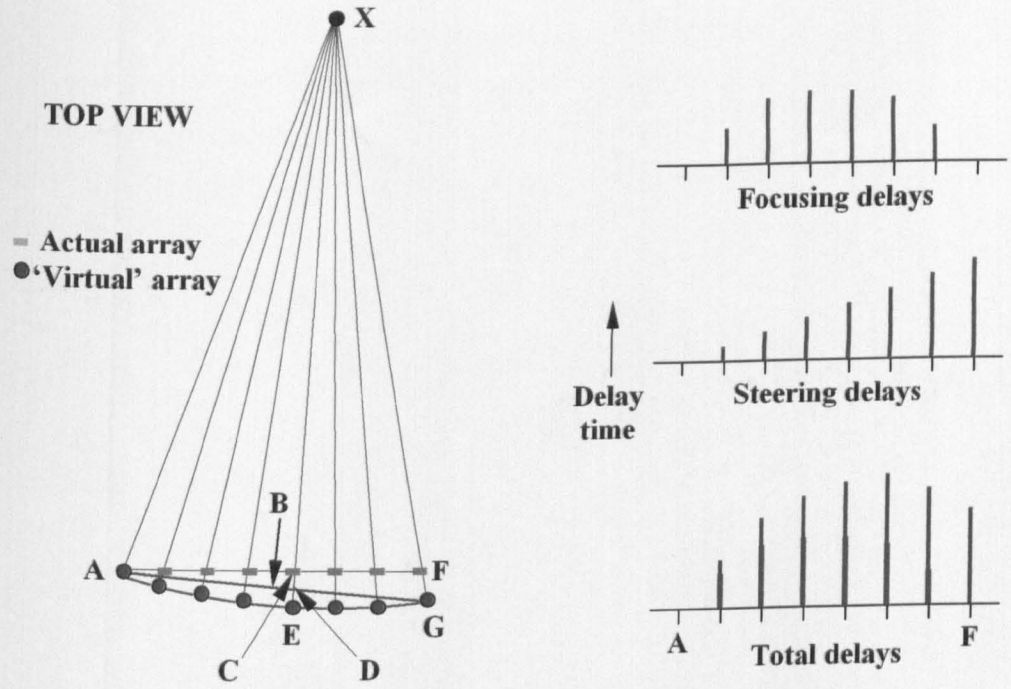

FIG.13.7 PRODUCTION OF VIRTUAL ARRAY

13.2.3) Determination of Point Spread Function

The point Spread Function (PSF) can be determined by vector addition of the array outputs for reflections off the object as it is moved in regular increments across the field at a fixed distance from the array. In the programme used to obtain the curves in Fig.13.8, the phase of the sound received by the array element closest to the object is taken as the reference. The path length difference, D on Fig.13.7 (a), between the closest point to the array and a particular array element, is calculated. The phase shift in radians is given by $2\pi d / \lambda$, where λ is the wavelength.

The amplitude of the output of a particular array element is assumed to be proportional to the cosine of the angle between the object and the normal. This will also make some allowance for the effect of obliquity [HECH89b].

The real and imaginary components of the outputs can then be calculated from the phase angles and relative amplitudes. These are summed separately to find the real and imaginary components of the resultant vector. Squaring this resultant gives the intensity. As absolute values are not necessary for the PSF, the resultant intensities are normalised by dividing them by the intensity when the object is on the axis.

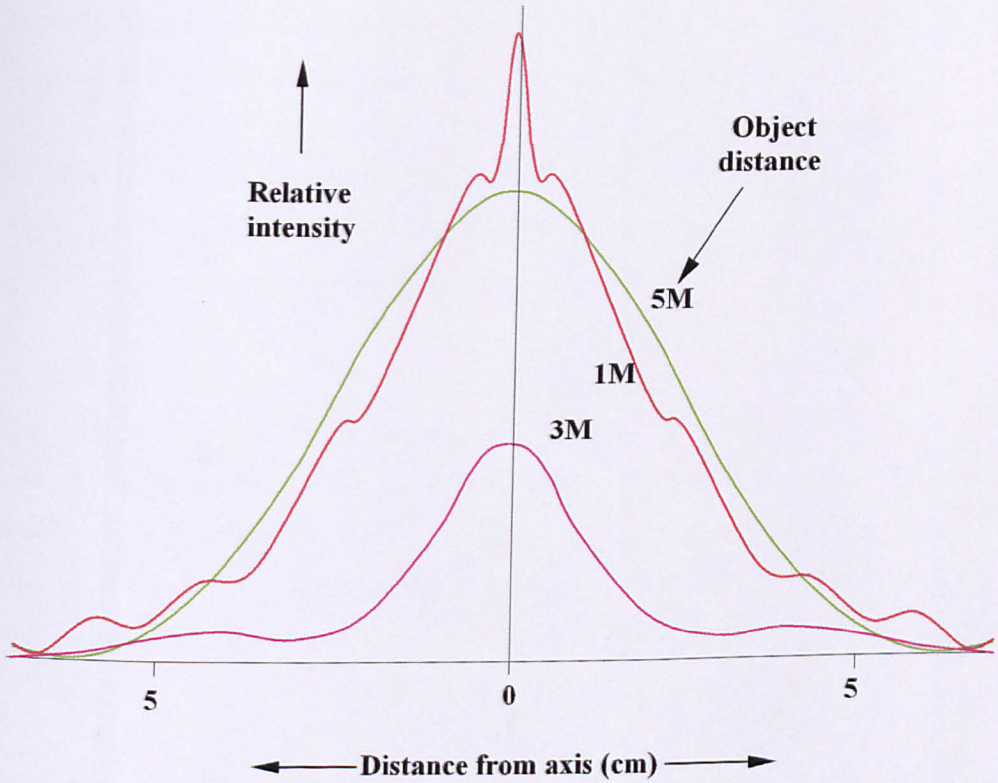

No. of array elements – 80
Array element spacing – 4 mm
Wavelength – 4 mm
Array focal length – 5m

FIG.13.8 ACOUSTIC ARRAY PSFs

The results for an 80-element array with a five-metre focal length, four-millimetre element spacing and a wavelength of four millimetres (82.9 kHz) are given in Fig.13.8. It can be seen that for the majority of PSFs for each of the object distances are within five centimetres of the axis. The array spacing is chosen to be the same as the wavelength so that only zero order wavelengths are detected, the first orders being at right angles to the array.

The curves in Fig.13.8 are drawn to actual horizontal scale. This is useful in visualising the relationship between the PSF and the head width, which is typically around 200 millimetres. The distance of the first minima from the axis for the curve for 5 metres is exactly 65 millimetres.

Families of curves calculated for other wavelengths and with 80 or 100 elements in the array all have the majority of their PSFs within the central ten centimetres whenever the spacing is made equal to the wavelength.

13.2.4) Advantages of Array Focusing

Although it *seems* fairly obvious that focusing the array is beneficial, the results actually show this to be the case. For example, in Fig.13.8 the maximum of the curve for five metres is not much less than for one metre. This is to be expected as all the outputs are in phase and reinforce each other. It has been found that his invariably counteracts the effect of the inverse square law.

Whereas the optical equivalent of an unfocused array is a case of Fresnel diffraction, when focused it is equivalent to Fraunhofer diffraction. The intensity distribution for this is the sinc^2 function where $\text{sinc}^2\theta = (\sin\theta / \theta)^2$ [STEW83b]. The PSF *can* be a very irregular function, especially where objects are close to the array and not in focus. This effect is the same as Frenel diffraction in optics and the PSFs produced are similar in shape to those produced by diffraction at a slit [FINC80b]. Incidentally, the fact that the calculated PSFs have the form of a sinc^2 function for objects at the focal plane provides a useful indication that the program is correct.

Deconvolution, i.e. effective de-blurring, is considered in the next section. This involves the use of Fourier transforms and inverse transforms. The Fourier transform of a $sinc^2$ function is a simple triangle function [BRAC85a]

If the transmission burst is sufficiently short, the focal length can be increased with time in order to match the increased distances of objects from which sound is reflected.

13.2.5) Deconvolution

As the PSF is around two-thirds the width of the average head, the acoustic image of the head will be very blurred. If a simple model of the head is used, where the eye-centre positions are assumed to be in the centre of the detected image, the blurred image might suffice. However, it may be useful to obtain higher resolution in order to obtain a more accurate indication of eye positions.

The blurred image in this case is the convolution of the PSF with the actual image. As the PSF is known, it will therefore be possible to sharpen up the image. An idealised object function and a $sinc^2$ function are shown in the top row of Fig.13.9. The majority of the PSF lies between the first minima as the relative values of the second, third and fourth maxima are 1/21, 1/61 and 1/120 respectively [HOUS38b]

If the object is 200 millimetres wide and the distance between the first minima is 120 millimetres (the distance between the first minima at focus in Fig.13.8), then the overall width of the blurred image will be 320 millimetres.

The lower figures in Fig.13.9 are the Fourier transforms of the object function, the PSF, and the convolution of these two which is the image intensity distribution function. The three columns of figures are in fact Fourier transform pairs where the upper figures are the transforms of the functions below them.

Convolution of two functions can be computationally simplified by multiplying their transforms and taking the inverse transform of the result [STEW83c]. This is an example of incoherent imaging (as opposed to coherent imaging where Fourier

transforms are applied to interference effects). The transform of a PSF is the modulation transfer function (MTF).

Dividing the transform of the image intensity *distribution function by the MTF*, and then taking the inverse transform of the result can perform deconvolution. In fig.13.9, the function (f) is divided by the triangular MTF (e) to give function (d) from which the original boxcar function can be obtained by taking the inverse transform.

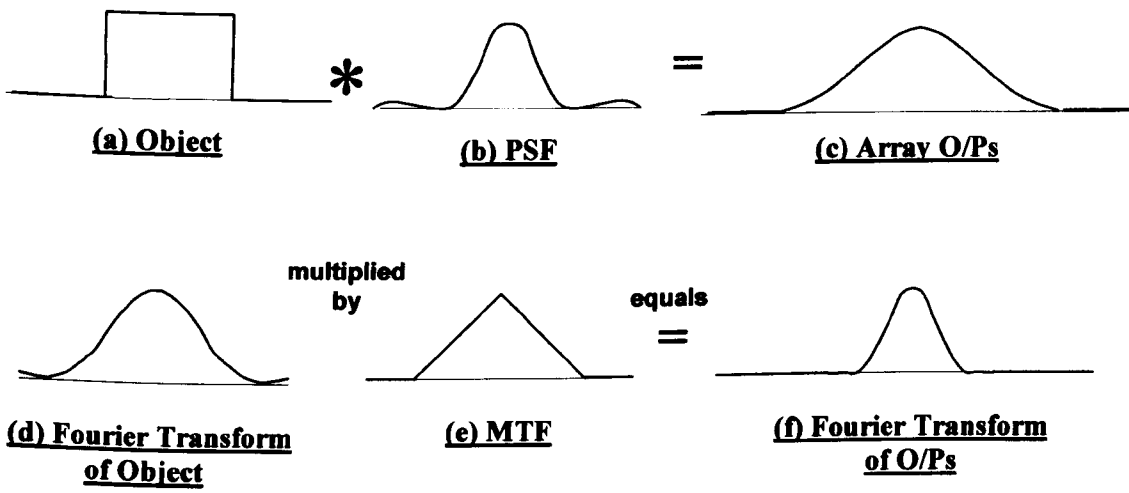

FIG.13.9 DECONVOLUTION OF ARRAY OUTPUTS

The acoustic 'image' is formed by simultaneously beaming the array in multiple directions as in Fig.13.10 (a). Consider direction 4, which is directed to the left of the object. Assuming that the PSF has around the same width of the object, it can be seen that the beam 4 will receive a small amount of the reflected sound from the object's left side. Likewise, beam 8 will receive some reflection off the right of the object.

Although the centres of beams 5 and 7 pass through the object, the object does not fall within the full width of the beam, hence the reduced amplitudes in these directions. In direction 6, the beam is completely within the object, so that the amplitude is a maximum. The envelope of the amplitudes in Fig.13.10 (b) represents a very blurred image of the object. If this function is deconvolved with the known PSF, the outputs of Fig.13.10(c) can be obtained.

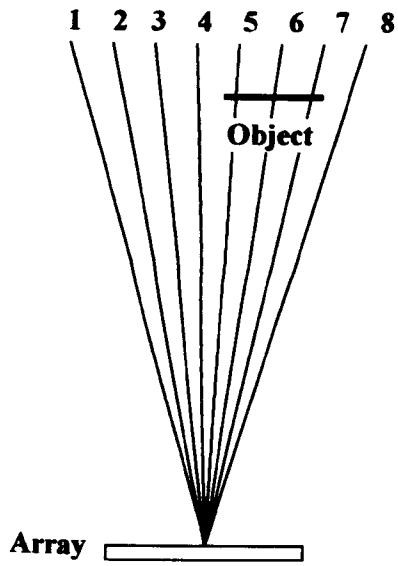

(a) Direction Quantization

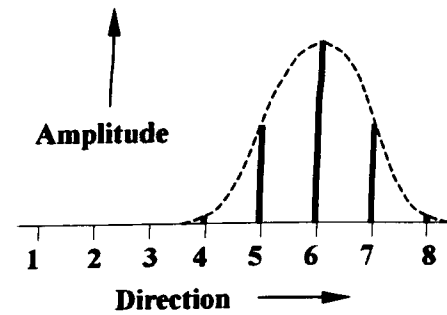

(b) Direction Outputs from Array

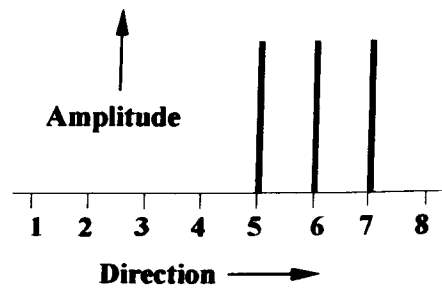

(c) Deconvolved Outputs

FIG.13.10 DECONVOLUTION OF QUANTIZED DIRECTION OUTPUTS

13.3) Possible Implementation

The complete system for using an array to determine head position is now considered. Firstly, a possible method of steering and deconvolution using Fourier transforms is outlined, followed by a description of how an actual head tracker could be implemented.

13.3.1) Functional Operation of a One Dimensional Array Processor

For ease of explanation, an eight-element only array is shown in Fig 13.11 – in practice this would need to be around a hundred elements. It should be noted that Fig.13.11 is only a functional diagram and would obviously not be a practical arrangement for processing the output of possibly a hundred or more element array. If there were one hundred discrete beam directions, there would be ten thousand parallel inputs at D-D. If the amplitude and phase are measured directly at the array outputs, the information can be converted to a more manageable form for serial processing.

In Fig.13.11 is a schematic diagram; and the waveforms produced when an object is positioned as in Fig.13.10 (a) are shown on Fig.13.12. The first four figures, which are of the amplitude and spatial information, are shown in polar form as this enables the operation of the delays to be seen clearly. Likewise the other outputs are better explained by showing their amplitudes only.

The outputs A-A exhibit an s-shape as at this point they have not been subjected to the focusing delays. The spatial positions of the complex outputs of the array on the figures are immaterial and they have been drawn nose-to-tail to indicate what the resultant will be. The focusing delays are time-dependent in order to match the focal length to the distance. The $f(t)$ generator is used to increase the focal length linearly with time. If the nearest and furthest head distances are one and five metres, the focal length will be one metre, six milliseconds after the transmission of the sound pulse, and five metres after 30.2 milliseconds.

In this case, the same delays are used for all beam directions. If the viewing field of the television is wide, say 80°, then correction might have to be made for off-axis

aberrations. Only a certain number of fixed delays would be needed, each one serving many adjacent summation processors. There certainly would not need to be separate off-axis correction for each processor. The optical analogue of these delays is the Schmidt corrector that is used in wide-angle telescopes to correct for spherical aberration.

Focusing will line up the vectors as in B-B. When the object is not in the focal plane that exists at a given time, the vectors will have an s-shape. However if, the focal length varies in time to match the distance of the object, the vectors can be considered lined-up for all practical purposes.

Eight sets of outputs are connected through the line D-D. For simplicity, the figure only shows the first and eighth connections, steering delays and summation processors. The object is assumed to be centred on the axis of direction 6 as in Fig.13.10 (a), therefore the vectors from the output of delay 6 will line up as in figure D-D. As the output becomes further away from 6, the vectors progress towards a more circular form and give smaller resultants.

The summation outputs of F-F correspond to the shape of the object convolved with the PSF. This is the polar form of Fig.13.10 (b), where magnitudes only are shown. By the very nature of the capture of the information by an array, the inputs at F-F are quantized. In any event, a Fourier transform can realistically only be evaluated in discrete form. A discrete Fourier transform (DFT) processes input information that is in the form of a series of impulse functions, and gives an output in the same form [BRIG74]. The nature of the input information is particularly suitable for DFT processing for two reasons. Firstly: it can be assumed that the objects, heads, fall entirely within a given width in the viewing field so that the image is never truncated by the edge of the inputs F-F. Secondly, the nature of the shape of the head in relation the effective sampling intervals produced by direction quantization is unlikely to cause any aliasing effects.

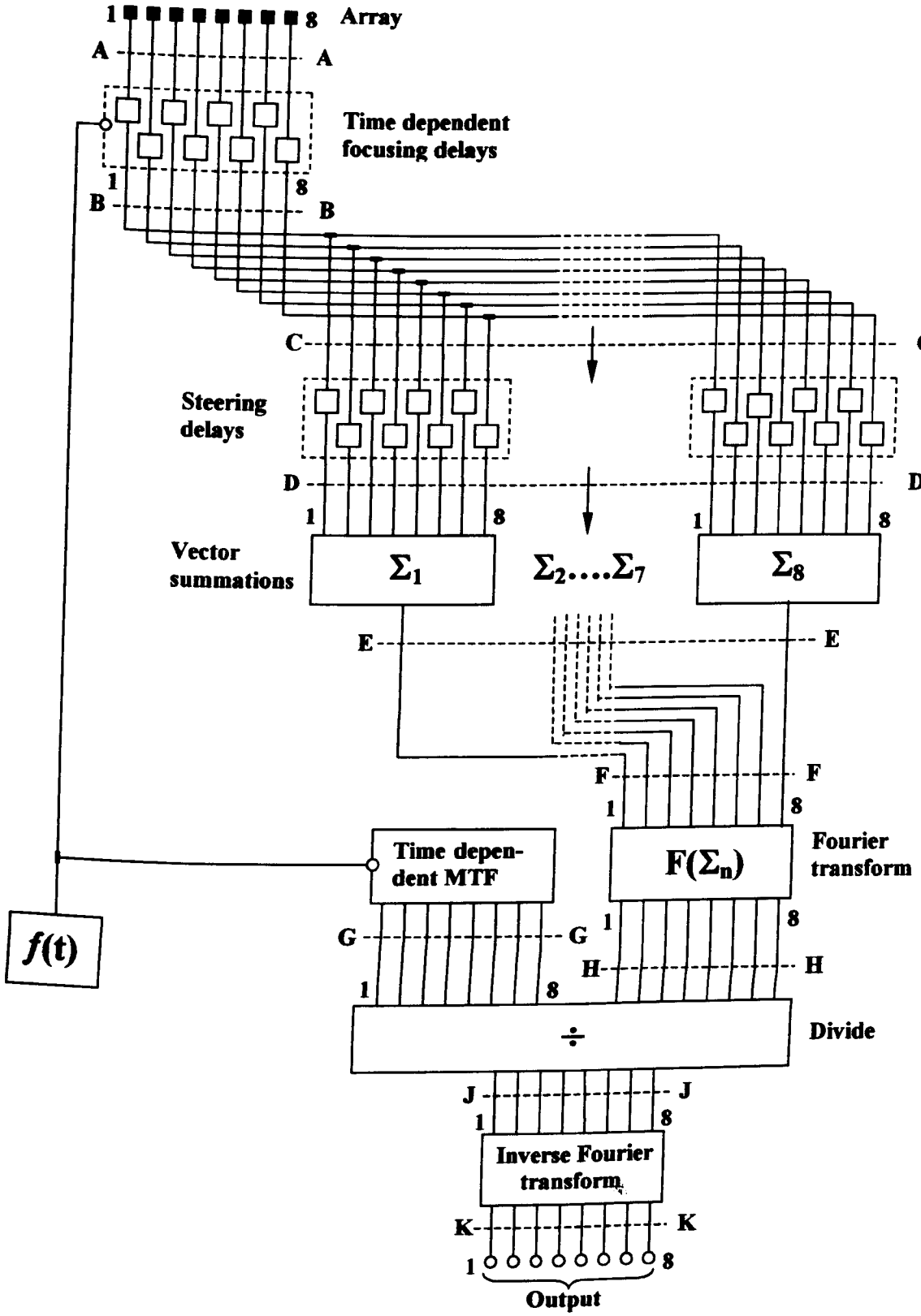

FIG.13.11 SCHEMATIC OF COMPLETE ARRAY PROCESSOR

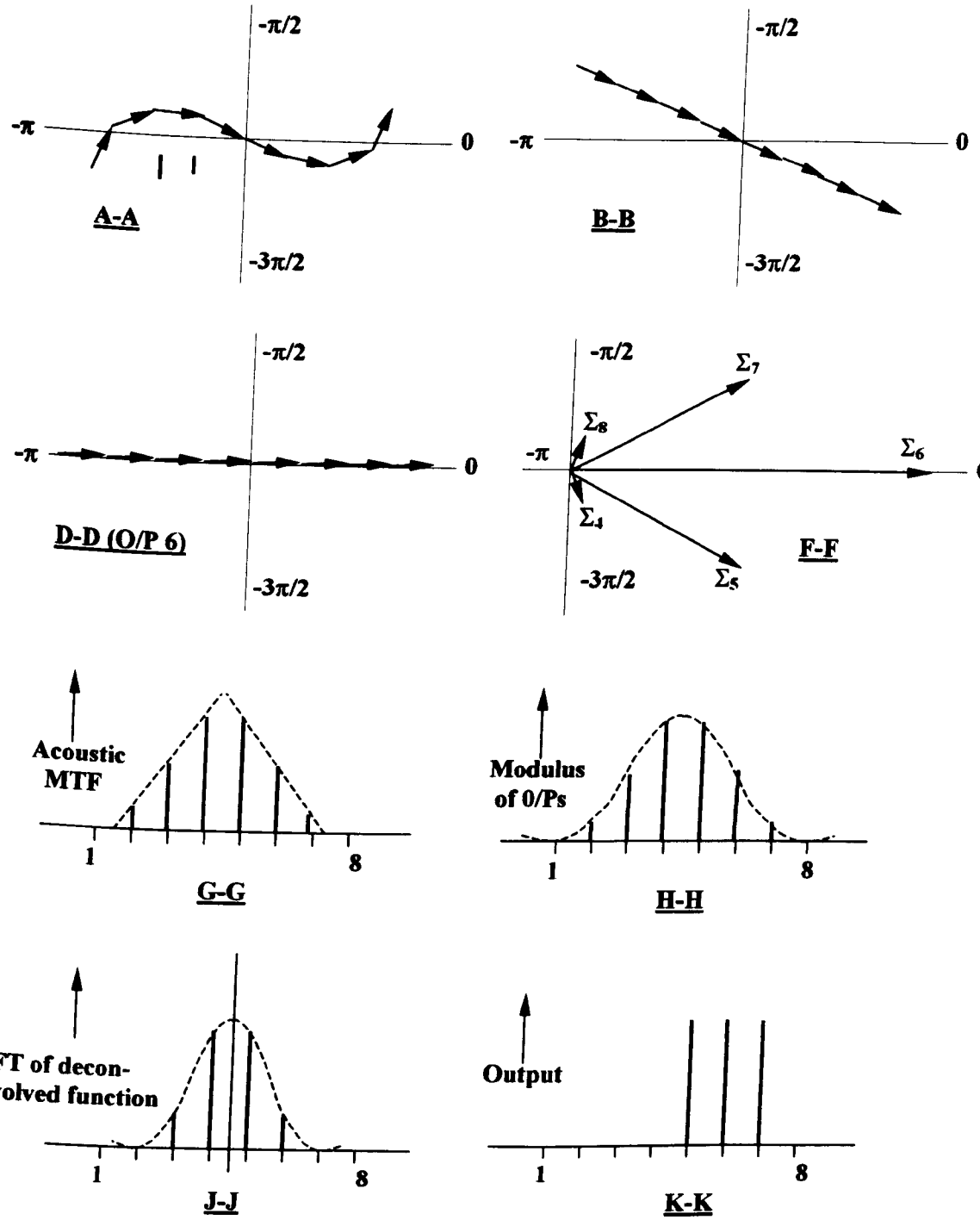

FIG.13.12 WAVEFORMS ON SCHEMATIC DIAGRAM

Many families of calculated curves for eighty and one hundred element arrays show that PSFs always have around a hundred milliimetre width, regardless of distance, whenever the array pitch is the same as the wavelength. With the distance across the field being discretized in angular, as opposed distance, intervals, the PSF spans a wider angle at closer ranges. Therefore the triangular envelope of the MTF in figure G-G increases in width with increasing distance, and hence, also time. This width is controlled by the output of $f(t)$. Whereas the inputs at F-F are in the spatial domain, those at G-G and H-H are in the spatial frequency domain where the mid-point between outputs 4 and 5 represents zero spatial frequency.

H-H is the DFT of the function F-F. This process could possibly be speeded-up by application if the fast Fourier transform (FFT) [BRIG67]. Whereas the envelope of the amplitude function is centred on output 6 in correspondence with the head position in the viewing field, however, the envelope of its Fourier transform amplitudes is central. The shape of the head determines the shape of the envelope. Information on the head's lateral position is held by the phase of the outputs - this is a consequence of the shift theorem [BRAC85b].

The next step is to divide the transform by the MTF to give the function J-J which is the Fourier transform of the object. This involves eight separate complex divisions, that is (H-H)1 by (G-G)1, et cetera.

The final stage is to perform an inverse transform on J-J to give the deconvolved object function K-K. Again this will be an FFT as is also carried out by the $F(\Sigma_n)$ processor.

Although an actual array would have around a hundred elements, and a direction quantization of one centimetre maximum, it would be computationally simpler to perform the deconvolution without resorting to operating in the Fourier transform domain. The head and PSF will be around eighteen-point and twelve-point functions respectively, and the spatial resolution is likely to be improved by a factor of around five. The method outlined is unlikely to be used in practice as it is probably not the easiest way of performing deconvolution, if indeed deconvolution is actually

necessary in the determination of eye-centre position. However this analysis may prove to be useful for any possible future design work.

13.3.2) Two-dimensional Array

On its own, a single linear array would not be of any use as it would integrate the reflections in the vertical direction. Some form of vertical scanning, or at least fixed beam forming, is required in order to discriminate between heads and other objects, for instance the bodies to which the heads are attached, or furniture.

If the viewing area was scanned with the same resolution in the vertical direction, a two-dimensional array with the same number of rows as columns would be required , i.e. around 100 x 100. An array with ten thousand elements is clearly not practicable in terms of either expense or size.

Fortunately, the same resolution is not required - all that is needed is to determine the lateral positions of the heads. If a display with a limited viewing area is proposed, such as would be the case for a prototype, then it would be safe to assume that all the viewers' heads lie close to one vertical plane. If this is the case then vertical scanning can be dispensed with and only a beam with a limited height will need to be formed.

This could be created by using a two-dimensional array, but with a much smaller number of rows than columns. Consider an array with just ten rows. This is sufficiently smaller than the number of columns for the vertical beam forming to be analysed separately, i.e. for all practical purposes the array length can be considered to be infinite. This saves having to calculate the response of a two-dimensional array, which would be a tedious exercise for the current work, which is merely an assessment of the viability of acoustic head tracking.

The calculation is also simplified by the fact that the wavefront is approximately flat in the vertical direction. For example, for an object two metres away, a ten-row array and a wavelength of four millimetres, the path length is only 0.081 millimetres greater at the outer array elements than the central elements (a phase lag of 0.13 radians).

On the other hand, ten rows is sufficiently large to make another assumption – that the shape of the response will be substantially the same as for an array with a large number of rows. On this basis the response will be $sinc^2$, with the first minima being from reflections $\lambda D / A$ from the axis where λ is the wavelength, D the distance of the object and A the height of the array. As the height of an array with N rows is $\lambda(N-1)$, the distance M of first minima from the axis is given more simply by $D/(N-1)$. This approximate relationship shows that the beam width is independent of wavelength, proportional to distance and more or less inversely proportional to the number of array rows.

With a ten-row array, the distance *between* the first minima is 444 millimetres. This is rather large compared to the average head height of 220 millimetres and would probably include too much of the body, possibly causing excessive error in the head position accuracy. Fifteen rows would give 286 millimetres between the first two minima. Fig.13.13, where the sensitivity curve (the PSF) is drawn to the same scale as the simplified head, indicates that this is likely to be sufficiently narrow.

The array forms a beam by virtue of the elements of each column receiving sound in phase – no delays are required. If the heads are assumed to lie in the region, say from one metre to three metres from the screen, the elements could have a curvature in the vertical direction centred at the geometrical mean, i.e. 1.7 metres. This would optimise the vertical resolution with very little, if any, additional construction cost. Scanning also would be possible, but the processing would be rather complicated, especially if vertical deconvolution is also carried out. However, if it *were* found to be practicable, then the array would be only 56 x 396 millimetres for a 15 x 100 array with a wavelength of four millimetres. This could easily be located between the display screen and the outer edge of the front panel.

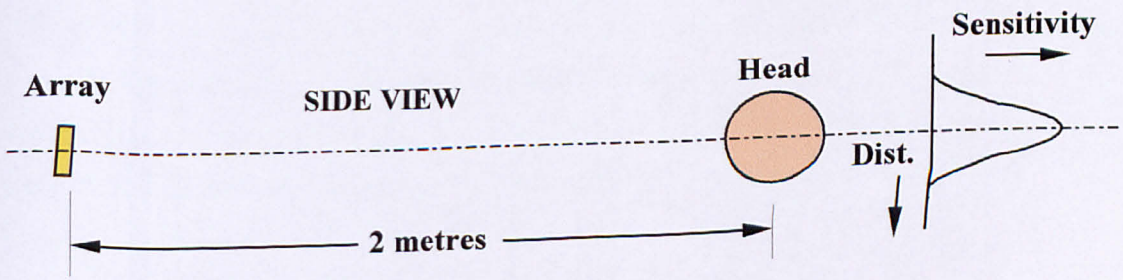

FIG.13.3 SCALE DIAGRAM OF ARRAY, HEAD AND PF

13.3.3) Simplified Head Tracker

If the viewing field is not very large and viewers' heads are assumed to be situated in approximately the same plane, then strategies in addition the absence of vertical scanning can be used in order to simplify the head tracker.

Horizontal focusing could be achieved by curving the array as opposed to applying delays to the array outputs. As in the previous section, the centre of curvature could be set at the geometrical mean between the nearest and furthest head distances.

With no vertical scanning, there is no reason in principle why the array needs to be two dimensional. One method of beam forming would be to simply place a horizontal slit aperture in front of a linear array. The effect of diffraction could be predicted rigorously by laborious calculation or with the use of a ripple tank. Unfortunately, the Cornu spiral cannot be used as this is only applicable where a slit moves in relation to two fixed conjugate points – movement of a fixed length along the curve corresponds to movement of the slit. When the response from reflections in different directions is required, these conjugate points effectively move in relation to each other.

As a fixed sound frequency will be used, the equivalent of coherent light techniques could possibly be applied. Coherent light can be focused using a Fresnel zone plate [HOUS38c]. This is a screen where alternate half-period zones are either opaque or are subjected to a phase change of π, a half-period zone being a region whose boundaries have a phase difference of π. Zone plates are usually shown in text books as concentric circles that are able to focus a spherical wavefront to a point; however, it is also possible for a series of strips to focus a cylindrical wavefront to a line.

The easiest implementation of a zone plate will be to use the inner half-period zone only. In this case there is a π phase difference between the sound from the top and bottom edges of the aperture and the direct path. If the aperture height is increased, more of the second half-period zone is included and the point will be reached when the array lies at a minima.

The analysis of the single slit can be simplified by making certain assumptions. These yield results that are approximate, but which are sufficiently accurate in this application. It should be noted that although the sound source was considered to be a notional vertical line source in Section **13.2)**, in practice the sound would originate from a single transducer so that the wavefront will be spherical.

Consider sound with a wavelength of four millimetres, and the object two metres from the aperture. If the aperture is fifteen wavelengths high, the distance between the first minima will be 267 millimetres (applying Equation (13.2) in Section **13.3.4**) and the phase lag at the aperture edges is 0.35 radians. If this lag is neglected, then the wavefront can be considered as effectively plane as in Fig.13.14 (b), so that the $sinc^2$ distribution applies.

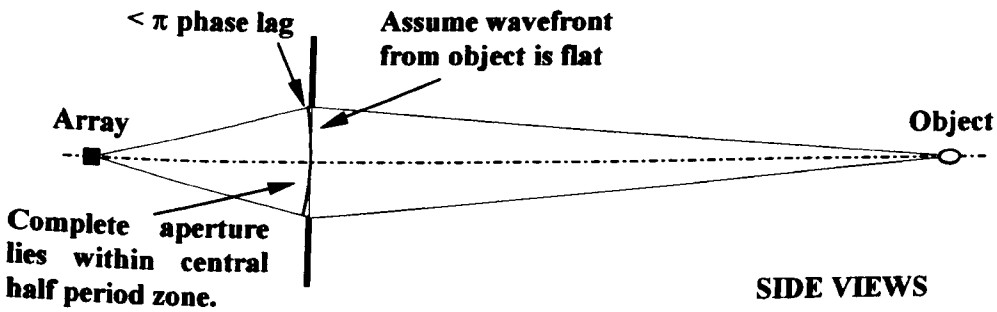

(a) Object on Axis

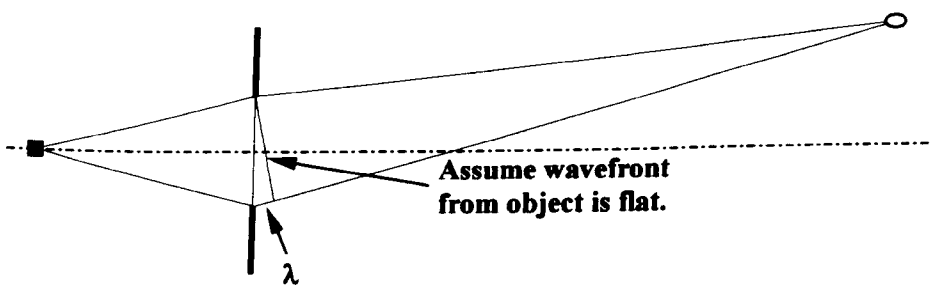

(b) Object at First Minima

FIG.13.14 SIMPLIFIED CONSIDERATIONOF APERTURE BEAM FORMATION

The wavefront behind the aperture shown in Fig.13.14 can now be treated separately. If an acoustic head tracker was used for the prototypes currently under construction, the maximum distance allowed by the housing between the array and the aperture would be three hundred millimetres. A fifteen-wavelength aperture will be sixty millimetres high. The path length difference between the axial distance and to the aperture edge, this corresponds to a phase difference of 2.35 radians. This puts the complete height of the aperture within the central half-period zone so that constructive interference occurs at the array. When the sound is off-axis, this phase difference will be even less.

The worst-case condition occurs at the minimum head distance. If this assumed to be one metre, then the phase lag given by the difference between the axial distance and the path via the aperture edge is 3.06 radians. This means that even under the worst-case conditions the aperture still lies completely within the central half-period zone.

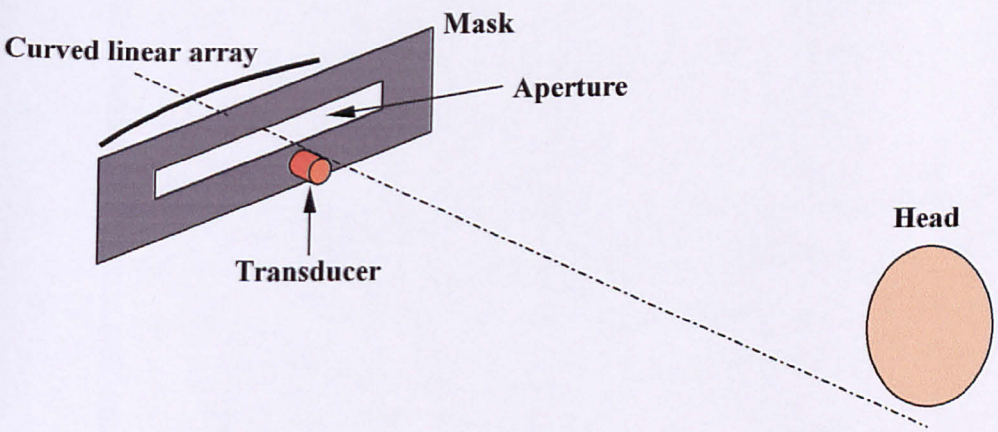

FIG.13.15 SIMPLIFIED ACOUSTIC HEAD TRACKER

One strategy that could possibly be employed to reduce the aperture-to-array distance would be to position a phase retarding strip, i.e. one that delays the sound, along the centre of the aperture. If material suitable for such a strip is available then it begs the

question whether some form of acoustic lens could be used. As it is not envisaged that acoustic head tracking will be used for the prototype, it is beyond the scope of this research to investigate this possibility.

Fig.13.15 shows the arrangement of the simplified acoustic head tracker that could be used with a prototype that served only two or three viewers who had more restricted freedom of movement than in a 3D TV display environment.

The processing can be simplified if deconvolution is not carried out. If the eye-centre position is assumed to be in the centre of the 'silhouette' of the head as detected by the array, then the centre of the convolution of this with a symmetrical PSF will give as good an indication of the eye-centre as the silhouette itself. Deconvolution is useful when the more detailed profile of the head obtained from the higher spatial resolution is processed to obtain a more precise determination of position. The assumption that the eye-centre coincides with the silhouette or 'shadow' position is used in the infra-red tracking method described in Chapter 12. This approach is also used in the lenticular 3D display of ATR in Japan where a retro-reflector is attached to the viewer's chin [OMUR98].

The processor required in this case will be considerably simpler than that given in Fig.13.11. The focusing delays will not be necessary as the focus will be fixed by the curvature of the array. As deconvolution is not being performed, the output will be at E-E. The operations of producing a Fourier transform, division and inverse Fourier transform will not be required in this case.

13.3.4) Aperture Equations

Although in the previous section the phase for the particular conditions was determined for a given wavelength, first minima position, aperture width, et cetera, it would be useful to provide some general equations in order to facilitate any possible future design work.

The greater the amount of the two second half-period zones the aperture includes, the smaller will be the response at the array. Therefore it is preferable to keep the aperture

height within the central half-period zone. As increasing the aperture height decreases the height of the PSF as described in Section **13.3.2)**, the optimum aperture height is that of the central half-period zone.

For the edge of the central half-period zone boundaries to coincide with aperture edges, the path length difference between the axial distance from the array to the aperture and the distance from the array to the aperture edge will need to be half a wavelength as in Fig.13.16 (a).

In this figure it can be seen that

$$(E + \lambda / 2)^2 = E^2 + (\lambda / 2)^2$$

Taking the square root of both sides of this equation yields

$$E + \lambda / 2 = E\,(1 + (\lambda / 2E)^2)^{1/2}$$

As $(n\lambda / 2E) << 1$ the binomial approximation can be applied, therefore

$$E + \lambda / 2 = E\,(1 + \tfrac{1}{2}(\lambda / 2E)^2)$$

Solving for E

$$E = \lambda / 4 \quad \text{.....(13.1)}$$

If the distance of the first minima of the PSF from the axis M is given by –

$$M = D / n \quad \text{.....(13.2)}$$

Rearranging (13.2)

$$n = D / M \quad \text{.....(13.3)}$$

Note that in this case, n is the height of the aperture expressed in wavelengths, as opposed to the number of array elements N in section 13.3.2).

Substituting (13.3) into (13.1)

$$E = \lambda / 4 (D / M)^2 \quad .....(13.4)$$

Therefore in order to ensure that the complete height of the aperture lies within the central half-period zone

$$E > \lambda / 4 (D / M)^2$$

This expression yields the minimum preferable value for the array to aperture distance. If E is smaller, the sensitivity will be reduced, and if E is greater the sensitivity will be improved, but the array to aperture distance may become impracticably large. What this relationship does is to provide a design guideline. D is the *maximum* head distance.

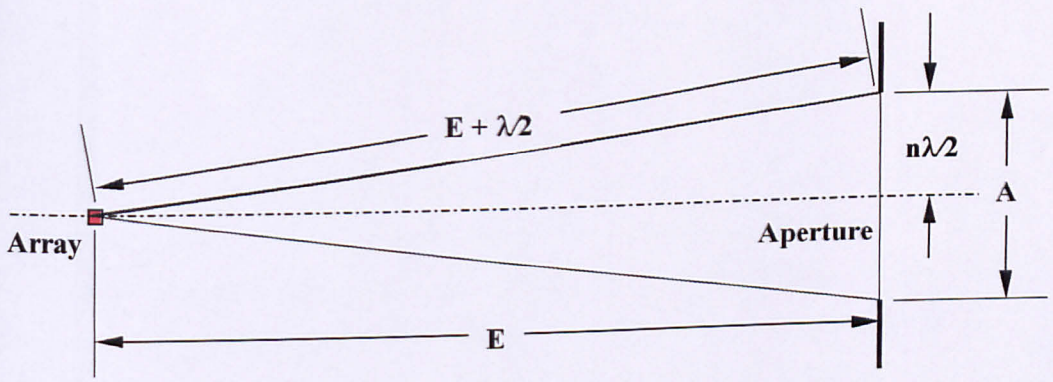

(a) Aperture Edges at Inner Half Period Zone Boundaries

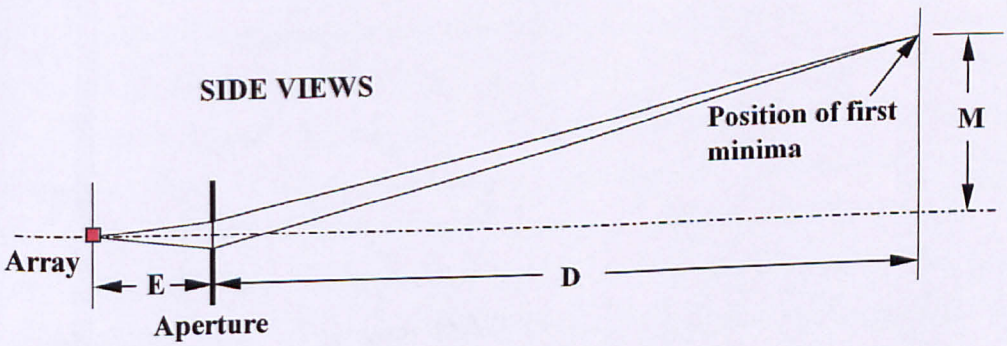

(b) First Minima

FIG.13.16 INNER HALF-PERIOD ZONE AND FIRST MINIMA

It is useful to summarise the equations

$$A = n\lambda \qquad \text{.....(13.4)}$$

$$M = D/n \qquad \text{.....(13.5)}$$

$$E = \lambda / 4(D/M)^2 \qquad \text{.....(13.4)}$$

Where

λ = wavelength

M = distance of first PSF minima from axis

D = maximum head distance

A = aperture height

n = aperture height expressed in wavelengths

E = array to aperture distance

13.4) Summary

In section 12.3.1), the information has been treated as a succession of one-dimensional functions where deconvolution is only carried out with respect to values along a line parallel to the array. Provided the z-resolution is sufficiently high, two-dimensional deconvolution could be worthwhile. However, a wavelength of four millimetres might be rather large in relation to the size of facial features to provide sufficient resolution.

If the z-resolution is sufficiently high, there are techniques that can be used to sharpen up the image. The B-scan mode, where 'slices' of the object are produced by an array of transducers, is used widely in medical imaging. In general, any ultrasonic images produced in this mode suffer from three causes of degradation. These are convolution blurring caused by finite aperture size (the array width in this case), out-of-focus blurring and noise. These problems are approached by the use of a Wiener filter in a method adapted from 3D optical microscopy [SAPI98]. If the array focal length is variable, out-of-focus blurring does not occur and noise is an issue that is beyond the scope of the current work.

Medical imaging has the additional problem of scattering in tissue, this has been addressed by the application of a deconvolution algorithm, which incorporates a Kalman filter and was previously used in seismic work [JENS98]. This operates on one-dimensional data and is capable of producing an increase in resolution of a factor of 2.4 with negligible increase in the signal to noise ratio. This technique would not be necessary for head tracking as the target is situated in air, which is a homogenous medium.

Increases by factors of 2.5 to 5.2 in lateral resolution, and 1.5 to 1.9 in radial resolution, of B-scan images have been reported [ABEY00] by using separate one-dimensional radial and lateral distortion kernels. As the tissue response is unknown, its contribution to the overall deconvolution function can be isolated by varying the transducer characteristics; such as frequency, aperture shape or size, or spatial arrangement [REID00]. Again, these methods make allowances for the tissue, and the ultrasonic system response. This would not be necessary for head tracking.

Most benefit would be obtained from increasing the resolution if the position of the nose could be determined. This is the natural position of the boundary between the left and right exit pupils. As the nose is in the order of two centimetres across, this could never be resolved with a PSF around ten centimetres wide.

In the simplified head tracker, where the eye-centre position is assumed to be mid-way across the 'silhouette' of the head, errors could arise certain under circumstances but much simpler processing and greatly reduced z-resolution requirement might justify this, at least for a prototype.

This consideration of the possibility of acoustic head tracking is really only a feasibility study into whether or not, in theory, this approach is viable. No attempt has been made to investigate the practical issues such as the absorption of sound in air, or suitable materials for the transducers. However, the conclusion is that acoustic methods *could* be used principle if other methods such as machine vision or infrared reflection prove too difficult. Well-established optical techniques have been applied in the analysis as these are also applicable to sound.

CHAPTER 14
CONCLUSIONS

14.1) Preface

The research carried out so far has provided a valuable starting point for ongoing work whose ultimate goal is the production of a 3D display that will used in the first commercially feasible 3D television broadcasting system. The surveys of other autostereoscopic methods carried out in Chapters 2 and 3 indicate that at the present time, at least amongst work that is published, there is no other 3D display being developed that is suitable for this purpose.

Although holographic wavefront reconstruction of the image could *possibly* provide a solution in the long term, it is unlikely to be used for the next generation of television display that will probably be on the market within the next ten years or so. The major problem with this approach is that, even when vertical motion parallax is dispensed with, large amounts of information still have to be displayed This is being addressed by the QinetiQ display [STAN00], but it seems unlikely it could be viable within the near future. In any event, the problems of image-capture considered in Section **8.3)**, and the reproduction of naturally lit scenes, still have to be overcome.

Volumetric displays suffer from image transparency, and multi-view displays have a restricted depth of viewing field that becomes smaller with increasing screen width. Head tracking appears to provide the solution to providing a television display in the foreseeable future as the minimum amount of information, that is two images only, needs to be displayed. This places the least demands on the display, and also enables image capture with a simple camera-pair that need not occupy a large width.

The disadvantages of a simple two-image system are the lack of motion parallax, and the difference between the accommodation and convergence of the eyes. This can cause fatigue and eyestrain, but it appears that insufficient research has been carried out into the *prolonged* viewing of 3D that would occur with 3D television. It is possible some researchers have overstated this problem, as there may be strategies, for example the reduction of disparity, that can overcome this.

An interesting example of the effect of reduced disparity was seen by the author at Philips Research Laboratories in Eindhoven in March 2002. A 3D image, with a maximum disparity of only a few pixels, was presented on a polarized glasses type 3D display. This disparity is sufficiently small for the two views to be observed without the use of the glasses with no noticeable blurring. However, when the screen was viewed with the glasses, a 3D image was seen. The 3D effect had a slightly unnatural appearance, but did give a striking example of the stereo effect of disparities that are possibly sufficiently small to cause no viewing problems.

On balance, it appears that any problems associated with a two-image display method are far outweighed by the advantages. The only way the same image-pair can be presented to one or more viewers, who do not have fixed viewing positions, is to use head position tracking to steer the regions where these images are seen (the exit pupils) to the positions occupied by the eyes..

In previous research carried out by the author, the use of projection to produce these exit pupils was investigated [SURM97]. Although, at first sight, projection appears to be a suitable candidate to perform this function, unfortunately, this was found not to be the case. However, the cost of LCDs has fallen dramatically in recent years, and their use in a 3D television display has now become a viable option.

Given the points referred to in this section, it does appear that two-image head tracking display, using a direct-view LCD with a novel backlighting assembly to steer the positions where the images are seen, is likely to be the optimum solution for 3D television.

14.2) Current State of Prototypes

The 12" / 10" prototype is currently still under construction. Originally, the display was built as a 12" version, but unfortunately, the LCD was damaged whilst being converted to operate in the 'projection' mode, i.e. where light from an external source can pass through its complete area without obstruction. A backlightless 10" LCD is available for use in a high brightness display and the housing was modified in order to accommodate this smaller panel and also to magnify the image. The construction of

this version is not finished as a parallax barrier image multiplexer has not yet been made. The 5.6" version has also not been completed for the same reason.

The ATTEST project will provide considerable funding for De Montfort University's 3D television display work. Although the University's role on the project is to produce two multiple-viewer prototypes, a single-viewer 21" display will also be built. This will operate on the same principle as the 5.6" and 10" displays described in Chapters 9 and 10, and the purpose of this is to quickly provide a display that can be used for evaluation and demonstration purposes. Due to this, the work on the smaller prototypes might be discontinued.

The LCD used for this display is an NEC 21.3" panel with UXGA resolution (1600 x 1200) pixels. This will enable two 576-line images to be displayed on alternate pixel rows with the loss of only 48 lines. The row and column drivers are located within the aluminium frame that houses the panel, therefore making the construction of the display more suited to passing light from an external source through its complete area. The remainder of the drive electronics can be easily folded out of the light path. The only connections between the row and column drivers, and the remainder of the drive electronics is through three flexible strip cables that have a total of around forty connections.

The vertical diffuser is a holographic Light Shaping Diffuser (LSD) that has an elliptical output 40° high by 0.2° wide. The sheet is 0.5 millimetres thick and is mounted to the LCD front substrate by sealer around its edge. As the front surface of the LCD has a diffusing antireflection coating, the gap between the substrate and the flat face of the diffuser is filled with glycerine.

In the first version of the display, image multiplexing will utilise a mask a mask produced on five-millimetre glass. A company in Finland, Terapixel, is currently making a mask to our specification. As the barrier material is chrome, reflections from its surface might be unacceptably high. In this case, the mask will be used in the fabrication of another mask with a more suitable opaque layer.

The exit pupils are produced with a Fresnel lens that has a focal length of 500 millimetres. Having the illumination sources 667 millimetres behind the screen produces the optimum viewing distance of two metres. Construction of the display is progressing well with the LCD, driving circuitry, vertical diffuser and Fresnel lens mounted in a lightweight aluminium frame. The multiplexing barrier and illumination sources have yet to be mounted to the frame.

Folding mirrors will not be used initially as these are not necessary for evaluating the display performance. However, as it is planned to loan one of these displays to The Technical University of Eindhoven (TU/e) for human factors experiments, folding will probably be used on this model in order to keep the size down. The complete screen, i.e. the multiplexing screen, the LCD, the diffuser, and the Fresnel lens are mounted in a sub-assembly that is attached to the frame by four easily removed set screws. It will therefore be relatively simple to convert the optics to the folded type.

The illumination sources will probably consist of a pair of white LED arrays. However, if the parallax barrier causes too much light attenuation, halogen lamps will be used.

The 48-element infrared camera, that uses discrete components, will continue to be used as a demonstrator of the principle of using retroreflection in determining the effective 'shadow' of the target. The unit still contains the electronics described in Section **12.4.2),** but the majority of this is now redundant.

The camera using a 128-element array on a single chip is still under development, and will be used for tracking on the single viewer 21" prototype. As this incorporates a single linear array, it effectively captures a horizontal 'slice' of the target head. The viewer's head position is sufficiently restricted for this to be adequate for this prototype.

14.3) ATTEST

Describing the ATTEST project puts the research carried out to date into context more clearly. ATTEST is a two-year project that started on 1st March 2002. It is part of the Information Society Technologies programme sponsored by the European

Commission and comprises a consortium of eight partners whose goal is to develop an entire 3D video chain, from content creation through to the display.

The content will be provided in two ways. The first method is to use a camera that can determine range in addition to picture content. This is based on the Zcam^{TM} that is used for 'depth keying', that is segmenting objects in the foreground of the scene from the background by determining their distance. The existing camera is being modified to make it suitable for the resolution and accuracy demands of 3D television. This operates by measuring the time-of -flight of infrared light from a source located close to the camera lens. The other approach is to develop algorithms that synthesise 3D images from existing 2D content. Investigation into performing this function at the receiver, and the broadcast end, is being carried out.

The transmitted signal is encoded using a base layer that contains the standard 2D digital signal, and enhancement layers that enable the addition of 3D information at various levels to be encoded, for instance for a single user, or for multiple users. This scheme enables the coding to be backwards compatible so that the signal can be used for existing 2D receivers.

Two displays are under development, these are the single user version of Heinrich Hertz Institut (HHI) mentioned in Section **3.4.2)** [HHI02], and the multiple viewer version to be built at De Montfort University (DMU). The multiple viewer display will present 3D to up to four viewers who may be situated between one and three metres from the screen, and up to 30° from the axis.

One useful outcome of the collaborative effort is that the lenticular screen used by HHI can also be used as a multiplexing screen in the DMU display. The screen is located in front used for exit pupil formation in the HHI display, and behind the LCD for image multiplexing in the DMU display. Fortunately, the geometry is similar in each case.

A Flemish broadcaster is producing material in 3D, and human factors aspects of coding artefacts and 3D displays is being carried out by TU/e. Philips are leading the project and are also working on the rendering for the displays.

14.4) Relevance of Research Carried out to Date

Much of the research carried out for this thesis is now proving extremely useful in the ATTEST project. This section considers the usefulness of each specific area of work in relation to both the single-viewer 21" prototype under construction, and to the proposed multiple viewer version that will be built.

a) **Folding:** The simple expedient of folding a paper template, as described in Section **4.2)**, provides a very quick method of determining the optimum position of the vertically folding mirrors in both the single and the multiple-viewer versions. The folding efficacy is less of an issue in prototypes where the size of the housing in not a critical issue, but will be important in a production model where the housing needs to be as small as possible.

b) **Image Multiplexing:** The equations derived in Chapter 5 were used calculate the dimensions of the barrier ordered from Terapixel. A lenticular screen has also been ordered to perform the same function as it enables almost 100% light throughput. However, the barrier is an attractive option as it can be inexpensive to manufacture, and, with careful design, can enable a light throughput up to 50% of the amount passing without the barrier.

c) **LCD Scattering:** Scattering by the LCD is a major factor contributing to crosstalk. The scattering patterns obtained in Chapter 6 indicate that this scattering is caused by diffraction at the RGB sub-pixels. The scattering characteristics of the LCDs used in the prototypes will be measured in order to assess its importance in relation to all the other factors conspiring to cause crosstalk.

d) **Vertical Diffuser:** In the single-viewer prototype, viewer movement is restricted due to spherical aberration in the Fresnel lens forming the exit pupils. For this reason, the results in Chapter 7 indicate that the amount of horizontal deviation will be negligible. The situation is different in the multiple-viewer version with its much larger viewing field. The curvature of the deviation characteristic of the various diffusers examined, namely; lenticular sheet, Light Shaping Diffuser and holographic, cause an increase in the boundary zone width between the left and right exit pupils. This can be an appreciable proportion of the interocular distance

when the viewer is far off-axis, or close to the maximum viewing distance, and can contribute to crosstalk.

e) **Image Space Geometry:** This has no bearing on the actual design of the display optics. However, as the distortions are an inevitable consequence of any two-image 3D display that does not have motion parallax, it is helpful to know the magnitude of these distortions when human factors aspects of the displays are examined.

f) **Screen Intensity Variation:** The results obtained in Section **8.4)** do not apply to the single-viewer displays as the exit pupils are formed by a Fresnel lens. Investigation into the steering optics required by a multiple-viewer display indicates that a discontinuous illumination source might be required. If this is the case, then the acceptable levels of intensity variation needs to be known.

g) **Head Tracking Accuracy Requirements:** It is unlikely that head tracking accuracy will be of particular importance in the single-viewer displays. In the multiple viewer display, the viewer may be as much as three metres from the screen and any small angular inaccuracy in the steering optics output could give rise to appreciable errors at this distance. Also, in the single-viewer version, the magnification between the illumination source and the viewing field is relatively small (3 x in the case of the 21" display), so that any increment in the position of the illumination source is not magnified unduly in the viewing field. In the multiple-viewer display, it is possible this magnification could be much greater, thereby giving large positional increments in the viewing field.

h) **Retroreflecting Infrared Head Tracker:** As previously mentioned, the existing 128-element infrared tracker will be used in the 21" single-viewer version. The multiple viewer display will also require distance and vertical position of the viewers' heads to be determined. This will necessitate the use of two two-dimensional infrared arrays to capture the reflection images. This system will be developed from the existing one-dimensional tracker.

i) **Acoustic Head Tracking:** This method of tracking was investigated several years ago. As ultrasonic time-of-flight distance measurement is simple, determining lateral position ultrasonically also appeared to be an interesting possibility. The method does not require the wearing of any attachment to the head, or a rerroreflector mounted behind the head. Also, the resolution could probably be made sufficiently high for head tracking. However, the author considered the method would require too much effort put into its development. Consequently, this approach will not be adopted.

14.5) Conclusion

This thesis outlines the world-wide interest and developments in the pursuit of 3D television, and the author is convinced that the optical techniques adopted by De Montfort University are the way forward. The earlier prototypes developed during the research offer no significant advantages over methods of other groups working in this field. However, unlike these, the prototypes have the *potential* to be developed into a multiple viewer version with a large viewing field that will be suitable for television. This work will be undertaken within the ATTEST project.

PAGE
MISSING
IN
ORIGINAL

REFERENCES

ABEYRATNE U.R., Petropulu A.P. and Reid J.M. (2000), "Higher Order Spectra Based Deconvolution of Ultrasound Images", *Biomedical Engineering and Science Institute, Drexel University, Philadelphia, PA19104.*

ARIMOTO A., Ooshima T., Tani T. and Kaneko Y. (1998). "Wide Viewing Area Glassless Stereoscopic Display using Multiple Projectors", *SPIE Proceedings, "Stereoscopic Displays and Applications IX",* Vol.3295, pp186-191.

BARDSLEY T. (1995a). "The Design and Evaluation of an Autostereoscopic Computer Graphics Display", *Thesis submitted to De Montfort University,* pp46-47.

BARDSLEY T. (1995b). "The Design and Evaluation of an Autostereoscopic Computer Graphics Display", *Thesis submitted to De Montfort University,* pp107-125.

BARDSLEY T. (1995c). "The Design and Evaluation of an Autostereoscopic Computer Graphics Display", *Thesis submitted to De Montfort University,* p144.

BENTON S.A., Slowe T.E., Kropp A.B. and Smith S.L. (1999). "Micropolarizer-based multiple-viewer Autostereoscopic Display", *SPIE Proceedings, "Stereoscopic Displays and Applications X",* Vol.3639, pp76-83.

BENTON S.A. (2002). "Autostereoscopic Display System", *United States Patent No. 6,351,280.*

BERKEL C., Parker D.W. and Franklin A.R. (1996). "Multview 3D-LCD", *"SPIE Proceedings, Stereoscopic Displays and Virtual Reality Systems IV",* Vol.2653, pp 32-39.

BERKEL C. and Clarke J.A. (1997). "Characterisation and Optimisation of 3D-LCD Module Design", *SPIE Proceedings, "Stereoscopic Displays and Virtual Reality Systems IV",* Vol.3012, pp179-186.

BERKEL C. (1999). "Image Preparation for 3D-LCD", *SPIE Proceedings, "Stereoscopic Displays and Applications X",* Vol.3639, pp84-91.

BRACEWELL R.N. (1985a). *"The Fourier Transform and its Applications", McGraw-Hill,* pp 411-426.

BRACEWELL R.N. (1985b). *"The Fourier Transform and its Applications", McGraw-Hill,* pp 104-107.

BRIGHAM E.O. and Morrow R.E. (1967). "The Fast Fourier Transform", *IEEE Spectrum,* December 1967, pp 63-70.

BRIGHAM E.O. (1974). *"The Fast Fourier Transform and its Applications", Prentice-Hall,* pp 81-92 & 118-121.

BROWNING J. (1996). "Cyber View - New Stars for the New Media", *Scientific American*, Vol.274 No.7, pp.20-21.

COLLENDER R. (1986). "3-D Television, Movies and Computer Graphics Without Glasses", *IEEE Transactions on Consumer Electronics*, Vol.CE-32, No.1, pp 56-61.

COLLENDER R. (1987). "Moving Autostereoscopy using all Static Components", *IEEE Transactions on Consumer Electronics*, Vol. CE-33 No.2, pp 65-70.

DENISYUK Y., Orlov V.V. and Brui J.B. (1998). "One-dimensional Diffuse Screen for 3-D Image Projection", *SPIE Proceedings*, Vol.3293, pp78-82.

DODGSON N.A., Moore J.R., Lang S.R., Martin G, and Canepa P. (2000). "A 50" Time-multiplexed Autostereoscopic Display", *SPIE Proceedings, "Stereoscopic Displays and Virtual Reality Systems VII"* Vol.3957, pp 177-183.

DOLGOFF G. (1997). "Real-Depth™ Imaging: A New Imaging Technology with Inexpensive Direct-view (no Glasses) Video and other Applications", *SPIE Proceedings, "Stereoscopic Displays and Virtual Reality Systems IV"*, Vol.3012, pp282-288.

EICHENLAUB J. (1993). "Developments in Autostereoscopic Technology at Dimension Technologies Inc.", *SPIE Proceedings, "Stereoscopic Displays and Applications"* Vol.1915, pp177-186.

EICHENLAUB J. (1994). "An Autostereoscopic Display with High Brightness and Power Efficiency", *SPIE Proceedings, "Stereoscopic Displays and Virtual Reality Systems"*, Vol.2177, pp 143-149.

EICHENLAUB J. and Hutchins J. (1995). "Autostereoscopic Projection Displays" *SPIE Proceedings, "Stereoscopic Displays and Virtual Reality Systems II"*, Vol.2409, pp 48-54.

EICHENLAUB J. (1996). "Prototype Magnified and Collimated Autostereoscopic Displays" *SPIE Proceedings, "Steroscopic Displays and Virtual Reality Systems IV"*, Vol.2653, pp 20-31.

EICHENLAUB J. (1997). "A Lightweight, Compact 2D/3D Autostereoscopic LCD Backlight for Games, Monitor and Notebook Applications", *SPIE Proceedings, "Stereoscopic Displays and Virtual Reality Systems IV"*, Vol.3012, pp274-281.

EZRA D., Woodgate G.J., Omar B.A., Holliman N.S., Harrold J. and Shapiro L.S. (1995). "New Autostereoscopic Display System", *SPIE Proceedings, "Stereoscopic Displays and Virtual Reality Systems II"*, Vol.2409, pp 31-40.

FAJANS J. (1992). "Xyzscope – A New Option in 3-D Display Technology", *SPIE Proceedings, "Visual Date Interpretation"*, Vol.1668, pp25-26.

FARIS S.M. (1994). "Novel 3-D Stereoscopic Imaging Technology", *SPIE Proceedings, "Stereoscopic Displays and Virtual Reality Systems"* Vol.2177, pp 180-195.

FARIS S. (2001). "Multi-mode Stereoscopic Imaging System", *United States Patent No.6,195,205 B1.*

FAVALORA G.E., Dorval R.K., Hall D.M., Giovinco M. and Napoli J. (2001). "Volumetric Three-dimensional Display System with Rasterization Hardware", *SPIE Proceedings, "Stereoscopic Displays and Virtual Reality SystemsVIII"* Vol.4297, pp 227-235.

FHM – Staff writer (1998). "Teutonic 3D", FHM, *Emap, Elan Network,* Nov 1998, article in 'Reporter' section.

FINCHAM W.H.A. and Freeman M. (1980a) *"Optics", Butterworths,* p322.

FINCHAM W.H.A. and Freeman M. (1980b) *"Optics", Butterworths,* p 307.

FORSHAW M.R.B. (1978a). "Three Dimensional Television", *Optica Acta,* Vol.25, pp 828-835.

GOVE R.J. (1994). "DMD Display Systems: The Impact of an All-digital Display", *Texas Instruments publication – reprint from: SID 1994 International Symposium, Seminar, Exhibition, San Jose, California,* June 12-17, 1994.

HAMASAKI J. (1995). "Aberration Theories of Lenticular and Related Screens", *International Workshop on Stereoscopic and Three Dimensional Imaging,* Santorini, *Greece, September* 6-8, 1995, pp 14-31.

HARMAN P. (1996). "Autostereoscopic Display System", *SPIE Proceedings, "Stereoscopic Displays and Virtual Reality Systems IV",* Vol.2653, pp56-64.

HARMAN P. (1997). "Retroreflective Screens and their Application to Autostereoscopic Displays" *SPIE Proceedings, "Stereoscopic Displays and Virtual Reality Systems IV",* Vol.3012, pp145-153.

HARMAN P. (2000). "Autostereoscopic Teleconferencing System", *SPIE Proceedings, "Stereoscopic Displays and Virtual Reality Systems VII",* Vol.3957, pp 293-301.

HASHIMOTO N. , Morokawa S. and Kitamura K. (1991). "Real Time Holography using the High-resolution LCTV-SLM", *SPIE Proceedings, "Practical Holography V",* Vol.1461, pp 291-302.

HATTORI T. (1993). "Stereoscopic Display Employing Head-position Tracking using Large Format Lenses", *SPIE Proceedings, "Stereoscopic Displays and Applications IV"* Vol.1915, pp 2-5.

HATTORI T., Sakuma S., Katayama K., Omori S., Hayashi M. and Midori Y. (1994a). "Stereoscopic Liquid Crystal Display 1 (General Description)", *SPIE Proceedings, "Stereoscopic Displays and Virtual Reality Systems"* Vol.2177, pp 143-145.

HATTORI T., Sakuma S., Katayama K., Omori S., Hayashi M. and Midori Y. (1994b). "Stereoscopic Liquid Crystal Display 1 (General Description)", *SPIE Proceedings, "Stereoscopic Displays and Virtual Reality Systems"* Vol.2177, pp 146-147.

HATTORI T, (1995). "On-the-wall Stereoscopic Liquid Crystal Display", *SPIE Proceeding,s "Stereoscopic Displays and Virtual Reality Systems II"*, Vol.2409, pp 41-47.

HATTORI T. (2000a). "Sea Phone 3D Display", *http://home.att.net/~SeaPhone/3display.htm* pp1-6

HATTORI T. (2000b). "Sea Phone 3D Display", *http://home.att.net/~SeaPhone/3display.htm* pp7-9.

HECHT E. (1989a). *"Optics, 2nd Edition", Addison-Wesley,* pp 449-453.

HECHT E. (1989b). *"Optics, 2nd Edition", Addison-Wesley,* pp 404 & 434.

HEIDRICH H., Schwerdtner A., Glatte A. and Mix H. (2000). "Eye Position Detection System", *SPIE Proceedings, "Stereoscopic Displays and Virtual Reality Systems VII"* Vol.3957, pp 192-197.

HEMBD C., Stevens R., Hutley M. (1997). "Imaging Properties of the Gabor Superlens", *European Optical Society, Topical Meetings Digest Series: 13 "Microlens Arrays"*, NPL Teddington, May 15-16 1997, pp101-104.

HHI (2002). "3-D Display", *http://atwww.hhi.de/~blick/3-D_Display/3-d_display.html*

HINES S. (1997). Autostereoscopic Video Display with Motion Parallax", *SPIE Proceedings, "Stereoscopic Displays and Virtual Reality Systems IV"*, Vol.3012, pp208-219.

HONDA T. (1995). "Dynamic Holographic 3D Using LCD", *Asia Display '95,* pp777-780.

HOUSTON R.A. (1938a). *"A Treatise on Light"*, Longmans, Green & Co., pp 166-177.

HOUSTON R.A. (1938b). *"A Treatise on Light", Longmans, Green & Co.,* pp 166-167.

HOUSTON R.A. (1938c). *"A Treatise on Light", Longmans, Green & Co.,* pp 164-166.

ICHINOSE S., Tetsutani N. and Ishibashi M. (1989). "Full-color Stereoscopic Video Pickup and Display Technique Without Special Glasses", *Proceedings of the SID,* Vol.3014, 1989, pp319-323.

IMAI H., Imai M., Yukio O. and Kubota K. (1996). "Eye-position Tracking Stereoscopic Display using Image Shifting Optics", *SPIE Proceedings, "Stereoscopic Displays and Virtual Reality Systems IV"*, Vol.2653, pp 49-55.

IMAI H., Susumu T. and Imai M. (1999). "Viewing Point Detection System using Specific ImageProcessing for Eye-position Tracking Autostereoscopic Display", *SPIE Proceedings, "Stereoscopic Displays and Applications X"*, Vol.3639, pp92-98.

ISHIMA K., Yamada M., and Isono H. (1996). "A Study on Blinks while Watching 3D-HDTV", *NHK R&D Report*, No. 43 (November 1996)

ISONO H., Yasuda H., Kusaka H. and Morita T. (1990). "3D Flat-panel Displays without Glasses", *Proceedings of the SID*, Vol 31/3, 1990 pp263-266.

ISONO H., Komiyama S., Takemori D., Kanayama H., Yamada C. and Yoshida T. (1995). "A Novel Autostereoscopic 3D HDTV Display System: Creating a Superb Sensation of Reality and Presence", *Asia Displays '95*, pp795-798.

JENSEN J.A. (1998). "Deconvolution of in-vivo Ultrasound Images: Challenges and Solutions", *Seminar at the Signals and Systems Group*, Department of Information Technology, Technical University of Denmark.

JEON H-W, Travis A.R.L., Collings T.D., Wilkinson T.D. and Frauel Y. (2000). "Image Tiling System using Optically Addressed Spatial Light Modulator for High-resolution and Multiview 3-D Display", *SPIE Proceedings, "Stereoscopic Displays and Virtual Reality Systems VII"*, Vol.3957, pp165-176.

KAJIKI Y., Yoshikawa H. and Honda T. (1996). "Three-Dimensional Display with Focused Light Array" *SPIE Proceedings, "Practical Holography X"*, Vol.2652, pp 106-116.

KAJIKI Y. (1997). "Hologram-Like Video Images by 45-View Stereoscopic Display", *SPIE Proceedings, "Stereoscopic Displays and Virtual Reality Systems IV"*, Vol.3012, pp154-166.

KANOLT C.W. (1918). United States Patent 1260682.

KIM S.-S., Sohn K.H., Savaljev V., Pen E.F., Son J.Y. and Chun J.-H. (2001). "The Optical Design and Analysis for Super Multiview Three-dimensional Imaging System", *SPIE Proceedings, "Stereoscopic Displays and Virtual Reality Systems VIII"*, Vol.4297, pp222-226.

KINGSLAKE R. (1983). ***Optical System Design,*** Academic Press pp174-175.

KLEIN S. and Dultz W. (1990). "Perfect 3-Dimensional Movies and Stereoscopic Movies on TV- and Projection Screens; An Appraisement", *SPIE Proceedings, "Stereoscopic Displays and Applications"* Vol.1256, pp 289-295.

KNAPP A.G. (1990). Television Applications", *SID Residential Summer School,* 1990.

KONRAD J. (1999). "Enhancement of Viewer Comfort in Stereoscopic Viewing: Parallax Adjustment", *SPIE Proceedings, "Stereoscopic Displays and Applications X"* Vol.3639, pp179-189.

LIPPMANN M.G. (1908). "Epreuves Reversibles Donnant la Sensation du Relief", *J. Phys.*, 4th series, November, pp821-825.

LIPTON L. (1982). *Foundations of the Stereoscopic Cinema: A Study in Depth,* Amsterdam: Van Nostrand.

LUCENTE M., Benton S.A. and St.-Hilaire P. (1994). "Electronic Holography: The Newest", *International Symposium on 3-D Imaging and Holography,* Osaka, Japan Nov. 1994.

LUCENTE M. and Galyean T.A. (1995). "Rendering Interactive Holographic Images", *Computer Graphics Proceedings, Annual Conference Series,* 1995, pp 387-393.

LUCENTE M. (1997). "Interactive Three-dimensional Displays ; Seeing the Future in Depth", *Siggraph "Computer Graphics - Current, New and Emerging Display Systems".*

LYTLE D. (1995). "High-Speed Scanner Key to 3-D Imager", *Photonics Spectra,* October 1995, p48.

MACFARLANE D.L. and Schultz G.R. (1994). "A Voxel Based Spatial Display" *SPIE Proceedings, "Stereoscopic Displays and Virtual Reality Systems",* Vol.2177,pp 196-202.

MAENO K., Fukaya N., Nishikawa O. , Sato K. and Honda T. (1996) "Electro-holographic Display using 15-megapixel LCD" *SPIE Proceedings, "Practical Holography X",* Vol.2652, pp15-23.

MARR D, (1982). *"Vision",* W.H Freeman and Company, New York., pp147-148.

MASHITANI K, (1997). Personal communication from R & D Headquarters, Sanyo Electric Co. Ltd.

MAXWELL C.A. (1992). "Flicker Science and the Consumer", *Information Display,* 11/92, pp7-10.

MAYER U., Nuemann M.D., Kubbat W. and Landau K. (2000). "Is Eye Damage Caused by Stereoscopic Displays", *SPIE Proceedings, "Stereoscopic Displays and Virtual Reality Systems VII",* Vol.3957, pp4-11.

MCCORMICK M., Davies N. and Chowanietz E.G. (1992). "Restricted Parallax images for 3D T.V.", *IEE Colloquium "Stereoscopic Television"*, Digest No: 1992/173, pp 3/1-3/4.

MCKAY S., Mason S., Mair L.S., Waddell P. and Fraser S.M. (1999), "Stereoscopic Display using a 1.3 Diameter Stretchable Membrane Mirror", *SPIE Proceedings, "Stereoscopic Displays and Virtual Reality Systems VI"*, Vol.3639, pp122-131.

MCKAY S., Mair G.M., Mason S., and Revie K. (2000), "Membrane-mirror-based Autostereoscopic Display for Teleoperation and Telepresence Applications", *SPIE Proceedings, "Stereoscopic Displays and Virtual Reality Systems VII"*, Vol.3957, pp198-207.

MONTGOMERY D.J., Woodgate G.J., Jacobs A., Harrold J. and Ezra D. (2001). "Analysis of the Performance of a Flat Panel Display System Convertible between 2D and Autostereoscopic 3D Modes", *SPIE Proceedings, "Stereoscopic Displays and Virtual Reality Systems VIII"* Vol.4297, pp148-159.

MOORE J.R., Travis A.R.L., Lang S.R. and Castle O.M. (1992). "The Implementation of a Multi-view Autostereoscopic Display", *IEE Colloquium "Stereoscopic Television"*, Digest No: 1992/173, pp 4/1-4/16.

MOORE J.R., Dodgson N.A., Travis A.R.L., Lang S.R. (1996). "Time-multiplexed Color Autostereoscopic Display" *SPIE Proceedings, "Steroscopic Displays and Virtual Reality Systems IV"*, Vol.2653, pp 10-19.

MORIMOTO C.H., Koons D., Amir A. and Flickner M. (2000). "Pupil Detection and Tracking using Multiple Light Sources", *Image and Vision Computing 18,* Elsevier Science BV, pp331-335.

MORISHIMA H., Nose H., Yaniguchi N., Inoguchi K and Matsumura S. (1998). "Rear Cross Lenticular 3D Display without Eyeglasses", *SPIE Proceedings, "Stereoscopic Displays and Applications IX"*, Vol.3295, pp193-201.

MULKENS E. and Roberts J.W. (2001). "Effects of Display Geometry and Pixel Structure on Stereo Display Usability", *SPIE Proceedings, "Stereoscopic Displays and Virtual Reality SystemsVIII"* Vol.4297, pp 276-289

NISHIDA Y., Hattori T., Sakuma S., Katayama K., Omori S. and Fukuyo T. (1994). "Stereoscopic Liquid Crystal Display II (Practical Application)", *SPIE Proceedings "Stereoscopic Displays and Virtual Reality Systems"*, Vol.2177, pp 150-155.

NISHIDA Y., Hattori T., Omori S., Suzuki J., Katayama K. and Sakuma S. (1995). "Simplification of Infrared Illumination of Stereoscopic Liquid Crystal TV", *SPIE Proceedings, "Stereoscopic Displays and Virtual Reality Systems II"*, Vol.2409, pp 96-100.

OHSHIMA T., Komoda O., Kaneko Y. and Arimoto A. (1997). "A Stereoscopic Projection Display Using Curved Directional Reflection Screen", *SPIE Proceedings, "Stereoscopic Displays and Virtual Reality Systems IV",* Vol.3012, pp140-144.

OKOSHI T. (1976a). *"Three Dimensional Imaging Techniques"*, New York: Academic Press, p129.

OKOSHI T. (1976b). *"Three Dimensional Imaging Techniques"*, New York: Academic Press, p140.

OKOSHI T. (1976c). *"Three Dimensional Imaging Techniques"*, New York: Academic Press, p141.

OKOSHI T. (1976d). *"Three Dimensional Imaging Techniques"*, New York: Academic Press, p142.

OKOSHI T. (1976e). *"Three Dimensional Imaging Techniques"*, New York: Academic Press, pp362-363.

O'MARA W.C. (1996). "Liquid-Crystal Displays Tackle the Desktop", *Information Display,* Vol.12, No.7 pp 35-36.

OMURA K., Tetsutani N. and Kishino F. (1994). "Lenticular Stereoscopic Display System with Eye-Position Tracking and without Special-Equipment Needs", *SID 94 Digest,* pp 187-190.

OMURA K., Shiwa S. and Tsutomu M. (1998). "Lenticular Autostereoscopic Display System: Multiple Images for Multiple Viewers", *Journal of the SID,* 6/4 1998 pp 313-324

PALEY W. (1992). "Head-Tracking Stereo Display: Experiments and Applications", *SPIE Proceedings, "Stereoscopic Displays And Applications III",* Vol.1669, p 88.

PASTOOR S. (1991a). "3D-television: A Survey of Recent Research Results on Subjective Requirements", *Signal Processing: Image Communication,* (1991), Elsevier Science Publishers B.V., pp 21-32.

PASTOOR S. (1991b). "3D-television: A Survey of Recent Research Results on Subjective Requirements", *Signal Processing: Image Communication,* (1991), Elsevier Science Publishers B.V., p23.

PASTOOR S. (1991c). "3D-television: A Survey of Recent Research Results on Subjective Requirements", *Signal Processing: Image Communication,* (1991), Elsevier Science Publishers B.V., p24.

PASTOOR S. (1992). "Human Factors of 3DTV: An overview of Current research at Heinrich-Hertz-Institut Berlin", *IEE Colloquium "Stereoscopic Television"* Digest No. 1992/173, p11/3.

PASTOOR S. and Wopking M. (1997). "3-D Displays: A Review of Current Technologies", *http://atwww.hhi.de/~blick/papers/displays97/displays97.html*

PERLIN K. (1999). "A Displayer and a Method for Displaying", *Patent Application, International Publication No. WO 99/38334.*

PERLIN K. (2000). "Displayer and a Method for Displaying", *Patent Application, International Publication No. WO 00/70882.*

PERLIN K., Poultney C., Kollin J.S., Kristjansson D.T. and Paxia S. (2001). "Recent Advances in the NYU Autostereoscopic Display", *SPIE Proceedings, "Stereoscopic Displays and Virtual Reality Systems VIII",* Vol.4297, pp196-203.

REID J.M., Forsberg F. and Goldberg B. (2000). "Improvement of Resolution of Ultrasound Images", *Biomedical Engineering and Science Institute, Drexel University, Philadelphia, PA19104.*

SAKAMOTO K., Ueda H., Takahashi H and Shimizu E. (1995). "Real-time Three-dimensional Display Using a Holographic Optical Element", *SPIE Proceedings,* Vol.2577, 22-32.

SANDLIN D.J., Margolis T., Dawe G,. Leigh J. and DeFanti T.A. (2001). *SPIE Proceedings "Stereoscopic Displays and Virtual Reality Systems VIII",* Vol.4297, pp204-211.

SANGER D., Miyake Y. and Haneishi H. (1995). "Automatic Extraction of Facial Pattern from Colour Reversal Film Using Knowledge-Based Multistep Filtering Technique", *Asia Display '92, pp311-314.*

SAPIA M.A., Loew L.M., Fox.M.D. and Schaff J.C. (1998). "Ultrasound Deconvolution Using Adaptive Inverse Filtering", *Proceedings of the 12th IEEE Symposium on Computer-Based Medical Systems.*

SCHWEIWILLER P.M., Dumbreck A.A. and Chapman A.D. (1990). "Videotape Recording of 3D Television Pictures", *SPIE Proceedings, "Stereoscopic Displays and Applications",* Vol.1256, p239.

SCHWERDTNER A. and Heidrich H. (1998). "The Dresden 3D Display (D4D)", *SPIE Proceedings, "Stereoscopic Displays and Applications IX",* Vol.3295, pp203-210.

SCHWARTZ A. (1985). "Head Tracking Stereoscopic Display", *Proceedings of IEEE International Display Research Conference,* pp 141-144.

SEXTON I. (1992). "Parallax Barrier Display Systems" *IEE Colloquium "Stereoscopic Television"* Digest No: 1992/173, pp 5/1-5/5.

SIEGEL M. (2001). "Perceptions of Crosstalk and the Possibilities of a Zoneless Autostereoscopic Display", *SPIE Proceedings, "Stereoscopic Displays and Virtual Reality Systems VIII",* Vol.4297, pp34-41.

SMITH C.W. and Dumbreck A.A. (1988a). "3-D TV: The Practical Requirements", *Television: Journal of the Royal Television Society,* January/February 1988, pp 9-15.

SMITH C.W. and Dumbreck A.A. (1988b). "3-D TV: The Practical Requirements", *Television: Journal of the Royal Television Society,* January/February 1988, p10.

SMITH C.W. and Dumbreck A.A. (1988c). "3-D TV: The Practical Requirements", *Television: Journal of the Royal Television Society,* January/February 1988, pp10-12.

SMITH C.W. and Dumbreck A.A. (1988d). "3-D TV: The Practical Requirements", *Television: Journal of the Royal Television Society,* January/February 1988, p12.

SON J.-Y., Shestak S. A., Lee S.-K. and Jeon H.-W. (1996). "Pulsed Laser Holographic Video" *SPIE Proceedings, "Practical Holography X",* Vol .2652, pp24-28.

SON J.-Y., Shostak S.A., Choi Y.-J. and Kim K.-T. (1997). "Emitting Diagram Control Method for Solid Objects 3-D Display", *SPIE Proceedings, "Stereoscopic Displays and Virtual Reality Systems IV",* Vol.3012, pp262-272.

SON J.Y., Smirnov V. V., Asnis L. N., Volkonsky V. B., Chun J. H. and Kuznetzov S. V. and Lee H. S. (1999a). "Real-time 3D Display with Acousto-optical Deflectors", *SPIE Proceedings, "Stereoscopic Displays and Virtual Reality Systems VI",* Vol.3639, pp 137-142.

SON J.Y., Smirnov v.v., Chun Y.S. and Kim S.S. (1999b). "Non-glasses Type Stereoscopic Display System Based on Polarization", *SPIE Proceedings, "Stereoscopic Displays and Virtual Reality Systems VI",* Vol.3639, pp 132-136.

SON J.Y., Shestak S.A., KIM S.-S. and Choi Y.J. (2001). "A Desktop Autostereoscopic Display with Head Tracking Capability", *SPIE Proceedings, "Stereoscopic Displays and Virtual Reality Systems VIII",* Vol.4297, pp 160-164.

SPOTISWOODE N, and SPOTISWOODE R. (1953a). *Stereoscopic Transmission,* University of California Press, pp19-22.

SPOTISWOODE N. and SPOTISWOODE R. (1953b). *Stereoscopic Transmission* University of California Press, p22.

SPOTISWOODE N. and SPOTISWOODE R. (1953c). *Stereoscopic Transmission* University of California Press, p13.

STANLEY M., Conway P.B., Coomber S., Jones J.C., Scattergood D.C., Slinger C.W., Bannister B.W., Brown C.V., Crossland W.A. and Travis A.R.L. (2000). "A Novel Electro-optic Modulator System for the Production of Dynamic Images from Giga-pixel Computer Generated Holograms", *SPIE Proceedings, "Practical Holography XIV and Holographic Materials VI",* Vol.3956, pp13-22.

STEWARD E.G. (1983a). "Fourier Optics – An Introduction", *John Wiley and Sons,* pp24-25.

STEWARD E.G. (1983b). "Fourier Optics – An Introduction", *John Wiley and Sons,* pp 28-31.

STEWARD E.G. (1983c). "Fourier Optics – An Introduction", *John Wiley and Sons,* pp 86-90.

ST HILAIRE P. (1995). "Modulation Transfer Function of Holographic Stereograms" *Paper from Internet – originally published in "Applications of Optical Holography", 1995 SPIE Proceedings.*

STREET G.S.B. (1998). "Autostereoscopic Image Display Adjustable for Observer Location and Distance", *United States Patent 5,712,732.*

SURMAN P. (1997). "Head Tracking Two-image Stereo Displays", *Research Monograph 4 – Internal De Montfort University document,* 1997 pp14-33.

TAKAHASHI S., Toda T. and Iwata F. (1996). "Full Color 3D-Video System using Grating Image", *SPIE Proceeding, "Practical Holography X",* Vol.2652, pp 54-61.

TETSUTANI N., Ichinose S. and Ishibashi M. (1989). "3D-TV Projection Display System with Head Tracking", *Japan Display '89,* pp 56-59

TETSUTANI N., Omura K. and Kishino F. (1994). "A Study on a Stereoscopic Display System Employing Eye-position Tracking for Multi-viewers", *SPIE Proceedings, "Stereoscopic Displays and Virtual Reality Systems",* Vol.2177, pp 135-142.

TILTON H.B. (1985). "Large-CRT Holoform Display", *Proceedings of IEEE International Display Research Conference,* pp 145-146.

TOURIS T.C. (1994). "System Performance Requirements for a Head Tracking Autostereoscopic Display", *SPIE Proceedings, "Stereoscopic Displays and Virtual Reality Systems",* Vol.2177, pp16-25.

TRAVIS A.R.L. and Lang S.R. (1991). The Design and Evaluation of a CRT-based Autostereoscopic Display", *Proceedings of the SID,* Vol.32/4, pp279-283.

TRAUB A.C. (1966). "Three-dimensional Display", *United States Patent No 3,493,290.*

TRAUB A.C. (1967). "Stereoscopic Display using Rapid Varifocal Mirror Oscillations", *Applied Optics,* June 1967, Vol.6 No.6, pp1085-1087.

TRAYNER D and Orr E. (1996) "Autostereoscopic Display using Holographic Optical Elements", *SPIE Proceedings, "Stereoscopic Displays and Applications VII",* Vol.2653, pp 65-74.

TRAYNER D and Orr E. (1997) "Developments in Autostereoscopic Displays using Holographic Optical Elements", *SPIE Proceedings, "Stereoscopic Displays and Virtual Reality Systems IV",* Vol.3012, pp167-174.

TSAI C.H., Lee K. Hseuh W.J. and Lee C.K. (2001). "Flat Panel Autostereoscopic Display", *SPIE Proceedings, "Stereoscopic Displays and Virtual Reality SystemsVIII"* Vol.4297, pp 165-174.

VALYUS N.A. (1966a). *"Stereoscopy",* The Focal Press, pp117-161.

VALYUS N.A. (1966b). *"Stereoscopy",* The Focal Press, pp73-84.

VALYUS N.A. (1966c). *"Stereoscopy",* The Focal Press, pp161-168.

VALYUS N.A. (1966c). *"Stereoscopy",* The Focal Press, p259.

WILCOCK P.E. (1992). "HDTV: How Much is Enough" *IEE Colloquium, "Stereoscopic Television"* Digest No: 1992/173, pp 4/1-4/8.

WOODGATE G.J., Ezra D., Harrold J., Holliman N.S., Jones G.R. and Moseley R.R. (1997) "Observer Tracking Autostereoscopic 3D Display Systems", *SPIE Proceedings, "Stereoscopic Displays and Virtual Reality Systems IV",* Vol.3012, pp187-198.

YAMANOUE H. (1995). "the Relation between Size Distortion and Shooting Conditions for Stereoscopic Images", *Asia Displays '95,* pp681-664.

YAMANOUE H., Nagayama M., Bitou M. and Tanada J. (1998). "Orthostereoscopic Conditions for 3D HDTV", *SPIE Proceedings, "Stereoscopic Displays and Applications IX",* Vol.3295, pp111-112.

YANAGISAWA N., Kyung-Tae K., Son J-Y., Tatsuya M and Takatoshi O. (1997). "A Focus Distance Controlled 3DTV", *SPIE Proceedings,* Vol.3012, pp256-261.

YOUNSE J.M. (1993). "Mirrors on a Chip", *IEEE Spectrum,* November 1993, pp27-31.